Facultad de Ciencias
Departamento de Química Orgánica

Photosensitizers based on Ruthenium-bipyridyl complexes and porphyrins for dye-sensitized solar cells

MARÍA MEDEL GONZÁLEZ
Doctoral Thesis

Supervised by Prof. Tomás Torres Cebada
and Dr. Maxence Urbani

Madrid, 2015

This PhD Thesis has been done at the Department of Organic Chemistry at the Universidad Autónoma de Madrid under the supervisión of Prof. TomásTorres Cebada and Dr. Maxence Urbani.

El desarrollo de este trabajo ha sido posible gracias a las colaboraciones con el grupo de investigación del Prof. Grätzel and Nazeerudin, en Lausanne, Suiza, donde se llevo a cabo la caracterización física y el montaje de células solares fotosensibilizadas por colorante. Quisiera agradecerles su dedicación y esfuerzo en los proyectos comúnes. Asimismo, quiero dar las gracias al departamento de química orgánica y al servicio interdepartamental de investigación (el SidI), por haberme permitido disponer de todos los medios técnicos que fueron necesarios para esta tesis doctoral.

Sobra decir que todo esto no hubiera sido posible sin sin la confianza que el Prof. T. Torres depositó en mi, prestándome una vitrina y dándome la oportunidad de tener un contrato pre-doctoral y demostrar que no todo es una media en un papel. Agradecer la ayuda y paciencia para que todo esto llegara a buen puerto de mano de el Dr. M. Urbani, que siempre ha estado ahí para todas las preguntas.

Al resto de seniors también tengo que agradecerles por haber sacando tiempo para resolver dudas y por compartir su tiempo para poder aprender a mejorar en este mundo tan competitivo. En especial a la Dra. G. De la Torre, quería agradecerla por los consejos tanto profesionales como personales que me ha dado en este periodo.

A todos los compañeros de la tercera planta de la que siempre guardare un gran recuerdo, sobretodo del L307: de Juan y su música; Miguel que me enseño a hacer la TT1; Julia y su orden mas que necesario; Javi y su paciencia para todo. Y gracias a todos los que fueron pasando. En todo este tiempo que hemos coincidido, trabajo y diversión ha sido uno, haciendo todos vosotros de esta etapa un “algo” muy especial.

Mención especial para ciertas “personitas” que he conocido y me han permitido sobrellevar esto mucho mejor y espero que estén ahí por mucho tiempo: María “Pequeña” que fue mi compañera de complejos; el descubrimiento de esa cuarta planta (Bea, Nuria y Manu); gracias por esas tartas con grados de chocolate peligrosos para la vida y Nico, que aunque has llegado algo mas tarde me has vuelto a enseñar porque me enamore de esta carrera volviendo a ver la química con tus ojos, muchas gracias.

Y por supuesto, a Noemi que me ha acompañado en esta carrera y en muchas mas cosas y a Araceli que ya no se desde cuando froma parte de mi vida y que siempre me aguanta.

A mi Carol, yo ya se que podíamos con esto y con mas. Lo que dudo es si hacer otra tesis en Fisica o algo mas difícil… Nos hacemos un gran año!

Por ultimo, a toda mi familia. Gracias por ser como sois., los mejores padres que me podían haber tocado, Mabel y Jose Luis, por haberme querido, haberme dado todo siempre y por ello os tengo que agradecer la persona que soy. Alex por aguantarme siempre todo. A ti Maricarmen, por enseñarme que todo hay que tomárnoslo con una sonrisa en la cara, porque si pienso en ti es como vienes a mi memoria, con esa eterna sonrisa y ese positivismo que jamas has perdido. Y por supuesto a la familia que llego algo mas tarde pero que quiero igual, mi Paco que esta siempre y el mas pequeño pero el que mejor escucha, Altot. Os quiero.

Y a ti tia, esta dedicado todo esto, porque siempre confiaste en mi y te mereces todo.

Para ti y por esos 99 años de ejemplo a seguir. Siempre estarás conmigo.

To date, the results reported in this thesis have been published in the following journals:

• **Adapting Ruthenium Sensitizers to Cobalt Electrolyte Systems** S A Kumar, M Urbani, M Medel, M Ince, D González-Rodríguez, A K Chandiran, A N. Bhaskarwar, T Torres, Md. K. Nazeeruddin, and M Grätzel; J. Phys. Chem. Lett. 2014, 5, 501−505; doi: dx.doi.org/10.1021/jz402612h.

• **Cyclopentadithiophene-functionalized Ru(II)-bipyridine sensitizers for dye-sensitized solar cells** M Urbani, M Medel, S A Kumar, A K Chandiran, D González-Rodríguez, M Grätzel, Md.K. Nazeeruddin, T Torres; Polyhedron 2014, doi: http://dx.doi.org/10.1016/j.poly.2014.05.045

• **Synthesis of amphiphilic Ru(II) heteroleptic complexes based on benzo[1,2-b:4,5-b'] dithiophene: relevance of the half-sandwich complex intermediate and solvent compatibility** M Urbani, M Medel, S A Kumar, M Ince, A N. Bhaskarwar, D González-Rodríguez, M Grätzel, M K Nazeeruddin, T Torres ; Chemistry - A European Journal. 2015, doi: 10.1002/chem.201502417

Standars abbreviations and acronyms

CB	Conduction band
VB	Valence band
CNT	Carbon nanotube
CS	Charge separation
DBU	1,8-Diazabicyclo[5.4.0]undec-7-ene
o-DCB	**o**-Dichlorobenzene
DCM	Dichloromethane
DMAE	**N**,**N**-Dimethylaminoethanol
DMF	**N**,**N**-Dimethylformamide
DMSO	Dimethyl sulfoxide
DSSC	Dye-sensitized solar cell
EA	Elemental analysis
EI	Electronic impact
EQE	External quantum efficiency
FF	Fill factor
GPC	Gel permeation chromatography
HOMO	Highest occupied molecular orbital
IR	Infrared
IPCE	Incident photon-to-current efficiency
ITO	Indiun tin oxide
LUMO	Lowest unoccupied molecular orbital
MALDI	Matrix-assisted laser desorption/ionization
NMR	Nuclear magnetic resonance
OPV	Organic photovoltaic

Standars abbreviations and acronyms

OSC	Organic solar cell
Pc	Phthalocyanine
PCE	Power conversion efficiency
PD	Polidispersity
ppm	Parts per million
THF	Tetrahydrofuran
UV-Vis	Ultraviolet-visible spectrophotometry

INDEX

Resumen:

La presente tesis doctoral, que lleva por título *"Photosensitizers based on Ruthenium-bipyridyl complexes and porphyrins for dye-sensitized solar cells"* está centrada en el desarrollo y estudio de nuevos materiales funcionales con propiedades electrónicas para su utilización en fotovoltáica molecular. Se ha dividido en dos capítulos principales; en el primero de ellos se ha desarrollado síntesis, caractirzacion y aplicación de ocho nuevos complejos de rutenio. Estos complejos se componen de dos unidades de bipirina, una dadora y otra aceptora y dos ligandos tiocianato. En este este estudio todas ellas tienen en común la unidad aceptora o de anclaje a la superficie de la celula solar (bipiridina con dos grupos ácidos) y los ligandos lábiles tiocianatos y como unidades variables las unidades o bipiridinas dadoras.

Las bipiridinas dadoras se pueden dividir en dos grupos:

- Uididades de BDT en el que se han sintetizado cuatro complejos diferentes añadiendo un doble enlace en su anclaje entre la unidad y la bipirina para aumentar la conjugación; añadiendo cadenas alquílicas o no para aumentar su solubilidady evitar la agregación en el dispositivo.
- Unidades CDT en las que a su vez se han sintetizado tres complejos diferentes con las mismas premisa que las anteriores.

En todos los casos se midieron sus propiedades fotofisicas y se compararon entre ellas, escogiendose las mas favorable para la optimización de sus respectivos dispositivos. Introduciendo como novedad la utilización de complejos de cobalto como electrolito de la célula fotovoltáica, hasta ahora poco utilizados en etos casos.

En el segundo capitulo de esta tesis se ha centrado en la sintesis y caracterizacion de cuatro porfirinas "push-pull" con el fin de ser utilizadas en fotovoltáica molecular, análogas a las que en la actualidad poseen el record en este campo. Para ello se a legido un grupo voluminoso que evite agregación similar al de estudios reportados en el grupo con ftalocianinas, 2,5-difenilbenceno. Y por otro lado se han sintetizado diferentes grupos de anclaje ("Pull") con y sin unidad de benzo[*c*][1,2,5]tiadiazole y como unidad dadora dos aminas secundarias ("Push") mas o menos voluminosas para evitar agregación en el dispositivo final. Con estas convinaciones se han sonseguido cuatro porfirnas que en un futuro se medirán sus propiedades fotofisicas.

CHAPTER 1: INTRODUCTION

1.1 SOLAR ENERGY

The evolution of mankind before the industrial revolution was dependent on the annual cycle of plant photosynthesis for both heat (burning wood) and mechanical energy (human and animal muscle power derived from food and fodder). Steam locomotives, the quintessential machines of the industrial revolution, started to use existing energy resources, such as coal, more efficiently. Ever since, industrial development has depended on the availability of cheap and reliable energy sources. On the international scale, the energy required in 2005 was the equivalent of 13 terawatts (TW), which is 13 trillion watts of power. 85% of this energy came from fossil fuels, which has produced large quantities of greenhouse gases. These emissions result of global warming which turned out to be catastrophic consequences for the earth . As energy expenses keep growing, it has been estimated that the world's energy consumption will reach 28 TW in 2050.[1] This points out that the society is facing a dilemma: for further economic development, an increase in the energy consumption is necessary. However, this will lead to dramatic and irreversible consequences for the environment due to the emission of pollutants. The predicted exhaustion of fossil energy resources and the pressure of environmental constraints have urged an intensification of the research on renewable energy sources, which plays an essential role in the sustainable development of the environment, economy and society.

Solar, geothermal, ocean, wind, tides and hydropower and biomass are renewable energies that may meet these energy demands. As a matter of fact, solar energy alone possesses the potential of becoming the successor of fossil fuels, which could cover the world's current energetic needs.[2]Sunlight strikes the Earth's surface with enough energy every hour to supply world consumption per annum. This is by far the biggest source of available energy, and a great candidate for a transition to a more sustainable production of energy.

Solar energy[3] can be converted into electricity either thermodynamically or electronically. The first method, the solar thermal energy[4], is usually focused in the

design of optical collectors to generate electricity by heating a fluid to drive a turbine connected to an electrical generator. The second method, instead, converts directly the solar energy into electricity by opto-electronic devices, called solar cells. This efficient production of electricity by means of solar cells[5] is nowadays available and photovoltaics is one of the fastest growing renewable energy technology. In this context, silicon based solar cells are by far the most dominating type of photovoltaic devices with a market share of about 90% (single crystalline, polycrystalline and amorphous forms). Their broad recognition is attributed to their proven and reliable operational capacities, namely, good efficiencies and a lifetime of 20 years. Laboratory cell efficiencies have reached 25% (crystalline), but commercial module efficiencies are still in the range of 15-18%.[6] A combination of an increase in efficiency and a reduction of the production costs of the photovoltaic panels is still necessary to realistically compete with conventional fossil-fuel energy conversion systems. Fifty years of research and innovation have significantly reduced the price of silicon-based photovoltaic modules. However, despite these efforts, the cost of production remain high which hampers wider application. The main reson comes from the high purity of the silicon required to obtaine such high efficiency. Another drawback is that silicon panels are very heavy and rigid in shape. In this regard, both organic photovoltaics and hybrid devices with active inorganic and organic materials have attracted significant attention as viable alternative to Si-based due to their lower cost of production, flexibility and high-efficiency at low-light intensities.

Organic materials fulfill many requirements for solar cells, such as strong optical absorption, easy manufacturing in thin films, chemical tailoring to tune their properties, and low-cost synthesis[7]. However, long-term stability is still an issue that has to be solved.

1.1.1 Classification of solar cells

First reports on photovoltaic concepts date back to the end of the XIX century with two major contributions: one from Becquerel in 1839, describing photocurrent, and the first real reports on photoconductivity made by Smith and Adams in 1873 and 1876, respectively, working on selenium. It was not known until the beginning of the XX century that photoconductivity using an organic compound, namely, anthracene, could be observed. The commercial potential of

these photoconductive materials has encouraged the research in this area, and the variety of devices has broadened to encompass all fields of development. Solar cells can be broadly classified depending upon the type of active material used, manufacturing technique, type of junction formed or even the generation. A classification based on the type of material (inorganic, organic or hybrid when both are present) is shown below (the record conversion efficiencies for the different technologies reported in this section are updated until July 2015).

Inorganic solar cells

The technology used to make most of the solar cells fabricated so far, borrows heavily from the microelectronics industry, where silicon prevails as semiconductor. The first silicon solar cell was developed by the Bell Telephone Lab in 1954, showing an efficiency of 6%. Much research has followed this pioneer work since silicon is safe and the second most abundant element on Earth. The crystalline solar cells, either mono- or polycrystalline, are known as the 1st generation solar cells. Their maximum efficiencies, 25.0% and 20.4%, respectively, are close to the Shockley–Queisser theoretical limit, i.e. 33%. Crystalline silicon solar cells dominate the photovoltaic market, despite the fact that an important drawback of this kind of photovoltaic cells is to get highly pure silicon (>99.99%). The production costs of such modules are very high, which motivated engineers and scientists to develop a 2nd generation of solar cells by addressing factors such as easy and low-cost production, as well as higher performances.

The 2nd generation based on thin film inorganic solar cells, appeared in the early 60s (although they did not raise too much expectations until the 90s), as a consequence of the development of cost-efficient of the thin film technologies. Nowadays they have proved to be a strong alternative to classical silicon photovoltaics. Modules based primarily on chemical vapour deposited amorphous silicon (maximum efficiency of 13.4%, LG Electronics), as well as polycrystalline InSe, CdTe (maximum efficiency of 21.5%, First Solar), $CuInGaSe_2$ (known as CIGS ; maximum efficiency of 21.7%, ZSW) have yielded outstanding performances. When compared to the 1st generation of solar cells, they are, in general, less expensive, but also less efficient. Thin film solar cells are designed in such a way that they use less material, resulting in lower cost and easier manufacturing processes. Some drawbacks, like resource scarcity and toxicity of

the active materials, triggered research on a 3rd generation of solar cells during the last two decades.

In the latter generation, highly efficient solar cells are based on environmentally friendly materials that allow inexpensive solvent-based fabrication techniques. Leading examples are low-cost, thin-film solar cells based on novel concepts like hot carrier solar cells, multiple exciton generation, tandem or multijunction solar cells.[8] By means of these cells, the Shockley-Queisser limit as defined for the 1st generation of solar cells is expected to be bypassed.[9]

Figure 1.1 A tipical silicon solar cell with the layer configuration displayed

Organic solar cells.

All-organic photovoltaics, as well as hybrid solar cells, are considered also as a type of 3rd generation devices, and have the merits of low cost, stability, simple fabrication and flexibility.[10]

In the late 50s and 60s, it was discovered that many common dyes, such as methylene blue, many important biological molecules like carotenes and chlorophylls, and other porphyrins and related synthetic analogues such as phthalocyanines, had semiconducting properties. These dyes were among the first organic materials to exhibit a photovoltaic response. As early as 1958, Kearns et al. reported a cell based on a single layer (Schottky or monolayer solar cell) of a magnesium phthalocyanine, which had a photovoltage of 200 mV. Since then, organic materials have gained broader interest and several new concepts associated to the configuration of the device have been presented.

A milestone came in 1986 when Tang used a two-component, donor:acceptor active layer (planar bilayer heterojunction, PHJ, or p-n solar cell, Figure 1.2 a). This structural modification benefits from the facile formation of the charge carriers (electrons and holes) by electron transfer from the photoexcited donor to the acceptor component. Also, the separated charge transport layers

ensure connectivity with the correct electrode and give the separated charge carriers less chance to recombine with their counterparts. The drawback is that only excitons (i.e. electron-hole pairs formed by light excitation) formed very close the interface between donor and acceptor layers are able to dissociate. In an attempt to overcome this structural problem, the concept of bulk-heterojunction (BHJ, Figure 1.2 b) was introduced by Yu et al.[11] In such technology, the active layer is a blend composed of a donor and an acceptor component, in which a bicontinual phase separation is formed.[12] If the molecular mixing of the two active materials occurs properly to allow a good contact between each other (morphology control), the advantage of this type of cell is the large interface area that enables most of the excitons to reach the p-n interface.

Ultimately, another type of architectures called tandem solar cells (Figure 1.2 c), have gained a lot of attention. They consist in a combination of two or more single junction cells (one on top of the other) that absorb at different wavelength ranges. Their advantage is that a combination of absorbing molecules can allow spanning a larger spectral region of sunlight, which would be difficult to obtain with a single component, hence giving them the potential to reach higher efficiencies.

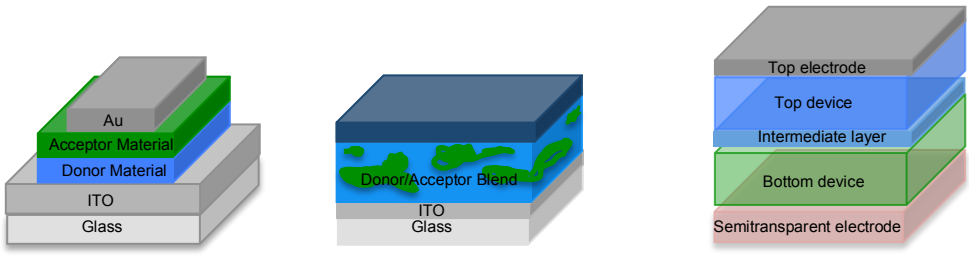

Figure 1.2 Schematic representation of a) planar bilayer, b) bulk heterojunction and c) tandem solar cell.

From a different point of view, another classification of the organic solar cells[13] based on the active material can be established: (1) polymer solar cells (PSC), also known as plastic solar cells, which are constituted by conjugated polymers; and (2) small molecule-based photovoltaic devices, in which discrete chromophores form the active layer.[14]

In general terms, the photovoltaic process for organic photovoltaic (OPV)[15] cells starts when light is absorbed by the organic active layer, and an electron from the HOMO is promoted to the LUMO by formation of an exciton (electron-hole pair). After exciton dissociation, the electron migrates to the cathode, and the hole moves to the anode. A fundamental difference in the working principle of solar cells based on organic materials with regard to conventional inorganic photovoltaic cells, is that, in the latter, the absorption of photons with energies greater than the bandgap of the semiconductor results in the direct generation of free charge carriers (electron and holes) that are able to diffuse under an externally applied electric field to their respective electrodes. On the other hand, organic materials have typically a much lower dielectric constant than their inorganic counterparts, and this results in the generation of tightly coulombically bounded electron-hole pairs upon photoabsorption, with a binding energy of about 0.5 eV, rather than free charge carriers.[16] In addition, organic semiconductors do not exhibit band-like transport behaviour, the charge carriers moving along by a hopping mechanism between localized states.[17] The charge carrier mobility in organic semiconductors is, therefore, inherently low, with typical values less than 10^{-2} cm^2/V. These differences between inorganic and organic materials drive the structural design of organic solar cells.[18]

Regarding the efficiencies, while polymeric tandem solar cells have reached a conversion efficiency of 10.6%,[19] it is worth noting that Heliatek helds the record in multi-junction architectures,[20] with a tandem oligomer-based device achieving a certified power conversion efficiency of 12%. For a single junction device, the best conversion efficiency was reported by Mitsubishi Chemical, achieving a PCE of 11.7%.[21]

Hybrid solar cells

Apart from the fully organic solar cells, combinations of organic-inorganic materials have been of great relevance in the recent years. In this sense, the development of dye-sensitized solar cells (DSSCs) in the 90s opened up new horizons in the area of photovoltaic, and entered dynamically the race for cost-efficient devices functioning at the molecular and nanoscale levels.[22] The seminal paper by O'Regan and Grätzel in 1991[23] introduced a pioneering architecture, in which an organic light-absorbing dye is anchored to a mesoporous inorganic n-type

semiconductor film (the semiconductor operates as photoanode) and filled in with a redox-active electrolyte.

This type of DSSCs has shown a tremendous potential and is nowadays a real alternative to the standard silicon photovoltaics,[24] with efficiencies growing from 7% in the seminal report, using ruthenium complexes as the dye, to the current 13.0% employing porphyrins. Alternatively, p-type DSSCs (an active photocathode) have been also explored but they have not exhibited yet energy conversion values as high as conventional n-type´s. This was ascribed to several drawbacks associated with the electrolytes and the p-type semiconductors,[25] and to date, there is just one example of comparable efficiency, i.e. 2.51%.[26] Nowadays, another important point is the growing tendency to develop all-solid-state devices versus the liquid-based DSSCs, which represents a step forward into the future commercialization.[27]

Beyond the architecture, there are some materials that need a special mention, like quantum dots[28] and perovskites.[29] The latter is the active component of a new family of solar cells, the perovskites solar cells (PSC), that has a very good chance to contribute to a large scale solar energy production based on their high efficiency (up to ca. 20%) and compatibility with scalable processes. Perovskites have the general formula of ABX_3 (Figure 1.3) where A and B are monovalent and divalent ions, respectively, and X is O, C, N or an halogen.

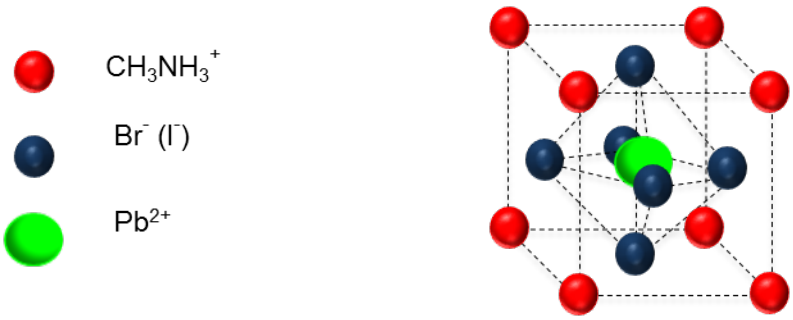

Figure 1.3 Structure for $CH_3NH_3PbBr_3$, a common perovskite currently used for solar cell applications

The field of perovskite-sensitized solar cells has grown exponentially since the first work of a perovskite-sensitized solar cell was published in 2009 by Miyasaka and co-workers, where a PCE 3.81% was obtained for a sensitized solar

cell employing $CH_3NH_3PbI_3$ as absorber and the iodide/triiodide redox couple was reported.[30] A first tremendous breakthrough came later in 2012 by Kim et al. who used *spiro*-MEOTAD as solid-state hole-transporting material (HTM), replacing the traditional liquid-electrolyte commonly used in DSSC, which improved the stability of the device to achieve a PCE exceeding 9.7%. One year later, in 2013, Burschka et al. reported a sequential deposition method to permit a much better control over the perovskite morphology during the fabrication of the device, resulting in an alluring PCE of 15%, beating the best DSSC at the time (YD2-oC8) with a PCE of ca. 12%. In view of the above, it is not surprising that, since then, research on PSC has soared in the last few years. Current progress in the area focuses mainly on the morphology optimization (thickness and homogeneity),[31] broadening the absorption and photostability.[32] The current record of PSC stands now at 20.1% (KRICT). Despite their indisputable leadership in terms of high-efficiency and low-cost production, PSC technology is facing, however, two important issues: first environment's, because of the toxicity of lead and second, the short-term stability due to high moisture-sensitivity of perovskites. These constitute two serious limitations for further large-scale applications in photovoltaics that need to be solved in the future.[33]

1.2.2 Photovoltaic parameters of a solar cell

The properties of a photovoltaic device can be characterized by plotting the measured current output J of the cell versus the voltage output V of the cell. In the dark, the J-V curve passes through the origin, since at that moment no electrons is flowing through the device and no potential is present. By exposing the photovoltaic device to light, the J-V curve shifts upwards, as can be seen in Figure 1.4. The most important characteristic parameters of photovoltaic devices can be found on this J-V curve.

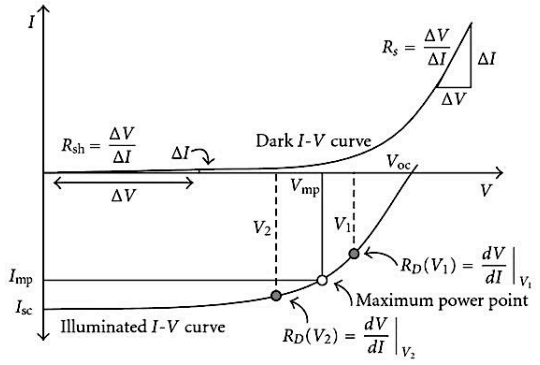

Figure 1.4 Typical I-V curve for a solar cell in the dark and under illumination

Open-circuit voltage (V_{OC}): It is the maximum possible voltage across a photovoltaic device. This is the voltage across the cell, in sunlight, when no current is flowing through the device.

Short-circuit current (I_{SC}): It is the current that flows through an illuminated solar cell when there is no external resistance *i.e.* when the electrodes are simply connected or short-circuited. I_{SC} is the maximum current that a photovoltaic device is able to produce. Under an external load, the current will always be less than I_{SC}. The short-circuit current depends on a number of factors, such as the area of the solar cell. To remove the dependence of the solar cell area, it is more common to list the short-circuit current density (J_{SC} in mA/cm^2), rather than the short circuit current (I_{SC} in mA).

Maximum power point (M_{pp}): It is the point (V_m, J_m) on the I-V curve at which the maximum power is produced. Power is the product of current I and voltage V. This is represented in Figure 1.4 as the area of the rectangle formed between a point on the I-V curve and the axes I and V. The maximum power point is that point on the I-V curve at which the area of the resulting rectangle, I x V, is largest.

Fill Factor (FF): It is the ratio of its actual maximum power output to its theoretical power output, if current and voltage would be at their maxima, I_{SC} and V_{OC}, respectively. This is a very important property used to measure photovoltaic device performance. It is a measure of the 'squareness' of the I-V curve. FF can be written down as follows (Eq1.1).

$$\text{FF} = \frac{\text{Jm}\times\text{Vm}}{\text{Jsc}\times\text{Voc}} \qquad \text{Eq1.1}$$

Power Conversion Efficiency (PCE or η): It is the ratio of the power output, (P_{out}) to power input (P_{in}). The PCE measures the amount of power produced by a photovoltaic device relative to the power available from the incident light radiation summed over all wavelengths. It is the most important parameter to characterize the performances of a solar cell. In order to compare the results from various devices, regardless of the design and active material, the cells are subject to the same standard test conditions. PCE can be written down as follows (Eq1.2).

$$\text{PCE}\ (\eta) = \frac{P_{out}}{P_{in}}\times 100\% = \frac{J_m\times V_m}{P_{in}}\times 100\% = \frac{J_{sc}\times V_{oc}\times \text{FF}}{P_{in}}\times 100\%$$

Eq1.2

For obvious realistic and practical reasons, the efficiency of a photovoltaic device is usually given under 1 sun illumination. In a sun simulator, an input power of 100 mW/cm^2 corresponds to the irradiation of ambient sunlight under standard conditions, with a spectrum consistent to an air mass global value of 1.5 (AM 1.5G) at a temperature of 25 ºC. These conditions are defined as the standard '1 Sun' value. Air mass describes the spectrum of radiation and can be defined as the amount of atmosphere though which sunlight has to travel to reach the Earth's surface. This is abbreviated as AM x, in which x is the inverse of the cosine of the zenith angle of the sun. The above-mentioned AM1.5G conditions correspond to the spectrum and irradiance of sunlight incident with a zenith angle of 48.2º (Figure 1.5).

External Quantum Efficiency (EQE): Also known as Incident Photon to Current Efficiency (IPCE), is another important parameter for solar cell characterization. It is calculated by the number of electrons extracted in an external circuit divided by the number of incident photons at a certain wavelength under short-circuit condition. EQE can be written down as follows (0) elementary charge, *h* is the Planck constant, and *c* is the speed of light in vacuum.

$$\text{EQE}\ (\eta) = \frac{\text{number of electrons}}{\text{number of incident photons}} = \frac{J_{sc}\ (\lambda)/e}{P_{in}\ (\lambda)/(hc/\lambda)} = \frac{J_{sc}(\lambda)hc}{P_{in}\ (\lambda)e\lambda}$$

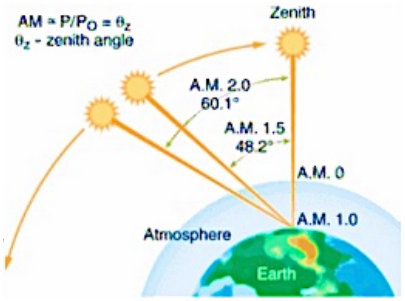

Figure 1.5 The air-mass value AM 0 equates to insolation at sea level with the Sun at its zenith. AM 1.0 represents sunlight with the Sun at zenith above the Earth's atmosphere. AM 1.5 is the same, but with the Sun at an oblique angle of 48.2º, which simulates a longer optical path through the Earth's atmosphere; AM 2.0 extends that oblique angle to 60.1º.

1.2. DYE-SENSITIZED SOLAR CELLS (DSSCs)

Dye-sensitized solar cells (DSSCs) are one of the most studied photovoltaic devices. These solar cells take sunlight and convert it directly into electricity using very cheap materials.

This type of solar cells is also known as photo-electrochemical solar cells. The DSSCs perform much better compared with other photovoltaic devices under diffuse light conditions due to the use of the mesoporous semiconductor (mesoporous surfaces). Last but not least, these solar cells offer also the possibilities to design solar cells with a large and flexible shape, colour and transparency, which aims for the integration into different products to opens up new eco-friendly commercial opportunities, because, at the moment, solar cells offer a lower-cost alternative to silicon photovoltaics because they are based on cheap materials and inexpensive manufacturing technology.

1.2.1 Principles of operation

One of the most important key-components of a DSSC is the "dye" or "sensitizer" inside the device. This provides a remarkable advantage to this technology because of the flexibility and easily tuneable photophysical, photochemical and electrochemical properties of the dye by molecular engineer, and for that are excellent candidates for light harvesting systems and energy conversion devices. A working and a counter electrode, and an electrolyte that can be liquid or a solid containing various additives and a redox shuttle composes all DSSCs. For the working electrode, a layer of a mesoporous metal oxide semiconductor, often TiO_2, is deposited onto a FTO/TCO transparent conducting oxide. The mesoporous film is coloured with a sensitizer that acts as the light harvesting material. Upon light absorption the sensitizer injects an electron into the semiconductor. The injected electrons to reach the counter electrode where the oxidised shuttle is regenerated, closing the electrical circuit. The counter electrode is made of an atomic layer of Pt that serves to catalyse this electron transfer. The main process occurring in an operative DSSC are represented in **¡Error! No se encuentra el origen de la referencia.**.[34]

Upon absorption of sunlight, the photosensitiser promotes an electron from its ground state to the excited state (absorption/excitation: **R.1**). This electron is subsequently injected into the conduction band of the semiconductor (injection: **R.2**).

The oxidized dye is regenerated to the ground state by the hole-transport shuttle present in the electrolyte (**R.4**). The injected electron in the photophoanode which arrives at the back contact and flows through an external circuit to reach the counter electrode. At the counter electrode, the electrons are transferred to the oxidized shuttle present in the electrolyte (regeneration of the oxidized shuttle: **R.3**). The most commonly used electrolyte contains the I^-/I_3^- redox couple.

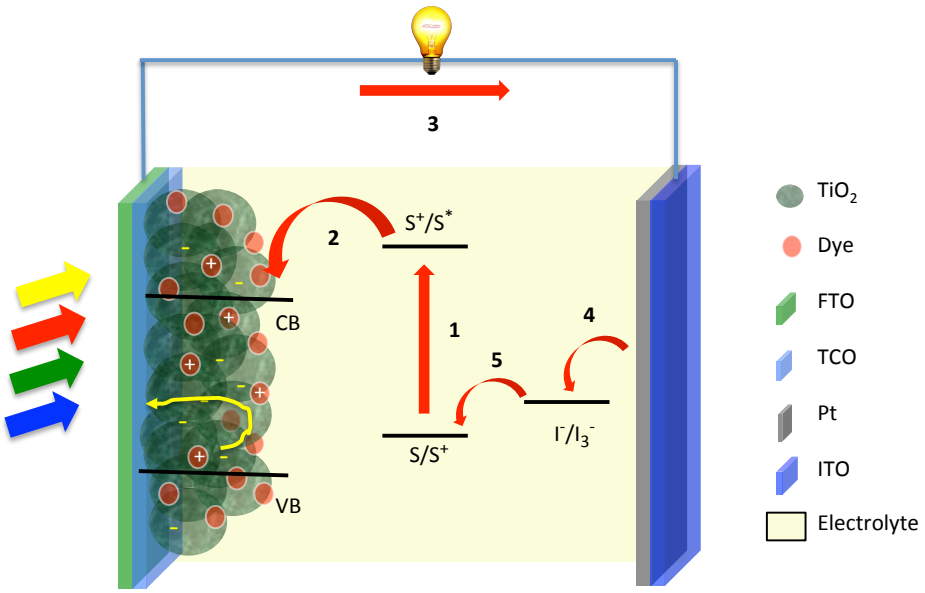

Figure 1.6 Schematic representation and main processes occurring in a DSSC . S, S+ and S* represent the dye in the ground, oxidized and excited state respectively. (1) Photoexcitation of the dye, (2) electron injection from the excited dye to the semiconductor, (3) external circuit, (4) regeneration of the electrolyte and (5) regeneration of the oxidized dye.

Photoexcitation: $S + h\nu \rightarrow S^*$ (**R.1**)

Electron injection: $S^* \rightarrow S^+ + e^-(TiO_2/CB)$ (**R.2**)

Electrolyte regeneration: $I_3^- + 2\ e^-(Pt) \rightarrow 3\ I^-$ (**R.3**)

Dye regeneration: $2\ S^+ + 3\ I^- \rightarrow 2\ S + I_3^-$ (**R.4**)

The regenerative cycle of a dye-sensitized solar cell is based on reversible reactions, and the devices can convert sunlight into electricity without suffering permanent chemical transformations.

However, this system has undesirable loss reactions, which decrease the total efficiency of the device (Figure 1.7) . The three main loss reaction processes are: (1a) deactivation of the dye excited-state (**R.5**), (2b) recombination of photoinjected electrons in the semiconductor with the oxidized photosensitizer (**R.6**), and (3c) recombination of photoinjected electrons in the semiconductor with the oxidized form of the redox mediator (**R.7**). The latter recombination reaction is also called the "dark current".

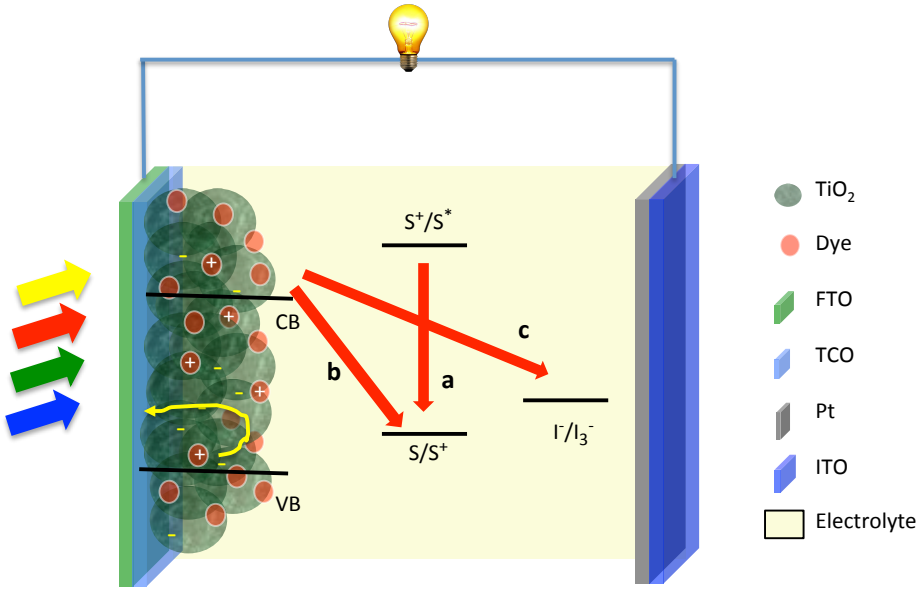

Figure 1.7 Scheme of the loss reactions occurring in a DSSC. (a) Dye excited state deactivation, (b) e^--TiO2 /S^+ back electron transfer, and (c) e^--TiO2 /I^- recombination reaction.

Dye excited state deactivation: S* ➔ S + heat/h ν (**R.5**)

Back electron transfer: $S^+ + e^-$ (TiO_2/CB) ➔ S (**R.6**)

Electron recombination with the redox couple: $I_3^- + 2\ e^-$(TiO_2/CB) ➔ $3I^-$ (**R.7**)

Despite the loss processes occurring in a DSSC, the reason for the relatively high efficiencies observed in optimised devices is due to the rather favourably balanced kinetic competition which ensures forward electron transfer reactions dominate over the loss processes mentioned. For most dyes, loss reactions are several orders of magnitude slower than the forward processes when the devices are working under normal operating conditions, allowing efficient charge separation to occur (Table1.1).[35]

Table1.1 Timescales of forward and loss processes occurring in DSSC

Forward processes	**Loss processes**
Electron injection from the excited dye into the semiconductor conduction band (10^{-12} - 10^{-9} s)	Excited state deactivation (> 10^{-9} s)
Dye regeneration by the redox electrolyte (10^{-9} - 10^{-6} s)	Back electron transfer from the TiO_2 to the oxidised dye (10^{-6} - 10^{-3} s)
	Electron recombination between the TiO_2 and the electrolyte (10^{-3} - 10^{1} s)

1.2.2 Fundamental constituents of a dye-sensitized solar cell

In a DSSC, the semiconductor acts as a supporting material for dye adsorption and as an electron transport pathway. For the photoanode, the TiO_2 mesoporous nanoparticles are deposited onto a glass substrate (TCO = transparent conductive oxide) coated with a thin layer of a transparent conductive material. The most commonly used conductive material is fluorine-doped tin oxide (FTO). The photocathode is usually made of an ITO substrate (indium-tin oxide) coated with a thin layer of platinum or graphite carbon.

Three important processes take place in the working electrode: light harvesting, charge separation and electron transport. Light-harvesting is performed by the chromophoric agent, which consists of a photosensitize. Charge separation occurs at the Dye/TiO_2 interface, with electron travelling through the TiO_2 CB and holes through the electrolyte. Electron recombination can take place at the interface between the semiconductor and the dye or the electrolyte.

DSSCs are devices composed of multiple components, and their overall efficiency depends strongly on the individual properties of each constituent. Much effort have been spent on the optimisation of the materials used in the fabrication of solar cells, such as the semiconductor metal oxide, the photosensitiser, the electrolyte and the counter electrode.

1.2.2.1 The working electrode

As mentioned above, the mesoporous semiconductor film is attached to the TCO. The TCO consists in a glass coated with a thin layer of a transparent conductive material. In this type of devices, the most commonly used conductive material is fluorine doped tin oxide (FTO). In other devices, the material used is tin doped indium oxide (ITO), but the fabrication of DSSCs implies temperatures higher than 300^{o}C and although ITO presents higher conductivities, its thermal instability strongly increases the resistance of the material and, hence, most devices are fabricated using FTO.

It is also important to mention that mesoporous TiO_2 semiconductor still gives the highest efficiencies, but many other metal oxide systems have been tested, such as ZnO, SnO_2, and Nb_2O_5. Besides these simple oxides, ternary oxides, such as $SrTiO_3$ and Zn_2SnO_4, have been investigated, as well as core-shell structures, such as ZnO-coated SnO_2.

The TiO_2 is a stable, nontoxic oxide, which has a high refractive index (n = 2.4-2.5) and is widely used as a white pigment in paint, toothpaste, sunscreen, self-cleaning materials and food (E171). Several crystal forms of TiO_2 occur naturally: rutile, anatase and brookite. Although rutile is the thermodynamically most stable form, anatase is, however, the preferred structure in DSSCs because it has a larger bandgap (3.2 vs 3.0 eV for rutile) and the higher conduction band edge energy, Ec. This leads to a higher Fermi level and Voc in DSSCs for the same conduction band electron concentration.

For state-of-the-art DSSCs, the employed architecture for the mesoporous TiO_2 electrode is as follows:[36]

1. A TiO_2 blocking layer (thickness ~50 nm), coating the FTO plate to prevent contact between the redox mediator in the electrolyte and the FTO, prepared by chemical bath deposition, spray pyrolysis, or sputtering.[37]
2. An active layer consisting of a 5–12 μm thick film made with mesoporous TiO_2 (~20 nm particle size) that provides a large surface area for sensitizer

adsorption (in order to anchor a dye monolayer) and good electron transport to the substrate (porosity must be also controlled).

3. A light scattering layer on top of the mesoporous film, consisting of ca. 4 μ m thick porous layer containing ~400 nm sized TiO_2 particles. The aim of this layer is to reflect the unabsorbed light passing thought the device, which improve the light-harvesting efficiency of the device by giving a second "chance" of the dye to reabsorb a photon. This is particularly efficient for dyes that have low molecular extinction coefficients (such a Ru(II) N3, ε = 10,000-15,000). The most common method to deposit the nanoparticles (active and scattering layers) is based on the doctor Blade screen printing techniques (manual or automatic).
4. A $TiCl_4$ post-treatment, consisting of an ultrathin overcoating of TiO_2 on the whole structure, deposited by means of chemical bath deposition using a 2M $TiCl_4$ aqueous solution, followed by thermal treatment at 500ºC. This post-treatment leads to the deposition of an ultrapure TiO_2 shell (~1 nm) on the mesoporous TiO_2, acting as "cement" to fill the empty space default of the TiO_2 nanostructure. The aim of this process is to reduce electron recombination at the TiO_2 / electrolyte interface. However, this process also reduces the porosity of the TiO_2 films, which may let diffusion problems of the redox shuttle present in the electrolyte for dye-regeneration. For small molecules such as I_3^-/I^- ions the dye-regeneration efficiency is not affected, thus rendering this treatment beneficial to the overall efficiency of the device.

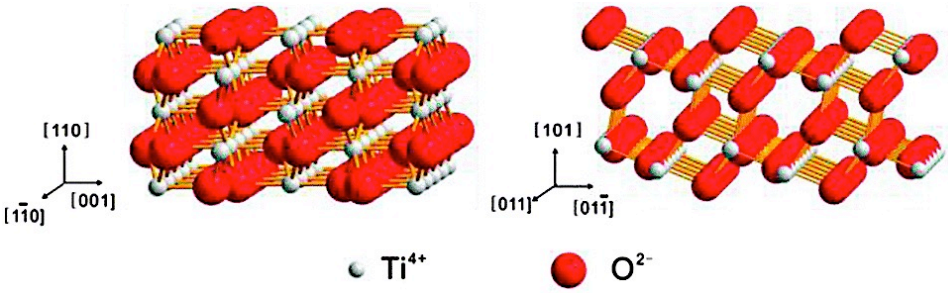

Figure 1.8 TiO_2 in Anatase form.

However, for big molecules such as $[Co(bpy)_3]^{3+/2+}$ complexes, dye-regeneration efficiency is strongly reduced because of diffusion limitation, which is why $TiCl_4$ post-

treatment is usually not performed when using cobalt-based electrolyte. The thermal post-treatment improves drastically the morphology of the TiO_2 nanostructure. The two main consequences are the lowering of the TiO_2 band edges levels (stabilized in energy) and an increase of the electron lifetime, which can improve the injection efficiency and increase the electron diffusion length, respectively.[38]

1.2.2.2 The photosensitizer

Characteristics of molecular sensitizers

To be efficient in a DSSCs, the sensitizer must absorb light across the widest portion of the visible spectrum, especially in the red and NIR region where the solar photon flux is maximum. It must display adequate HOMO/LUMO levels: a LUMO level higher than the TiO_2 CB and an HUMO level below the redox shuttle to ensure an efficient electron injection and for dye-regeneration, respectively. It must be functionalized with an anchoring group (usually carboxylic acid) that bind strongly the semiconductor surface, in order to ensure a strong electronic communication with the TiO_2 orbitals and avoid desorption process. In addition, it must be chemically and photochemically stable under light exposure and heating over time. Anchoring a dye to TiO_2 has been achieved through a number of anchoring groups, such as phosphonic acid, salicylate, carboxylic acid, sulphonic acid, phosphonic acid and acetyl-acetonate derivatives.

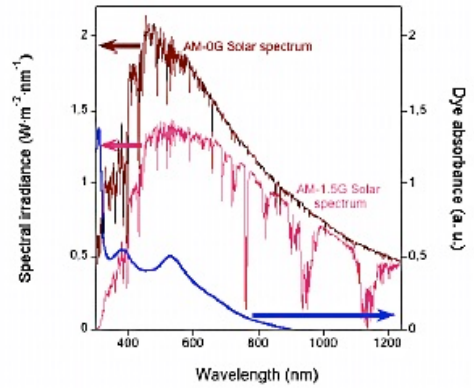

Figure 1.9 AM-0G solar spectra (-----), AM1.5G solar spectra17 (-----) and absorption spectra of cisdithiocyanato-bis-(4,4'-dicarboxy-2,2'-bipyridine)ruthenium(II) dye (-----)

These carboxyl and phosponic functional groups efficient can form various types of binding through the Brønsted acid sites of the TiO_2 surface (surface bound hydroxyl groups) of the semiconductor to obtain strongly bounded molecules and good electronic communication between the two parts. More recently, pyridyl have also proved to be efficient anchoring groups through coordinate bonding between the lone pair of electrons of the nitrogen atom and the Lewis acid sites of the TiO_2 surface (exposed Ti^{n+} cations).[39]

The spectrum of the solar irradiance is shown in Figure 1.9 Currently, most of efforts for improving the efficiency of DSSCs in engineering dye compounds that display extended absorption in the red and/or NIR region of the sun light.

The structure of the dye has to include one or more anchoring groups in order to bind strongly to the surface of the semiconductor and ensure an efficient electron injection. Photosensitizers can interact with the surface of metal oxides through covalent bonds, hydrogen bonding, electrostatic interactions, hydrophobic interaction, Van der Waals forces or entrapment inside the pores.[40] However, the formation of covalent bonds between the hydroxyl groups present at the surface of the semiconductor nanoparticles and the different anchoring groups of the dyes increases the amount of absorbed dye as well as the stability of the cell and the strength of the electronic coupling between the molecular orbital of the dye and the Ti 3d orbital of the semiconductor, and decreases the rate of dye desorption.[41] Although most of the sensitizers are linked to the semiconductor surface through carboxylic acid groups, a variety of different groups such as phosphonic acid,[42] boronic acid,[43] sylanes[44], other derivatives or moieties have been used.

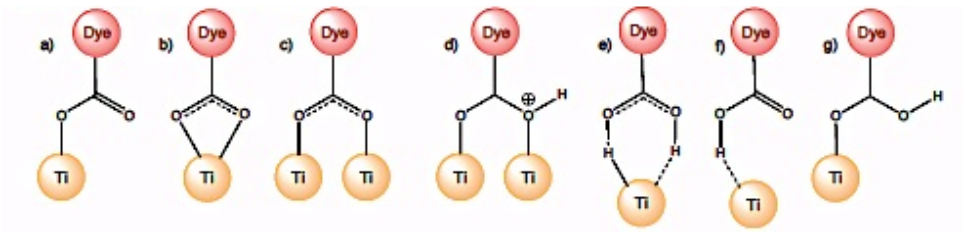

Figure 1.10 Possible binding modes of a carboxylic acid group to TiO_2 . (a) Ester linkage, (b) chelatebinding, (c, d) bidentate bridges, (e, f) hydrogen bonding interactions, and (g) monodentate binding through the CO.

A dye anchored through carboxylic acid groups can be desorbed from the films under basic conditions, which is useful to quantify the amount of dye loading. Furthermore, several binding modes of a carboxylic acid group to the surface of a metal oxide are possible depending on the dye structure, the binding groups, the crystalline form of the metal oxide and the surface environment (Figure 1.10).[45,46]

The redox properties of the dye are also important for efficient charge separation: the LUMO energy level must be higher than the conduction band energy level of the semiconductor in order to be able to inject electrons into the TiO_2, and the HOMO must be sufficiently low to permit fast electron regeneration by the electrolyte redox couple. The HOMO-LUMO band gap should be about 1.5 eV for optimum absorption of sunlight. Furthermore, the spatial orientation of the dye influences not only the electron injection of the dye into the semiconductor conduction band and the photosensitizer regeneration, but also the electron recombination between photoinjected electrons in the TiO_2 and the oxidized dye.[47] Another chemical aspect of photosensitizers regards their solubility in organic solvents. The dye should be soluble in a volatile solvent to permit their adsorption onto the surface of the semiconductor, but should not be desorbed by the electrolyte solution. Finally, the redox reactions involving the dyes must be reversible and the photosensitisers should be stable enough to permit many oxidation/reduction cycles without decomposition of the molecules.

Classes of molecular sensitizers:

Many different classes of compounds have been investigated for solar cell applications. They can be divided in four main groups: d^6-transition metal coordination complexes (such as or $Ru(II)L_8$ octahedral complexes; with L = Ligand),[48] free-base or metallated macrocycles (porphyrins and phthalocyanines), metal-free all-organic dyes[49] and natural pigments (chlorophyll, carotene, etc…) have been designed and applied to DSSCs in the past decades.[50]

a) d^6-transition metal coordination complexes

The architecture of this family of photosensitizers consists of a central metal ion coordinated by various ligands (typically polypyrydil) having at least one anchoring group. Light absorption in the visible part of the solar spectrum is due to metal-to-ligand charge transfer (MLCT) transitions with moderate absorption coefficients (typically $\varepsilon \approx 10{,}000–20{,}000\ cm^{-1}\ M^{-1}$). The central metal ion is a crucial part of the overall properties of the complexes. Ancillary ligands, typically bipyridines or

terpyridines, can be tuned by using different substituents (alkyl, aryl, heterocycle, etc.) to change the photophysical and electrochemicalproperties and therefore improve the photovoltaic performance. Among the d^6-transition metal coordination complexes, ruthenium (II) have shown the best photovoltaic properties: a broad absorption spectrum, appropriate excited and ground state energy levels, long excited-state lifetime

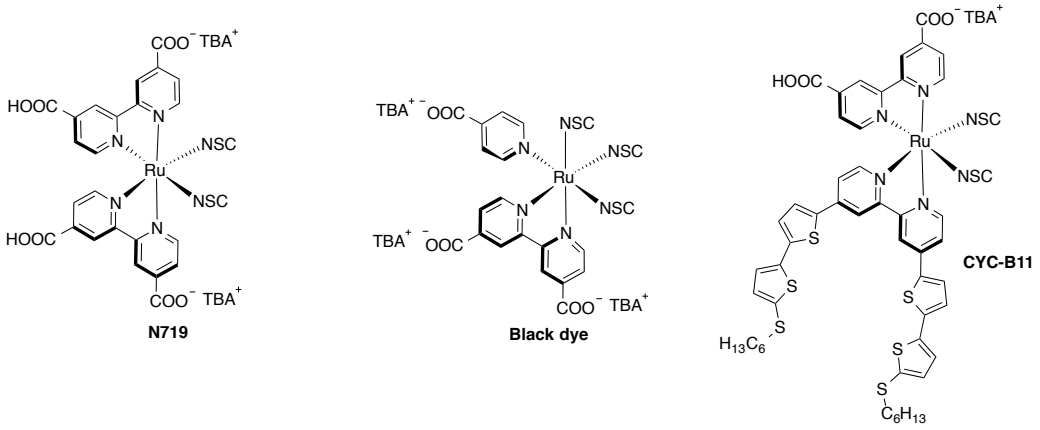

and good electrochemical stability.

Figure 1.11 Structures of Ru-sensitizers used in DSSCs

Several ruthenium complexes used in DSSCs have reached more than 10% solar cell efficiency under standard measurement conditions. Some representative ruthenium dyes are depicted in Figure 1.11. Many attempts have also been made to use other metal ions such as Os(II),[51] Re(I),[52] Fe(II),[53] Pt(II)[54] or Cu(I),[55] but these analogues dyes gave in general lower efficiencies than Ru(II) ones. Record efficiencies exceeding 11% have been obtained using ruthenium polypyridyl complexes as molecular sensitizers, the first and the most extensively investigated class of dyes, mainly by the group of M. Grätzel.

Among them, **N3**[56], **N719**,[57] **black dye** (also called **N749**),[58] and **CYC-B11**,[59] present the best reported efficiencies: 11.18%, 11.10%, and 11.50%, respectively (Figure 1.11). Ru(II) polypyridil complexes have been for a long time the champion dyes in DSSC maintained for a long time, and remain one of the most efficient class of sensitizer. However, the high cost of Ru metal and the low extinction coefficients of

Ru-based complexes have prompted the research on DSSCs to focus on other classes of Ru(II)-free dyes.

b) free-base or metallated macrocycles (porphyrins and phthalocyanines)

Porphyrins. During the last years, an effort was made in order to replace the ruthenium complexes by other dyes. Ideally, earth abundant, non-toxic metals components or no metal ion at all can be easily envisaged. Moreover, avoiding the use of ruthenium will also decrease the production cost of the final device.[60] Porphyrins were introduced as photosensitizers in DSSCs due their primary role in photosynthesis and their outstanding absorption properties and excellent flexibility in tuning photophysical and electrochemical properties through structural changes (centre metal ion and/or peripheral substituions at tha *meso*- or β-positions).[61] Porphyrins are fully conjugated aromatic macrocycles characterized by the presence of four modified pyrrole subunits interconnected at their carbon atoms via methine bridges. Typical porphyrin absorption spectra consist of an intense Soret band centered at 400-450 nm (~ 300,000-500,000 cm^{-1} M^{-1}) and a series of moderately absorbing Q bands at 500-650 nm (~ 15,000-30,000 cm^{-1} M^{-1}).[62]

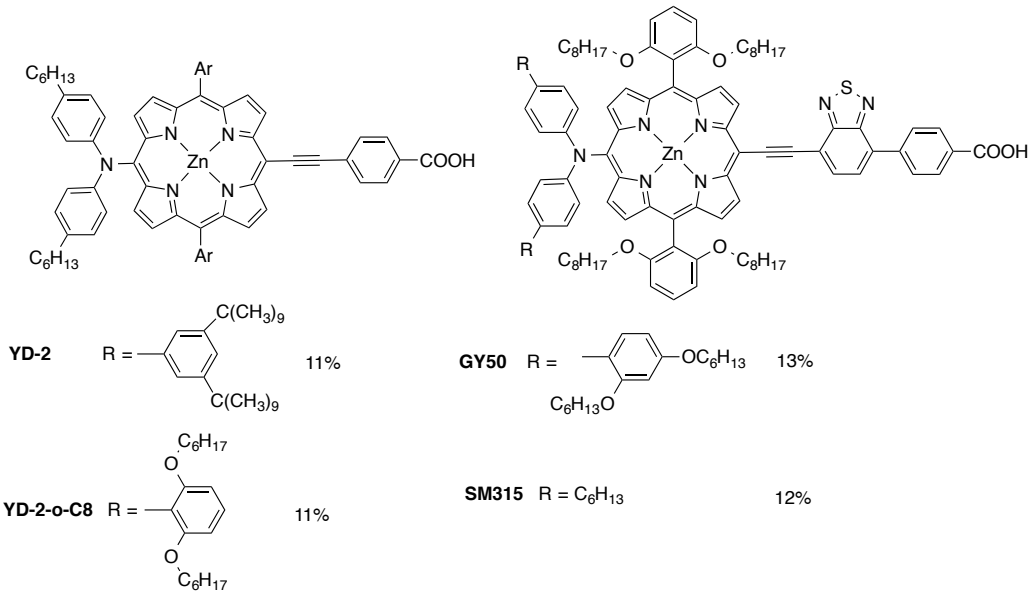

Figure 1.12 Structures of the best efficient porphyrin dyes reported in DSSCs

The most commonly porphyrins used in DSSCs are Zn(II)-based (Figure 1.12), knomn for their excellent photo- physical and -chemical properties. Self-aggregation by p-p stacking interaction is a well-know properties of these large aromatic macrocycle that have been largely exploited in chemistry for the construction of supramolecular systems, or as recognition element with others π-rich aromatic systems, especially with fullerene C_{60}. Stacking phenomena usually induced low electron injection yields due to deactivation of excited state before the electron injection into the TiO_2 CB occurs, so co-adsorbents are usual needed to improve the device performance. Aggregation of porphyrins is usually rather lows in comparison with other aromatic systems (such as Pcs, vide infra) so the necessary amount of co-adsorbent present in the dye-uptake solution CHENO to avoid aggregation rather slow. The introduction of 3,5-ditert-buthylphenyl (in YD2) or dioctyloxyphenyl (YD2OC8) meso-groups at the 5,15 positions of the porphyrin have proved to be an efficient structural design to supress efficiently aggregation, making the use of CHENO often unnecessary or in a very low proportion (typically 2eq of CHENO per porphyrin).

Furthermore, the D-π-A configuration[63] of dye molecules has emerged as a premium model for high-efficient porphyrin dyes. The integration of a porphyrin chromophore as a π-bridge into a D-π-A structure, has provided efficiencies comparable to the best ruthenium polypyridyl dyes; for instance push-pull porphyrin **YD-2** (PCE = 11.0%)[64] and the improved **YD2-oC8** (PCE = 11.9%, and 12.3% in co-sensitized cells),[65] in which the 3,5-bis(*tert*-butyl)phenyl substituents in YD-2 are replaced by 2,6-dioctoxyphenyl groups, as shown in Figure 1.13. **YD-2** are replaced by 2,6-dioctoxyphenyl groups, as shown in Figure 1.13. Further structural optimization of porphyrins dyes involved the introduction of a benzothiadiazole (BTD) ring between the porphyrin and the anchoring group, which yielded the porphyrins **GY50** (PCE = 12.75%)[66] and **SM315** (PCE = 13.0%),[67] (Figure 1.12). The intyroduction of the BTD spacer was successful in filling the gap between the Soret band and the Q band in the absorption spectrum, giving rise to panchromatic sensitizers. In addition, it also proved to enhance the "pulling" effect providing a better electron injection efficiency.

Phtalocyanines**.** Phtalocyanines are 18 electron planar macrocycles and are extremely used as dyes and pigments. These compounds possess intense absorption in the Q-band (around 700 nm), as well as promising electrochemical, photochemical and thermal properties, and are thus of interest to use as NIR photosensitizers for DSSCs. The solubility of these dyes is normally very poor and needs to be improved by

structural optimization in order to facilitate the dye-sensitization process. Another major problem with phthalocyanines is their strong tendency to aggregate on the semiconductor surface, which requires very high concentration of a co-adsorbent to

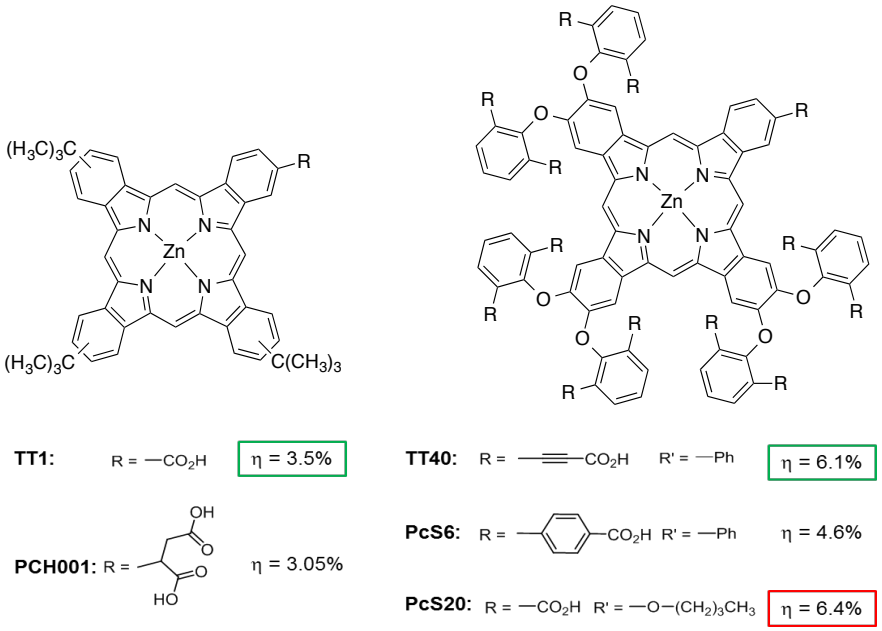

prevent dye aggregation (typically 100 eqv. of CHENO per Pc), and hence reached the optimal performances in DSSC. Recently, a significant breakthrough came through the rational design of the peripheral substitution in **TT40**[68] and **PcS20** to suppress efficiently the aggregation of Pcs. Consequently; the optimal performances of these dyes were obtained without co-adsorbent.

Figure 1.13 Structures of phthalocianines dyes used in DSSCs.

There are different strategies to avoid the formation of molecular aggregates onto the semiconductor nanoparticles: 1) Introduction of bulky groups in the periphery of the scaffold;[69] 2) axial substitution of Pcs, and 3) addition of co-adsorbents,[70] that strongly bind to the surface and displace a certain number of dye molecules from the TiO_2, reducing their probability of aggregation. Chenodeoxycolic acid (CHENO or CDCA)[71] is the most commonly used co-adsorbent, but other examples such as 1-decylphosphonic (DPA)[72] or ω-guanidinoalkyl[73] acids that were also reported.

c) metal-free all-organic dyes

Donor-π-bridge-Acceptor organic dyes. The D-π-A structure consists of electron-donating and electron-withdrawing groups linked covalently through a π conjugate spacer. Within this architecture, it is easy to tune the properties of the dye by rational molecular design, and in particular extend the absorption spectra, adjust the HOMO and LUMO levels and obtain systems with a strong push-pull character to facilitate the intramolecular charge separation. When a dye absorbs light, the intramolecular charge transfer occurs from subunit A to D mediated through the π-bridge. This "ballistic" configuration usually favours a better charge separation and hence a more efficient electron injection from the excited state of the photosensitizer into the TiO_2 conduction band.

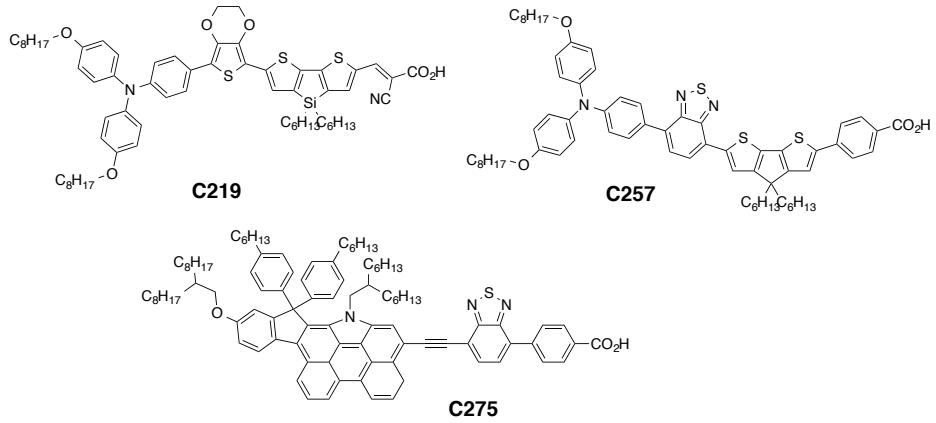

Figure 1.14 Structures of metal-free organic dyes used in DSSCs

After light-absorption, the excited dye promotes an electron injection from its LUMO to the TiO_2 CB. For an efficient sensitizer, the LUMO is usually located at the electron-acceptor moiety, which also plays the role of the anchoring group, close to the semiconductor surface in order to facilitate the electron injection process. In general, efficiencies consistently remain in the range of 6.0-8.0% with a few exceptions, and thus far only a few D/A organic dyes have achieved PCEs over 10.0% (**C219** and **C257** for instance, Figure 1.15). The current efficiency record for pure organic dyes, 12.5%, has been achieved by a *N*-annulated indenoperylene electron-donor, decorated with an electron-acceptor benzothiadiazole moiety (**C275**, Figure 1.14).[74] Further explorations of other exotic polycyclic aromatic materials seem to be steps in the right direction.[75] In this regard, some organic small molecules derived from the coplanar perylene skeleton

are endowed with a large molar absorption coefficient, high luminescence yield, and excellent photostability, had the new record of this kind of molecules whit 11.5% and 12% (**C277** and **C278**).[76]

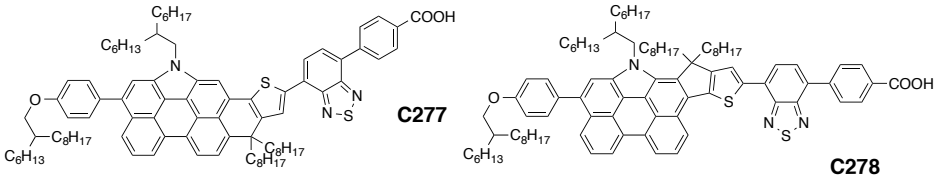

Figure 1.15 Structures of record metal-free organic dyes used in DSSCs

1.2.2.3 Electrolyte

The electrolyte is the hole transporting material in a DSSCs. Different requirements are needed to have a good electrolyte:

- It must have a good contact between the working and the counter electrodes.
- It needs high conductivity to permit fast charge transport between the platinum counter electrode and the oxidized dye.
- The electrolyte should neither degrade nor desorb the photosensitizer from the metal oxide surface.
- It should also be thermally, optically, chemically and electrochemically stable.
- The potential of the redox couple must allow efficient dye regeneration.

A great number of redox mediators and electrolyte systems have been explored, including I_3^-/I^- in either solid polymer,[77] gel,[78] ionic liquid[79] or plastic crystal[81] systems; solid inorganic materials;[80] Co(III)/Co(II)[81], $(SeCN)_3^-/SeCN^-$ redox couples,[79] hole-conducting organic polymers[82] and small organic molecule.[83] To date, the best performances have been obtained with I_3^-/I^-or the Co(III)/Co(II) redox couple.

Liquid electrolytes. In these electrolytes the redox pair is dissolved in organic solvents with high dielectric constants such as acetonitrile, *N*-methylpyrrolidine and valeronitrile, or a combination of those solvents.

Ionic liquids. The addition of ionic liquids in organic solvent based electrolytes often increases the ionic conductivity.[84] The ionic liquid electrolytes were divided into

two sections, pure ionic liquids and quasi-solid (gel-based materials with dispersed amounts of liquid electrolyte) electrolytes based on ionic liquids. The area is vastly dominated by imidazolium-based electrolytes, and some of the main conclusions were that the combination of photochemical stability and low viscosity, and thus ion mobility, remains a challenge.[85] Ionic liquids presents also very low vapour pressure, non-flammability, high ionic conductivity and wide electrochemical window, which are very useful properties for long-term stability of the devices.[86]

Solid electrolytes. Volatile liquid electrolyte remains a several issue for long-term stability of the DSSC, which has prompted the development of all-solid electrolyte. Yet, the solid hole conductors present several disadvantages: (1) the efficiencies of the DSSC remain constantly lower that those obtained with common iodine-based liquid electrolytes, (2) surface wetting (percolation inside the nanoporous of the semiconductor oxide is an important issue), (3) moderate stability in air that requires a perfect sealing and encapsulation, (4) partial absorption of light by the material acting as a filter for the sensitized films. The most common and efficient solid electrolyte is spiro-OMeTAD.

Additives. These compounds play a central role in the enhancement of photoelectrochemical performance of DSCs. Their effects are often attributed to modification of redox couple potential, shifts of the semiconductor conduction bands, effects of surface blocking and organization of the dye on the surface. Most additives that have been reported contain an electron donating nitrogen heterocycle, the most commonly used being 4-*tert*butylpyridine (TBP).[85] TBP modify the surface of the semiconductor by coordination to the defective sites of the surface where no dyes are adsorbed. The first consequence is the reduction of the dark current (i.e. recombination electrolyte/e-(CB) which improves the FF. The second effect of TBP is to shift upwards the conduction band edge of the semiconductor, which enhance the open circuit voltage, but at the same time this shift also decrease the injection driving force, which may reduce the electron efficiency and hence the photocurrent of the cell.[87]

1.2.2.4 The counter electrode

The function of the counter electrode is the reduction of the oxidized species present in the electrolyte redox couple. It should presents low resistance to be efficient. The best and most used material for the counter-electrode remains platinum because it is easy to prepare by thermal decomposition and give the best performances in DSSC.

Because of the high-coast of Pt, other materials have been envisaged and tested such as carbon graphite, black carbon, or conducting polymers such as PEDOT or cobalt sulphide, which has proved to be competitive and represent serious alternative.

CHAPTER 2: RUTHENIUM COMPLEXES

2.1 INTRODUCTION

The photophysical and photochemical properties of ruthenium(II) diimine complexes have been investigated by virtually thousands of researchers over the past 50 years. The reason being that they are not only interesting for fundamental studies of, for instance, light-induced electron[8890] and energy-transfer processes,[91] but they are also becoming increasingly important in technological and biomedical applications, such as solar energy conversion,[92] photo-catalysis,[93] cancer phototherapy,[94] and sensors.[95]

The use of ruthenium pyridyl complexes as sensitizer in DSSCs has now more than thirty years of development history. As early in 1977, Clark and Sutin[96] already used a tris-bipyridyl ruthenium complex to sensitize titanium dioxide to sub-band gap illumination but in solution only. Charge transfer could only occur after diffusion of the ion to the semiconductor, so the efficiency of the sensitization was very low. By 1980, the idea of chemisorption of the dye through an acid carboxylate group bonding to the metal oxide surface has been established so that the sensitizer was immobilized and it formed the required monomolecular film on the semiconductor substrate, which facilitated charge transfer, by electron injection.[23] The anatase form of TiO_2 became more dominant as a substrate for chemisorption of dyes for its advantageous photochemical and photoelectrochemical properties, being a low-cost, widely available, non-toxic and biocompatible material, and it is even used in health care products and domestic applications such as paint pigments. In 1991, the remarkable success of sensitized electrochemical solar cell was announced with the conversion efficiency of 7.1% under solar illumination, a synergy of structure substrate roughness, dye photochemistry, counter electrode kinetics and electrolyte redox chemistry. After these successes in photovoltaics, the field of application of Ru(II) dyes had evolved to focus on photovoltaic devices rather than on photosynthesis. That improvement has continued progressively since then, to reach now more than 11%.[97]

2.1.1 Structural aspects of a Ruthenium complex.

2.1.1.1 Metal centre

Ruthenium was discovered in 1844 in Tartu, Estonia, by Karl Karlovitch Klaus, who named this new metal Ruthenia, the Latin name for Russia. This element, just like osmium, is a unique metal due to its ability to form coordination complexes and covering the widest range of oxidation states theoretically allowed for a transition metal: from 8 in $[RuO_4]$ to -2 in $[Ru(CO)_4]$, the most common being Ru(II) and Ru(III) oxidation states.[98] The choice of ruthenium (II) metal is interesting for a number of reasons:

- Its octahedral geometrical structure allows extending of specific ligands in a controlled manner.
- The photophysical, photochemical and the electrochemical properties of Ru (II) complexes can be tuned in a predictable way.
- It possesses stable and accessible oxidation states from I to IV.
- It forms very inert bonds with imine nitrogen centres.[99]

2.1.1.2 Bipyridines

Pyridine is an important aromatic heterocyclic organic compound, and its structure is present in many natural products and synthetic molecules.[100] Pyridyl moieties are versatile building blocks for the preparation of polypyridyl ligands[101] like oligopyridines, which are molecules of great importance due to their ability to form stable complexes with numerous metal centres. The structure of these ligands strongly affects their optical and electrochemical properties. The functionalization of polypyridyl ligands with different groups allows their use in a wide range of applications, which exploit their photophysical, photochemical and redox properties. Among the great variety, bipyridines and terpyridines are the most employed. They are heterocyclic aromatic molecules based on 6-membered nitrogen containing rings, linked through a single bond between the different carbon positions of the pyridyl moieties.

The most used and best studied bipyridine is the bidentate chelate 2,2'-bipyridine (bpy), due to its ability to form stable complexes with metals[102]. However, six possible bipyridine regioisomers can be distinguished (Figure 2.1), from which three are

symmetrical isomers (2,2'-, 3,3'- and 4,4'-), while the other three are asymmetrical isomers (2,3'-, 2,'4'- and 3,4'-).

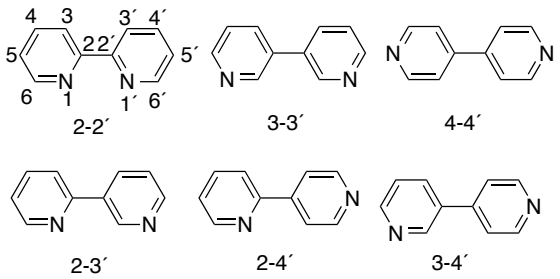

Figure 2.1. Molecular structure of the 6 possible isomers of bipyridine.

The major application of nitrogen containing aromatic heterocycles involves the formation of complexes with numerous metal centers.[102, 104] Polypyridyl ligands interact with the *d* orbitals of transition metals through both donor and acceptor molecular orbitals located on the nitrogen atoms and the conjugated aromatic system, respectively. Furthermore, the geometry and the angle between the different nitrogen donor atoms strongly affect the nature of the bond between the pyridine-based chelating ligands and the metal center.[101] The pyridyl moieties of non-coordinated 2,2'-bipyridine can rotate around the inter-ring C-C bond, and its torsional angle reaches a minimum in energy when the two pyridyl moieties are coplanar and with the nitrogens in a trans conformation[105]. This planar spatial disposition is favourable due to the π-conjugation of the rings, while the repulsive interaction between the hydrogens H3 and H3´ induces a twist of 180 º to the angle between the pyridyl rings. On the other hand, this molecule adopts a *cis* planar conformation when linked in a bidentate mode to a metal centre, forming a stable five-membered ring (Figure 2.2)

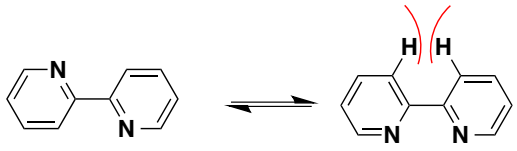

Figure 2.2. Molecular conformation of 2,2'-bipyridine as free ligand (on the left) and coordinated to a metal ion (on the right)

Polypyridyl ligands, when non-coordinated to metals, exhibit intense absorption bands in the ultraviolet (UV) region. The absorption spectrum is red shifted under

acidic conditions, indicative of the protonation of the nitrogen atoms.[106] Most of bipyridines, terpyridines and phenanthrolines display π - π * transitions of low energy that enable non-radiative relaxation of the excited state through an intersystem crossing and/or internal conversion and, thus, the molecules are not fluorescent in organic solvents.[107] However, the introduction of substituents, such as highly extended conjugated moieties or electron donor groups can increase the luminescence quantum yield.[108]

The major application of polypyridyl ligands is due to the photophysical, photochemical and electrochemical properties, which are derived from their complexation with almost all the transition, alkaline earth and lanthanide metals. Polypyridyl complexes have been extensively studied and used in a wide range of applications, such as supramolecular chemistry,[109] solar light harvesting, luminescence labelling of biological molecules,[110] catalysis[111] and light emitting devices.[112]

2.1.1.2 Ruthenium polypyridyl complexes

From chemistry perspective, ruthenium-based molecules belong to a class of metal complexes (organometallics).[113,114] The crystal field and molecular orbital theories can be explained the properties of ruthenium complexes bonding. The properties of ruthenium complexes arise from electrostatic interactions between the metal ion and chelating ligands, which result in the splitting of *d*-orbital energies. From the molecular orbital theory point of view, their coordination bonds can be explained by the charge transfer transitions between the metal and chelating ligands due to the interaction between the *s*, *p* and *d* atomic orbitals of the metal centre and those of the chelating ligands, which have appropriate geometry to allow a strong overlap.

The kinetic stability of the ruthenium complexes in a broad range of oxidation states, the reversible nature of most of their redox pairs and the wide range of well-known synthetic reactions for their preparation, make these compounds very attractive for use in a wide range of research areas. In this work, attention has been particularly focused on the study of Ru(II) complexes and their applications in DSSC.

2.1.2 Properties of ruthenium complexes with polypyridyl ligands.

Owing to the wide diversity ligands available, ruthenium polypyridyl complexes are extremely versatile compounds with a large panel of photophysical, photochemical and redox properties that can be easily tuned and optimised for a particular purpose.

A photochemical or photophysical process takes place when a molecule absorbs a photon and promotes an electron from the ground state to the excited state. This high energy state is unstable and thus, the molecule tends to undergo some type of deactivation process. Excited state deactivation can occur via[115]:

1. The emission of light (luminescence),
2. The liberation of the excess energy in form of heat (thermal deactivation),
3. The interaction with other molecules present in the local environment (quenching process)
4. The formation of a new species (photochemical reaction).
5. A charge transfer process (hole or electron) to a donor or an acceptor leading to either the oxidized or the reduced specie, respectively.

2.1.2.1 Absorption spectroscopy

The photophysical and electrochemical properties of ruthenium complexes are usually described through a simplified linear combination of atomic orbitals (Figure 2.3). Each molecular orbital is denominated as metal (M) or ligand (L) in agreement with its prevalent localisation. The molecular orbital diagram for an octahedral complex of a transition metal such as Ru(II) indicates that different transitions between the different chelating ligands and metal orbitals can take place upon the absorption of light. These transitions can be classified as:

- Metal-centred transitions (MC), also called d-d transitions, when the electrons are promoted from a π_M metal orbital to a σ_M orbital;
- Ligand-centred (LC) or π - π^* ligand to ligand transitions, for transitions mainly localised on the chelating ligands,
- Transitions between molecular orbitals with different localisation: metal-to-ligand charge transfer (MLCT), or ligand-to-metal charge

transfer transitions (LMCT). Electronic transitions that occur to a lesser extent are those from a metal-centred orbital to solvent (charge transfer to solvent, CTTS).[116]

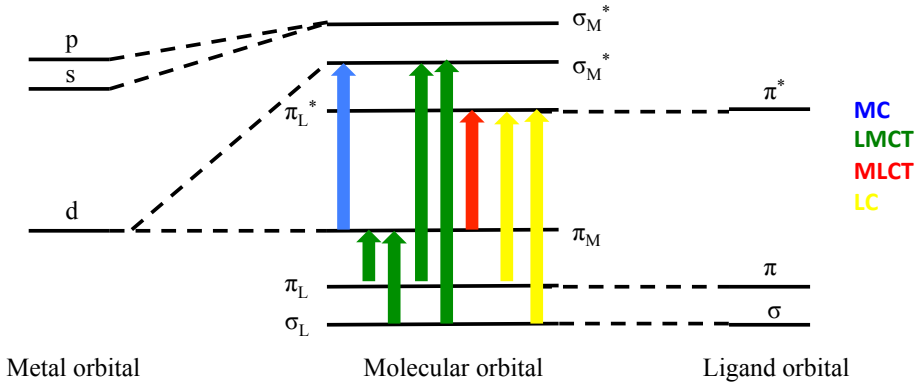

Figure 2.3. Simplified molecular orbital diagram for a transition metal complex in an octahedral geometry showing different electronic transitions.

The light absorption processes are only allowed for transitions in which the ground and the excited state have the same spin value. These transitions can be observed as intense bands in the absorption spectra of the molecules. Some of them are an electronic transition from metal t_{2g} orbitals to empty ligand orbitals without spin change allowed, is called a singlet-singlet optical transition. The allowed transitions are characterized by large extinction coefficients. In contrast, transitions from the ground state to excited states with different spin are called single-triplet optical transitions, which are forbidden from symmetrical rules (Pauli exclusion principle) and hence are associated with small extinction coefficients. However, the excited singlet state may also undergo a spin, resulting in an excited triplet state. This process is called intersystem crossing (ISC) (Figure 2.4). Although not formally triplet or singlet in nature, the predominantly triplet character of the lowest-energy excited state and singlet character of the initial Franck-Condon state rationalizes why the transition between them is often termed intersystem crossing.

The MC, MLCT and LC transitions of an octahedral transition metal complex are related to the ligand field strength, the redox potential of the metal complex and the intrinsic properties of the ligands, respectively.[117] For this reason, changes in the molecular structure of the ligands attached to the ruthenium metal ion can vary

dramatically the relative energy positions of the excited states, with the consequent changes in their photophysical properties.[118]

Most ruthenium bipyridyl complexes display a lowest excited state as a long-lived triplet T_1, whose deactivation results in an intense phosphorescence. However, at high temperatures, non-radiative deactivation can take place via thermally activated T_2 metal.

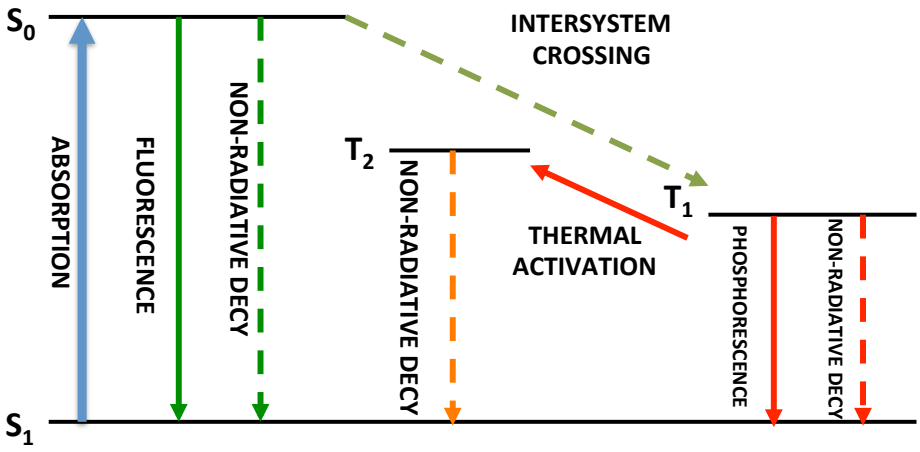

Figure 2.4. Jablonski diagram for ruthenium polypyridyl complexes.

2.1.2.2 Emission spectroscopy

The behaviour of excited species is usually represented in a Jablonski diagram (Figure 2.4). In most of the ruthenium polypyridyl complexes, three states are involved in the photochemical activation process: a singlet ground state, and singlet and triplet excited states.

The multiplicity of the ground state for most ruthenium (II) polypyridyl complexes is a singlet (S_0) and the absorption of a photon leads to the promotion of an electron from an occupied orbital to a higher energy unoccupied orbital with the same spin multiplicity (S_1). However, the lowest excited state is often a triplet (T_1) and, although it cannot be populated directly upon light absorption, it can be achieved through the deactivation of higher excited states. The S_1 state rapidly decays via intersystem crossing to the T_1 due to the strong spin-orbital coupling in metal complexes.[118] The quantum yield for the formation of the lowest triplet excited state is

often equal to unity, yielding deactivation though both a radiative (phosphorescence) and a non-radiative way (Figure 2.4).

2.1.2.3 Redox properties

Ru(II) polypyridyl complexes are octahedral and diamagnetic, with a t_{2g} configuration[119]. The electrochemical behaviour of polypyridyl ruthenium complexes depends on the nature of the ligands surrounding the metal ion. However, due to their high number of stable oxidation states, ruthenium polypyridyl complexes serve as both electron acceptor and electron donors.[120] The oxidation of a d_6 Ru(II) polypyridine complex involves removal of an electron from the highest energy occupied molecular orbital (HOMO), usually a σ_M (t_{2g}) metal centred orbital, with the formation of paramagnetic low spin d^5-Ru(III) complexes, which are inert to ligand substitution.

On the other hand, the reduction of a Ru(II) polypyridyl complex may involve the introduction of one electron into the lowest unoccupied molecular orbital (LUMO), located either into a metal-centred (σ^*_M) or into a ligand-centred orbital (π^*_L), depending on their relative energy level arrangement. In general, the reduction process of these complexes takes place on the polypyridyl ligand because they are easy to reduce once coordinated to the ruthenium metal centre. In this case, the ruthenium metal ion maintain its d^6 low-spin configuration. These species are usually very stable making the reduction reaction fully reversible. However, when the LUMO is metal centred, the reduction of these complexes produce unstable ruthenium complex with a low spin d^7 electronic configuration followed by a rapid ligand dissociation, making this reaction process irreversible.

2.1.2.4 Tuning the photophysical and electrochemical properties

The structure of the polypyridyl ligand determines the redox and optical properties of ruthenium complex, which can be modified by the introduction of appropriate chelating ligands.

Generally, two strategies are used to tune these properties:

- Modification of the LUMO energy level by introducing a ligand with a low-lying π^* molecular orbital involved in the MLCT.
- By destabilisation of the t_{2g} metal orbital (HOMO energy level), which is affected by the donor or acceptor properties of the ligand.[121]

The modification of the HOMO and LUMO energy levels has a direct effect over the MLCT transitions of a ruthenium complex, and consequently induces changes in the absorption spectrum. Fine-tuning of the excited state energy levels can be achieved by choosing an appropriate ligand involved in the MLCT.

2.1.2.5 Stereochemistry of ruthenium polypyridyl complexes

Another characteristic of octahedral metal complexes such as Ru(II) with bidentate ligands is their stereoisomerism.[122] For homoleptic tris(bidentate) complexes with symmetrical ligands (L), two enantiomers are possible, called Δ and Λ (Figure 1.1A). Two geometrical isomers (facial (*fac*) and meridional (*mer*)) are possible for complexes with non-symmetrical bidentate chelate ligands (R-L) (Figure 2.5B).

However, the number of isomers increases to four and eight, respectively, when two [Ru(R_1-L)(R_2-L)(L)] or three [Ru(R_1-L)(R_2-L)(R_3-L)] unsymmetrical substituted ligands are linked to the ruthenium metal center (R_1-L, R_2-L and R_3-L are different unsymmetrical nitrogen containing bidentate chelate ligands). For bis(bidentate) complexes two geometrical isomers can be formed (cis/trans) as well as two enantiomers of the cis form (Figure 2.5A). Furthermore, the number of possible isomers increases exponentially with the number of metal ions in the synthesis of polynuclear complexes.

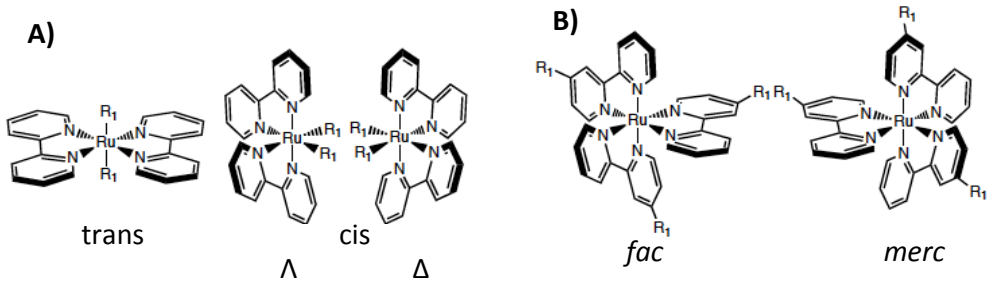

Figure 2.5. Δ and Λ geometrical isomers of Ru(II) symmetrical tris(bidentate) complexes trans and two cis isomers of bis(bidentate) ruthenium complexes or *fac* and *mer* isomers of Ru(II) tris(bidentate) complexes containing an unsymmetrical ligand.

2.1.3 Applications of ruthenium complexes with polypyridyl ligands.

Because of their excellent photophysical properties and rich electrochemistry, Ru(II) polypyridyl complexes have been widely studied and used in many fields during the last 30 years:[123, 124]

- Solar energy conversion. The potential of ruthenium polypyridyl complexes to act as photosensitisers in the conversion of solar energy into electrical energy has become an attractive subject of study.[125,126] Through an appropriate molecular design, ruthenium polypyridyl complexes can exhibit a wide range of colours absorbing in different regions of the UV-visible spectrum, and a panel of different redox properties.
- Water splitting and CO_2 reduction. The main goal of artificial photosynthesis is to mimic the conversion of water and sunlight carried out by plants and other photosynthetic organisms to obtain environmentally friendly energy sources.[127] An interesting reaction, which results in the formation of carbon free fuels (H_2), is the splitting of water.
- Optical molecular chemosensors. Chemosensors are molecules which display a specific response to a particular analyte species. Optical chemosensors offer a variation in their absorption or emission spectra, intensity or lifetime in the presence of specific species. Ruthenium polypyridyl complexes have been extensively us for the detection of O_2, since diatomic oxygen is a well-known luminescence quencher.[128]
- Interaction with biomolecules. Transition metal complexes, which are stable, inert and water-soluble, are extensively used in chemotherapy and in the development of highly sensitive diagnostic agents.[129] Furthermore, the sensitivity of their absorption and emission spectra, intensity and lifetime to different biomolecule microenvironments such as DNA or proteins make these complexes attractive candidates for biomolecule sensing.[130] By changing the ligands of the ruthenium complex, the nature and the strength of binding with biomolecules can be modified. For this reason, ruthenium polypyridyl complexes used as chemosensors can interact with biomolecules trough covalent or non-covalent bonds.

2.1.4 Ruthenium(II) complexes as dyes for DSSCs.

Generally, transition metal complex used in DSSC consist of a central metal ion coordinated by ancillary and anchoring ligands. The number of ligands per metal centre is generally either four or six, with others being rare. From the free form to the octahedral complex, the ligand orbitals split into three sets of degenerated ones: t_{2g} (d_{xy}; d_{xz}; d_{yz}) and eg (d_{x2-y2} ; d_{z2}).

The splitting value increases by 40% as one moves from the first row (3*d*) to the second (4*d*) and third (5*d*) raw transition elements.[131] A Ru(II) complexes can be visualized as an electronic attraction between a positive charged metal ion and negative charged ions. A metal ion or atom can act as a discrete centre surrounded by a set of ligands arranged in a way that donate their electron pair to the central metal atom.

There is at least one anchor group on one of the available ligand to attach the dye to the semiconductor surface and facilitate the electron injection. The light absorption in the visible region is mainly coming from the MLCTs, which is the most important contribution to light-harvesting. An electron will be excited from the metal d orbitals to the ligand π^* orbitals when light irradiates the dye. As exemplified for **Z907**, **C101**, and **C106** (Figure 2.6), the HOMO level is commonly localized on the ruthenium centre and electron-donating ligands (NCS),[132] and the LUMO on the polypyridyl ligand.

Ancillary ligands of Ru-based dyes can be tuned by different substituents like heterocycle and aryl to improve the dye performance in DSSCs. For efficient charge injection, generally, the electron cloud should situate close to the supporting semiconduction oxide in excited state. group has the lowest LUMO, facilitating an efficient electronic coupling of excited dye molecules and titania nanocrystals. In place of alkyl on dnbpy, introducing alkylthiophene not only lifts the HOMO, it also lowers the LUMO. Insertion of sulfur between thiophene and alkyl further depresses the LUMO due to the well-known electronic substituent effects of alkylthio compared to alkyl.

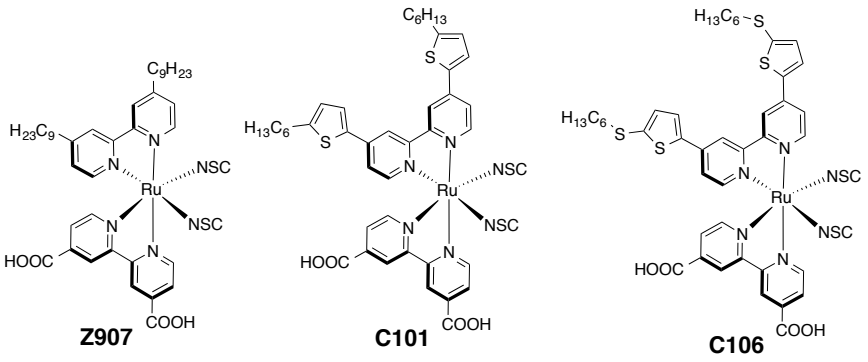

Figure 2.6. Molecular structures of **Z907**, **C101**, and **C106**.

The red-shifted low-energy MLCT transitions observed in the preceding discussion, we detailed the electron transitions by calculating the electronic states of **Z907**, **C101**, and **C106** as well as their bipyridyl ligands. The only variation in the molecular structures of these three sensitizers is in their ancillary ligands. Moreover, among these ligands dcbpy with the carboxylate anchoring.

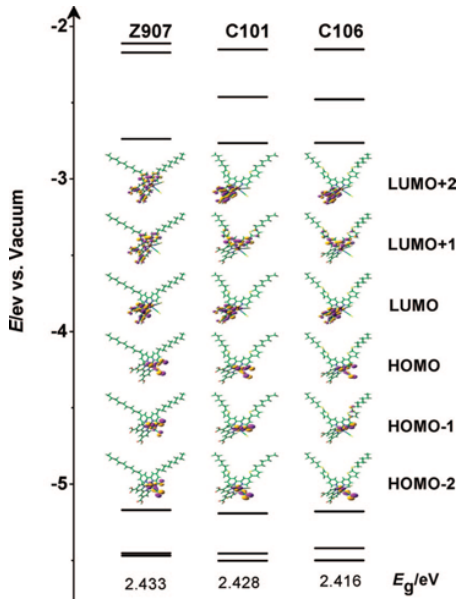

Figure 2.7. Energy diagram and isodensity surface plots of the first three HOMOs and the first three LUMOs of Z907, C101, and C106. All theisodensity surface values are fixed at 0.04.[133]

The experimental energy diagram and isodensity surface plots are shown in Figure 2.7. The red-shifted MLCT bands of **C101** and **C106** compared to **Z907** can be easily comprehended from their low-lying LUMO+1 orbitals, because the energy levels of their first three HOMOs do not differ remarkably. In comparison to **C101**, a slightly uplifted HOMO as well as HOMO-1 of **C106** and a depressed LUMO+1 stemming from the sulfur insertion can be explaining the small bathochromic absorption. For **Z907** and **C101**, the first three HOMOs own ruthenium t_{2g} character with sizable contribution from the thiocyanate ligand. However, the HOMO-1 of **C106** exhibits a distinctive feature, with a certain distribution on 4,4′-Bis(5-(hexylthio)thiophen-2-yl)-2,2′-bipyridine, apart from the Ru-NCS combination. In addition, its HOMO-3, which is also involved in the visible excitation, is completely localized on 4,4′-Bis(5-(hexylthio)thiophen-2-yl)-2,2′-bipyridine like LUMO+1. This scenario can be understood in terms of the Franck-Condon principle, stating that during an electronic transition, a change from one vibrational energy level to another will be more likely to happen if the two wave functions overlap more significantly.

On the other hand, other exemplified is for N621 (**¡Error! No se encuentra el origen de la referencia.**), the HOMO level is commonly localized on the ruthenium centre and electron-donating ligands (NCS), and the LUMO on the polypyridyl ligand.

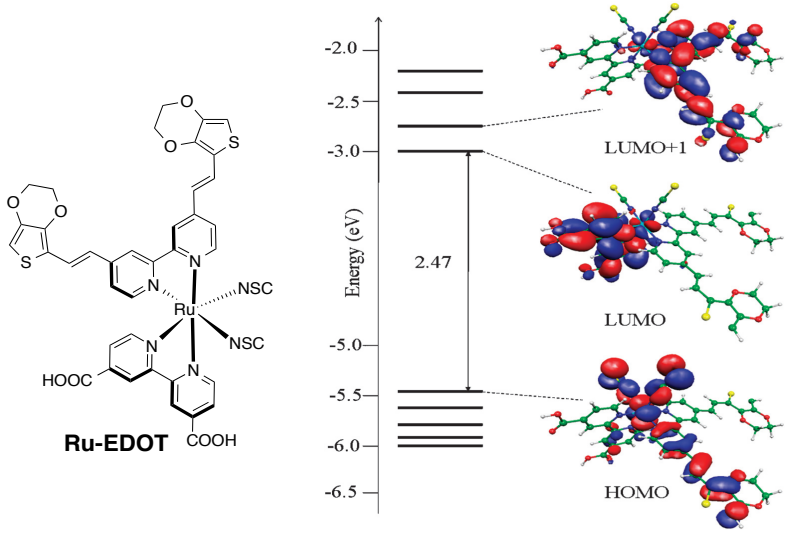

Figure 2.8. Molecular structures of Ru-EDOT (on the left) and molecular orbital energy diagram of Ru-EDOT (on the right).[134]

A schematic representation of the molecular orbitals for Ru-EDOT is shown in The HOMO is a combination of Ru t_{2g} and SCN π orbitals, as found in similar compounds showed previously, appreciably mixed with π EDOT carácter.

The lowest-energy state of Ru-complex is three-fold symmetric and is best described by the symmetry label D_3 as shown in Figure 2.9 Based on the Franck-Condon principle, immediately following excitation the initial excited state ought to possess the same structural symmetry as the ground state.[135] Thus, the initial, Franck-Condon excited state formed via a MLCT transition[136] in Ru-complex could consist of a delocalized electronic wavefunction on all three bpy ligands each formally possessing 1/3 of an electronic charge.

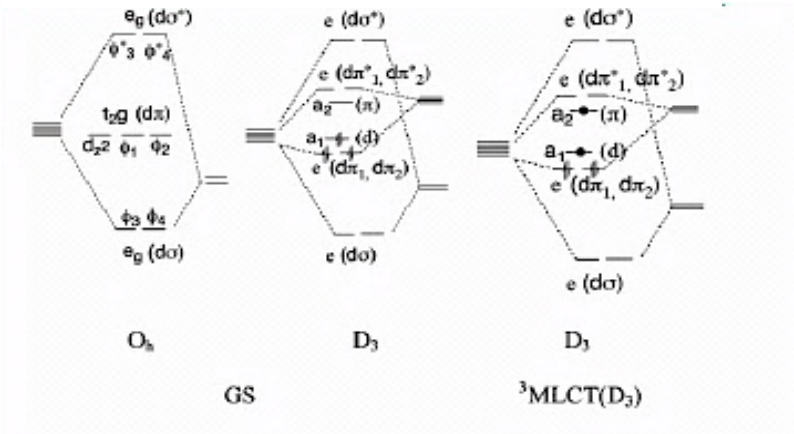

Figure 2.9. Molecular-orbital diagrams for Ru-complexes in their ground state with GS-Oh) octahedral, Oh symmetry; or GS-D3) reduced D3 symmetry, like for Ru(bpy)32+ . Also shown are excited-state molecular-orbital diagrams for: 3MLCT-D3) the initial, Franck- Condon excited state formed under the ground-state D3 symmetry .

In 1979, Ru-based dyes with carboxylated bipyridine ligands were used to sensitize TiO_2 for the first time.[137] Later in 1985, Desilvestro *et al*. used Ru-complexes with three carboxylated bipyridine ligands to obtain the first efficient DSSC with IPCE over 40 % in the wavelength of 450–500 nm.[138] However, the major breakthrough came in 1991 when Grätzel and co-workers achieved an efficiency of 7.9 % by using a trimeric trinuclear Ru-complex (Figure 2.10) and a new mesoporous TiO_2 film as photoanode.[139]

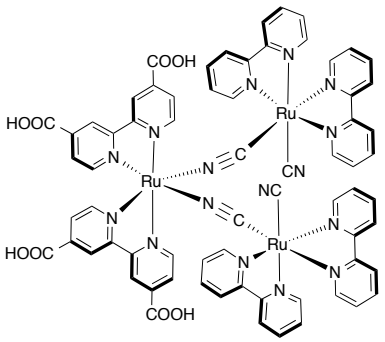

$[Ru(bpy)_2\text{-}(CN)_2]_2Ru(\ bpy(COO)_2)^{2-}]$

Figure 2.10. Molecular structures of **$[Ru(bpy)_2\text{-}(CN)_2]_2Ru(\ bpy(COO)_2)^{2-}]$**

Following this pioneer work, Grätzel and coworkers synthesized a series of mononuclear Ru(II) complexes including *cis*-bis(isothiocyanato) bis(2,2'-bipyridyl-4,4'-dicarboxylato ruthenium(II), known as **N3** dye, which displays outstanding photovoltaic properties.[140] DSSC with **N3** (Figure 2.11) can achieve an overall solar-to-electric energy conversion efficiency of 10 %.

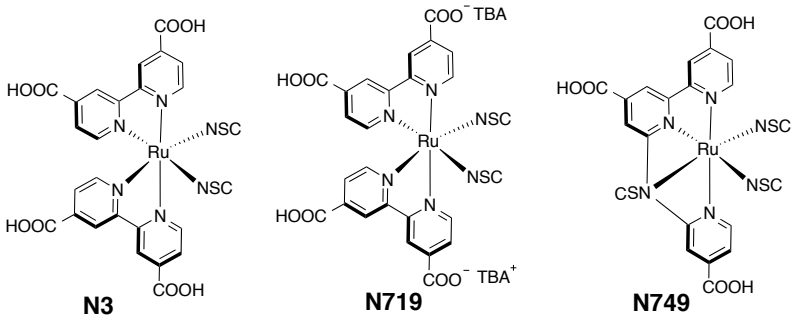

Figure 2.11. Typical ruthenium-based dyes N3; N719; N749.

In order to improve the light-harvesting capability and extend the absorption over the NIR region Grätzel and coworkers reported later on the dye **N749** (known as black dye) using a terpyridine tridentate ligand. Figure 2.12 shows the photocurrent action spectrum, where the incident photon to current conversion efficiency is plotted as a function of wavelength. In comparison with its predecessor **N3** this new dye exhibited extended absorption toward the NIR region, which resulted in a larger and impressive J_{SC} of 20.5 mA/cm^2 with an IPCE response extended up to 920nm, yielding an improved overall PCE of 10.4%.

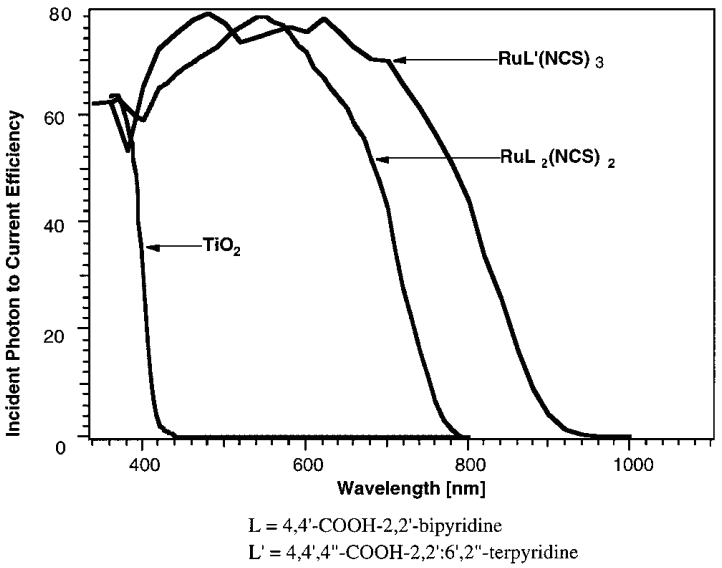

Figure 2.12. Photocurrent action spectrum obtained with the black dye attached to nanocrystalline TiO_2 films. The incident photon to current conversion efficiency is plotted as a function of the wavelength of the exciting light. Photocurrent action spectra for bare TiO_2 and TiO_2 doped with N3 have been included for comparison.

After that, most Ru-based dyes were designed based on basis of **N3** replacing one of the two dicarboxylic acid bipyridine by various ancillary ligands. Changing properly the ancillary ligand can extend the absorption to the red and near infrared region (NIR)[141] regions by increasing the effective π-electron conjugation, suppress dye aggregation, tune the HOMO and LUMO levels, increase thermal stability of DSSC,[142] and decrease recombination processes.

2.1.5 Structural Optimization of Ruthenium (II) complexes for N3 performance in DSSCs.

After the tremendous success of **N3** in DSSC, various modified Ru(II)-analogues have been designed in an attempt to improve the efficiency and long-term stability. Several approaches were followed and can be classified in three categories:

1) Introduction of an ancillary group, which consists in replacing one of the two dicarboxylic acid bipyridine of the **N3** dye by a bipyridine ancillary ligand.
2) Structural modification of the anchoring group.
3) Thiocyanate-free Ru(II) complex.

On the basis of the **N3** structure, changing properly the different ligands can extend the absorption toward the red and near infrared region (NIR)[143] regions, suppress dye aggregation, tune the HOMO and LUMO levels, increase thermal stability of DSSC, [144] and/or decrease recombination processes. To absorb long- wavelength photons (*i.e.* absorption in the red and NIR regions), the HOMO-LUMO gap of the sensitizer should be as narrow as possible. However, to be efficient in a DSSC, it must display an HOMO level below than that of the redox couple and low enough to ensure an efficient dye-regeneration (i.e. large driving force for dye-regeneration: ΔG_{Reg}), while the LUMO must be higher than the TiO_2 CB level to make the electron injection process thermodynamically possible and high enough to make it efficient (i.e. large driving force for electron injection : ΔG_{Inj}).

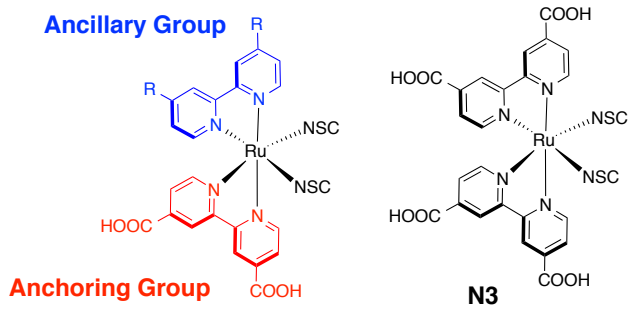

Figure 2.13. General diagram of a ruthenium complex (on the left) and dye **N3** (on the right)

2.1.5.1 Tuning the property of heteroleptic Ru(II)complexes trough modification of the ancillary ligand

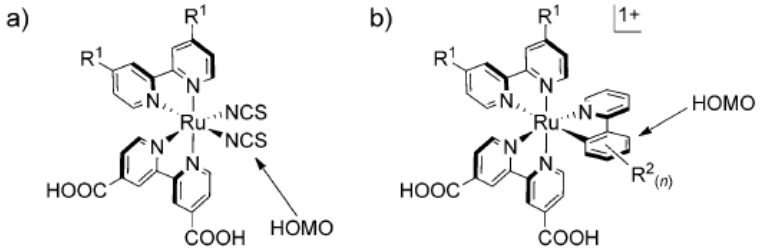

Figure 2.14. Molecular design elements that can be manipulated to render high-performance Ru-based DSSC dyes with a) NSC^- groups and b) cyclometalating ligands. The HOMO is localized at the metal and the anionic case of the cyclometalated complexes

The most commonly used strategy to improve the light-harvesting efficiency of Ru-based dyes was the preparation of tris-heteroleptic Ru(II)complexes [RuLL'(NCS)$_2$] modified analogues of the bis-heteroleptic dye **N3** [RuL'$_2$(NCS)$_2$], (Figure 2.14).

Changing ligands can tune the HOMO and LUMO levels of the dye to extend absorption region to the NIR region. The HOMO must be low enough for redox couple to regenerate the oxidized dye, while the LUMO should be high enough for efficient electron injection into the conduction band of TiO_2. Meanwhile, the HOMO-LUMO gap should be as narrow as possible to absorb longer wavelength light. A successful example is **N749**, as mentioned before. Nazeeruddin reported that dyes **K9** and **K23** can generate high Jsc in DSSC when compared with **Z907**, which was due to the increased absorption in NIR regions.[145]

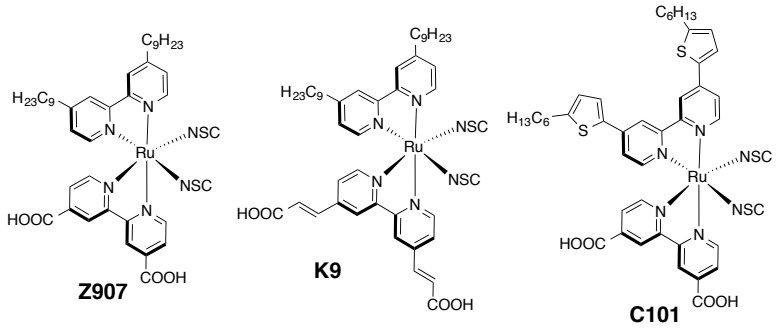

Figure 2.15. Typical ruthenium-based dyes **Z907**, **K9** and **C101**.

Extend the π-conjugated System to Enhance Light Harvesting

When the conjugation of the bipyridine ancillary ligand in a Ru(II) complex is extended thought electron-rich atoms and/or π-extended subunits, better light-harvesting can be expected, especially higher molar extinction coefficients and a redshift of the absorption spectrum. A typical example is the dye C101 that incorporates two alkyl-substituted thiophenes at the ancillary ligand part. Thanks to this structural modification, the DSSC device made with **C101** showed improved performances when compared to **N3** for instance, because of the redshift of the IPCE response. The C101/DSSC achieved an overall efficiency of 11 % under AM 1.5G using an iodine-based electrolyte.[146] Another intersting example was the introduction of 3-methoxystyryl moieties in **Z910** dye (Figure 2.15) that reached an efficiency of 10.2 % in DSSC.[147] After that, many analogues dyes incorporating other types of conjugated

electron-rich units such as alkyl- or thioalkyl- thiophene, dithiophene, furan, selenophene, thieno[3,2-b]thiophene, ethylenedioxythienyl (EDOT), and carbazole, have been extensively reported in DSSC. [148-151] Grafting strong chromophore subunits, acting as antennae, is also a common strategy to boost the light-harvesting properties of the Ru(II) complexes, although it is not often accompanied by an improvement of the performances in DSSC. A successful attempt was obtained with **JK56** that reached a maximum IPCE value of 83 % and achieved an overall PCE of 9.2 % under AM 1.5G standard conditions.

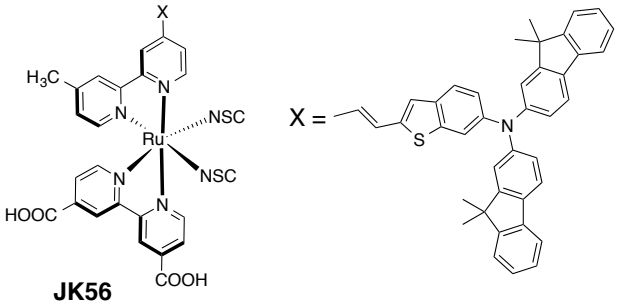

Figure 2.16. Typical ruthenium-based dyes **JK56**.

Increase the stability of the device by incorporating of hydrophobic chains in the ancillary group.

In parallel with the huge research efforts devoted to improve the photovoltaic performances of a DSSC, the stability of device under operative condition is also parameter of crucial importance for further large-scale commercialization. The latter have been less considered, and remain an important drawback for this kind of solar cells (as for organic-based solar cells in general), considering that most stable devices can perform around 1000 h without significant drop in the photovoltaic performances.

Attaching hydrophobic alkyl chains to the dye can retard desorption of the dye from TiO_2 surface and increase the thermal stability, making the DSSC more stable.[152, 153] In addition, they are useful to retard the recombination processes between the electrolyte and the TiO_2 surface, acting as a blocking layer, which is helpful to improve the photovoltaic performances and especially the V_{OC}. One of the first examples was reported with **Z907** in DSSC, which showed much more stability when compared to **N719**. Another advantage to incorporate these hydrophobic chains is when solid-state

electrolyte because they enhance the interaction between dye and hole conducting material, increasing the of relative permeability the TiO_2.[154]

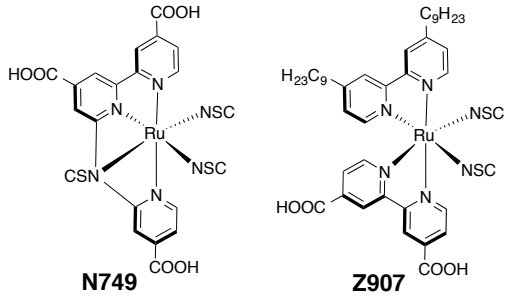

Figure 2.17. Dyes **N749** and **Z907**

Retard Charge Recombination

Some modification of ancillary ligands of ruthenium complexes can decrease recombination rate effectively. Therefore, there is a charged space at the interface between the dye and TiO_2, retarding charge recombination between injected electrons and the left positive charges[155].

Attachment of hydrophobic ligands to Ru(II) complexes may increase the stabilityas well. The anchoring states of dyes to TiO_2 tend to break in trace amount of water, and the dye molecules will desorb from the surface. Attaching hydrophobic chains to ruthenium center as ligands can retard desorption of the dye from TiO_2 surface. Thus, it can make DSSC more stable in a long term.

One example was observed in the influence of the hydrophobic hydrocarbon chain length of amphiphilic ruthenium dyes on the device performance in solid-state DSSCs[156]. By varying the hydrocarbon chain length of an amphiphilic ruthenium dye (Figure 2.18), the efficiency can be improved significantly. The results reported in this example suggest that a slightly longer hydrocarbon chain length might be advantageous and could lead to even higher efficiencies, and a hydrophobic chain attached to the dye can be used to suppress recombination.

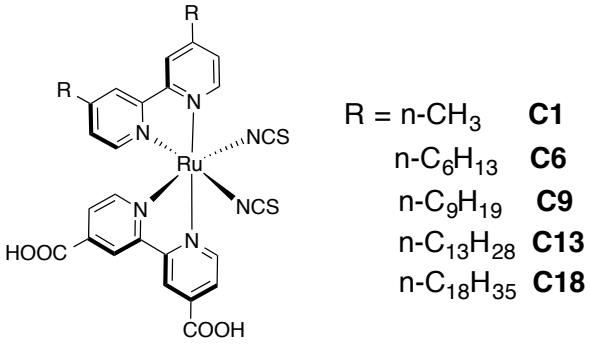

Figure 2.18. Molecular structures of the dyes with different chain lengths (a) and the hole conductor (b) used for the device preparation are shown next to a schematic of the device structure (c) the devices consist of a glass substrate covered by a conductive transparent electrode (F-doped SnO_2)[156]

This leads to a linear increase in device efficiency with chain length (Figure 2.19). Also, the fill factor (FF) = $(V_m J_m)/(V_{OC} J_{SC})$, where V_m and J_m are current and voltage for maximum power output and J_{SC} and V_{OC} are short-circuit current and open-circuit voltage, respectively) seems to follow this increase. Just for the longest chain, **C18**, we observe a dramatic decrease in open-circuit voltage, current density, and efficiency. Already the devices with **C9** and **C13** dye show no difference in the current density, but the open-circuit voltage still increases.

We attribute this behavior to the arrangement of the dye molecules onto the TiO_2 surface, which is strongly influenced by the hole conductor that surrounds the dye. We find an interaction between the hole conductor and dye, which leads to a higher absorption of the dye. The hydrophobic chains of the dyes seem to extend and arrange themselves in the presence of the hole conductor to form an effective spacer between the TiO_2 layer and the hole conductor, which suppresses charge recombination at this interface.

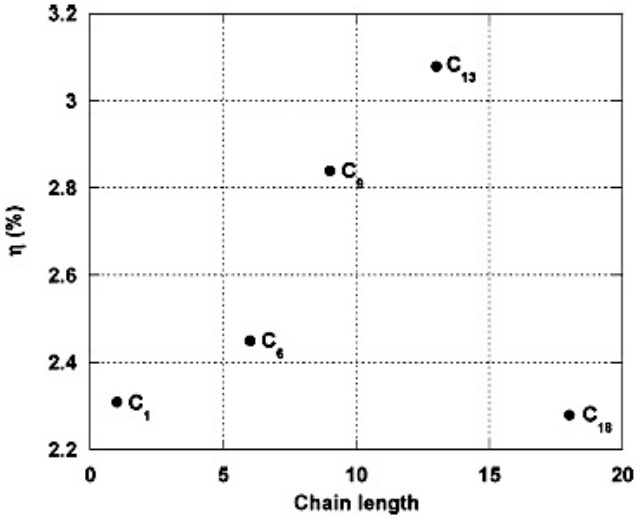

Figure 2.19. Device efficiency (in %) vs chain length of amphiphilic dyes with different hydrophobic hydrocarbon chain lengths. Up to the dye with a **C13** chain, a linear increase in efficiency can be observed with the increase of the length of the hydrocarbon chain.

For these dyes explained here, the highest increase in absorption it were for the **C9** and **C13** dye followed by the **C6**, **C1**, and **C18** dye, successively. The reason of this higher absorption coefficient lies in the extension of the carbon chains. The longer the chain is, the higher the increase in absorption. Only the decrease of the absorption for the **C18** dye. It is assumed that this very long chain collapses and tends to curl up and does not swell to its full length in the presence of the hole conductor, as seems to be the case for the shorter chains. Therefore, the effective length of the chain does not increase further and the blocking effect is even smaller than that for the dyes with shorter chains.

2.1.5.2 Tuning the property of heteroleptic Ru(II)complexes trough structural modification of the anchoring ligand

Some modification of ancillary ligands of ruthenium complexes can decrease recombination rate effectively. We will introduce the mechanism to retard recombination first. As the excited electrons in the LUMO of the dye are injected to TiO_2 rapidly, the dye is left with positive charge density. The positive charge density is distributed over the metal ruthenium, even to the thiocyanate ligand. So there is a charged space in the interface between dye and TiO_2, retarding charge recombination

between injected electrons and the left positive charges[157]. One example was observed in the triarylamine moiety connecting with a conjugated link helped to increase the extinction coefficient. This is the result of faster intramolecular hole transfer from the ruthenium center to the donor and longer-lived charged separation between the injected electrons in TiO_2 and oxidized donor group of the dye. Dyes with triarylamine moiety achieved 3.4 % overall efficiency in solid-state dye-sensitized solar cells while **N719** was only 0.7 % in the same condition.[158] The results showed that charge recombination between electrons in TiO_2 and holes in dye can be retarded by introduction of triarylamine donor groups.

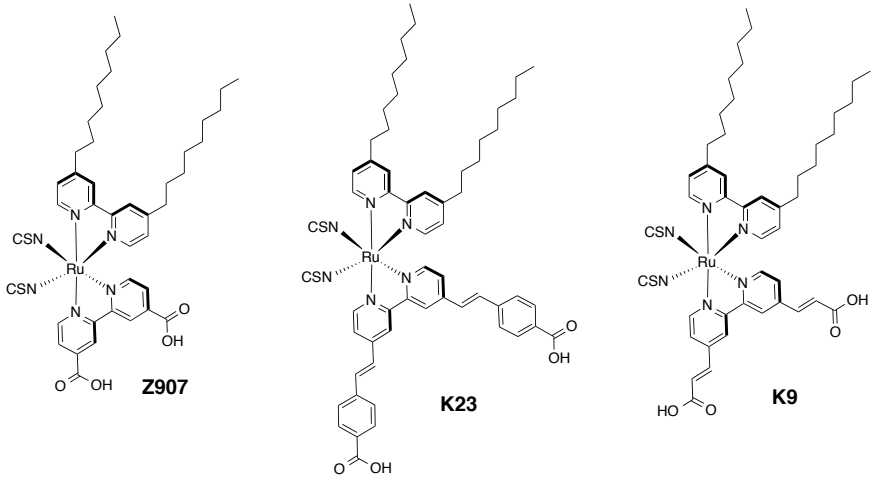

Figure 2.20. Typcal ruthenium-based dyes K9; K23 and Z907.

2.1.5.3.Thiocyanate-free Ru(II) dyes

The thiocyanate ligands are usually considered as the most fragile part of the ruthenium dyes. Firstly, since it is a monodentate ligand, it is easier to decoordinate than a bidentate ligand like bipyridine. Secondly, it is an ambidentate ligand which can attach at either the sulfur atom or the nitrogen atom. Many attempts to replace the thiocyanate donor ligands have been made.

In recent times the need of designing and investigating thiocyanate-free Ru sensitizers clearly emerged in the scientific community, as evidenced by the many research reports appeared in the recent DSSC literature.[159] Accordingly, a collection of the literature reports on this important class of novel Ru(II) DSSC sensitizers for improved chemical long-term stability could have been particularly useful to the

researcher dealing with DSSC. The two most representative series based on (Figure 2.21):

1. The commonly used 2,2'-bipyridine ligand, that is ruthenium(II) bis-bipyridyl complexes bearing a cyclometallated bidentate ligand
2. Ruthenium(II) bipyridyl complexes bearing non-cyclometallated bidentate ligands.

In the last three years many novel and stable dyes pertaining to these two families have been synthesized, fully characterized in their structural, optical, and energetic properties and employed as sensitizers in DSSC. Though their PCE is still lower than the best thiocyanate-based Ru(II) complexes, in some cases remarkable performances were obtained, clearly showing the great potential of this class of Ru(II) dyes. In conclusion, in the near future the use of properly optimized thiocyanate-free ruthenium(II) bipyridyl complexes in combination with more performing and tailored liquid or quasi-solid electrolyte mixtures could contribute to pave the way to efficient solar devices endowed with long-term chemical and thermal stability for viable large-scale commercialization of DSSCs.

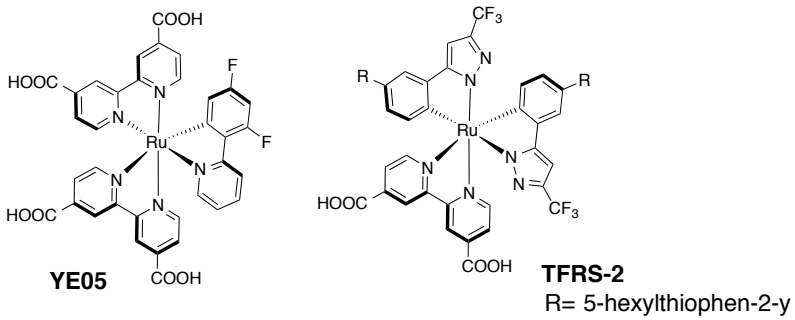

Figure 2.21. The commonly used 2,2'-bipyridine ligand: cyclometallated bidentate ligand Ruthenium and non-cyclometallated bidentate ligands.

On the other hand the thiocyanate ligang can cahnge for other ligands. For these series of Ruthenium bipyridyl dyes (Figure 2.22: **1-4**), the spatial separation of the dye cation state from the electrode surface was determined by semiempirical calculations . All dyes in this series have the same structural components for achieving binding to the metal oxide surface (two dicarboxy bipyridyl groups) and are therefore expected to bind to the electrode surface with a similar orientation

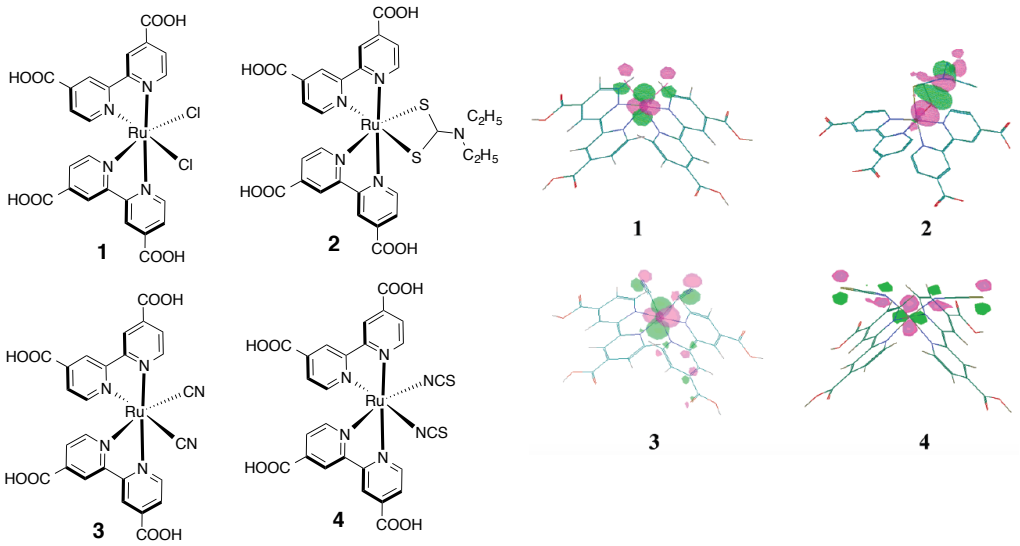

Figure 2.22. Graphical representation for the HOMO of $Ru(dcbpy)_2Cl_2$ (**1**), $Ru(dcbpy)_2DTC$ (**2**), $Ru(dcbpy)_2(CN)_2$ (**3**), and $Ru(dcbpy)_2(NCS)_2$ (**4**) catión states[155]

It is apparent from that for dye **1** the cation wave function is metal-localized, whereas for dye **4** the cation is localized on the NCS ligands. Dyes **2** and **3** lie intermediate between these two extremes.

Finally, the syntheses and electrochemical spectroscopic properties of a suite of asymmetrical bistridentate-cyclometalated Ru(II) complexes (Figure 2.39) bearing terminal triphenylamine (TPA) substituents were reported[160]. The placement of the anionic ring on the flanking position of the tridentate ligand proximate to the TPA unit maximizes light harvesting in the visible region, maintains sufficient vectoral electron transfer toward the semiconductor surface, and ensures that the LUMO is situated on the anchoring ligand to enable facile charge injection into the TiO_2. This study also highlights the ability to independently manipulate the thermodynamic energy levels of the redox-active TPA and metal units.

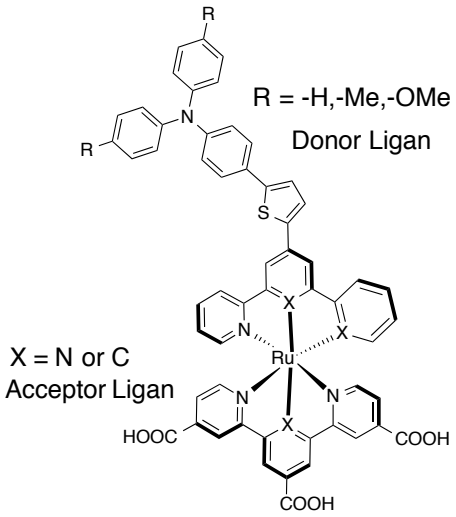

Figure 2.23. "Donor Ligand" and "Acceptor Ligand" descriptors reflect the relative position of the electron-rich TPA substituents only.

2.2 OBJECTIVES

The main objective of this chapter is to explore two new families of ancillary ligands to design Ru(II)-complexes, one based on benzo[1,2-b:4,5-b']dithiophene and a second one on cyclopentadithiophene (CDT) (Figure 2.24), in order to evaluate their potential as sensitizers in DSSC. In addition, these dyes wiil be functionalize with numerous alkyl chains at the lateral and/or terminal positions making them highly hydrophobic, which is expect to enhance the robustness of the device (long-term stability) and improve the photovoltaic performance in DSSC by decreasing charge recombination at the electrolyte/TiO_2 interface. These two families of novel ruthenium(II) polypyridyl complexes will bw design, synthesize, characterize, and finally test in DSSC in collaboration with the group of professors Grätzel and Nazeerudin, at Lausanne, Switzerland.

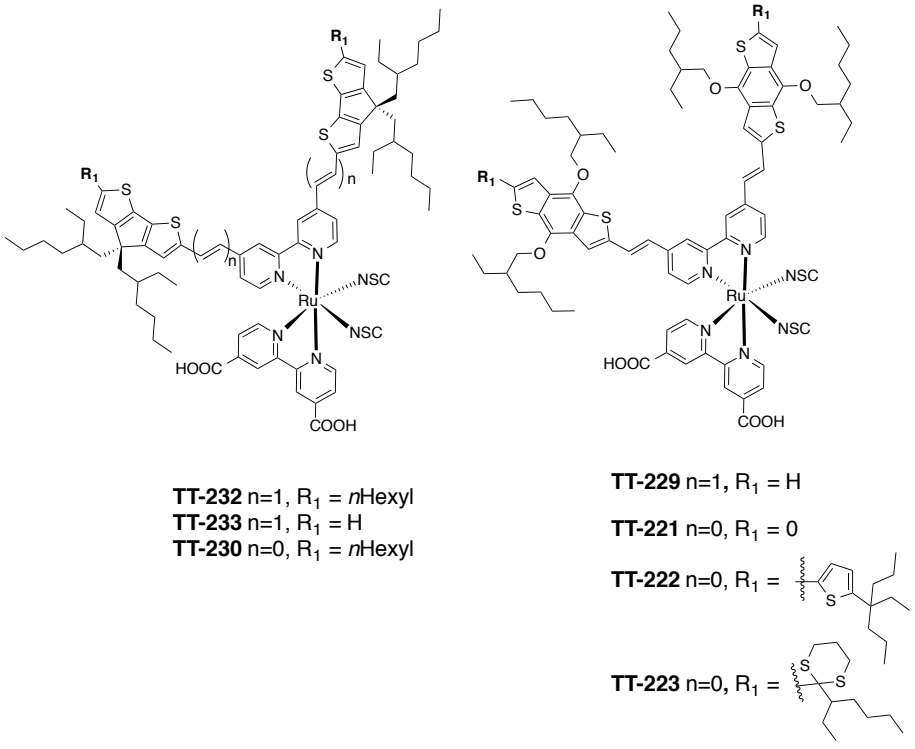

TT-232 n=1, R_1 = *n*Hexyl
TT-233 n=1, R_1 = H
TT-230 n=0, R_1 = *n*Hexyl

TT-229 n=1, R_1 = H
TT-221 n=0, R_1 = 0
TT-222 n=0, R_1 =
TT-223 n=0, R_1 =

Figure 2.24. Two series of novel ruthenium(II) polypyridyl complexes: a) based on benzo[1,2-b:4,5-b']dithiophene (on the right) (BDT) (on the left) b) based on cyclopentadithiophene (CDT) (on the left)

These dyes of general formula $Ru(L)(L')(NCS)_2$ feature the same 4,4'-dicarboxylic acid 2,2'-bipyridine moiety acting as the anchoring group (L´), whose function is to attach the dye to the semiconductor surface, two thiocyanate groups, which shift the absorption spectra to the red, and a second bipyridine ligand differently substituted at the 4,4' positions with BDT or CDT subunits, acting as the ancillary ligand (L):

1. Those based on benzo[1,2-b:4,5-b']dithiophene derivatives (**BDT**): the ancillary ligand is a bipyridine functionalize with two BDT either directly-linked (n=0) or vinylene-linked (n = 1). The π-extended conjugation either through a vinylene bride in the case of **TT229** (n = 1) and trough additional thiophene moieties (**TT222**) that cause significant redshift and broadening of the absorption bands (Figure 2.24 *a*). For all these complexes, various hydrophobic chains will be introduced at the terminal and/or lateral positions of the BDT subunits. The reaction conditions will be adapt and optimize for the preparation of these amphiphilic complexes with a strong lipophilic character.

2. Those based on cyclopentadithiophene derivatives (CDT): the ancillary ligand will be a bipyridine functionalized with two CDT subunits, either directly-linked (n=0) or vinylene-linked (n=1). As well, a remarkable difference between all of them is the π-extended conjugation through the vinylene bridges in the case **TT231** and **TT232** (n = 1) that will be cause a significant redshift and broadening of the absorption bands in comparison with **TT230** (n = 0) (Figure 2.24 *b*).

2.3 RESULTS AND DISCUSSION

2.3.1 Synthesis of functionalized bipyridines

2.3.1.1 Synthesis of 4,4'-dibromo-2,2'-bipyridine

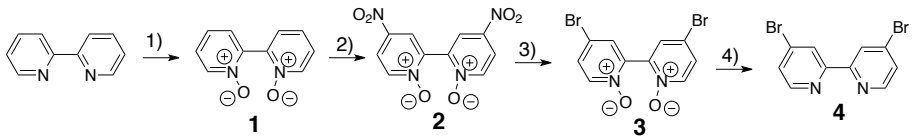

Scheme 2.1. Synthesis of 4,4-dibromo-2,2-bipyridine: 1) AcOH, H_2O_2 (94%); 2) H_2SO_4, HNO_3; (70%); 3) AcOH, acetyl bromide (44%); 4) Phosphorus tribromide, CH_2Cl_2 (66%).

A method for synthesis of 4,4- dibromo-2,2-bipyridine, wherein a four-step process, by oxidation the nitrogen atom in good yields to activated the 4 position and protected these atoms, followed the nitration, using concentrated sulfuric acid and fuming nitric acid, to produce 4,40-dinitro-2,20-bipyridine-N,N-dioxide **2** in 86% yield. A sustitution nucleophile of the nitro group using brome derivative. This is followed by the reduction of **3**, catalyzed by phosphorus tribromide, to form **4** in 73%.

2.3.1.2 Synthesis of the BDT-functionalized bipyridines.

Synthesis of the BDT precursors: Building block (8)

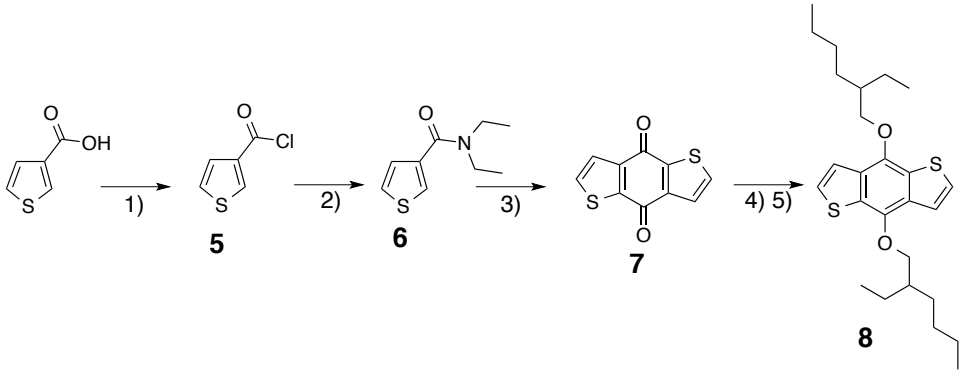

Synthesis of the BDT starting building block **8:** 1) Oxalyl chloride in CH_2Cl_2 (quant.); 2) diethylamine in CH_2Cl_2 (quant.); 3) n-BuLi in THF (76%); 4) KOH, Zn in DMF; 5) 2-ethylhexylbromide (87%).

The synthetic approach to prepare the BDT building block **8** is depicted in 0. First, the commercially available 3-carboxylic acid thiophene was treated with an

excess of oxalyl chloride to yield the activated acid chloride **5**. After removal of the solvents and excess of oxalyl chloride under high-vacum, this compound was used without purification in the next step because it is too reactive to be purified on column chromatography (decomposition), and the yield was assumed quantitative for this step. The activated derivated **5** was subjected to a direct amidation reaction with diethylamine to afford compound **6** (*N,N*-Diethylthiophene-3-carboxamide) in yield exceeding 95%. Once the lithiated species of the thiophene derivated is generated (at the 2-position), it can react with the amide group of another molecule (nucleophilic attack) through an intermolecular (bimolecular) process to produce a dimeric species. In this case, the intramolecular reaction of the lithiated specie cannot occur for obvious geometrical constrain reasons. Next, the generated dimeric species react with a second equivalent of nBuLi to produce the corresponding dimeric-monolithiated species, which can evolve either to a trimeric species by reaction with another monomeric molecule (intermolecular process, and so on it can evolved to polymeric species by the same reaction sequences) or to the cyclic product through an intramolecular reaction. The intramolecular reaction being kinetically much faster than the intermolecular one, the formation of the cyclic product is favoured. Consequently, the reaction conditions (concentration, temperature and equivalent of nBuLi) were crucial to obtain compound **7** in a good yield. Subsequently, diketone **7** was reduced by zinc dust / KOH in DMF at 60°C to afford the dialkolate intermediate. This reaction is strongly favoured because of the gain in aromaticity from the 1,4-benzoquinone form of the central ring (non-aromatic) to the hydroquinone or benzene-1,4-diol (aromatic), which can be appreciated by the change of colour produced during the reaction, starting from light yellow to deep dark-green. When the reduction reaction was completed, an excess of dodecyl bromide was added to the solution to afford the dialkoxyl compound by a double *O*-alkylation reaction. After additional 12 h of reflux, 4,8-bis(dodecyloxy)benzo[1,2-*b*:4,5-*b*]dithiophene, compound **8**, was obtained in 78% yield.

Synthesis of the BDT precursors:

The bipyridine ligands **L-221**, **L-222**, **L-223** and **L-229** were synthetized by multi-steps reactions from the BDT starting building block **8**, as depicted in 0. The first key-step consisted of the mono-functionalization of 1 by a two-stage reaction sequence (0:, routes a–d): treatment of **8** with *n*BuLi at -78°C was followed by the addition of the appropriate electrophilic reagent, $SnBu_3Cl$, Br_2, 2-ethylhexanoyl chloride or DMF, to

afford the corresponding mono-substituted derivatives **9**, **10**, **13** and **16**, respectively. When an equimolar amount of *n*BuLi was used, the starting material (i.e. compound **8**) and the bis-substituted product were always obtained in a significant proportion (ratio 1/mono/bis of c.a. 2:6:2).

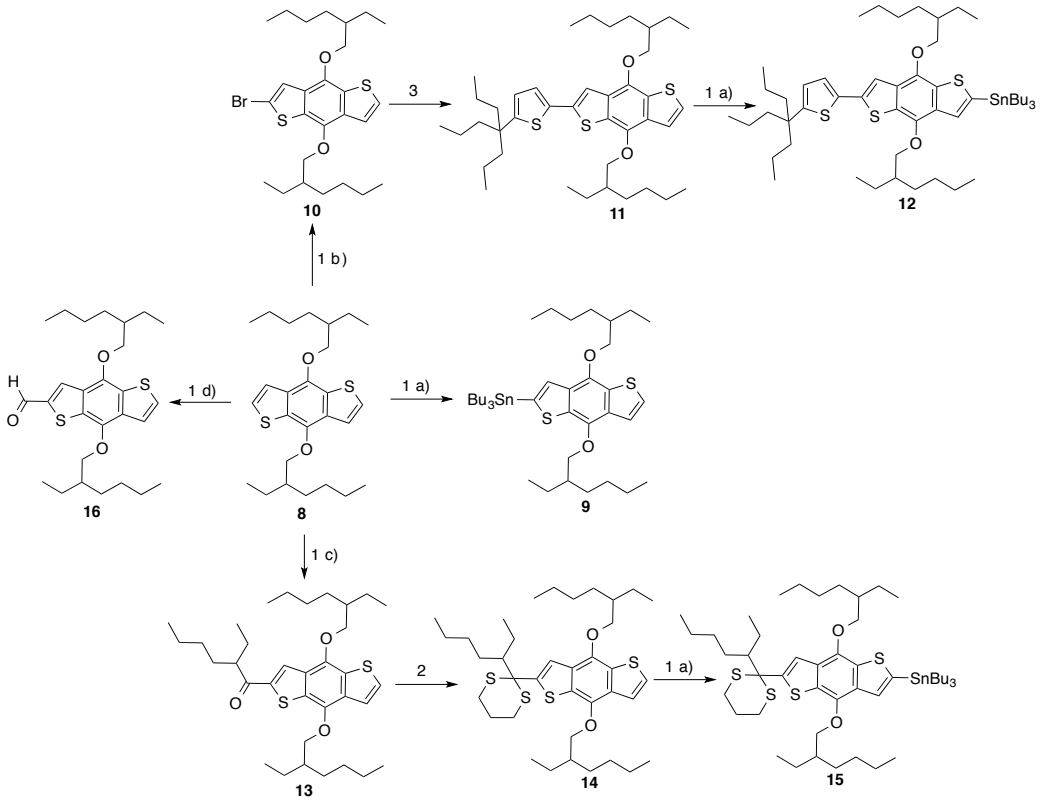

Scheme 2.2. 1) nBuLi, 1.1–1.2 or 1.3–1.6 eq, THF, -78°C to -60°C, 1–2h followed by a) SnBu3Cl (1.5–1.6 eq), -60°C to rt, 2–3h (**9**: n.d., **12**, **15**: quantitative yields); b) Br2 (1eq), -60°C to rt, 2–3h (**10**: 67%); c) 2 ethylhexanoyl chloride (3eq) in THF, -60°C to -20°C, 2–3h (**13**: 44%); d) DMF (1.5 eq), -60°C → rt 2–3h, then H2O (**16**: 69%); 2) propane-1,3-dithiol (28 eq), BF3•Et2O (25 eq), CH2Cl2, rt 48h (7: quantitative); 3) tributyl(5-(4-propylheptan-4-yl)thiophen-2-yl)stannane (85%)

In this Figure 2.25 it show the signals of this serie of compounds: in red (8-7ppm) the aromatic signals; in blue de -CH_2- (α around 4.5ppm) and in green the aliphatic chain of all of them. The symmetry of this bulding block in compound **8**

showed a simplified spectra. These molecules broken the simetry and the stectrum of all of them were more complicated aparing pair of signals of the similar atoms of carbon (see in blue the alfa of alkyl chain or the carbon of the protection of the keton in compound 14).

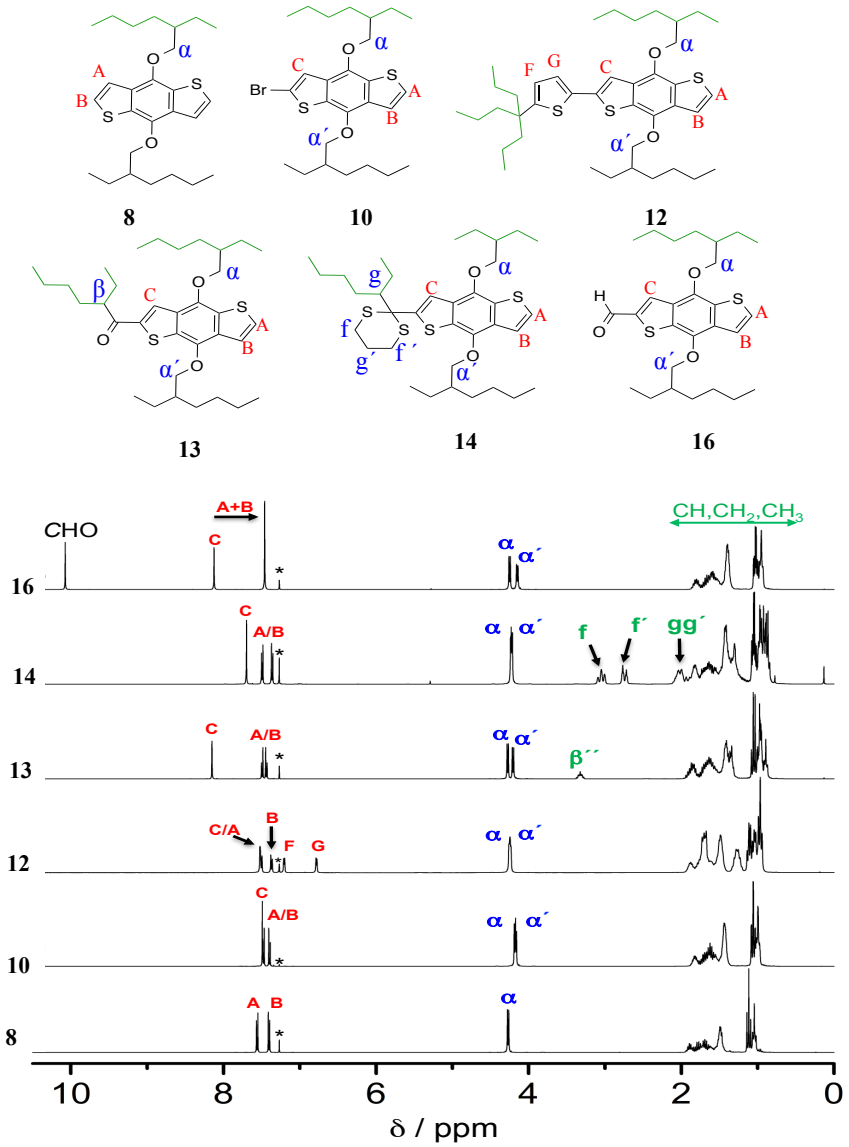

Figure 2.25. ^{1}H-NMR spectrum of some intermediates of BDT ($CDCl_3$; 300 MHz); * denotes the residual solvent peak of $CDCl_3$.

It can be explained by proton exchange phenomena either between the mono-lithiated specie of **8** and the generated mono-functionalized product as reported for other classes of thiophene-based derivatives, or most probably in our case by an equilibrium mono- and bis- lithiated intermediates of **8**.

By using only a slight excess of *n*BuLi (1.1–1.2 eq) and an excess of electrophilic reagent (1.5 eq), this ratio could be optimized to c.a. 0:7:3 of 1/mono/bis products respectively. After separation by column chromatography on SiO_2, the mono-substituted products could be obtained in good yields (**10**: 67%, **16**: 69%).

In the case of the stannyl derivative **9**, chromatographic separation was not possible due to the strong tendency of these derivatives to decompose on SiO_2. Therefore, the crude mixture containing the mono-**9** and the bis- stannyl derivatives was used as well without further purification in the next step. In the case of the acyl derivative (0: route 1c), a solution of the in situ formed lithiated product of **8** in THF was transferred into an excess of 2-ethylhexanoyl chloride (3 eq) in THF at -60°C, in order to avoid subsequent reaction with the generated carbonyl group.

However, the formation of by-product could not be fully avoided in that case, thus leading to a lower 44 % yield for **13**. Carbonyl group of ketone **13** was then converted into dithioacetal by treatment with an excess of propane-1,3-dithiol in the presence of BF_3•Et_2O in CH_2Cl_2 at r.t. for 48h, affording **15** in quantitative yield (Scheme 2.1 2). On the other hand, the mono-bromide derivative **9** was subjected to a palladium-catalysed Stille cross-coupling with tributyl(5-(4-propylheptan-4-yl)thiophen-2-yl)stannane to afford 4 in 86% yield. (0: 3 a)

Next, compounds **11** and **12** were treated another time with *n*BuLi (1.3–1.6 eq) at -60°C, followed by the addition of $SnBu_3Cl$ (1.6 eq), to afford the corresponding stannyl derivatives **12** and **15** in quantitative yields. In these cases, one could use an excess of *n*BuLi because only one free reactive proton remains at the α-position of the thiophene moiety (the other position being already substituted).

Synthesis of the BDT-functionalized bipyridines

Stille couplings between 4,4'-dibromo,2,2'-bipyridine and stannyl derivatives **9**, **12**, or **15**, afforded the corresponding free ligand **L221** in low yield (23%), and **L222** (91%) and **L223** (96%) in excellent yields (Scheme 2.3). The low yield obtained for **L221** came from the formation of by-products (oligomers) during the reaction, caused

by the presence of the bis-stannyl by-product in the starting material (26 mol%, vide supra), associated with many purifications steps required to isolate **L-221** from the reaction mixture.

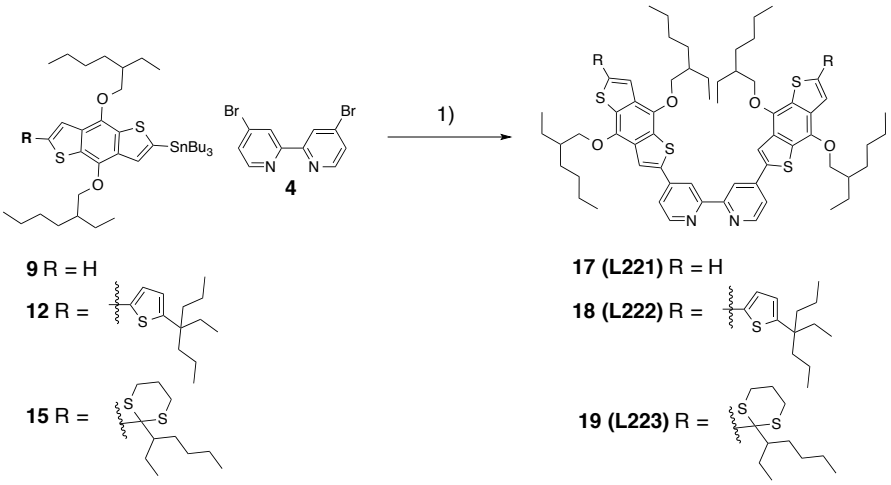

Scheme 2.3. Stille couplings between 4,4'-dibromo,2,2'-bipyridine and stannyl derivatives: 1) 4 and $Pd(PPh_3)_4$ in toluene at reflux (**17**: 29%, **18**: 91%, **19**: 96%)

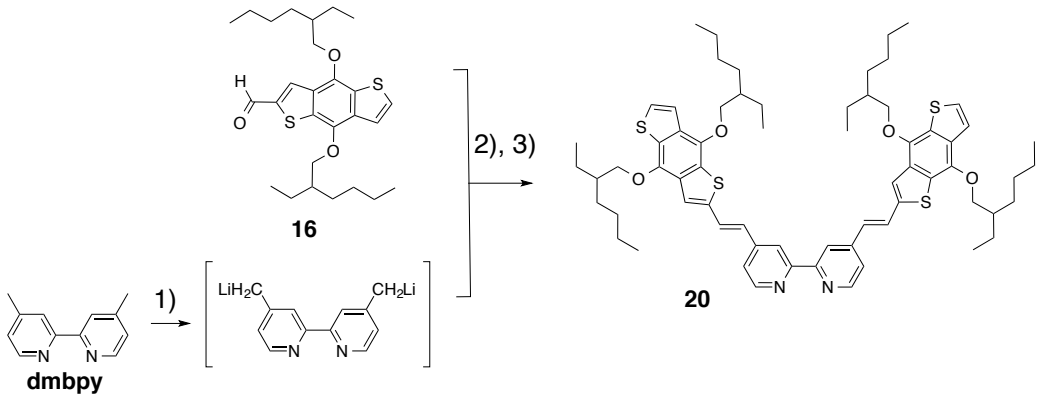

Scheme 2.4. 1) LDA (2.2 eq), THF, -78°C, 25 min→ -10°C, 20 min, then 2) **16** (2.6 eq) in THF -78°C → rt 2–3h, then H_2O, followed by 3) PTPS, I_2 (cat.), toluene reflux, Dean-Stark trap, overnight (**20**: 35% (three steps from dmbpy)

Compound **20 (L229)** was synthetized by modified procedures previously reported in the literature.[161,162] The first step involves a double deprotonation /

dilithiation of the commercially available 4,4'-dimethyl,2,2'-bipyridine (dmbpy) with lithium diisopropylamide in THF at low temperature (-78°C to -60°C) to afford the corresponding *in-situ* generated bis-anion (Scheme 2.6). Subsequent reaction with an excess of aldehyde **16**, followed by hydrolysis, afforded a bipyridine$(BDT)_2$ diol under a stereo-isomeric mixture due to the two generated stereogenic centres (R or S configuration of the two C^*-OH sp^3 carbons Figure 2.26). This diol was then dehydrated under mild conditions in a Dean-Stark apparatus at reflux of toluene for 48h using pyridinium toluene-*p*-sulfonate salt (PTPS) as catalyst, to afford the corresponding bis-ethylenic derivative. The dehydration reaction proceeded smoothly and cleanly with high *trans*-stereoselectivity.

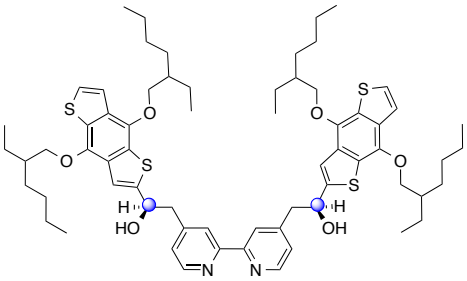

Figure 2.26. Bipyridine$(BDT)_2$ diol under a stereo-isomeric mixture with stereogenic centres (R or S configuration of the two C*-OH sp^3 carbons)

However, the presence of *cis*-isomers as minor by-products formed during the reaction (*Z/E* and *Z/Z*) were always detected by ^{1}H NMR after purification and estimated to be less than 5%. This prompted us to use a catalytic amount of I_2 during the third reaction-step (6) (Scheme 2.4) to ensure the all-*trans* configuration of the double bonds. Following this strategy, isomerically pure (*E/E*)-**34** was obtained in a straightforward one-pot dehydration/isomerization reaction in an overall moderate 35% yield after purification by column chromatography on SiO_2 (three reaction steps from dmbpy; yield not optimized).

2.3.1.3 Synthesis of the CDT-functionalized bipyridines

Synthesis of the CDT precursors: Building block (24)

The CDT precursor **25** was obtained in a five-step reaction sequence (Scheme 2.5 steps 1–4) from the commercially available 3-bromo thiophene. The first step involved a one-pot five-step reaction (Scheme 2.5 steps 1.1–1.5). First, an halogen-Li exchange reaction by treatment of 3-bromo thiophene with nBuLi at low temperature generated the corresponding lithiated intermediate, which then reacted with thiophene-

3-carbaldehyde to afford the lithium dithienyl-methoxide intermediate. Subsequently, treatment with two more equivalents of *n*-BuLi generated the trilithiated species, which then reacted with three equivalents of iodine to afford, after hydrolysis, the diiodoalcohol **21** in good yield.

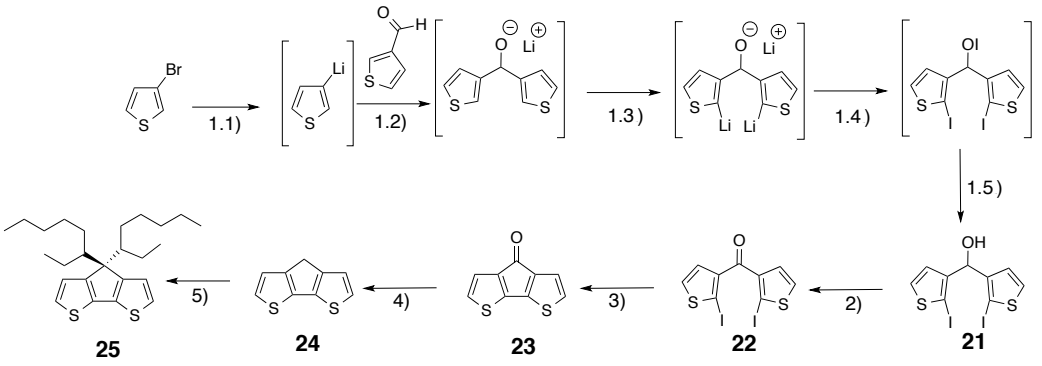

Scheme 2.5. Synthesis of the CDT starting building block **21**: 1) 1.- 3-bromothiophen, nBuLi in Ether 2.- thiophene-3-carbaldehyde (65%); 2) PCC in CH_2Cl_2 (94%) 3) Cu (power) in DMF (60%); 4) Hydrazine in ethylene glycol (54%) 5) 2-ethylhexyl bromide in DMSO (48%).

It cannot be excluded that iodination of the tri-lithiated derivative proceeded via the hypoiodite since, when only two equivalents of iodine were used, the formation of the mono-iodo alcohol was observed in a significant proportion decreasing the yield of the diiodoalcohol **21** to 51%. In the second step, alcohol **21** was oxidized with pyridinium chlorochromate (PCC) giving the diiodo-ketone **22** in good yield. Compound **22** was subjected to an intramolecular Ullmann coupling reaction to afford **23** in 90% yield.

Finally, the target compound **24** (4H-cyclopenta[2,1-b:3,4-b]dithiophene) was obtained by a reduction reaction of ketone **23**, following a procedure described by Turner et al.[163] Reduction of **23** according to a Huang-Minlon modification of the Wolff-Kischner procedure afforded **24** in satisfactory yield using like reducing agent hydrazine at high temperature. Cyclopentadithiophene **24** was alkylated to form **25** in standar condition (base and bromo derivative).

The synthetic approach to prepare all the final bulding blocks for CDT is shown in Scheme 2.5 It was synthesized starting from compound **25** previously described elsewhere.[164] The first step involved a Friedel-Crafts mono acylation of compound **25**

with hexanoyl chloride (1.2 eq) using $AlCl_3$ (1.5 eq) as Lewis acid catalyst. The key-step was the acylation of the α-position of a thiophene moiety, but was poorly controlled under the experimental conditions. Indeed, the presence of unreacted starting material and the formation of the undesired bis-acyl product were always observed even using an equimolar or a default amount of any of the reagents.

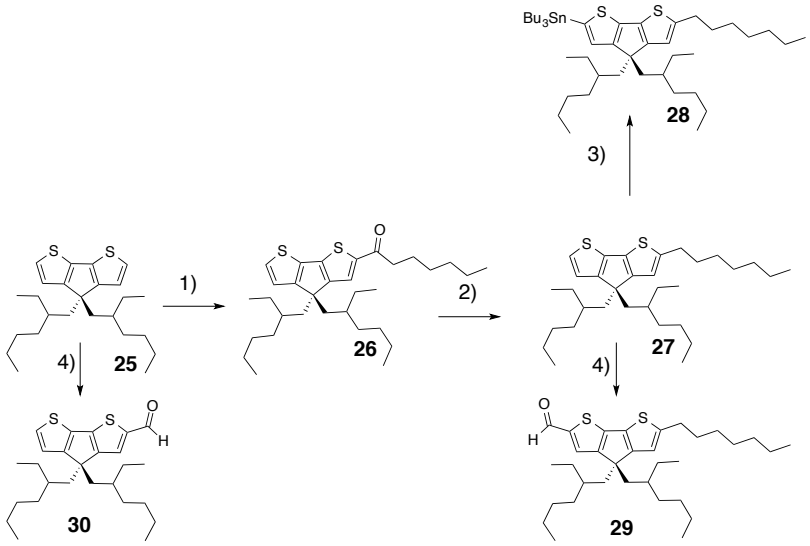

Scheme 2.6. 1) $AlCl_3$, hexanoyl chloride, dry CH_2Cl_2, 0°C to rt overnight. (30%) 2) $LiAlH_4$, $AlCl_3$, Et_2O, 0°C rt 2 h. (82%) 3) n-BuLi, THF, -10°C, 45 min then $SnBu_3Cl$, -10°C (2 h) to rt overnight (quant.) 4) LDA (2.2 eq), THF, -78°C, 25 min→ -10°C, 20 min, DMF 16h (**29**: 73% and **30**: 30%)

Under optimized experimental conditions, the mono acyl product **26** could be isolated in moderate 53% yield from the reaction mixture after chromatography column on silica gel. Next, the reduction of the ketone group was achieved by a metal-hydride reduction using $LiAlH_4$ and $AlCl_3$ to afford the mono-hexyl derivative **27** in 46% yield, which was then converted into its corresponding stannyl derivative in quantitative yield by treatment with *n*BuLi followed by $SnBu_3Cl$.

Finally, compounds **29** and **30** was obtained by first a Mc Murry formylation of **25** or **27** using an excess of DMF and $POCl_3$ at reflux in 1,2-dichloroethane (DCE) overnight to afford, after hydrolysis, an aldehyde.

Synthesis of the CDT-functionalized bipyridines

The bipyridine ligand **31** was further obtained from a Stille coupling between the stannyl derivative **28** and 4,4'-Dibromo-2,2'-bipyridine.[165,166] The relative low yield obtained for **31** (46%) mainly came from difficulties of purification.

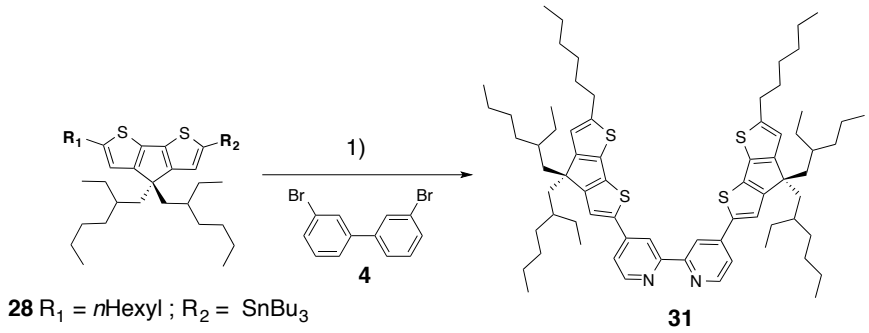

Scheme 2.7. Stille couplings between 4,4'-dibromo,2,2'-bipyridine and stannyl derivatives: 4, $Pd(PPh_3)_4$, refluxing in toluene, 3 days. (41%)

As a typical example for this family of compound, the ^{1}H-NMR spectrum of **L230** is depicted in (Scheme 2.7).

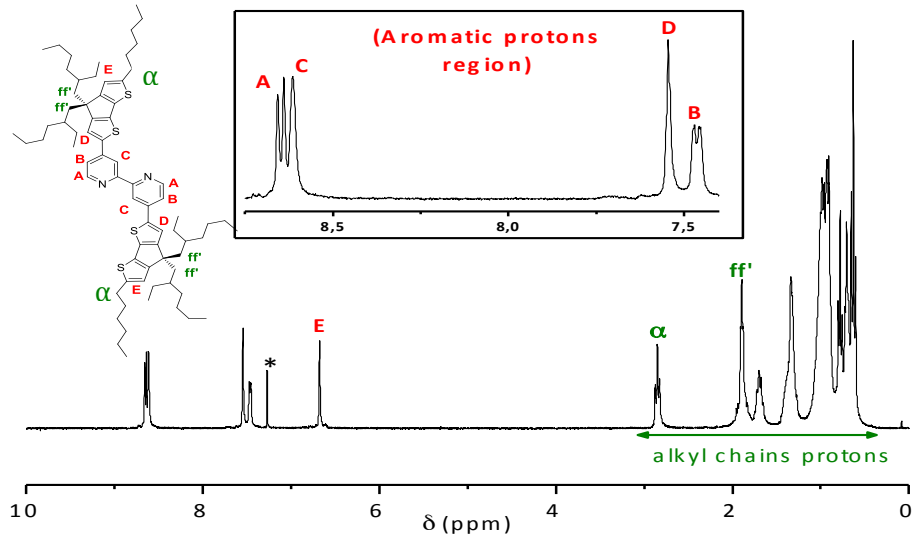

Figure 2.27. ^{1}H-NMR spectrum of 26 (CDCl3; 300 MHz); * denotes the residual solvent peak of CDCl3.

The synthetic approach to prepare the ligand of the dye (**L232** and **L233)** is shown in Scheme 2.8. The step is a double deprotonation/lithiation of dimethyl 2,2'-bipyridine (1eq) with LDA (2eq), in THF at low temperature.

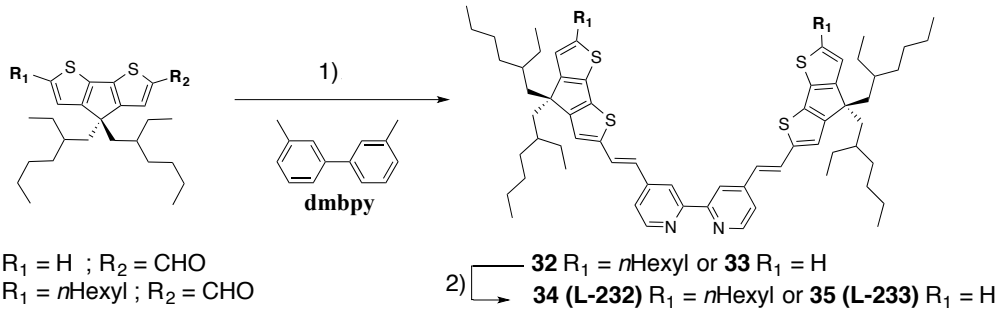

29 R_1 = H ; R_2 = CHO
30 R_1 = *n*Hexyl ; R_2 = CHO

32 R_1 = *n*Hexyl or **33** R_1 = H
34 (L-232) R_1 = *n*Hexyl or **35 (L-233)** R_1 = H

Scheme 2.8. LDA (2.2 eq), THF, -78°C, 25 min→ -10°C, 20 min, then 2.1) (2.6 eq) in THF -78°C → rt 2–3h, then H_2O, followed by 2.2) PTPS, I_2 (cat.), toluene reflux, Dean-Stark trap, overnight (**34**: 70% and **35**: 70%)

Subsequent quenching of the in-situ generated bis-anion with an excess of aldehyde **29** or **30** afforded, after hydrolysis, the functionalized (bis)hydroxy bipyridine (**32** or **33)** in good yields, obtained as racemic mixtures of alcohols. Finally, bipyridines **34** and **35** were obtained under smooth conditions using pyridinium p-toluene sulfonate salt (PPTS) as a dehydrating agent, in refluxing toluene for 48h. The presence of a catalytic amount of iodine was found to be necessary to ensure the formation of all-trans type double bonds.

2.3.2 Synthesis of the (cis)tris-heteroleptic Ru(II) complexes

2.3.2.1 Optimization procedures

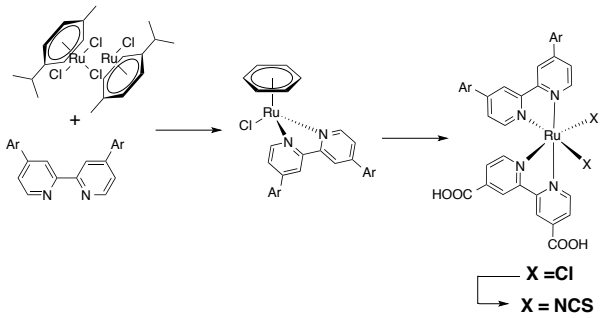

Figure 2.28. Formation of trisruthenium complex under standard conditons.

Starting from dichloro(*p*-cymene)-Ru(II) dimer as the ruthenium precursor, the next step was the synthesis of the Ru(II) complexes *cis*-RuLL'$(NCS)_2$ in a one pot, three-steps reaction by successive coordination of 1) the BDT-functionalized bipyridine (**L**) at 70ºC for 4h, 2) the (2,2'-bipyridine)- 4,4'-dicarboxylic acid (**L´**) at 140ºC for 4h, and finally 3) two NCS monodentate ligands at 140ºC for 4h, using DMF as solvent and a thermal heating source.

However, under these standard conditions commonly described in the literature for the synthesis of such complexes,[167–172] no formation of the target compounds were detected, and only the *bis*-heteroleptic Ru(II) complexes were obtained as the major products, as exemplified in, together with minor degradation products. Switching the order of introduction of the bipyridines ligands (i.e. first **L** and then **L´**) was also attempted but gave the same results under these conditions. These unsuccessful attempts should be explained by the difference in lipophilicity between the two bipyridines ligands.

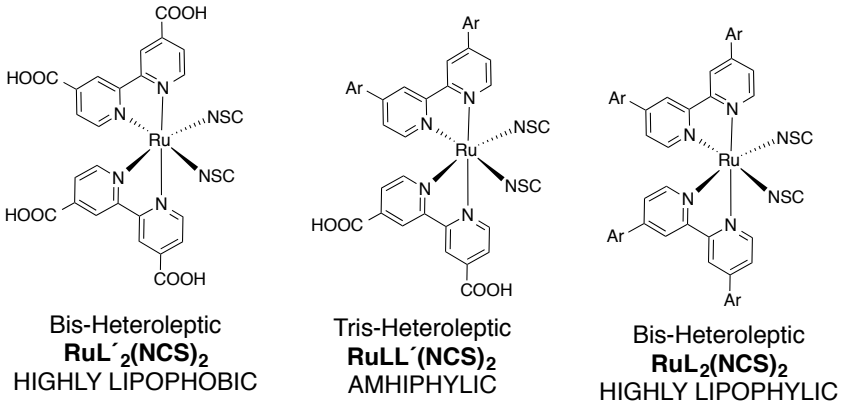

Figure 2.29. General molecular structures of the bis- and tris- heteroleptic Ru(II)complexes formed during a general reaction

To find out suitable conditions, we first screened and optimized the first reaction step. In this step, it is admitted that the coordination of the bipyridine to the ruthenium metal centre takes place from the cleavage of the double-chlorinated bridge of Ru_2Cl_4(*p*-cymene)$_2$[169,172] to afford a cationic, mononuclear, (arene)Ru(II) half-sandwich chelate complex {[(η^6-*p*-cymene)(k^2-*N*,*N*-bipy)(must not exceed 70–90°C and an equimolar ratio [Ru(II)]/[bipyridine ligand] is necessary k-Cl)]$^+$} with a chloride counter anion.[173,174] It was reported that the temperature, both crucial factors to avoid

the undesired formation of *bis*-heteroleptic complex in this first step (resulting from the coordination of a second bipyridine to the Ru metal centre). In this context, we focused on $CHCl_3$ and mixtures $CHCl_3$ and EtOH as solvent of reaction. On the other hand, microwave heating was previously reported as a powerful method for the synthesis of such complexes.[175–177]

To optimize this reaction-step, the commercially available 4,4'-dimethyl 2,2'-bipyridine (**dmbpy**) was chosen as a model ligand for trials because it displays good solubility in organic solvents such as $CHCl_3$ (Figure 2.30). Three representative experiments were carried out in parallel and are summarized in Table 2.1, using in each cases an equimolar amount of **dmbpy** and Ru(II) (*i.e.* 0.5 eq of the dimer Ru_2Cl_4(*p*-cymene)$_2$ per eq. of **dmbpy**) at a concentration of 30 mM.

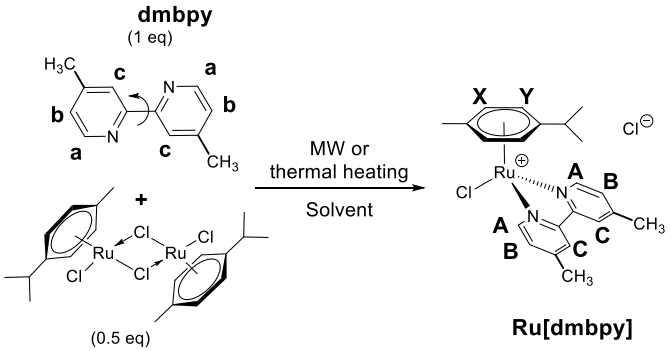

Figure 2.30. Formation of the half-sandwich Ru(II) complex Ru[dmbpy] from4,4'-dimethyl 2,2'-bipyridine (dmbpy) and dichloro(p-cymene)-ruthenium(II) dimer, and 1H nomenclature of the aromatic protons.

Table 2.1. Optimization of conditions for the formation of **Ru[dmbpy]**.

Entry	Solv.	Heating[b] source	Time	**dmbpy**[a] mol%	Ru[dmbpy][a] mol%
I	$CHCl_3$	thermal	4h	<5	>95
II	$CHCl_3$	MW	30 min	32	68
III	$CHCl_3$/ EtOH (1:1)	MW	45 min	0	100

[a] ratios **dmbpy**/**Ru[dmbpy]** were determined based on the integration of the ^{1}H NMR protons signals. [b] Heating to reflux.

Based on ^{1}H NMR spectra of the crude products this reaction step proceeded smoothly and cleanly (Figure 2.31) under MW to afford the half-sandwich complex quantitatively under optimized conditions (III): MW heating to reflux in a 1:1 mixture of $CHCl_3$ and EtOH for 45 min. Following this procedure, the intermediate complexes

Ru[L] were synthetized from the functionalized bipyridine ligands (**L**) using in this case a slight excess of formal Ru metal atom (1.1–1.3 eq per bipyridine, *i.e.* 0.55–0.65 eq of Ru(II) dimer) in order to ensure the full consumption of the highly-valuable bipyridines starting material.

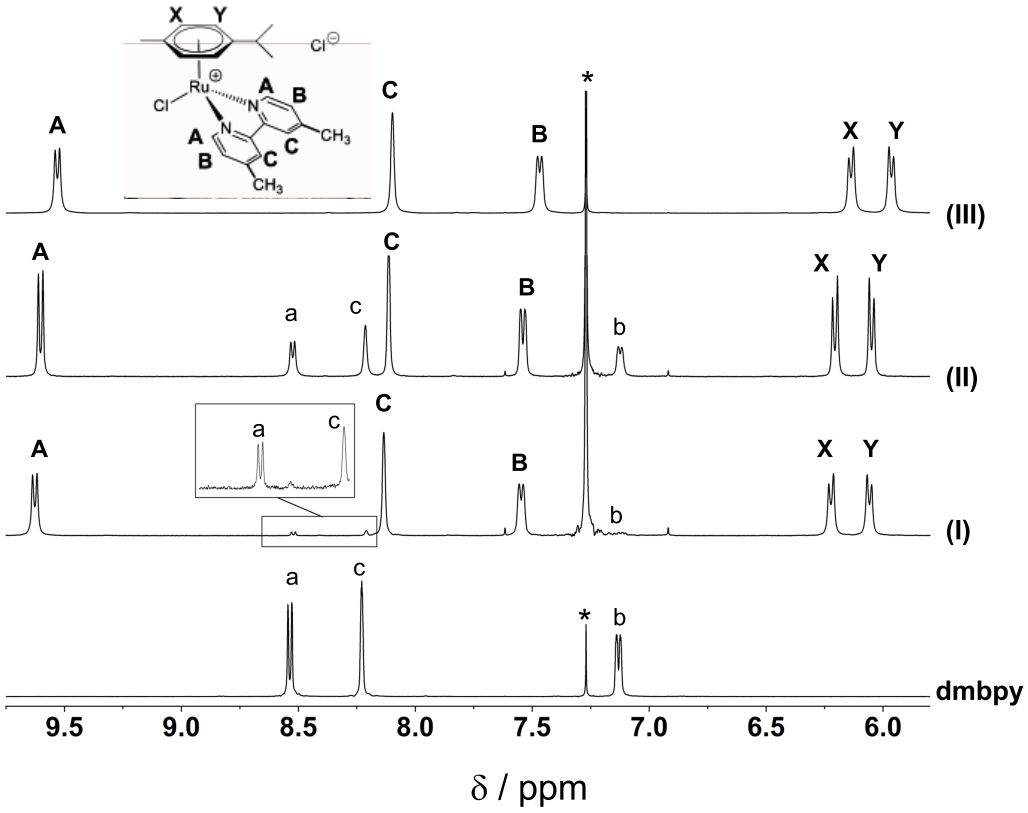

Figure 2.31. ^{1}H NMR spectra (300 MHz; $CDCl_3$; 25°C) of 4,4'-dimethyl-2,2'-bipyridine (dmbpy; bottom trace) and after each experiment (I)–(III) (* denote the residual solvent peak of $CDCl_3$).

The next step was the coordination of the second bipyridine ligand (**L´**= **dcbpy**=(2,2'-bipyridine)- 4,4'-dicarboxylic acid) to the Ru metal centre of the above-mentioned intermediate complex **Ru[L]** to afford the *tris*-heteroleptic Ru (II) octahedral complex $RuNN_1NN_2(Cl)_2$ under *cis*- isomeric form, which require higher temperature (140–160°C; step 2). The **Ru[L]** complex tailored with a positively-charged moiety displayed better solubility in DMF than the highly lipophilic starting bipyridine free ligands (**L**). As well, to balance lipophilicity against lipophobicity, **dcbpy** was dissolved in DMF (90% v/v) and added to a solution of **Ru[L]** in PhCl (10% v/v), and

the resulting solution heated to reflux under MW at 130–140°C for 45 min. In this mixture of solvents, all materials were soluble. In addition PhCl, was also chosen because of its high boiling point (131ºC) close enough to that of DMF (153ºC) to reach temperatures in the range of c.a. 130–140ºC within this mixture (DMF/PhCl 9:1), required for the energetically more demanding coordination of a second bipyridine to form the octahedral (*cis)tris*-heteroleptic Ru(II) complex. Subsequently, a large excess of NH_4NCS (50–75 eq) was added and the mixture irradiated again at 130–140°C for additional 45 min, resulting in the exchange of the chloride by isothiocyanate k^1-bonded ligands (step 3). The use of a slight excess of formal Ru metal in the first step and the appropriate amount of **dcbpy** in the second step induced the expected formation of the *bis*-heteroleptic Ru (II) complex *cis*-$Ru(L')_2(NCS)_2$ *(cis*- bis (isothiocyanato) bis(2,2′-bipyridyl-4,4′-dicarboxylato) ruthenium(II), also called "N3 dye") as a minor secondary product, which was nevertheless easily removed during the work-up by washing the crude with MeOH, while the excess of NH_4NCS was removed with water. The purification of the complexes was achieved by size-exclusion chromatography (eluent THF/MeOH 7:3) affording dyes in acceptable to good yields.

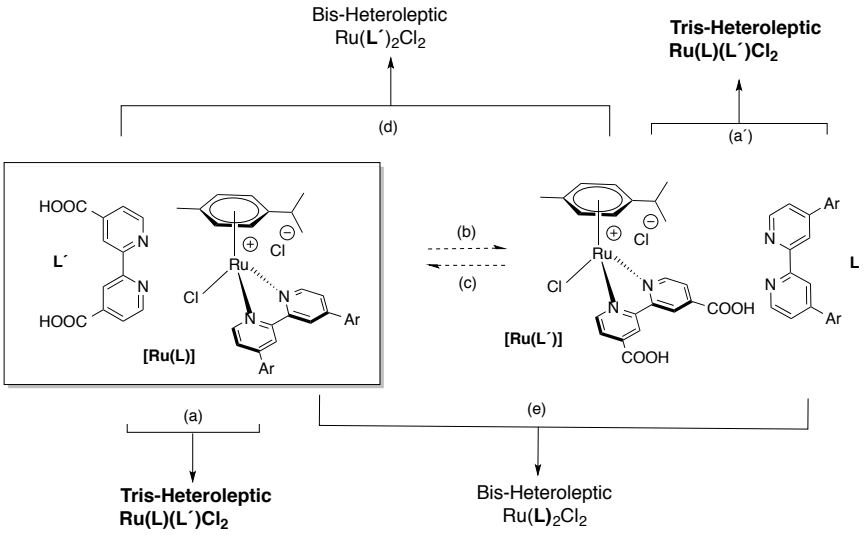

Figure 2.32. Proposed pathways for the partial scrambling process that takes place during the synthesis of the tris-heteroleptic Ru(II) complex upon heating Ru[L] and L′ (starting materials) at 130–140°C (MW) in DMF/$PhCl_3$ 9:1.

Unexpectedly, we still always obtained the *bis*-heteroleptic complex $Ru(L)_2(NCS)_2$ in variable proportion (5–30% yield) as by-product. Indeed, considering

that the intermediate **Ru[L]** was formed quantitatively in the first step in every cases (*vide supra*), the formation of $Ru(L)_2(NCS)_2$ can be therefore explained by a partial scrambling reaction process through bipyridine ligands exchange (de- coordination / coordination process), either from $RuLL´X_2$ (X= Cl or NCS) or most probably from **Ru[L]** (Figure 2.32)

2.3.2.2 Synthesis of the Ru(II) complexes based on BDT

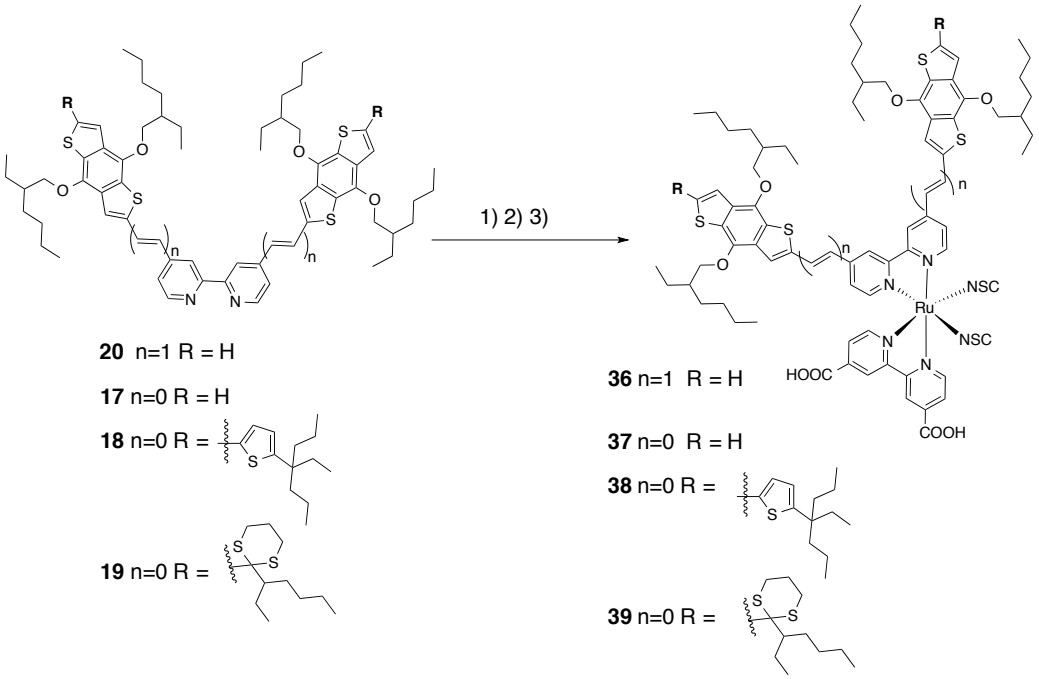

Scheme 2.9. Microwave-assisted synthesis of the (cis)tris-heteroleptic Ru(II) complexes whit CDT subunits. Reagents: 1) CHCl3/EtOH (1:1), MW 60–70°C, 45 min. 2) dcbpy, DMF/PhCl (9:1), MW 130–140°C, 45 min, followed by 3) NH_4NCS, MW 140°C, 45 min (**36**: 94%, **37**: 76%, **38**: 51% and **39**: 73%)

Following our optimized procedure, we prepared the four half-sandwich **Ru[L]** complexes from the four BDT-bipyridine (**36, 37, 38 and 39**).

The starting BDT-bipyridines are highly soluble in fat and non-polar solvent (hexanes, chloroform, toluene), insoluble in polar solvent such as DMSO or methanol, and fairly soluble in DMF, whereas dcbpy displays a strong lipophobic carácter (insoluble in fat and non-polar solvents, soluble in DMSO and DMF).

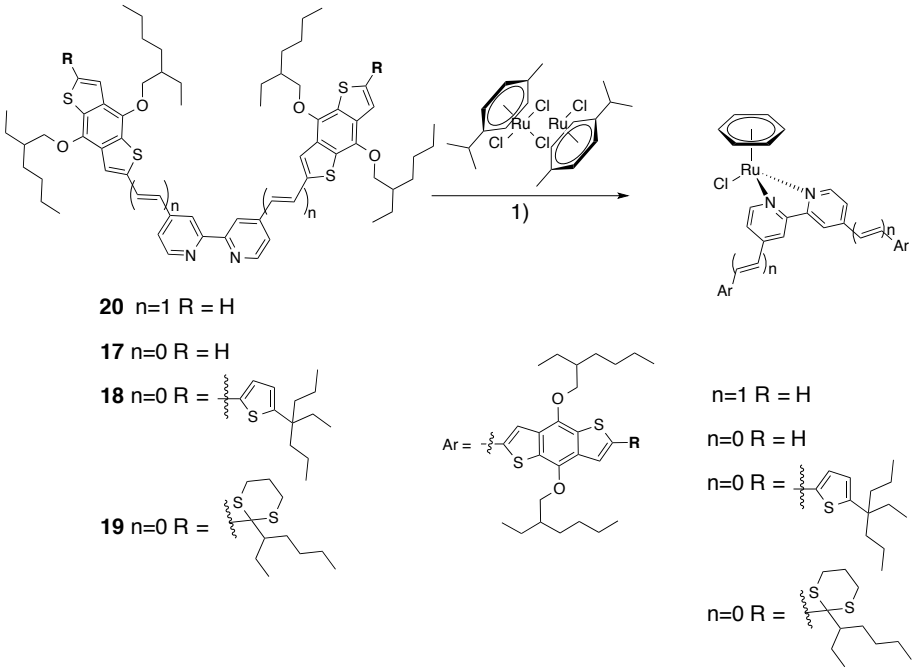

Scheme 2.10. Microwave-assisted synthesis of the (cis)*tris*-heteroleptic Ru(II) complexes under optimized conditions. Reagents and conditions: 1) $CHCl_3$/EtOH (1:1), MW 60–70°C, 45 min.

Following this procedure, the intermediate complexes **Ru[L]** were synthetized from the BDT-functionalized bipyridine ligands (L) using in this case a slight excess of formal Ru metal atom (1.1–1.3 eq per bipyridine, i.e. 0.55–0.65 eq of Ru(II) dimer) in order to ensure the full consumption of the highly-valuable BDT-bipyridines starting material (Scheme 2.10). Although the concentration was much lower in these cases (3–5 mM) it did not influence the reaction. Indeed, the **Ru[L]** complex was still formed quantitatively in every cases too, as confirmed by the ^{1}H NMR spectra of the crude products (Figure 2.33)

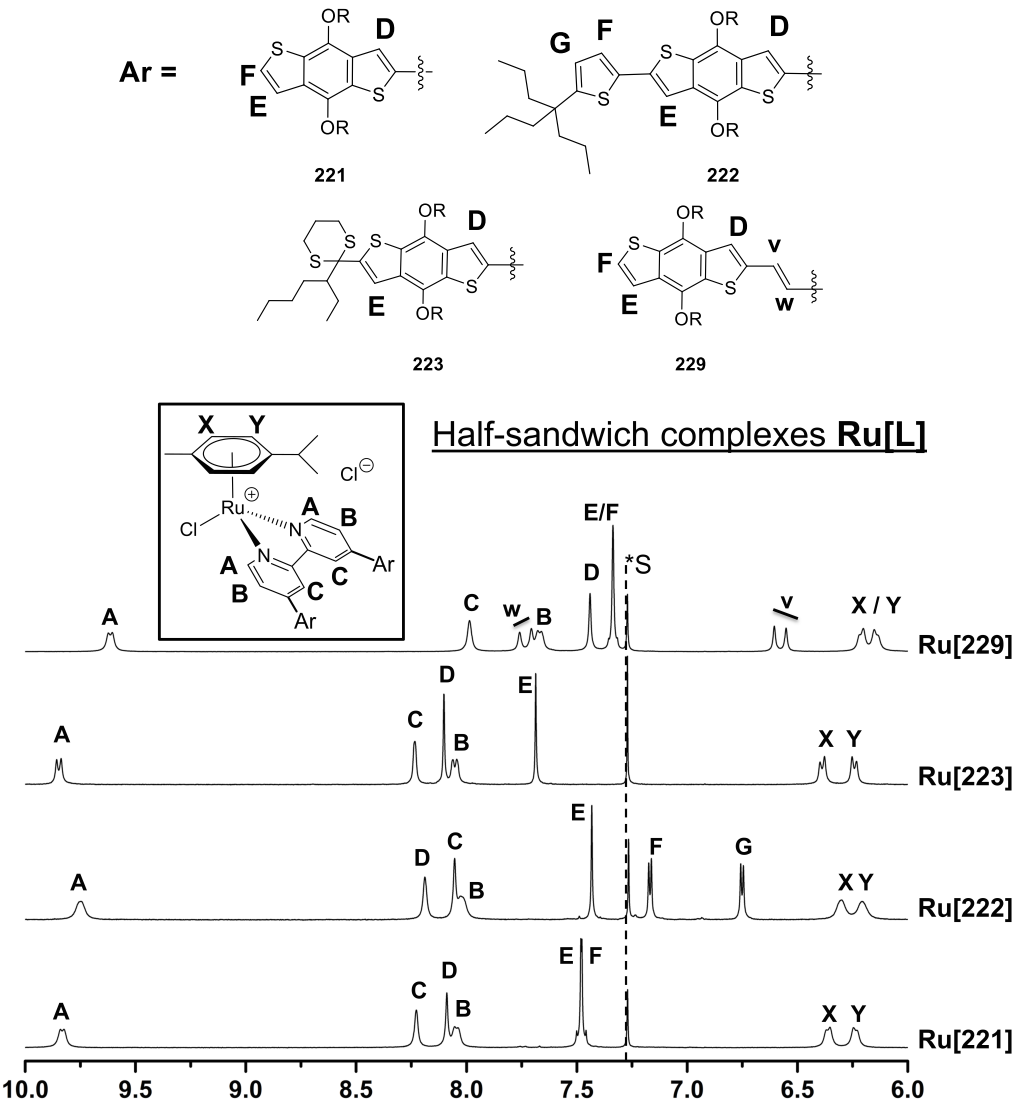

Figure 2.33. Partial ^{1}H NMR spectra ($CDCl_3$, 300 MHz; aromatic protons region) Ru(II) half-sandwich complex intermediates **Ru[L]** (right; crude products), and proposed assignment; *S denotes the residual chloroform signal of $CDCl_3$. Top: ^{1}H NMR nomenclature.

The next step was the coordination of the second bipyridine ligand (L´= **dcbpy**) to the Ru metal centre of the above-mentioned intermediate complex **Ru[L]** to afford the *tris*-heteroleptic Ru (II) octahedral complex $RuLL´(Cl)_2$ under *cis*- isomeric form, which require higher temperature (140–160°C; Scheme 2.11, step 2).

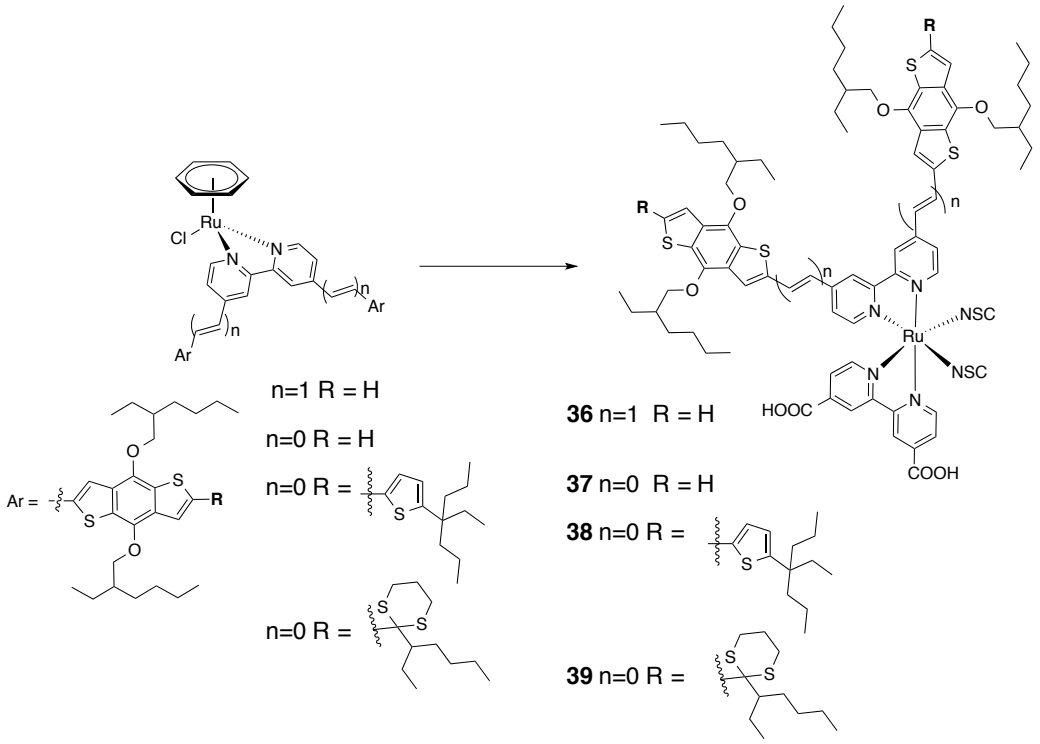

Scheme 2.11. Microwave-assisted synthesis of the (cis)*tris*-heteroleptic Ru(II) complexes under optimized conditions. Reagents and conditions: 1) **dcbpy**, DMF/PhCl (9:1), MW 130–140°C, 45 min, followed by 2) NH_4NCS, MW 140°C, 45 min (**36**: 94%; **37**: 51%; **38**: 73%; **39**: 76%). MW = Microwave, DMF = *N*,*N*-dimethylformamide, dcbpy = (2,2'-bipyridine)- 4,4'-dicarboxylic acid, PhCl = chlorobenzene

To afford the *tris*-heteroleptic Ru (II) octahedral complex $RuLL'(Cl)_2$ under *cis*-isomeric form, which require higher temperature (140–160°C; Scheme 2, step 2). The **Ru[L]** complex tailored with a positively-charged moiety displayed better solubility in DMF than the highly lipophilic starting BDT-bipyridine free ligands (**L**). As well, to balance lipophilicity against lipophobicity, **dcbpy** was dissolved in DMF (90% v/v) and added to a solution of **Ru[L]** in PhCl (10% v/v), and the resulting solution heated to reflux under MW at 130–140°C for 45 min. In this mixture of solvents, all materials were soluble. In addition PhCl, was also chosen because of its high boiling point (131ºC) close enough to that of DMF (153ºC) to reach temperatures in the range of c.a. 130–140ºC within this mixture (DMF/PhCl 9:1), required for the energetically more demanding coordination of a second bipyridine to form the octahedral (*cis)tris*-

heteroleptic Ru(II) complex. Subsequently, a large excess of NH_4NCS (50–75 eq) was added and the mixture irradiated again at 130–140°C for additional 45 min, resulting in the exchange of the chloride by isothiocyanate k^1-bonded ligands (Scheme 2, step 3). The use of a slight excess of formal Ru metal (1.1–1.3 eq) in the first step and the appropriate amount of **dcbpy** in the second step (*i.e.* 1 eq per **Ru[L]** + 2 eq per excess of Ru), induced the expected formation of the *bis*-heteroleptic Ru (II) complex *cis*-$Ru(L')_2(NCS)_2$ (*cis*- bis(isothiocyanato) bis(2,2′-bipyridyl-4,4′-dicarboxylato) ruthenium(II), also called "N3 dye") as a minor secondary product, which was nevertheless easily removed during the work-up by washing the crude with MeOH, while the excess of NH_4NCS was removed with water.

The purification of the complexes was achieved by size-exclusion chromatography (eluent THF/MeOH 7:3) affording **TT221 or 36**, **TT222 or 37**, **TT223 or 38** and **TT229 or 39** in acceptable to good yields (94%, 51%, 73%, and 76% yield, respectively). The yields were found to be quite heterogeneous, even though they always exceed at least 50% (after purification) under our optimized conditions (best yield obtained over 2–3 runs is reported for each complex). Unexpectedly, we still always obtained the *bis*-heteroleptic complex $RuL_2(NCS)_2$ (with L= $bpy(BDT)_2$) in variable proportion (c.a. 5–30% yield) as by-product. Indeed, considering that the intermediate **Ru[L]** was formed quantitatively in the first step in every cases (*vide supra*), the formation of $RuL_2(NCS)_2$ can be therefore explained by a partial scrambling reaction process through bipyridine ligands exchange (de-coordination / coordination process), either from $RuLL'X_2$ (X= Cl or NCS) or most probably from **Ru[L]**

To support our latter hypothesis, a solution of **TT229** (1eq) and **dcbpy** (2 eq) in PhCl/DMF (1:9) was heated under MW at 130–140ºC for 90 min. Under these similar conditions than those used for the synthesis, only the starting materials were recovered without formation of *bis*-heteroleptic complexes, hence supporting that the partial scrambling process must occur from **Ru[L]**.

NMR Characterisation: Example of TT221

^1H NMR spectra were obtained in $CDCl_3$, DMF [d_8], or THF [d_6] (almost insoluble in DMSO [d_6], MeOD [d_4] and acetone [d_6]). As well as for the synthesis, we had to find a proper mixture of deuterated solvents. We could record well-defined ^1H NMR spectra with sharp signals when using mixtures of $CDCl_3$ and MeOD[d4] (8:3 or 7:4). As a typical example, the ^1H NMR spectrum of **TT221** (**III**) is depicted in,

together with its corresponding free ligand **L221** (**I**), and half-sandwich complex intermediate **Ru[221]** (**II**). (Figure 2.35)

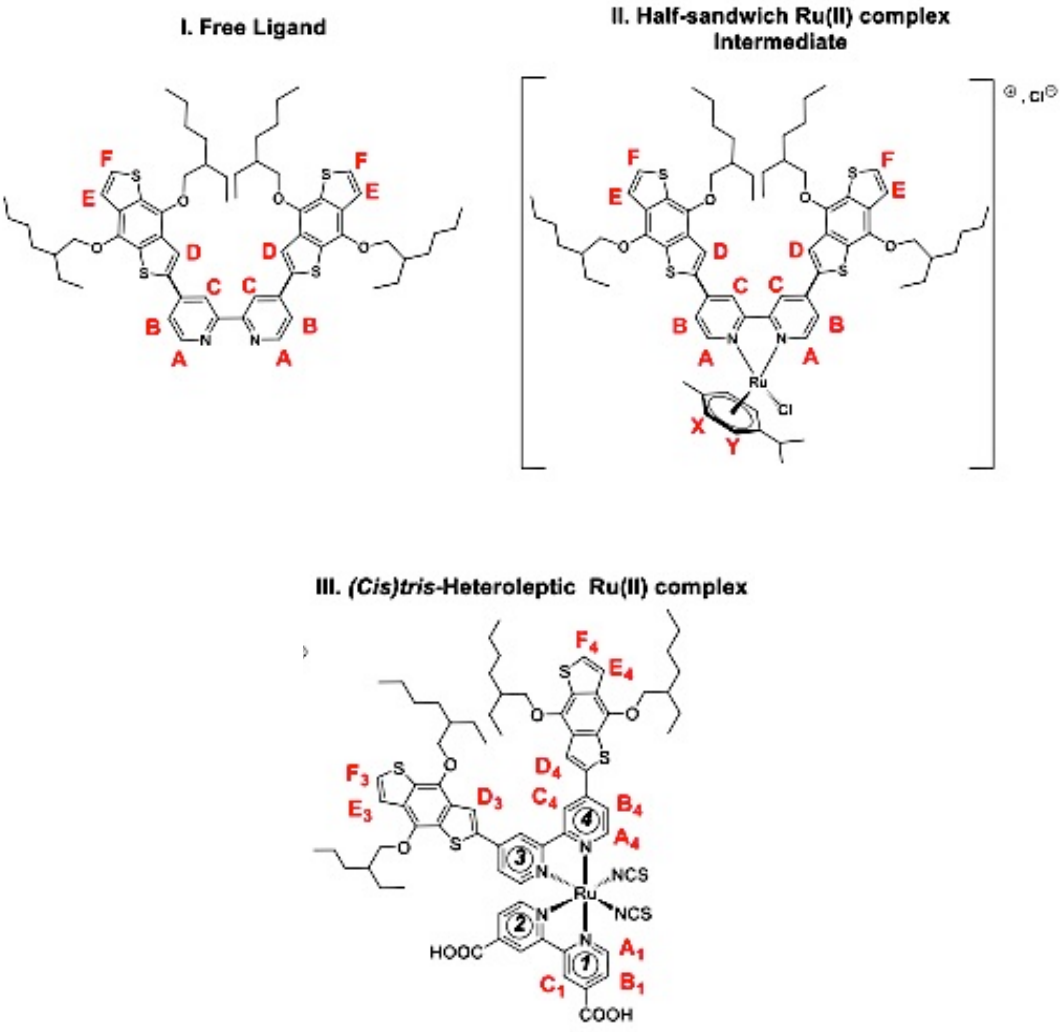

Figure 2.34. Different steps of the sinthesys of Ruthenium complex for NMR

The bipyridine moiety usually displays a characteristic AMX-type pattern of second order (300 MHz) for the A, B, C protons (with $^{3}J_{AB} \approx 5$ Hz and $^{4}J_{BC} < 1–1.5$ Hz). In addition, the two BDT-pyridine arms appear magnetically equivalent to each other, as exemplified in the NMR spectrum of **L221** that shows a characteristic AB quartet for the E and F protons and a singlet for the D protons. The half-sandwich Ru(II) complex **Ru[221]** displays similar features for the pyridil protons than the parent ligand, but with strong deshielding of the A protons (Dd ≈ +1 ppm) and shielding of the

C protons (Dd ≈ -0.7 ppm), a characteristic and general trend due to the coordination of the bipyridine ligand to the ruthenium metal centre.

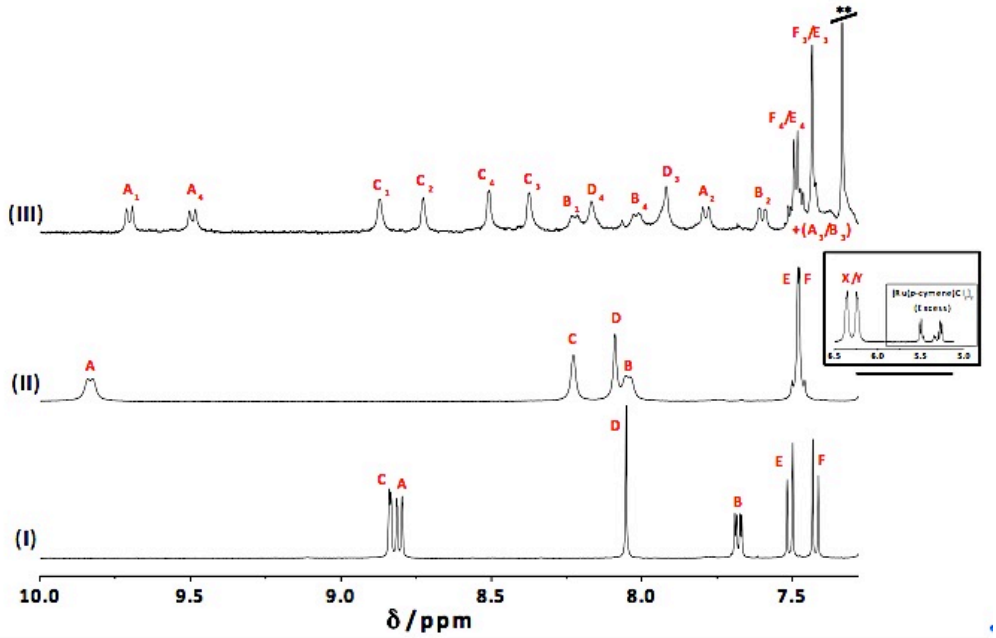

Figure 2.35. Partial ^{1}H NMR spectra (300 MHz) of (I) **L221** in $CDCl_3$, (II) crude **Ru[L221]** in $CDCl_3$, and (III) **TT221** in $CDCl_3$/MeOD[d4] (8:3), and proposed assignment based on 2D-COSY $^{1}H/^{1}H$ experiments; ** denotes the residual $CHCl_3$ peak of the $CDCl_3$ solvent.

In contrast, all pyridil protons (L and L') appear magnetically non-equivalent for the octahedral (*cis*)tris-heteroleptic Ru(II) complex. As a result, four sets of AX systems and four singlets can be observed in the NMR spectrum of **TT221**, for the twelve non-equivalent protons $A_{1\text{-}4}$, $B_{1\text{-}4}$ and $C_{1\text{-}4}$ protons. This is also evidenced by the loss of equivalency of the two BDT moieties, showing, for instance, a splitting of the aromatic protons signals ($D_{3/4}$, $E_{3/4}$ and $F_{3/4}$) and four AB systems for the methylenoxy OCH_2 protons

2.3.2.3 Synthesis of the Ru(II) complexes based on CDT

Folowing the same procedures described for the BDT complexes, the three CDT complexes **TT230 or 40**, **TT231 or 41**, and **TT232 or 42** were syntghestiseds. The ruthenium heteroleptic complex was obtained in a one-pot, three-step reaction, according to general procedures described previously for BDT .

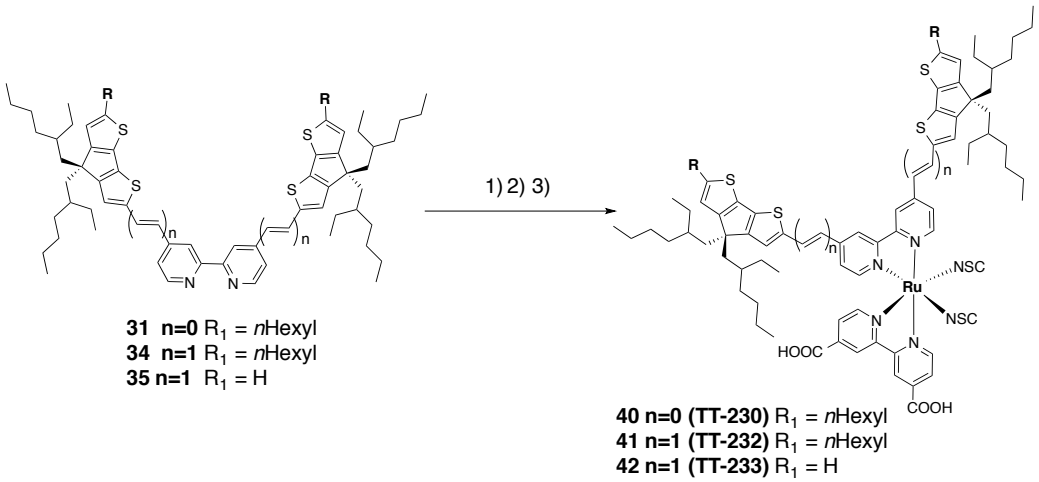

Scheme2.4. Microwave-assisted synthesis of the (cis)*tris*-heteroleptic Ru(II) complexes based on CDT Reagents: 1) $CHCl_3$/EtOH (1:1), MW 60–70°C, 45 min. 2) dcbpy, DMF/PhCl (9:1), MW 130–140°C, 45 min, followed by 3) NH_4NCS, MW 140°C, 45 min (**40**: 40%, **41**: 70% and **42**: 70%)

All bipyridyl donor-antenna derivatives (**31**, **32** and **35**) were converted into the desired complexes by using dichloro(p-cymene)ruthenium(II) dimer as reagent for the metallation reaction. This particular Ru(II) precursor provides the opportunity to obtain the desired heteroleptic octahedral ruthenium(II)bis(bipyridyl)$(NCS)_2$ complexes via an efficient one-pot synthesis by subsequent addition of the respective ligands followed by the anchoring molecule and finally adding an excess of NH_4SCN.

NMR Characterisation: Example of TT230

The bipyridine moiety usually displays a characteristic AMX-type pattern of second order (300 MHz) for the A, B, C protons (with $^3J_{AB} \approx 5$ Hz and $^4J_{BC} < 1–1.5$ Hz). In addition, the two CDT-pyridine arms appear magnetically equivalent to each other, like in the BDT-bipyridine. On the other hand and in the same path ok BDT, all pyridyl protons (L and L') appear magnetically non-equivalent for the octahedral (cis)trisheteroleptic Ru(II) complex. As a result, four sets of AX systems and four singlets can be observed in the NMR spectrum of **TT230**, for the twelve non-equivalent protons A1-4, B1-4 and C1-4protons

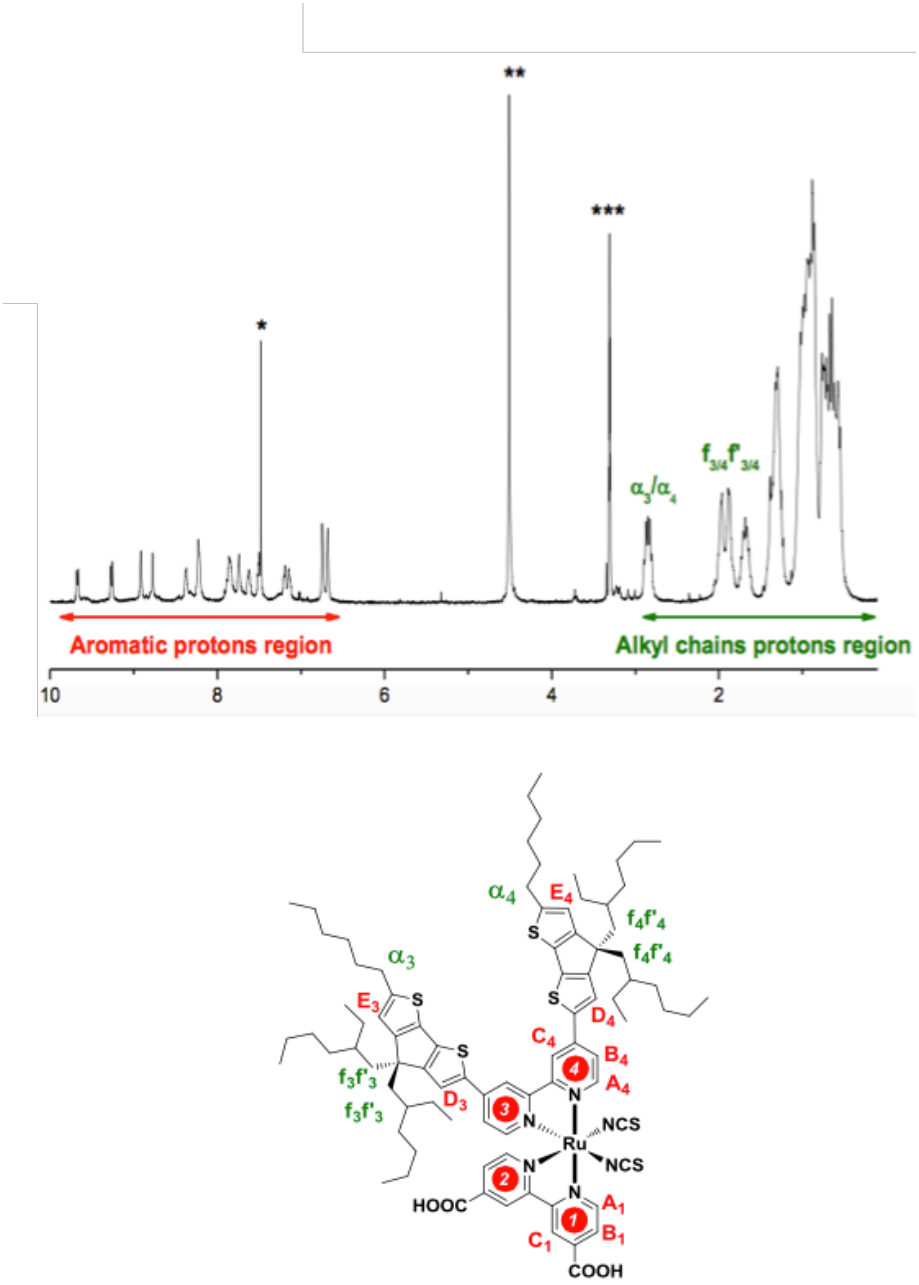

Figure 2.36. ^{1}H NMR spectrum of TT-230 (CDCl3 /MeOD-d4; 300 MHz) (* denotes the residual peak of CDCl3, ** and ***denotes the residual solvent peaks of MeOD-d4).

2.3.3 Spectral properties

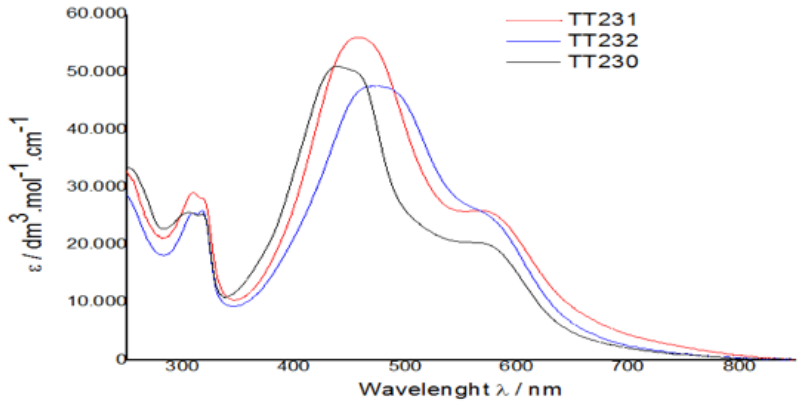

Figure 2.37. Uv- Spectral of Rutenium Colplex with CDT ligands base Ruthenium complex in DCM

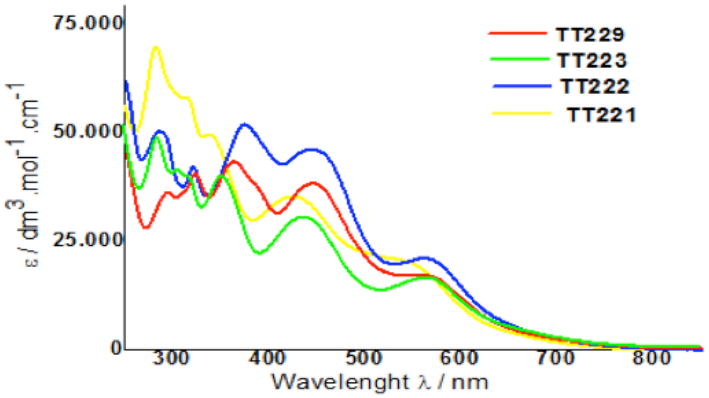

Figure 2.38. Uv- Spectral of Rutenium Colplex with BDT ligands base Ruthenium complex in DCM

The UV-visible spectra of dyes in solution (CH_2Cl_2) are depicted in Figure 2.37 and Figure 2.38, and absorption data summed up in Table 2.2. Both dyes display there distinct bands: the first one in the UV region centered at around 320 nm was attributed to the intraligand charge-transfer transition of the dcapy moiety ($\pi \rightarrow \pi *$ transition, $ILCT_1$); the main band centered at 440-500 nm was attributed to the overlap between

the intraligand charge-transfer band of the ancillary group bipy$(BDT)_2$ or bipy$(CDT)_2$ moiety ($\pi \rightarrow \pi^*$ transition, $ILCT_2$) with major contribution, and the first metal-to-ligand charge-transfer transition (MLCT) Ru(II) heteroleptic complex with minor contribution. The third band (shoulder) at around 580 nm was attributed to the second MLCT transition.

All dyes display strong absorption, especially in the 400-700 nm visible range with relatively similar and high absorption coefficients up to 50 000 $mol^{-1}.cm^{-1}L$.

Remarkably, the extension of π-conjugation between the two CDT moieties and bipyridine unit trough the vinylene linkage in **TT232** causes important changes of the main absorption band (ILCT2+MLCT1), with a maximum redshifted by 34 nm and extended to the red region of about 80 nm, with respect to TT-230.

Table 2.2. UV-visible data of the ruthenium(II) complexes in solution (CH_2Cl_2).

Complex	$l_{max}1$[a] (log e)[b]	$l_{max}2$[a] (log e)[b] ILCT1	$l_{max}3$[a] (log e)[b] ILCT2[d] + MLCT1	$l_{max}4$[a] (log e)[b] MLCT2
36-TT221	282 (4.85)	338 (4.70)	425 (4.55)	≈ 560[c] (4.28)
37-TT222	285 (4.71)	320 / 373 (4.63 / 4.72)	441 (4.67)	559 (4.33)
38-TT223	285 (4.68)	352 (4.60)	437 (4.48)	565 (4.21)
39-TT229	294 (4.56)	322 /362 (4.61 / 4.64)	446 (4.58)	≈ 560[c] (4.20)
40-TT230	297	317 (2.55)	439 (5.11)	≈ 581 [c] (1.95)
41-TT232	297	318 (2.60)	473 (4.77)	≈ 582 [c] (2.41)
42-TT233	297	318 (2.60)	473 (4.77)	≈ 582 [c] (2.41)

[a] λ_{max} are given in nm.; [b] ε are given in $mol^{-1} \cdot dm^3 \cdot cm^{-1}$;[c] Broad shoulder; [d] Main contribution iscoming from the ILCT2 band; ILCT1= $\pi - \pi^*$ dcapy intraligand charge-transfer transition; ILCT2= $\pi - \pi^*$ bipy(CDT)2; intraligand charge-transfer transition MLCT= Metal-to-Ligand Charge-Transfer transition

2.3.4 Photovoltaic performances in TiO_2-DSSC

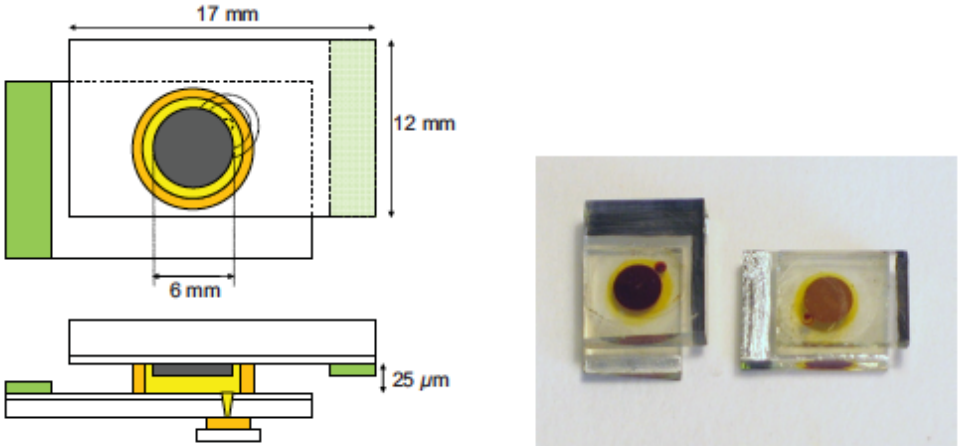

Figure 2.39. A sketch of DSC device and a picture of fabricated ones used for photovoltaic tests

2.3.4.1 Photovoltaic performances in TiO_2-DSSC of CDT

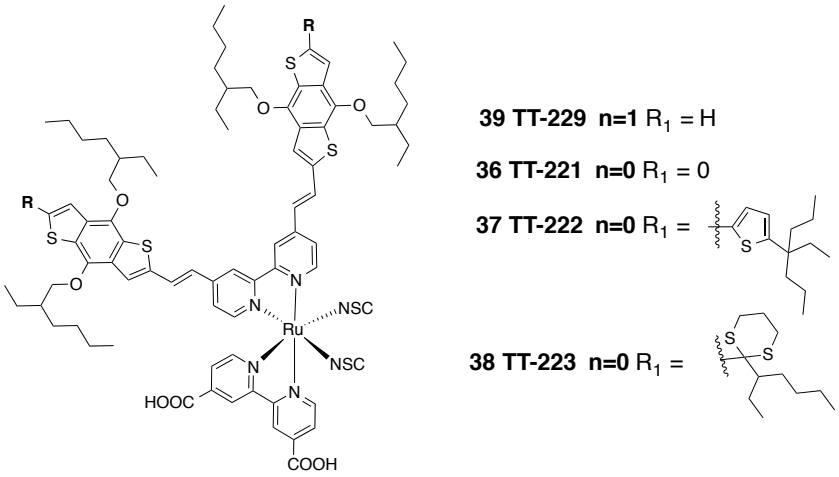

Figure 2.40. Sensitizers TT-221, TT-222, TT-223 and TT-229

The photovoltaic performances of the four complexes were tested in TiO_2-DSSC on [5+4] mm thick films, which consist of a 5 mm thick active layer and an additional 4 mm scattering layer, and using an iodine-based electrolyte A (Table 2.5). Under

identical conditions, the device made with **TT222** gave significantly larger V_{OC} (687 mV) and JSC (8.66 mA•cm^{-2}) than those made with the other sensitizers, achieving the best overall efficiency of 4.0%. The better optical properties of **TT222** due to the extension of conjugation through the additional thiophene moieties (redshift, and broadening of the absorption bands, accompanied with higher molecular extinction coefficients) should explain the larger observed JSC. On the other hand, the terminal bulky 1,1-dipropylbutyl groups in **TT222** should reduce the electron recombination process at the electrolyte/TiO_2 interface,[178-183] which explains well the 60–90 mV increase in the V_{OC} in comparison with the other dyes.

Table 2.5. Photovoltaic data of the devices[a] made with TT dyes on [5+4][b] mm thick TiO_2 films using the iodine-based liquid electrolyte A,[c] under simulated one sun illumination (AM1.5G) and active area of 0.159 cm^{-2}.

Dye	V_{OC} (mV)	J_{SC} (mA/cm²)	FF (%)	h (%)
TT221	630	7.60	70	3.4
TT222	687	8.66	67	4.0
TT223	610	6.05	76	2.8
TT229	598	6.81	75	3.1

[a] Two devices of equal quality were made for each dyes; the values obtained for the best cell are presented in each case. [b] The TiO_2 films have a total thickness of 9 mm consisting of a 5 mm thick TiO_2 active layer and an additional 4 mm of scattering layer. [c] Electrolyte A is composed of 1 M propyl methyl imidazolium, 0.5 M 4-tertbutyl pyridine, 0.03 M iodide, 0.05 M guanidinium thiocyanate, 0.05 M lithium iodide, in a mixture of acetonitrile and butylnitrile.

Optimization of the photovoltaic performances of TT222/DSSC

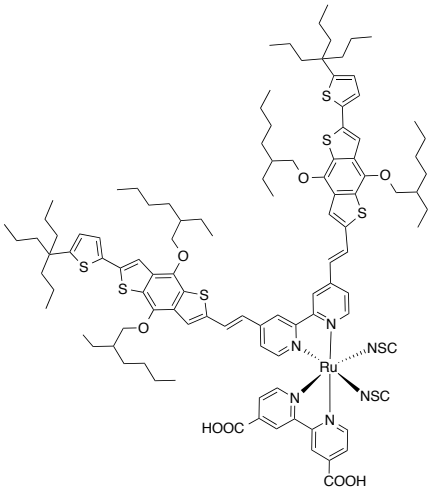

Figure 2.41. Sensitizers **TT222.**

TT222 gave significantly larger V_{OC} (687 mV) and J_{SC} (8.66 mA•cm^{-2}) than those made with the other sensitizers, achieving the best overall efficiency of 4.0%. The better optical properties of **TT222** due to the extension of conjugation thought the additional thiophene moieties (redshift, and broadening of the absorption bands, accompanied with higher molecular extinction coefficients) should explain the larger observed J_{SC}. On the other hand, the terminal bulky 1,1-dipropylbutyl groups in **TT222** should reduce the electron recombination process at the electrolyte/TiO_2 interface,[184] which explains well the 60–90 mV increase in the V_{OC} in comparison with the other dyes. Next, we carried out the optimization of the **TT222**/DSSC devices regarding the addition of co-adsorbent (CHENO) or neutral surfactant (Triton) in the dye-uptake solution, electrolyte composition and thickness of the active layer (Table 2.6). The role of the co-adsorbent is to decrease dye-aggregation, but except slightly improved FF, the V_{OC} and J_{SC} were found significantly lower in the presence of CHENO, resulting in a drop of the overall efficiency (3.3% *vs* 4.0% without CHENO under identical conditions). This seems to point out that dye-aggregation must be negligible in this case. The use of Triton did not help to improve the performance of the device neither.

Next, we examined three other types of electrolytes, one based on Co(III/II)tris(bipyridine) redox couple, and two other iodine-based (B and C) which

mainly differ in higher content of LiI (0.1 M and 0.2 M, respectively) than electrolyte A (0.05 M). When using the cobalt-based electrolyte, an impressive 92 mV improvement in the V_{OC} was observed for the **TT222**+CHENO device in comparison with the iodine-based electrolyte A.

However, as reported in other cases for Ru(II) heteroleptic complex dyes,[185] the J_{SC} concurrently dropped drastically to 4.7 mA•cm^{-2} resulting in a lower overall PCE of 2.7%. Next, we focused on the optimization of LiI concentration for the iodine-based electrolyte. Higher content of LiI produce a downshift of the TiO_2 conduction band (CB), which can improve the electron-injection for dyes that have a low-lying LUMO, and hence produce larger J_{SC}. As a drawback, lowering the TiO_2 CB concurrently decreases the V_{OC}.

Under identical configuration (**TT222** adsorbed on [5+4] mm films), the J_{SC} increased significantly from 8.66 mA•cm^{-2} with electrolyte A at 0.05 M LiI, to 9.17 mA•cm^{-2} with electrolyte B at 0.1 M LiI. Higher content of LiI (0.2 M) in electrolyte C did not improve further the J_{SC}, which suggests that the electron-injection process is already optimum with electrolyte B. At the same time, the V_{OC} dropped from 687 mV (electrolyte A), to 665 mV (B) and 655 mV (C).

Thus, the better balance between the gain in the J_{SC} vs loss in the V_{OC} was obtained with electrolyte B, for which the device achieved the best overall PCE of 4.3%. Finally, we optimized the **TT222**/DSSC devices regarding the thickness of the active layer. Thicker films can help to improve the J_{SC} in two cases: if the dye-loading is low and/or for dyes that display low molecular absorption coefficient (the latter is usually the case for common Ru(II) complex). In these two cases, because higher amount of dyes are adsorbed on the surface, larger J_{SC} can be obtained. As a counterpart, thicker films results in lower V_{OC} because of higher resistance process, and lower fill factor because of increased recombination processes. Using the same electrolyte B, an improvement in the J_{SC} could be obtained with thicker [10+4] mm (9.84 mA•cm^{-2}) than thinner [5+4] mm films (9.14 mA•cm^{-2}), and did not improve much more on [12+4] mm films (10.11 mA•cm^{-2}). As a result, the overall efficiency was further improved to 4.5% for both devices on [10+4] mm and [12+4] mm thick films, using electrolyte B.

Table 2.6. Photovoltaic data of the devices[a] made with dye **TT222** using different configurations under simulated one sun illumination (AM1.5G) and active area of 0.159 cm^{-2}.

Electrolyte	Dye solution	TiO_2 thickness (mm) [b]	V_{OC} (mV)	J_{SC} (mA•cm²)	FF (%)	h (%)
A[c] (0.05 M LiI)	**TT222**	[5+4]	687	8.66	67	4.0
	TT222+Triton (1:1)	[5+4]	640	6.70	77	3.3
	TT222+Cheno (1:1)	[5+4]	642	6.61	77	3.3
Cobalt[d]	**TT222**+Cheno (1:1)	[4+4]	734	4.70	77	2.7
B[e] (0.1 M LiI)	**TT222**	[5+4]	665	9.17	71	4.3
	TT222	[10+4]	650	9.84	71	4.5
	TT222	[12+4]	653	10.11	69	4.5
C[f] (0.2 M LiI)	**TT222**	[5+4]	655	9.23	69	4.2
	TT222	[12+4]	616	9.76	68	4.1

[a] Two devices of equal quality were made for each configuration; the values obtained for the best device are presented [b] The first value in brackets refers to the TiO_2 active layer; the second one to the scattering layer. [c] For composition of electrolyte A, see footnote [c] of Table 2. [d] The cobalt-based electrolyte was composed of 0.05 M $Co(Bipy)_3(PF_6)_3$, 0.2 M $Co(Bipy)_3(PF_6)_2$, 0.1 M $LiClO_4$, and 0.2 M 4-tertbutyl pyridine in AcCN. [e] Electrolyte B was composed of 0.1 M lithium iodine, 0.6 M 1,3-dimethylimidazolium iodide, 0.5 M 4-tertbutyl pyridine, 0.03 M iodine and 0.1 M guanidinium thiocyanate, in AcCN. [f] Electrolyte C has the same composition than B, except 0.2 M of lithium iodine.

2.3.4.2 Photovoltaic performances in TiO_2-DSSC of CDT

A transparent fluorine-doped tin oxide conducting glass (NSG10, Japan) was cleaned using ethanol and water followed by an ultrasonic cleaning in DeconnexTM solution for 30 min. The electrodes were then washed with water and ethanol. To remove the organics, a further thermal treatment was done at 500 °C for 30 min. The clean FTO glass was treated twice with TiCl4 (40 mM, 30 min, 75 °C). Two different TiO2 pastes (transparent layer and scattering layer) were screen printed on to the $TiCl_4$ pretreated electrode and followed a series sintering step as described elsewhere in the literature. A 9 µm thickness for the transparent layer (20 nm particles) and another 5 µm for the scattering layer (400 nm particles) were estimated. The photoanodes were further treated with $TiCl_4$ following the steps described above. The $TiCl_4$ post treatment was done to ensure better electronic contact between nanoparticles.

The photovoltaic properties and dye-loading for each DSSC devices made with sensitizers **TT230**, **TT232**, **TT233** or benchmark **Z907** are summed up in Table 2.3. Both **TT-230**, **TT-232** and **TT-233** reached similar dye-coverage on the TiO_2 surface. Hence, considering better optical properties for **TT232** or **TT233** it can be assumed a superior light-harvesting efficiency (LHE) than for **TT230**.

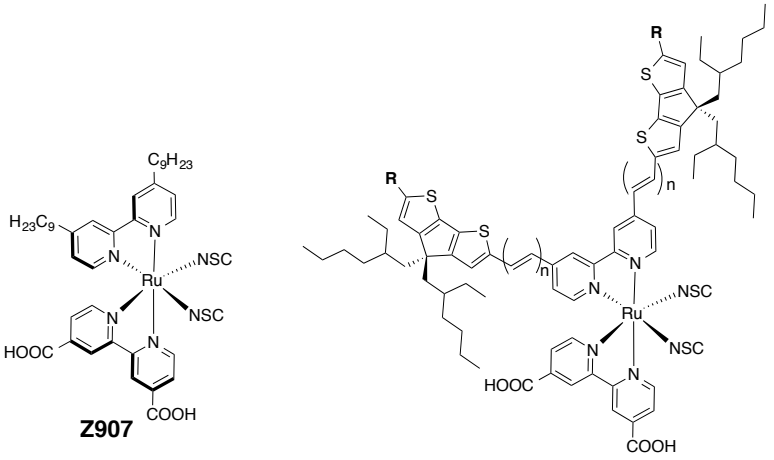

Figure 2.42. Sensitizers **TT230**, **TT232**, **TT233** and benchmark **Z907**

However, all individual photovoltaic parameters (JSC, VOC, FF) and hence the overall PCE were found to be much lower for **TT232** or **TT233** than **TT230**. Assuming superior LHE for **TT232** and **TT233** than for **TT230** and dye-loading surface coverage likewise similar for both dyes, the difference in the J_{SC} (7.4-7.6 vs 12.3 $mA.cm^{-2}$, respectively) can be directly ascribed to a much lower adsorbed photon-to-current efficiency for **TT232** or **TT233**. The presence of the double-bond linkages of the bipy$(CDT)_2$ moiety (ancillary group) in **TT232** and **TT233** should perturb and downshift significantly the LUMO levels of the dye, which should disfavor the electron-injection of the excited dye in the TiO_2 conduction band.

As the HOMO level is mostly delocalized over the Ru center and NCS moieties in **N3**-type analogues[186], we expect only few differences in regeneration of the three dyes **TT230**, **TT-232** and **TT-233**. Moreover, given the same bulky substitution for **TT230** and **TT-232**, we expect none or very little dye aggregation, which should disable any dye-dye* deactivation channel.

The use co-adsorbent (CHENO), surfactants or electrolite was tested to improve the photovoltaic properties, and resulted in a degradation of the overall efficiency of the cell. In two cases only had reprentative positive resultsin, it was explaining in this charter. The use co-adsorbent (CHENO) or surfactants did not help to improve the photovoltaic properties of the other dyes, and resulted in a degradation of the overall efficiency of the cell.

Table 2.3. Photovoltaic data of the devices[a] made with TT dyes on [5+4][b] mm thick TiO_2 films using the iodine-based liquid electrolyte A,[c] under simulated one sun illumination (AM1.5G) and active area of 0.159 cm^{-2}.

Dye	V_{OC} (mV)	J_{SC} (mA/cm²)	FF (%)	h (%)
Z907	698.7	12.8	78	7.0
TT-230	**654.8**	**12.3**	**76**	**6.1**
TT-232	603.2	7.4	72	3.2
TT-233	605.2	7.6	70	3.1

[a] Two devices of equal quality were made for each dyes; the values obtained for the best cell are presented in each case. [b] The TiO_2 films have a total thickness of 9 mm consisting of a 5 mm thick TiO_2 active layer and an additional 4 mm of scattering layer. [c] Electrolyte A is composed of 1 M propyl methyl imidazolium, 0.5 M 4-tertbutyl pyridine, 0.03 M iodide, 0.05 M guanidinium thiocyanate, 0.05 M lithium iodide, in a mixture of acetonitrile and butylnitrile.

Optimization of the photovoltaic performances of TT230/DSSC

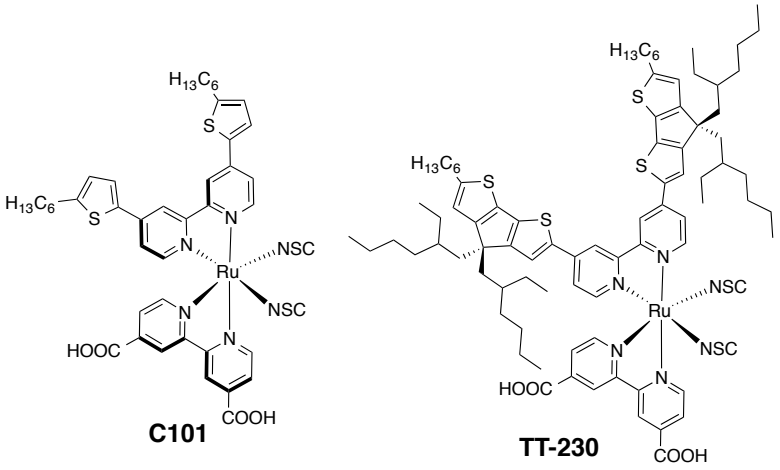

Figure 2.43. Sensitizers **TT-230**, and **C101**

The current-voltage characteristics of **TT230** and **C101** dye-sensitized solar cells (Figure 2.43) were measured at AM 1.5 G solar conditions (100 mW/cm^2). With the $[Co(bpy)_3]^{3+/2+}$ redox mediator, the reference **C101** exhibits an open-circuit potential of 735 mV with the current density of 6.5 mA/cm^2. When using the **TT230** dye that contains bulky substitutions, the V_{OC} increased to ~775 mV, which is 40 mV higher than our reference device **C101**. The coadsorbent chenodeoxycholic acid (cheno) in the dye solution further enhanced the V_{OC} to ~805 mV. The photovoltaic data and *J*-V curves are displayed in Figure 2.44 and Table 2.4.

The current-voltage properties measured under dark shows a dark current onset at 550 mV for the reference device made with **C101** sensitizer, whereas the onset shifts to higher voltages at around 625 mV for **TT230**, which is 75 mV higher. The dark current represents the back flow of electrons from the titanium dioxide to the redox mediator.[187,-189] When the $_nE_F$ of electrons in TiO_2 reaches a potential of 550 mV with respect to the Nernst potential of the redox mediator, the electrons already start to flow from the TiO_2 to the electrolyte. However, when the **TT230** dye is used, the onset shifts to 75 mV, which is responsible for higher open-circuit potential in the latter case.

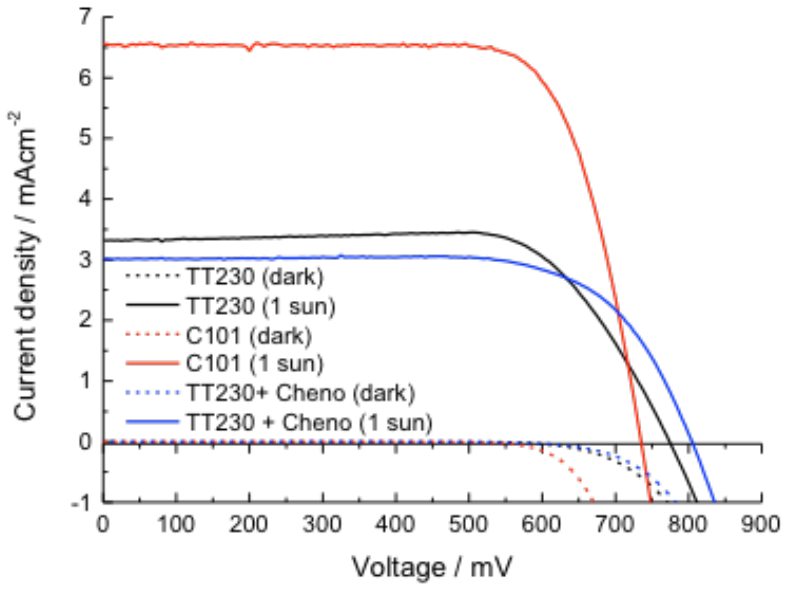

Figure 2.44. Current-voltage curves of the dye-sensitized solar cell under dark and under illumination (AM 1.5 G solar irradiance, 100 mW/cm^2 photon flux).

Table 2.4. **Photovoltaic parameters measured at AM1.5G solar irradiance (100 mW/cm^2) of the dyes sensitized solar cells employing the cobalt-based electrolyte.**[a]

[a] **The cobalt complex used in this study is the Co(III/II) tris(2,2'-bipyridine) complex, $[Co(bpy)_3]^{3+/2+}$.**

Dye	J_{SC} (mA/cm^2)	V_{OC} (mV)	Fill factor (%)	Ƞ (%)
TT230	3.3	**774.0**	72.5	1.8
C101	6.5	**735.1**	74.7	3.6
TT230+Cheno	3.0	804.4	70.0	1.6

The open-circuit potential of a standard DSC is affected by three different factors, namely the distribution of the surface trap states in TiO_2, the recombination rate (k_{rr}) of the photogenerated electrons from the conduction band of titanium dioxide to

the oxidized redox species, and the redox potential of the electrolyte. In the discussion below, we analyzed each parameter separately to find the origin of the change in the open-circuit potential. As the electrolyte used in this study is based only on the $[Co(bpy)_3]^{3+/2+}$ redox mediator, the change in V_{OC} due to the variation in the redox potential is negligible. Shows Figure 2.45 the trap state distribution of electrons measured as a function of voltage by the transient photocurrent decay technique.

The distribution shows an exponentially increasing trend when moving towards the conduction band of the titanium dioxide, consistent with the literature.[190] However, there exists a difference when using **C101** or **TT230** dyes. Due to the possible variation in the dipole moment of the dyes, **C101** possesses deeper trap states distribution compared to **TT230**, with and without cheno. Therefore, for a given charge density and recombination rate, the electron quasi-Fermi level of electrons in TiO_2 is positioned more negatively for **TT230** than for **C101**.

The second parameter, the recombination rate of the photogenerated electrons for two different dyes, was analyzed using transient photovoltage decay measurements). (Figure 2.45)

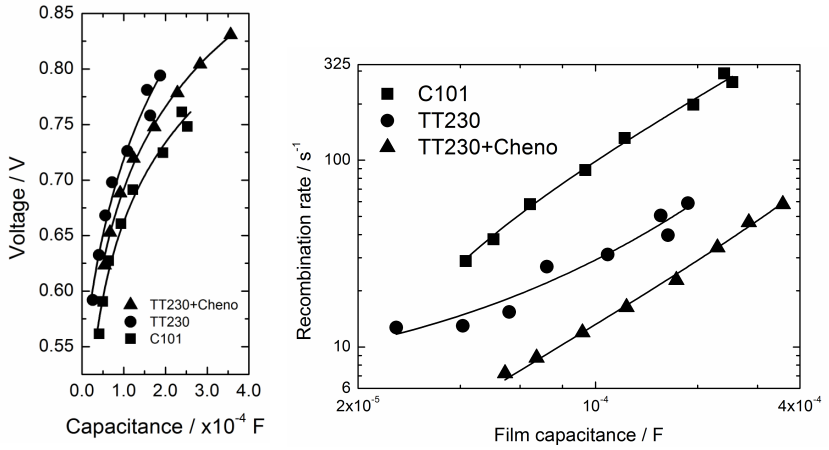

Figure 2.45. The distribution of surface electronic trap states in the titanium dioxide film sensitized with TT-230 and C101 dye molecules.(on the left) The recombination rate of the photogenerated electrons measured as a function of charge density for TT-230 and C101 dye sensitizers.(on the right)

It can be noticed that, at any given charge density (proportional to the capacitance), the k_{rr} is higher for the solar cells sensitized with the **C101** compared to

the **TT230** dye. Following the electron injection from the excited state of the dye into the TiO_2 conduction band, the steady state electron density maintained in TiO_2 is higher for the devices made with **TT230** (due to slower electron back reaction kinetics), which in turn shifts negatively the quasi-Fermi level of electrons increasing the open-circuit potential of the device. The reduction in the recombination kinetics can be visualized based on the structure of the dye-sensitizers. Compared to the reference **C101**, the **TT230** dye has bulkier substituents that tend to keep the $[Co(bpy)_3]^{3+}$ complex away from the TiO_2 surface, which in turn reduces the recombination loss of electrons to the oxidized redox mediator. Thus, in the case of Ru(II) bipyridyl complex sensitizers, a bulky attachment is needed to attain higher V_{OC} similar to all-organic dyes. The short-circuit current is found to be lower for **TT230**, which could be attributed to the lower dye loading on the titania mesoporous film (Table 2.4).

In this work we identified that bulky substituents are needed to block the back reaction in the Ru(II) complex based DSC when employing Co^{2+}/Co^{3+} redox mediator. We have compared two different Ru(II) dye sensitizers, with different substituents (**C101** and **TT-230**). The device made with the bulky **TT230** sensitizer exhibits higher open-circuit potential compared to our reference **C101** dye. The reason for this variation is correlated to the higher dark current density for the latter. Our recombination studies show that devices made with **TT-230** exhibit lower recombination rate and explain why the dark current onsets at higher voltages compared to the reference **C101**.

2.4 SUMMARY AND CONCLUSIONS

This study reports on the synthesis, characterisation and performance as photosensitizers in DSSSC of two family of Ru(II) complexes incorporating either benzofuseddithiophene (BDT)- or cyclopentanedithiophene functionalized bipyridine moieties , acting as ancillary ligands, meanwhile the other 4,4'-dicarboxylic acid 2,2'-bipyridine acts as the anchoring group and acceptor part in the complex (Figure 2.8). The BDT and CDT ligands are connected either through a single- or a double bounded type of linkage to the bypiridine (n = 0 or 1) and decorated with different lateral and/or terminal hydrophobic alkyl chains. These complexes showed remarkable difference in terms of optical properties and performances in DSSC.

- The CDT-dyes differ in the type of linkages of their ancillary group, either directly linked (**TT230**) or vinylene-linked (**TT232** or **TT232**). **TT230** sensitized cell achieved the best efficieny with a maximum solar-to-electric power conversion (PCE) of 6.1 % under standard AM 1.5 G standard conditions. The vinylene-linked dyes **TT232** and **TT232 (**with and without the lateral alkyl chains, respectively) achieved lower PCE of about 3% under same experimental conditions despite improved light-harvesting properties; namely, broader and redshift absorption.
- **TT-230** sensitizer was adapting to cobalt electrolyte systems. The dye provides an example of a bulky Ru(II)-dye reaching high open circuit voltage (V_{OC} = 774.0 mV) in DSC in combination with the Co^{3+}/Co^{2+} redox couple, and hence opens up an avenue to engineer a new generation of highly efficient sensitizers.
- Four (cis)tris-heteroleptic Ru(II) complexes based on benzo[1,2-b:4,5-b']dithiophene (BDT) were successfully synthetized. Owing to their amphiphilic character with high lipophilicity induced by the BDT moieties against lipophobicity brought by the two COOH groups, the synthetic conditions were found crucial and needed to be adapted, as well as the relevance of the intermediate halfsandwichcomplex involved in the first step reaction. After optimization of conditions using a MW-assisted method andadequate mixture of solvents, the target complexes wereobtained in good to excellent yields (50–91%), although partialscrambling were still observed in variable proportion in every cases. This work provides a guideline for the synthesis of other amphiphile tris-heteroleptic Ru(II) complexes with high

lipophiliccharacter, and reports on the first examples of Ru(II) complex based on BDT and their application in DSSC.

2.4 RESUMEN Y CONCLUSIONES

En este capitulo se presentan dos series de complejos de Ru(II) en fotosensibiliadores DSSSC, coordinados con ligandos bipiridinicos derivador del CDT o BDT con diferentes sustisuciones laterales y con doble enlace o no entre el ligando y la bipirina (n = 0 o n = 1). Dotados de con un grupo acido como grupo de anclaje. No todos ellos mostraron eficiencias similares.

- Los ligandos derivados del CDT ya sea directamente unidos a la bipiridina (**TT230**) o unidos por medio un enlace vinileno (**TT232** o **TT233**). Las células solares sensibilizadas con **TT230** lograron una conversión máxima de energía solar a eléctrica (PCE) de 6,1% bajo las siguientes condiciones: AM 1,5G estándar; mientras que el que posee el vinileno con o sin cadenas laterales los valores en iguales condiciones no superan el 3,2%
- Por otra parte, se adapta al electrolito de complejos de cobalto el dispositivo sensibilizado con TT-230. Este dispositivo es un ejemplo de DSSSC de complejos de Ru(II) voluminosos en los que se ha alcanzado un voltaje de tencion de circuito abierto (V_{OC} = 774.0 mV) elevado y por lo tanto se abre una nueva via para diseñar una nueva generación de sensibilizadores eficientes.
- Por ultimo, se han sintetizado cuatro complejos derivados de BDT con carácter amfifilico debido a las unidades de BDT que le dan caractes lipófilo y por otro lado las unidades con los dos grupos COOH que le proporcionan carácter lipofoba. Por otro lado, con este ejemplo se ha explicado el mecanismo intermedio de la formacin de los complejos para proporciona una guía para la síntesis de Ru (II) complejos de tris heteroléptico en microondas consiguiendo rendimientos excelentes (50-91%)

2.5 EXPERIMENTAL SECTION

In this Experimental Section, the preparation and characterization of the compounds has been organized following the order as they appear in the text.

Chemical reagents were purchased from Aldrich Chemical Co., Acros Organics, or Fluka Chemie, Alfa Aesar and were used without further purification. The monitoring of the reactions has been carried out by thin layer chromatography (TLC), employing aluminium sheets coated with silica gel type 60 F254 (0.2 mm thick, Merck). Purification and separation of the synthesized products was performed by column chromatography, using silica gel Merck-60 (230-400 mesh). The Size Exclusion Chromatography (SEC) was performed using Bio-Beads S-X1 (200-400 mesh).

2.5.1 Synthesis of functionalized bipyridines:

2.5.1.1 Synthesis of 4,4'-dibromo-2,2'-bipyridine

Compound (1)

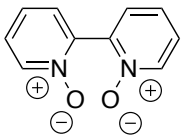

To a stirred solution of 2,2´-bypiridine (6 g, 38.5 mmol, 1 eq) in acetic acid glacial (40 ml) was added drop by drop a 30 wt.% solution of H_2O_2 in H_2O (15 ml) the temperature was keeped between 70-80 °C. At the end of the addition, the reaction mixture was heated to 80 °C for 8h. After cooling to r.t., the colourless solution was added over acetone (500 ml) yielding a white solid precipitate. The solid was filtrated off, washed with hexanes and recrystallize in water to obtain the product as a white solid (6.4 mg). Yield : 94%.

^{1}H-RMN (300 MHz, CDCl3), δ (ppm): 8.49-8.44 (m, 2H), 7.88-7.80 (m, 2H), 7.78-7.71 (m, 4H).

IR-TF (KBr) ν (cm^{-1}): 3481 (ArC-H), 3077, 1595, 1560, 1498 (C=C), 1326, 1254, 1132, 751.

EM (IE), *m/z*: 188.2 $[M]^+$ (100%).

Compound (2)

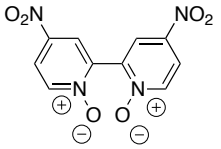

To a stirred solution of 2,2'-bipyridine-1,1'-dioxide (**1**) (4.5 g, 23.9 mol) in H_2SO_4 (13 ml) was added carefully fuming HNO_3 (10 ml) at 0 °C. Next, the reaction mixture was heated to 100 °C for 10h. After cooling to rt, the colourless solution was added carefully over a mixture of ice/N_2(l) under vigorous stirring, which produced gas release (N_2O_4). The mixture was stirred and let to reach r.t., resulting to the formation of a yellow precipitate. The solid was filtrated off, washed with H_2O (3x50ml) to obtain the product as a yellow solid. (4.5g). Yield : 70%

^{1}H-NMR (300 MHz, $CDCl_3$), δ (ppm): 8.68 (d, 2H, $J_{m,3\text{-}5}$ = 3.42 Hz H-3, H-3'), 8.58 (d, 2H, $J_{o,5\text{-}6}$ = 7.32, H-6, H-6'), 8.36 (dd, 2H, $J_{o,5\text{-}6}$ = 7.30, $J_{m,3\text{-}5}$ = 2.92 Hz, H-5, H-5').

IR-TF (KBr) ν (cm^{-1}): 3077, 1510 (NO_2), 1498 (C=C), 1340 (NO_2) 1326, 1290 (N-O), 1254, 759.

EM (IE), m/z: 278.2 $[M]^+$ (100%).

Compound (3)

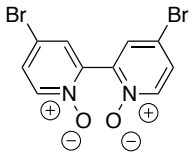

To a stirred suspension of 4,4'-dinitro-2,2'-bipyridine-1,1'-dioxide (**2**) (2.0 g, 7.0 mmol) in AcOH glacial (30 ml) at 60 °C, was added, drop by drop acetyl bromide (15.6 ml, 21 mmol). The reaction mixture was heated to reflux for 2 h. After cooling to r.t., the solution was poured over 300 g of crushed ice, and acidic media neutralized by

the addition of a 15% $NaHCO_3$ aqueous solution. The resulting precipitate was filtrated off to obtain the product as a yellow solid. (1.1 g). Yield : 44%

Pf: 227-230 °C.

^{1}H-RMN (300 MHz, DMSO-*d_6*), δ (ppm): 8.25 (d, $J_{o,5-6}$ = 7.30Hz, 2H, H-6, H-6'), 7.99 (d, $J_{o,5-6}$ = 2.80Hz, 2H ,H-3, H-3'), 7.74 (dd, $J_{m,3-5}$ = 2.80, $J_{o,5-6}$ = 7.01Hz, 2H,H-5, H-5').

IR-TF (KBr) ν (cm^{-1}): 3077, 1595, 1498 (C=C), 1248, 1261, 752.

EM (IE), *m/z*: 345.9 $[M]^+$ (100%).

Compound (4)

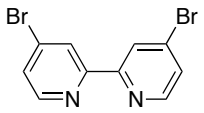

To a stirred suspension of 4,4'-dibromo-2,2'-bipyridine 1,1'-dioxide (**3**) (1.0 g, 2.9 mmol) in dry $CHCl_3$ (25 ml) at -5 °C was added drop by drop phosphorus tribromide (4 ml, 42 mmol). At the end of the addition, the reaction mixture was heated to reflux for 1 h. After cooling to r.t., the solution was poured over 300 g of crushed ice and was quenched by the addition of a 25% NaOH aqueous solution. The precipitate was filtrated off to obtain the product as a yellow solid.Yield : 66%

Pf: 141-144 °C.

^{1}H-RMN (300 MHz, $CDCl_3$), δ (ppm): 8.64 (d, J = 1.66, 2H, H-3, H-3'), 8.52 (d, J = 5.22, 2H ,H-6, H-6'), 7.53 (dd, J = 1.70 J = 5.17 , 2H ,H-5, H-5').

IR-TF (KBr) ν (cm^{-1}): 3077, 1595, 1498 (C=C), 1270, 772.

EM (IE), *m/z*: 313.9 $[M]^+$ (100%).

2.5.1.2 Synthesis of the BDT-functionalized bipyridines.

Synthesis of the BDT precursors: Building block

Compound (5)

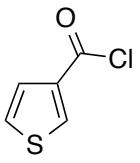

Thiophene 3-carboxylic acid (10.0 g; 0.76 mol) was dissolved in dry CH_2Cl_2 (10 mL) under argon. The solution was cooled at 0ºC with an ice bath, and then oxalyl chloride (14 mL, 1.62 mmol) was added in small portion in the solution. The obtained mixture was stirred at 0ºC for 2–3 h, then let at RT overnight. A clear solution was obtained. After removing CH_2Cl_2 solvent under reduced pressure, the excess of oxalyl chloride was removed by high-vacuum distillation to afford a white-beige solid, used as well without further purification in the next step (yield supposed quantitative for this step).

Compound (6)

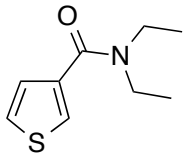

A solution of compound **5** (5.72 g; 0.76 mol) in 15 mL of CH_2Cl_2 was slowly and carefully added at 0ºC in a solution of diethylamine (5.70 g; 0.78 mmol) in CH_2Cl_2. At the end of theaddition, the mixture was stirred for additional 30 min at RT. Afterwards, the mixture was taken up with CH_2Cl_2, and the organic phase washed with deionized water till neutral pH, then dried over $MgSO_4$, filtrated and evaporated to dryness. The crude was pre-purified by flash chromatography on SiO_2 (Eluent CH_2Cl_2 100%, then AcOEt 100%). The obtained clear yellow oil was then purified by distillation under reduced pressure (140ºC, 4 mbar), to afford compound **6** (14.0 g; 0.76 mol) in quantitate yield (2 steps).

^{1}H-NMR (300 MHz, $CDCl_3$)), δ (ppm): 7.48 (dd, ^4J(C,A)= 3.0 Hz, ^4J(C,B)= 1.3 Hz, 1H; H-C), 7.32 (dd, ^3J(A,B)= 5.0 Hz, ^4J(A,C)= 3.0 Hz, 1H; H-A), 7.19 (dd, ^4J(B,A)= 5.0 Hz, ^4J(B,C)= 1.3 Hz, 1H; H-B), 3.32–3.58 (m, 4H; 2CH_2), 1.13–1.28 (m, 6H; 2CH_3).

Compound (7)

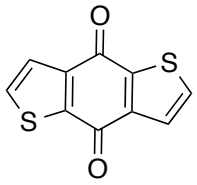

We synthetized this compound under modified conditions: in a Schleck flask, compound **6** (14.0 g; 0.764 mol) was dissolved in dry THF (160 mL) under Ar steam. The solution was cooled at -50ºC with an N_2(l) bath, and a 2.5 M solution of *n*BuLi in *n*-hexane (37 mL; 0.925 mol) was added drop by drop in the mixture within c.a. 30 min. At the end of the addition, the mixture was stirred at -20ºC for additional 2h at this temperature. Afterwards, the mixture was carefully poured in 200 g of crushed ice resulting in precipitation of a yellow solid. After 1h of stirring at RT, the precipitate was filtrated-off and the aqueous phase extracted 3 times with $CHCl_3$ (3×200 mL). The organic phase was evaporated to dryness and the remaining solid put together with the first precipitate. The solid was then successively dionied washed with water, cold MeOH (10 mL), cold hexanes (10 mL), and air-dried, yielding compound **7** as a yellow powder in 76% yield (6.42 g; 0.291 mol).

^{1}H-NMR (300 MHz, $CDCl_3$), δ (ppm): 7.72 (d, ^3J(A,B)= 5.0 Hz, H-A), 7.69 (d, ^3J(B,A)= 5.0 Hz, H-B).

Compound (8)

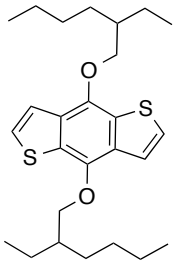

KOH pellets (4.50 g, 80.4 mmol) and zinc dust (4.45 g, 68.1 mmol) were added to a solution of **7** (0.906 g, 4.11 mmol) in DMF (100 mL). The mixture was heated at 80°C for 24h under argon (the colour of the mixture progressively turned from light yellow to deep dark green). Afterwards, 2-ethylhexyl bromide (4 mL, 22.5 mmol) was added with a syringe and the mixture heated at 80°C for additional 24h (the colour of the mixture progressively turned from deep dark green to yellow-brownish). After cooling to room temperature, the Zn/KOH suspension was filtered-off over Celite, and then DMF removed from the filtrate by high-vacuum distillation. The residue was extracted with hexanes and a 0.1 M HCl aqueous solution. After phase separation, the aqueous layer was extracted twice more with hexanes. The organic layers were combined, then successively washed with water (twice) until neutral pH, dried over $MgSO_4$, filtrated and evaporated to dryness. The yellow-brownish crude oil was purified by chromatography column on SiO_2, eluent CH_2Cl_2/Hexanes 2:8, to afford **8** (1.60 g, 3.58 mmol) as a clear yellow oil in 87% yield.

^{1}H-NMR (300 MHz, $CDCl_3$), δ (ppm): 7.56 (d, ^3J (A,B)= 5.5 Hz, 2H; H-A), 7.40 (d, ^3J(B,A) = 5.5 Hz, 2H; H-B), 4.27 (d, ^3J = 5 Hz, 4H; 2OCH_2), 1.90 (m, $^3J_{app} \approx$ 6 Hz, 2H; 2C$^*H$), 1.86–1.54 (m, 8H; 4CH_2), 1.54–1.43 (m, 80H; 40CH_2), 1.12 (t, ^3J = 7.5 Hz, 6H; 2CH_3), 1.05 (t, ^3J = 7.5 Hz, 6H; 2CH_3)

^{13}C-NMR (50 MHz, $CDCl_3$), δ (ppm): 144.6, 131.4, 129.9, 125.8, 120.2, 75.9 (OCH_2), 40.7, 30.5, 29.2, 23.9, 23.1, 14.1, 11.3.

MS (FAB+; *m*-NBA): *m/z* (%) found 222.0 (82) [M-2(ethylhexyl)]$^+$, 334.1 (12) [M-(ethylhexyl)+H]$^+$, 446.2 (100) [M]$^+$.

HRMS (FAB+; *m*-NBA + PEGH): *m/z* calcd for $C_{26}H_{38}O_2S_2$: 446.2313; found 446.2303 [M]$^+$.

Compound (9)

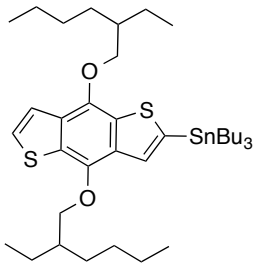

The benzodithiophene derivative **8** (597 mg, 1.34 mmol) was introduced in an oven-dried Schlenk flask, and then three cycles of vacuum-argon were realized. Under argon steam, dry THF (10 ml) was added by syringe in the flask through a septum/needle, and the resulting solution stirred at room temperature until the full dissolution of the starting material. Next, the flask was immerged in an acetone/$N_{2(l)}$ bath and cooled at -78°C for 5 min. Afterwards, a solution of *n*BuLi in THF/hexane (0.6 mL, 1.50 mmol, 2,5M) was added drop by drop by syringe to the solution through a septum/needle. At the end of the addition, the mixture was stirred for additional 60–90 min at the addition temperature and then $SnBu_3Cl$ (0.45 mL, 1.66 mmol) was added dropwise. The mixture was stirred at -60°C for an additional hour, and then allowed to warm slowly to room temperature within 1–2 hours. Finally, few drops of a saturated aqueous NH_4Cl solution were added to quench the reaction. The reaction mixture was diluted in a copious amount of hexane, then successively dried over $MgSO_4$, filtrated, and solvents evaporated to dryness The ratio mono-/ bis- substituted stannyl derivatives was estimated to be 74:26 by ^{1}H NMR. The crude yellow oil was used without further purification in the next step.

^{1}H-NMR (300 MHz, $CDCl_3$), δ (ppm): 7.52 (s, 1H), 7.47 (d, ^3J = 5.5 Hz, 1H), 7.38 (d, ^3J = 5.5 Hz, 1H), 4.21 (d, ^3J = 5 Hz, 2H), 4.19 (d, ^3J = 5 Hz, 2H), 1.88-1.73 (m, 2H), 1.74–1.14 (m, 34H), 1.07–0.90 (m, 21H).

Compound (10)

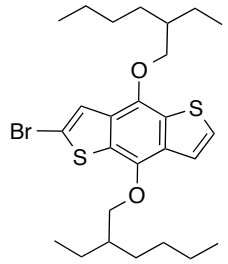

In an argon flushed Schlenk flask, a 1.6M *n*BuLi solution in hexanes (0.9 mL, 1.44 mmol) was added drop by drop to a solution of **1** (528 mg, 1.18 mmol) in dry THF (10 mL) at -78°C under argon. The mixture was stirred for 90 min at the addition temperature. Next, a 1.07 mM solution of Br_2 in hexanes (1 mL, 1.07 mmol) was added drop by drop within c.a. 10 min. At the end of the addition, the mixture stirred at -60°C for additional 90 min before allowing it to warm to RT and stirred overnight. Finally, few drops of a saturated aqueous NH_4Cl solution was added to quench the reaction. The mixture was diluted in 40 mL of hexanes, then dried over $MgSO_4$, filtrated, and solvents evaporated to dryness. The crude product was purified by chromatography column on SiO_2, eluent CH_2Cl_2/hexanes 1:9, to afford **3** (393 mg, 0.75 mmol) as a pale yellow oil in 64% yield.

^{1}H-NMR (300 MHz, $CDCl_3$), δ (ppm): .49 (s, 1H), 7.48 (d, ^3J = 5.5 Hz, 1H), 7.40 (d, ^3J = 5.5 Hz, 1H), 4.18 (d, ^3J = 5 Hz, 2H), 4.17 (d, ^3J = 5 Hz, 2H), 1.88–1.77 (m, 2H), 1.76–1.50 (m, 8H), 1.50–1.35 (m, 8H), 1.10–0.95 (m, 12H).

^{13}C-NMR (75 MHz, $CDCl_3$), δ (ppm): 143.7, 143.6, 131.4, 130.7, 130.3, 126.1, 123.1, 120.2, 114.5, 76.08, 76.06, 40.6, 30.4, 29.2, 23.8, 23.10, 23.08, 14.12, 14.11, 11.3.

MS (FAB+; *m*-NBA): *m/z* (%) found 299.9 (57), 301.9 (60) $[M\text{-}2(ethylhexyl)]^+$, 411.0 (9), 413.0 (12) $[M\text{-}(ethylhexyl)]^+$, 524.1 (93), 526.1 (100) $[M]^+$.

HRMS (FAB+; *m*-NBA + PEGH): *m/z* (%) calcd for $C_{26}H_{37}O_2S_2{}^{79}Br$: 524.1418 (90), $C_{26}H_{37}O_2S_2{}^{81}Br$: 526.1398 (100); found 524.1415 (93), 526.1401 (100) $[M]^+$.

UV-Vis: λmax(CH_2Cl_2)/nm= 300 (*e* /dm^3 mol^{-1} cm^{-1}: 9 780), 340 (8 500), 354 (11 200).

Compound (11)

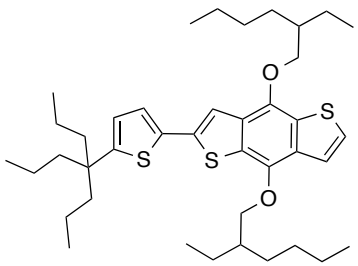

Prepared according to the general procedure described for Stille couplings, from **10** (486 mg, 0.92 mmol), tributyl(5-(4-propylheptan-4-yl)thiophen-2-yl)stannane (577 mg, 1.12 mmol), $Pd(PPh_3)_4$ (80 mg, 0.07 mmol) in refluxing toluene (40 mL) overnight. The crude was purified by chromatography column on SiO_2, eluent CH_2Cl_2/Hexanes 2:8, to afford **11** (532 mg, 0.78 mmol) as a yellow oil in 85% yield.

^{1}H-NMR (300 MHz, $CDCl_3$), δ (ppm): 7.45 (d, ^3J = 5.5 Hz, 1H), 7.44 (s, 1H), 7.35 (d, ^3J = 5.5 Hz, 1H), 7.15 (d, ^3J = 4 Hz, 1H), 6.74 (d, ^3J = 4 Hz, 1H), 4.18 (m, 4H), 1.88–1.77 (m, 2H), 1.75–1.49 (m, 12H), 1.48–1.33 (m, 8H), 1.29–1.12 (m, 8H), 1.09-0.82 (m, 21H).

^{13}C-NMR (75 MHz, $CDCl_3$), δ (ppm): 156.3, 144.3, 144.2, 137.3, 134.5, 132.3, 131.5, 130.4, 128.6, 125.6, 124.5, 123.9, 120.3, 114.8, 75.9, 44.1, 41.6, 40.7 (two s), 30.5 (two s), 29.3, 29.2, 23.9 (two s), 23.2, 23.1, 16.8, 14.7, 14.2, 14.1, 11.3 (two s).

MS (FAB+; *m*-NBA): *m/z* (%) **found** 443.1 (100) $[M\text{-}2(ethylhexyl)+H]^+$, 445.1 (33) [M-(propylheptanyl thiophene)], 556.2 (17) $[M\text{-}(ethylhexyl)+H]^+$, 668.3 (85) $[M]^+$.

HRMS (FAB+; *m*-NBA + PEGMMEH): *m/z* (%) calcd for $C_{40}H_{60}O_2S_3$: 668.3755; found 668.3750 $[M]^+$.

UV-Vis: λmax(CH_2Cl_2)/nm= 240 (*e* /dm^3 mol^{-1} cm^{-1}: 22 200), 292 (13 600), 336 (20 700), 351 (20 500), 375 (15 500).

Compound (12)

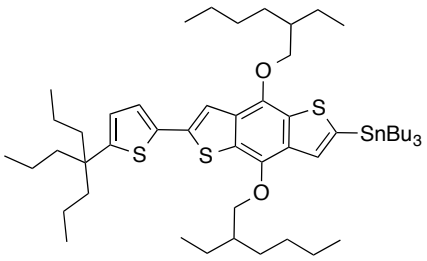

The **11** (268 mg, 0.40 mmol),was introduced in an oven-dried Schlenk flask, and then three cycles of vacuum-argon were realized. Under argon steam, dry THF (6ml) was added by syringe in the flask through a septum/needle, and the resulting solution stirred at room temperature until the full dissolution of the starting material. Next, the flask was immerged in an acetone/$N_{2(l)}$ bath and cooled at -78°C for 5 min. Afterwards, a solution of *n*BuLi in THF/hexane 0.25 M *n*BuLi solution in hexanes (2.1 mL, 0.53 mmol) was added drop by drop by syringe to the solution through a septum/needle. At the end of the addition, the mixture was stirred for additional 60–90 min at the addition temperature and then tributyltin chloride (0.2 mL, 0.74 mmol), was added dropwise. The mixture was stirred at -60°C for an additional hour, and then allowed to warm slowly to room temperature within 1–2 hours. Finally, few drops of a saturated aqueous NH_4Cl solution were added to quench the reaction. The reaction mixture was diluted in a copious amount of hexane, then successively dried over $MgSO_4$, filtrated, and solvents evaporated to dryness. The crude yellow oil was used without further purification in the next step (yield supposed to be quantitative for this step).

^{1}H-NMR (300 MHz, $CDCl_3$), δ (ppm): 7.49 (s, 1H), 7.43 (s, 1H), 7.13 (d, ^3J = 4 Hz, 1H), 6.73 (d, ^3J = 4 Hz, 1H), 4.20 (d, ^3J = 5.5 Hz, 2H), 4.18 (d, ^3J = 6 Hz, 2H), 1.88–1.77 (m, 2H), 1.75–1.14 (m, 46H), 1.08–0.82 (m, 30H).

Compound (13)

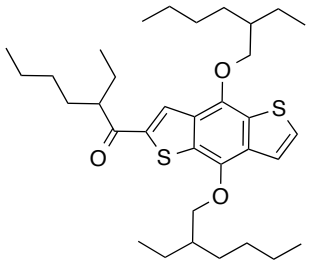

In an argon flushed Schlenk flask, a 2.5 M *n*BuLi solution in hexanes (0.70 mL, 1.75 mmol) was added drop by drop by syringe to a solution of **15** (665 mg, 1.49 mmol) in dry THF (8 mL) at -78°C under argon steam. The mixture was stirred for 90 min at the addition temperature. Next, this solution was transferred through a cannula in a solution of 2-ethylhexanoyl chloride in THF (2 mL) at -60°C. 2x1 mL of dry THF was used to wash the cannula. The solution was allowed to reach slowly -20°C within 90 min and then stirred at RT for additional 90 min. Finally, few drops of a saturated NH_4Cl aqueous solution was added to quench the reaction. The reaction mixture was then diluted in hexanes (40 mL), successively dried over $MgSO_4$, filtrated and solvents evaporated. The crude product was purified by chromatography column on SiO_2, eluent CH_2Cl_2/Hexanes 4:6, to afford **13** (380 mg, 0.66 mmol) as a bright yellow oil in 44% yield.

^{1}H-NMR (300 MHz, $CDCl_3$), δ (ppm): 8.15 (s, 1H), 7.49 (d, ^3J = 5.5 Hz, 1H), 7.44 (d, ^3J = 5.5 Hz, 1H), 4.27 (d, ^3J = 5.5 Hz, 2H), 4.21 (d, ^3J = 5.5 Hz, 2H), 3.32 (tt, ^3J = 8 and 5.5 Hz, 1H) 1.96–1.76 (m, 6H), 1.76–1.49 (m, 8H), 1.50–1.27 (m, 12H), 1.09–0.85 (m, 18H).

^{13}C-NMR (75 MHz, $CDCl_3$), δ (ppm): 198.8, 146.7, 144.5, 144.1, 134.3, 131.3, 131.0, 129.5, 127.6, 125.2, 120.4, 76.1, 76.0, 49.6, 40.6, 32.3, 30.5, 30.4, 29.9, 29.2, 29.1, 26.0, 23.8 (two s), 23.1, 23.0, 22.8, 14.0, 13.8, 12.1, 11.2.

MS (FAB+; *m*-NBA): *m/z* (%) found 348.0 (100) $[M\text{-}2(ethylhexyl)+2H]^+$, 572.3 (94) $[M]^+$, 573.3 (82) $[M]^+/[M+H]^+$.

HRMS (FAB+; *m*-NBA + PEGH): *m/z* calc for $C_{34}H_{52}O_3S_2$: 572.3358; found 572.3340 $[M]^+$.

UV-Vis: $\lambda_{max}(CH_2Cl_2)$/nm = 277 (*e* /dm^3 mol^{-1} cm^{-1}: 29 300), 327 (16 700), 410 (9 300).

Compound (14)

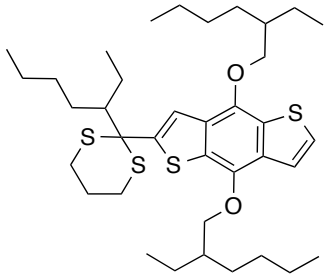

A commercial 7.93 M solution of BF_3•Et_2O in Et_2O (0.8 mL, 6.34 mmol) was added by syringe to a solution of **23** (143 mg, 0.250 mmol) and propane-1,3-dithiol (0.7 mL; 755 mg, 6.98 mmol) in dry CH_2Cl_2 under argon. The solution was stirred at room temperature for 48h. Afterwards, the resulting mixture was taken up with hexanes, and the organic layer successively washed with a saturated aqueous $NaHCO_3$ solution (three times), deionised water, dried over Na_2SO_4, filtrated and evaporated to dryness. The crude was purified by chromatography column on SiO_2, eluent CH_2Cl_2/hexanes 3:7, to afford **14** (166 mg, 0.250 mmol) as a pale yellow oil in a quantitative yield.

^{1}H-NMR (300 MHz, $CDCl_3$), δ (ppm): 7.70 (s, 1H), 7.49 (d, ^3J = 5.5 Hz, 1H), 7.36 (d, ^3J = 5.5 Hz, 1H), 4.23 (d, ^3J = 5.5 Hz, 2H), 4.22 (d, ^3J = 5 Hz, 2H), 3.06 (d, ^2J = 11 Hz, 1H), 3.03 (d, ^2J = 11 Hz, 1H), 2.75 (d, ^2J = 11 Hz, 1H), 2.74 (d, ^2J = 11 Hz, 1H), 2.09–1.18 (m, 27H), 1.08–0.81 (18H).

^{13}C-NMR (75 MHz, CDCl3), δ (ppm): 150.0, 144.3, 144.1, 131.5, 131.3, 130.6, 129.7, 125.6, 122.5, 120.4, 75.9, 62.5, 53.4, 40.7, 40.6, 31.7, 31.6, 31.0, 30.5, 30.4, 29.2, 29.0, 28.0, 25.2, 25.0, 24.5, 23.9, 23.8, 23.1, 22.9, 22.6 (two s), 14.1 (two s), 14.0, 13.7, 11.4, 11.3, 11.2.

MS (MALDI–TOF; DCTB): *m/z* (%) found 557.5 (34) [M-($C_3H_8S_2$)+H]$^+$, 662.4 (100) [M]$^+$.

HRMS (**MALDI-TOF; DCTB + PEGNa600):** *m/z* calc for $C_{37}H_{58}O_2S_4$: 662.3314; found 662.3313 [M]$^+$.

UV-Vis: $\lambda_{max}(CH_2Cl_2)$/nm = 233 (e /dm^3 mol^{-1} cm^{-1}: 40 800), 264 (55 900), 291 (16 000), 303 (20 800), 344 (14 300), 358 (21 500).

Compound (15)

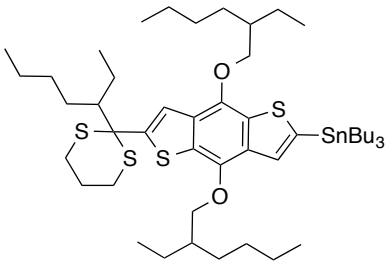

Compound **14** (139 mg, 0.21 mmol), was introduced in an oven-dried Schlenk flask, and then three cycles of vacuum-argon were realized. Under argon steam, dry THF (10ml) was added by syringe in the flask through a septum/needle, and the resulting solution stirred at room temperature until the full dissolution of the starting material. Next, the flask was immerged in an acetone/$N_{2(l)}$ bath and cooled at -78°C for 5 min. Afterwards, a solution of *n*BuLi in THF/hexane (1.3 mL, 0.33 mmol), was added drop by drop by syringe to the solution through a septum/needle. At the end of the addition, the mixture was stirred for additional 60–90 min at the addition temperature and then tributyltin chloride was added dropwise, 0.37 M solution of $SnBu_3Cl$ in hexanes (0.45 mL, 1.66 mmol). The mixture was stirred at -60°C for an additional hour, and then allowed to warm slowly to room temperature within 1–2 hours. Finally, few drops of a saturated aqueous NH_4Cl solution were added to quench the reaction. The reaction mixture was diluted in a copious amount of hexane, then successively dried over $MgSO_4$, filtrated, and solvents evaporated to dryness. The crude yellow oil was used without further purification in the next step (yield supposed to be quantitative for this step).

^{1}H-NMR (300 MHz, $CDCl_3$), δ (ppm): 7.68 (s, 1H), 7.54 (s, 1H), 4.24 (d, ^3J = 5 Hz, 2H), 4.23 (d, ^3J = 5 Hz, 2H), 3.07 (d, ^2J = 11 Hz, 1H), 3.03 (d, ^2J = 11 Hz, 1H), 2.74 (d, ^2J = 11 Hz, 1H), 2.73 (d, ^2J = 11 Hz, 1H), 2.10–1.15 (m, 45H), 1.08–0.81 (27H).

Compound (16)

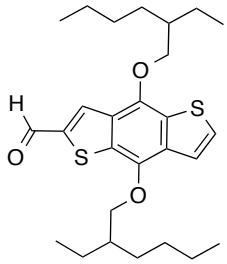

In an argon flushed Schlenk flask, a 2.5 M commercial solution of *n*BuLi in hexanes (0.43 mL, 1.075 mmol) was added drop by drop by syringe to a solution of **8** (433 mg, 0.97 mmol) in dry THF (8 mL) at -78°C under argon. The mixture was stirred for 90 min at the addition temperature (meanwhile, the colour of the mixture progressively turned from light yellow to deep dark brown). Next, dry DMF (0.3 mL, 3.87 mmol) was added dropwise and the mixture was stirred at -60°C for additional 90 min before allowing it to warm slowly to RT within 1h. Finally, few drops of a saturated NH_4Cl aqueous solution were added to quench the reaction (the colour of the mixture turned immediately to bright yellow. The reaction mixture was diluted in hexanes (50 mL), then successively dried over $MgSO_4$, filtrated, and solvents evaporated. The crude product was purified by chromatography column on SiO_2, eluent hexanes/CH_2Cl_2 6:4, to afford **16** in 69 % yield, as a deep-yellow viscous oil.

^{1}H-NMR (300 MHz, $CDCl_3$), δ (ppm): 10.07 (s, 1H), 8.13 (s, 1H), 7.46 (br s, 2H), 4.25 (d, ^3J = 5.5 Hz, 2H), 4.15 (d, ^3J = 5.5 Hz, 2H), 1.87–1.30 (m, 18H), 1.08–0.90 (m, 12H).

^{13}C-NMR (75 MHz, $CDCl_3$), δ (ppm): 184.2, 147.1, 144.4, 142.4, 134.9, 131.4, 131.2, 130.0, 129.6, 128.3, 120.3, 76.3, 76.0, 40.6, 30.3, 29.1 (two s), 23.7, 23.0 (two s), 14.0, 11.2.

MS (FAB+; *m*-NBA): *m/z* (%) found 249.9 (100) ([M-2(ethylhexyl)+2H]$^+$, 474.0 (71) [M]$^+$, 475.0 (53) [M]$^+$/[M+H]$^+$.

HRMS (FAB+; *m*-NBA + PEGH): *m/z* calc for $C_{27}H_{38}O_3S_2$: 474.2262; found 474.2274 [M]$^+$.

UV-Vis: $\lambda_{max}(CH_2Cl_2)$/nm = 278 (*e* /dm^3 mol^{-1} cm^{-1}: 25 000), 329 (16 300), 418 (8 900).

Synthesis of the BDT-functionalized bipyridines

General procedure :

In an argon flushed two-necked flask, the appropriate stannyl derivative and 4,4'-dibromo-2,2'-bipyridine were dissolved in dry toluene. The solution was stirred and degassed vigorously by bubbling argon through a needle/septum for 30 min. Afterwards, $Pd(PPh_3)_4$ (5–20 mol%) was introduced in the flask and the mixture heated while keeping a gentle argon bubbling. Once refluxing, the solution was let under inert atmosphere (Ar) and the reflux maintained for 1–3 days. After cooling down to RT, toluene was evaporated under reduced pressure and the crude purified by the appropriate method(s) as outlined in the text.

Ligands : L-221 (17), L-222 (18) and L-223 (19)

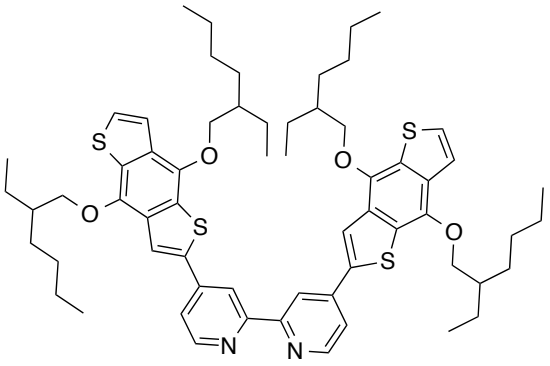

- Ligand **L-221** (**17**)

Prepared according to the general procedure described for Stille couplings, from **19** (1.95 g, 2.66 mmol), 4,4'-Dibromo-2,2',bipyridine (152 mg, 0.484 mmol), $Pd(PPh_3)_4$ (168 mg, 0.145 mmol) in refluxing toluene (75 mL) for 3 days. The crude product was purified by chromatography column on SiO_2, eluent CH_2Cl_2 containing MeOH (1%) and Et_3N (0.5%), followed by Gel permeation chromatography (Bio-rad, Bio-beds SX-1, eluent toluene). Purification was achieved by recrystallizations by slow diffusion of EtOH in a solution of **L-221** in Et_2O. Pure fractions were combined, re-dissolved in

hexanes (≈ 5 mL) and slowly evaporated to dryness to afford **L-221** (148 mg, 0.142 mmol) in 29% yield as a fine pale yellow-green powder.

^{1}H-NMR (300 MHz, $CDCl_3$), δ (ppm):): 8.84 (dd, ^{3}J = 5 Hz and ^{4}J = 2 Hz, 2H), 8.81 (d, ^{3}J = 5 Hz, 2H), 8.05 (s, 2H), 7.68 (dd, ^{3}J = 5 Hz and ^{4}J = 2 Hz, 2H), 7.51 (d, ^{3}J = 5.5 Hz, 2H), 7.42 (d, ^{3}J = 5.5 Hz, 2H), 4.27 (d, ^{3}J = 5.5 Hz, 4H), 4.24 (d, ^{3}J = 5.5 Hz, 4H), 1.95–1.82 (m, 4H), 1.81–1.52 (m, 16H), 1.52–1.35 (m, 16H), 1.11–1.03 (m, 12H), 1.03–0.94 (m, 12H).

^{13}C-NMR (75 MHz, $CDCl_3$), δ (ppm): 156.5, 149.7, 145.2, 144.4, 142.3, 140.3, 132.5, 131.9, 130.2, 129.3, 126.5, 120.4, 120.3, 118.6, 117.8, 76.2, 76.0, 40.7, 30.5, 30.4, 29.2 (two s), 23.9, 23.14, 23.13, 14.1, 11.3 (two s).

MS (MALDI–TOF; DCTB): *m/z* (%) found 1044.5 (100) $[M]^+$.

HRMS(MALDI–TOF; DCTB + PEGNa2000): *m/z* calcd for $C_{62}H_{80}N_2O_4S_4$: 1044.4995; found 1044.5033 $[M]^+$.

UV-Vis: λ_{max}(CH_2Cl_2)/nm = 284 (*e* /dm^3 mol^{-1} cm^{-1}: 64 100), 335 (46 750), 398 (26 300).

- Ligand **L-222** (**18**)

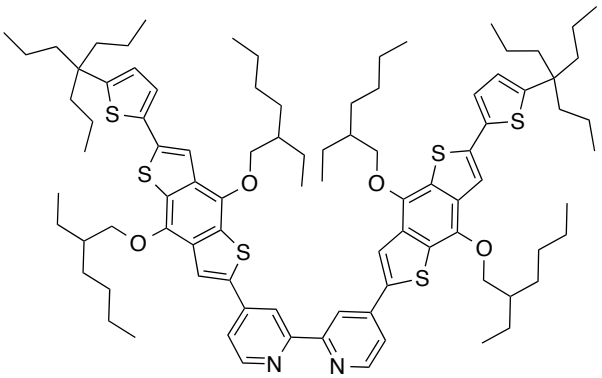

Prepared according to the general procedure described for Stille couplings, from **11** (383 mg, 400 µmol), 4,4'-Dibromo-2,2',bipyridine (41 mg, 131 µmol), $Pd(PPh_3)_4$ (40 mg, 34.6 µmol) in refluxing toluene (18 mL) for 3 days. The crude product was purified by chromatography column on SiO_2, eluent CH_2Cl_2 containing MeOH (1%) and Et_3N (0.5 %). The bright yellow viscous oil was re-dissolved in hexanes (≈ 5 mL) and slowly

evaporated to dryness, to afford **L-222** (181 mg, 121 μmol) in 91% yield, as a fine yellow powder.

^{1}H-NMR (300 MHz, $CDCl_3$), δ (ppm): 8.81 (d, ^4J = 2 Hz, 2H), 8.80 (d, ^3J = 5 Hz, 2H), 8.02 (s, 2H), 7.67 (dd, ^3J = 5 Hz and ^4J = 2 Hz, 2H), 7.45 (s, 2H), 7.18 (d, ^3J = 3.5 Hz, 2H), 6.75 (d, ^3J = 3.5 Hz, 2H), 4.25 (d, ^3J = 6 Hz, 4H), 4.23 (d, ^3J = 6 Hz, 4H), 1.94–1.83 (m, 4H), 1.80–1.38 (m, 44H), 1.31–1.13 (m, 12H), 1.12–1.04 (m, 12H), 1.03–0.95 (m, 12H), 0.94–0.87 (m, 18H).

^{13}C-NMR (75 MHz, $CDCl_3$), δ (ppm): 156.7, 156.6, 149.8, 144.9, 144.1, 142.6, 140.1, 138.1, 134.2, 133.4, 131.9, 129.9, 128.9, 124.8, 124.0, 120.6, 118.9, 117.9, 114.9, 76.3, 76.1, 44.2, 41.6, 40.8, 40.7, 30.5 (two s), 29.3, 29.2, 23.9 (two s), 23.2 (two s), 16.8, 14.7, 14.2 (two s), 11.4, 11.3.

MS (MALDI–TOF; DCTB): *m/z* (%) found 1488.7 (88), 1489.7 (100) $[M]^+$.

HRMS(MALDI–TOF; DCTB + PEGMeNa750 + PEGNa2000): *m/z* calcd for $C_{90}H_{124}N_2O_4S_6$: 1488.7880; found 1488.7880 $[M]^+$.

UV-Vis: $\lambda_{max}(CH_2Cl_2)$/nm = 245 (*e* /dm^3 mol^{-1} cm^{-1}: 62 700), 288 (51 900), 364 (68 800), 427 (61 900).

- Ligand **L-223** (**19**)

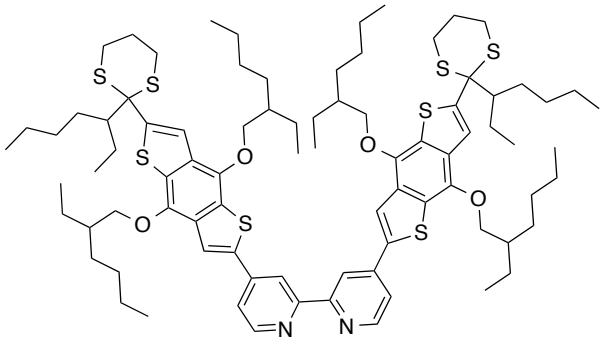

Prepared according to the general procedure described for Stille couplings, from **15** (200 mg, 210 μmol), 4,4'-Dibromo-2,2',bipyridine (24 mg, 131 μmol), $Pd(PPh_3)_4$ (40 mg, 76.4 μmol) in refluxing toluene (10 mL) for 3 days. The crude product was purified by chromatography column on SiO_2, eluent CH_2Cl_2 containing MeOH (1%) and Et_3N

(0.5%). The bright yellow viscous oil was re-dissolved in hexanes (≈ 5 mL) and slowly evaporated to dryness, to afford **L-223** (108 mg, 73.1 μmol) in 96% yield, as a fine yellow powder.

^{1}H-NMR (300 MHz, $CDCl_3$), δ (ppm): 8.85 (d, ^{4}J = 1.5 Hz, 2H), 8.81 (d, ^{3}J = 5 Hz, 2H), 8.06 (s, 2H), 7.70 (s, 2H), 7.69 (dd, ^{3}J = 5 Hz and ^{4}J = 1.5 Hz, 2H), 4.29 (d, ^{3}J = 5.5 Hz, 4H), 4.25 (d, ^{3}J = 5.5 Hz, 4H), 3.07 (d, ^{2}J = 11 Hz, 2H), 3.02 (d, ^{2}J = 11 Hz, 2H), 2.76 (d, ^{2}J = 11 Hz, 2H), 2.75 (d, ^{2}J = 11 Hz, 2H), 2.10–1.96 (m, 4H), 1.96–1.15 (m, 54H), 1.11–1.03 (m, 12H), 1.02–0.83 (m, 24H).

^{13}C-NMR (75 MHz, $CDCl_3$), δ (ppm): 156.6, 151.1, 149.8, 145.0, 143.9, 142.5, 140.1, 132.6, 131.8, 131.0, 129.2, 122.6, 120.6, 118.9, 117.9, 76.2, 76.1, 62.4, 53.5, 40.7 (two s), 31.7, 31.0, 30.5, 30.4, 29.2, 28.1, 25.0, 24.5, 23.9, 23.8, 23.1, 22.9, 14.2, 14.1, 14.0, 13.8, 11.3 (two s).

MS (MALDI–TOF; dithranol): *m/z* found (%) 1477.7 (96), 1478.7 (100), 1479.7 (98) $[M+H]^+$.

HRMS(MALDI–TOF; dithranol + PEGNa1500): *m/z* calc for $C_{84}H_{121}N_20_4S_8$: 1477.7087 found 1477.7050 $[M+H]^+$.

Ligand L-229 (20)

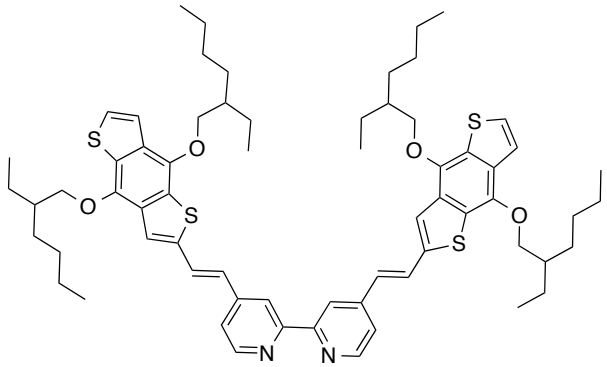

4,4'-Dimethyl,2,2'-bipyridine (50 mg, 0.27 mmol) was introduced in an oven dried 50 mL Schlenk, then three cycles of vacuum-argon were realized. Afterwards, THF (5 mL) was introduced under argon with a syringe and the obtained solution stirred at room temperature until the complete dissolution of the material. Next, the

mixture was cooled at –78°C for 10 min and a commercial 2.0 M solution of LDA in heptane/THF (0.32 mL, 0.64 mmol) was added by syringe to the colourless solution, which turned brown immediately. The solution was stirred at this temperature for 25 min, and then warmed at –10°C for additional 25 min (the solution progressively turned dark black-reddish). The mixture was cooled again at -78°C, and then a solution of **16** (340 mg, 0.72 mmol) in THF (5 mL) was transferred under argon in the Schlenk flask with a cannula. The mixture quickly turned light yellow, and was stirred at -60°C for additional 1–2h, then at -10°C for additional 30 min. Finally, few drops of an aqueous saturated NH_4Cl solution (≈ 0.1 mL) were added to quench the reaction. After 10 min of stirring, the reaction mixture was diluted in CH_2Cl_2 (40 mL), successively dried over Na_2SO_4, filtered over a small plug of Celite, and solvents removed under vacuum. The crude was then filtered on chromatography column through a small plug of SiO_2, and eluted first with CH_2Cl_2 as eluent (to remove unreacted aldehyde), followed by AcOEt/Et_3N (100:1) to recover the desired bipyridine product. The obtained crude diol was obtained as a streoisomeric mixture and used as well in the next step. Next, a 6.9 mM solution of I_2 in toluene (0.4 mL, 3 µmol, 1 mol%) was added to a solution of the above-mentioned diol and PTPS (27 mg, 107 µmol) in 20 mL of dry toluene. The mixture was refluxed in a Dean-Stark apparatus overnight (the colour of the solution progressively turned from light yellow to deep orange-reddish). After cooling down to room temperature, Et_3N (≈ 0.5 mL) was added to the solution (the colour of the solution immediately turned to bright yellow) and solvents removed under vacuum. The crude product was purified by chromatography column on SiO_2, eluent CH_2Cl_2 containing MeOH (0.2%) and Et_3N (0.2 %). The bright yellow viscous oil was re-dissolved in cold hexanes (5 mL) and the obtained solution slowly evaporated to dryness to afford **L-229** (105 mg, 94.3 µmol) in 35% yield, as a fine yellow powder.

^{1}H-NMR (300 MHz, $CDCl_3$), δ (ppm): 8.68 (d, ^3J = 5 Hz, 2H), 8.56 (bs, 2H), 7.67 (d, $^3J_{trans}$ = 16 Hz, 2H), 7.49 (s, 2H), 7.46 (d, ^3J = 5.5 Hz, 2H), 7.38 (d, ^3J = 5.5 Hz, 2H), 7.36 (dd, ^3J = 5 Hz and ^4J = 1.5 Hz, 2H), 6.96 (d, $^3J_{trans}$ = 16 Hz, 2H), 4.21 (d, ^3J = 6 Hz, 4H), 4.20 (d, ^3J = 6 Hz, 4H), (1.92–1.53 (m, 18H), 1.45 (bs, 18H), 1.11–1.03 (m, 12H), 1.03–0.95 (m, 12H).

^{13}C-NMR (75 MHz, $CDCl_3$), δ (ppm): 156.2, 149.5, 144.95, 144.85, 144.1, 141.0, 132.6, 131.4, 130.1, 128.7, 128.1, 126.8, 126.4, 122.1, 120.9, 120.4, 117.9, 76.1, 75.9, 40.6, 30.4, 29.2, 23.8, 23.1, 14.2, 11.3.

MS (MALDI–TOF; DCTB): *m/z* (%) found 1096.5 (100), 1097.5 (91) $[M]^+$.

HRMS(MALDI–TOF; DCTB + PEGMeNa750 + PEGNa2000): *m/z* calcd $C_{66}H_{84}N_20_4S_4$: 1096.5308; found 1096.5353 $[M]^+$.

UV-Vis: $\lambda_{max}(CH_2Cl_2)$/nm = 238 (ε /dm^3 mol^{-1} cm^{-1}: 46 500), 294 (36 000), 355 (61 400), 413 (31 800).

2.5.1.3 Synthesis of the CDT-functionalized bipyridines

Synthesis of the CDT precursors: Building block

Compound (21)

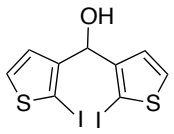

To a stirred solution of 3-bromothiophene (3 ml; 5.76 g, 30.0 mmol, 1eq) in dry Et_2O (25 mL) at - 78 ºC, was added with a syringe a 2.5M BuLi solution in hexanes (44.0 mmol, 17,6 ml, 1.2 eqv.). At the end of the addition, the solution was stirred for additional 1.5 h at -78ºC, and 1.5h at rt. Afterwards, the mixture was cooled again at -78 ºC and then a solution of thiophene-3-carbaldehyde (6.52 g, 40.0 mmol) in dry Et2O (20 mL) was added via syringe. The reaction mixture was stirred at –78ºC for 0.5 h, and then allowed to reach r.t., and stirred overnight. After cooling to -23 ºC, a 2.5M nBuLi solution in hexanes (36 ml, 88.0 mmol, 2eq) was added with a syringe. At the end of the addition, the solution was stirred at –23 ºC for additional 1 h, then the mixture was allowed to reach r.t., and stirred for additional 1 h. After cooling again the mixture at –23 ºC, a solution of I_2 (30 g, 252.0 mmol) in dry Et_2O (200 mL) was added dropwise. After that the reaction mixture was allowed to warm-up to room temperature. Them a 10% w/w aquos solution of Na_2SO_3 (200 mL) was added with vigorous stirring and the H_2O layer was acidified with a 10%w/w aquos solution of hydriodic acid to pH ~ 5. The organic layer was washed with water until neutral pH, and dried over MgSO4. The solvent was distilled under vacuo, the solid residue obtained was triturated with a mixture of CH_2Cl_2–hexane to obtained a solid. The solid was filtered off and washed. From the filtrate, solvents were distilled off under reduced pressure, the residue was purified by column chromatography on silica gel using CH_2Cl_2 as eluent and two fractions were collected.

After the solvent was distilled off under reduced pressure from the first fraction eluted, was obtained in total 8.57 g of tan solid (19.1 mmol, 65%)

^{1}H-NMR (300 MHz, $CDCl_3$), δ (ppm): 7.44 (dd, *J* = 5.6, 0.4 Hz, 2H), 6.93 (d, *J* = 5.6 Hz, 2H), 5.78 (d, *J* = 3.2 Hz, 1H), 2.24 (d, *J* = 3.3 Hz, 1H).

^{13}C-NMR (50 MHz, $CDCl_3$) δ (ppm): 71.6 (HOCH), 75.2 (2- and 2 -C),126.8 (4- and 4′-C or 5- and 5 -C), 131.3 (4- and 4 -C or 5- and 5 - C), 146.5 (3- and 3 -C).

Anal. Calcd for $C_9H_6I_2OS_2$: C, 24.12; H, 1.35; S, 14.31. Found: C, 4.20; H, 1.36; S, 14.41.

Compound (22)

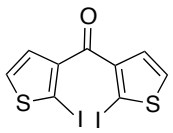

To a stirred solution of **21** (8.57 g, 19.1 mmol, 1 eqv.) in CH_2Cl_2 (110 mL) solid PCC (7.23 g, 28.7 mmol, 1.5 eqv.) was added in one portion at r.t. Stirring at r.t. was continued for 12 h. The reaction mixture was followed by TLC using CH_2Cl_2 as eluent. The resulting mixture was purified by column chromatography of silica gel using CH2Cl2 as eluent to obtain a light orange solid (**6**) (3.29 g, 7.3 mmol, 40%) (94%).

^{1}H-NMR (300 MHz, $CDCl_3$)), δ (ppm): 7.47 (d, *J* = 5.6 Hz, 2H), 7.06 (d, *J* = 5.6 Hz, 2H).

^{13}C-NMR (50 MHz, CDCl3), δ (ppm): 81.3 (2- and 2 -C), 129.8 (4- and 4 -C or 5- and 5 -C), 131.6 (4- and 4′-C or 5- and 5 -C), 143.2 (3- and 3 C), 185.5 (C=O).

Compound (23)

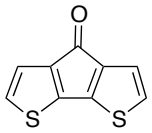

To a stirred solution of ketone **22** (1.21 g, 6.3 mmol, 1eqv.) in DMF (20 mL) Cu powder (1.39 g, 22.0 mmol, 3 eqv.) was added in one portion at r.t. The reaction mixture was heated under reflux for 15 h After cooling to r.t., the solid was filtered off and washed with Et_2O. The filtrate was washed with H_2O (150 mL), the layers were separated and the ether extracts was conbined, and dried over $MgSO_4$. After the solvent was distilled off under reduced pressure, the resulting solid was purified by column chromatography on silica gel using CH_2Cl_2 to obtain the product as a red solid (**23**) (8.13 mg, 4.2 mmol, 60%)

^{1}H-NMR (300 MHz, $CDCl_3$), δ (ppm): d = 6.97 (d, 2 H, J = 4.8, 3- and 5-H), 7.02 (d, 2 H, J = 4.8, 2- and 6-H).

^{13}C-NMR (50 MHz, $CDCl_3$), δ (ppm): d = 121.7 (2- and 6-C or 3- and 5-C), 127.2 (2- and 6-C or 3- and 5-C), 142.4 (3a- and 4a-C or 7a- and 7b-C), 149.2 (3a- and 4a-C or 7a- and 7b-C), 182.6 (C=O).

Compound (24)

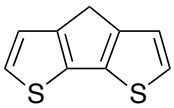

4HCyclopenta[2,1b:3,4b]dithiophen-4-one (1.21 mg, 6.1 mmol, 1eqv.) was mixed with 50% hydrazine (1.61 mg, 50.4 mmol, 1.52 ml, 2eqv.) and diethylene glycol (20 ml) at 70 ºC in a two-necked, 25 ml flask fitted with a condenser arranged for downward distillation. The mixture was heated to 70 ºC over a 2.5 hr period and maintained at this temperature until starting material was consumed and the hydrazone was formed (ornge solution). KOH (1.41 mg, 25.2 mmol, 4 eqv.) was added to the reaction mixture and the mixture was heated to 120 ºC. The mixture was followed by

TLC (haxane 100%). This green solution was then washed with ether (2 x 20 ml), wáter (2 x 20 ml), saturated solution of $Na_2S_2O_3$ (30 ml) and dried over Na_2SO_4. After filtration of the drying agent, the solvent was evaporated and the green solid obtained was subjected to column chromatography on silica gel using Hexane as eluent. Compound **24** was obtained (437.6 mg, 3.1 mmol) as a orange solid. Yiel: 54%

^{1}H-NMR (300 MHz, $CDCl_3$), δ (ppm): d = 7.19 (d, J = 4.8 Hz, 2H), 7.11 (d, J = 4.8 Hz, 2H), 3.57 (s, 2H).

^{13}C-NMR (50 MHz, $CDCl_3$), δ (ppm): 149.63, 138.59, 124.50, 123.00, 32.07.

Compound (25)

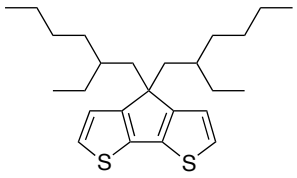

4H-Cyclopenta-[2,1-b:3,4-b']dithiophene (860 mg, 6.8 mmol, 1eqv.) was dissolved in DMSO 820 ml). The solution was purged with nitrogen, and ground 2-ethylhexyl bromide (2.83 g, 14,7 mmol, 2.7 ml, 2.2 eqv.) was added, followed by KI (22.2 mg, 0.13 mmol, 0.02 eqv.) at 0 °C during 15 min. At this temperatura KOH (855 mg,15.3 mmol, 2.3 eqv) was added in several portions.

The reaction was stirred overnight at room temperatura, under nitrogen. The mixture reaction was added into ice and extracted with ether. The organic layer was separated and dried over magnesium sulfate. Solvent was removed under vacuum, and the residue was purified by chromatography using hexanes as eluent. followed by vacuum distillation. The product was obtained as a colorless oil (1.31 g, 3.25 mmol) Yield: 48%)

^{1}H-NMR (250 MHz, $CDCl_3$), δ (ppm): 7.13 (m, 2H), 6.94 (m, 2H), 1.88 (m, 4H), 0.94 (m, 16H), 0.78 (t, 6.4 Hz, 6H), 0.61 (t, 7.3 Hz, 6H).

^{13}C-NMR (50 MHz, $CDCl_3$), δ (ppm): 158.01, 137.26, 124.39, 122.76, 53.67, 43.69, 35.43, 34.70, 29.03, 27.71, 23.18, 14.52, 11.08.

HRMS (FAB) m/z, Calc for $C_{25}H_{38}S_2$ (M+): 402.2415; found: 402.2417.

Compound (26)

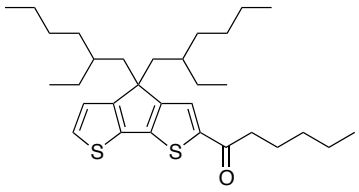

To a stirred solution of **25** (1.25 gr, 3.1 mmol, 1 eqv.) in dry dichloromethane (10 ml) was added hexanoyl chloride (500.7 mg, 3.7 mmol, 0.52 ml, 1.2 eqv.). The mixture was stirred for 1 h at r.t, cooled to 0 °C, and $AlCl_3$ (496.2 mg, 6.8 mmol, 2.2 eqv.) was added portionwise. The mixture was then allowed to warm to room temperature and stirred over night in argon atmosfere. The reaction was quenched by the addition of water (20 ml) and acidified with 2M aqueous HCl (40 ml). The mixture was extracted with dichloromethane. The organic layers were combined, washed with water (30 ml), dried ($MgSO_4$) and concentrated in vacuum to obtain a brown oil.

Purification by column chromatography (Hexanes/CH2Cl2, 1:1) yielded compound **26** (470 mg, 0.93 mmol) as a red viscous oil. Yield: 30 %

^{1}H-NMR (300 MHz, $CDCl_3$), δ (ppm): 7.54-7.49 (m, 1H), 7.32 (d, 3J = 5 Hz, 1H), 7.00-6.94 (m, 1H), 2.85 (t, 3J = 7.5, 2H), 1.98-1.83 (m, 4H), 1.77 (m, 3Japp ≈ 7.5 Hz, 2H), 1.43-1.32 (m, 3Japp ≈ 7.5 Hz, 4H), 1.05-0.81 (m, 18H), 0.75 (t, 3J = 7 Hz, 6H), 0.60 (2 x t, 9H: t, 3J = 7 Hz, 6H ; t, 3J = 7 Hz, 3H).

^{13}C-NMR (50 MHz, $CDCl_3$), δ (ppm): 193.6, 160.9, 157.5, 146.0, 143.2, 136.3, 128.0, 126.6, 122.5, 53.7, 43.14, 43.06, 39.0, 35.1, 34.3, 34.1, 31.6, 28.6, 27.3, 25.1, 22.8, 22.7, 22.5, 14.0, 13.9, 10.7, 10.6.

MS (FAB+, m-NBA): m/z (%) found 500.3 (67) [M]+, 501.3 (100) [M+H]+/[M]+.

HRMS (FAB+, m-NBA + PEGMMEH): m/z calc for $C_{31}H_{49}S_2O$: 501.3225; found 501.3220 [M+H]+.

UV-Vis: λmax(CH_2Cl_2)/nm = 284 (ε/dm^3 mol^{-1} cm^{-1} 8 420) ; 378 (28 500).

Compound (27)

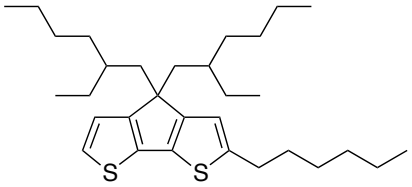

To a mixture of $LiAlH_4$ (480mg, 12.6 mmol, 10 eqv.) and $AlCl_3$ (504 mg, 3.8 mmol, 3 eqv.) in anhydrous ether (50 ml) at 0 °C was added compoun **11** (470 mg,0.93 mmol,1 eqv.) in dry ether. The mixture was allowed to warm to r.t. and then stirred in argon atmosferefor 2.5 h. The reaction was quenched by the careful addition of ether (4 ml) and 2 M aqueous HCl (10 ml). The product was extracted by washing the gray precipitate with ether. The combined organic layers were dried ($MgSO_4$). The resulting oil was purified by column chromatography on silica gel using Hexane to obtain the product as a orange oil (**11**) (500 mg, 1.02 mmol, 82%)

^{1}H-NMR (300 MHz, $CDCl_3$), δ (ppm): 7.05 (d, 3J = 5 Hz, 1H), 6.89(d, 3J = 5 Hz, 1H), 6.63 (s, 1H), 2.82 (t, 3J = 7.5 Hz, 2H), 1.90-1.74 (m, 4H), 1.67 (m, 3Japp ≈ 7 Hz, 2H), 1.10-0.82 (m, 20H), 0.81-0.72 (m, 6H), 0.81-0.72 (m, 6H), 0.66-0.56 (m, 9H).

^{13}C-NMR (50 MHz, $CDCl_3$), δ (ppm): 157.1, 156.2, 145.5, 137.4, 134.0, 122.9, 122.2, 119.7, 53.3, 43.2, 35.0, 34.2, 31.9, 31.6, 30.8, 28.6, 27.34, 27.29.

MS (FAB+, m-NBA): m/z found 486.3 [M]+.

HRMS (FAB+, m-NBA + PEGH): m/z calc for $C_{31}H_{50}S_2$: 436.3354, found 486.3348 [M]+.

UV-Vis: λmax(CH_2Cl_2)/nm = 296 (ε/dm^3 mol^{-1} cm^{-1} 5 340), 326 (broad sh, 5 000), 377 (broad sh, 3 800).

Compound (28)

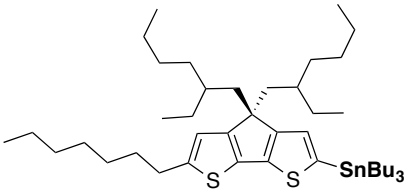

The **27** (268 mg, 0.40 mmol),was introduced in an oven-dried Schlenk flask, and then three cycles of vacuum-argon were realized. Under argon steam, dry THF (6ml) was added by syringe in the flask through a septum/needle, and the resulting solution stirred at room temperature until the full dissolution of the starting material. Next, the flask was immerged in an acetone/N_2(l) bath and cooled at -78°C for 5 min. Afterwards, a solution of *n*BuLi in THF/hexane 0.25 M *n*BuLi solution in hexanes (2.1 mL, 0.53 mmol) was added drop by drop by syringe to the solution through a septum/needle. At the end of the addition, the mixture was stirred for additional 60–90 min at the addition temperature and then tributyltin chloride (0.2 mL, 0.74 mmol), was added dropwise. The mixture was stirred at -60°C for an additional hour, and then allowed to warm slowly to room temperature within 1–2 hours. Finally, few drops of a saturated aqueous NH_4Cl solution were added to quench the reaction. The reaction mixture was diluted in a copious amount of hexane, then successively dried over $MgSO_4$, filtrated, and solvents evaporated to dryness. The crude yellow oil was used without further purification in the next step (yield supposed to be quantitative for this step).

Compound (29)

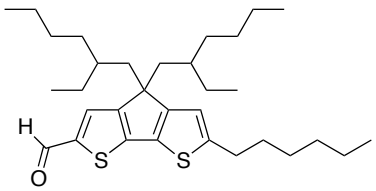

To a stirred solution of **27** (580 mgr, 1.26 mmol, 1 eqv.) in DCE (20 ml)under Ar, was added with a syringe $POCl_3$ (3.65 mmol, 0.22 ml, 2.9 eqv.) and DMF (2.40 mmol, 0.27 ml, 1.9 eqv.). The mixture was stirred for 1 h at r.t, then cooled to 0 °C, and

mixture was heated under reflux over night. After cooling to r.t., the reaction was quenched by the addition of a saturated aqueous solution of AcOK (8 ml) and the mixture was stirred for 30 min. Next, the mixture was extracted with DCM (2×30 ml), .The combined organic layers were dried ($MgSO_4$), and then evaporated to dryness. The resulting brown oil was purified by column chromatography on silica gel using a gradient (Hexane/AcOEt 10 : 2 to 8 : 1) to obtain the product as an orange oil (**29**) (470 mg, 0.96 mmol) Yield: 73 %

^{1}H-NMR (300 MHz, $CDCl_3$), δ (ppm): 9.77 (s, 1H, CHO), 7.51 (s, 1H, ArH), 6.68 (s, 1H, ArH), 2.81 (t, 2H, 3J= 7 Hz, CH_2(α) hexyl chain), 1.95-1.73 (m, 4H, $2CH_2$(α) ethylhexyl chain), 1.72-1.54 (m, 2H, 2 C*H ethylhexyl chain), 1.41-1.14 (m, 6H, 3 CH_2), 1.03-0.47 (m, 33H, $9CH_2$+ $5CH_3$).

^{13}C-NMR (50 MHz, $CDCl_3$), δ (ppm): 182.0 (CHO), 161.8 (3 signals), 156.3 (3s), 151.2, 148.7, 141.9, 133.1, 130.6, 119.9, 53.6, 42.9, 35.0, 34.1, 33.9, 31.6, 31.4, 30.9, 28.5, 28.4, 28.3, 27.3, 27.1, 22.6, 22.5, 22.4, 13.9, 10.5 (2s).

MS (FAB+, m-NBA): m/z found 515.3 (100) [M+H]+.

HRMS (FAB+, m-NBA + PEGH): m/z calc for $C_{32}H_{51}OS_2$: 515.3381 [M+H]+; found: 515.3369.

Compound (30)

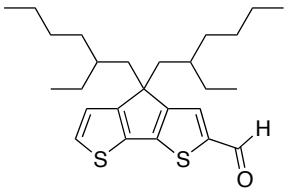

Compound (colorless oil, 500 mg, 1.24 mmol, 1 eqv.) was introduced in an oven dried Schlenk flask, and three cycles of vacuum-argon were realized. Under argon atmosfere, dry THF (8 mL) was then added with a syringe and the resulting solution was estirred at -78°C. Afterward, a 1.6M solution of nBuLi in Hexane (1.5 mmol, 0.93 ml) was added drop by drop with a syringe to the solution at -78°C and the mixture stirred for 2h at this temperature. The color of the solution was changed light orange to black. Next, DMF (126.4 mg, 1.7 mmol, 1.33 ml) by syringe al the same temperatura

for 2h room temperature. The mixture was then allowed to warm to room temperature and stirred over night in argon atmosfere.

Then water (0.5 mL) was added with stirring and the mixture was dried over MgSO4. The solvent was evaporated under vacuo to obtain a brown oil.

Purification by column chromatography (Hexanes 100% to Hexane/CDM, 1:1) yielded compound **12** (160.2 mg, 0.37 mmol) as a red viscous oil. Yield: 30 %

^{1}H-NMR (300 MHz, $CDCl_3$), δ (ppm): 9.77 (s, 1H, CHO), 7.51 (s, 1H, ArH), 6.68 (s, 1H, ArH), 2.81 (t, 2H, 3J= 7 Hz, CH_2(α) hexyl chain), 1.95-1.73 (m, 4H, $2CH_2$(α) ethylhexyl chain), 1.72-1.54 (m, 2H, 2 C*H ethylhexyl chain), 1.41-1.14 (m, 6H, 3 CH_2), 1.03-0.47 (m, 33H, $9CH_2$+ $5CH_3$).

^{13}C-NMR (50 MHz, $CDCl_3$), δ (ppm): 182.0 (CHO), 161.8 (3 signals), 156.3 (3s), 151.2, 148.7, 141.9, 133.1, 130.6, 119.9, 53.6, 42.9, 35.0, 34.1, 33.9, 31.6, 31.4, 30.9, 28.5, 28.4, 28.3, 27.3, 27.1, 22.6, 22.5, 22.4, 13.9, 10.5 (2s).

MS (FAB+, m-NBA): m/z found 515.3 (100) [M+H]+.

HRMS (FAB+, m-NBA + PEGH): m/z calc for $C_{32}H_{51}OS_2$: 515.3381 [M+H]+; found: 515.3369.

Synthesis of the BDT-functionalized bipyridines

Ligand L-230 (31)

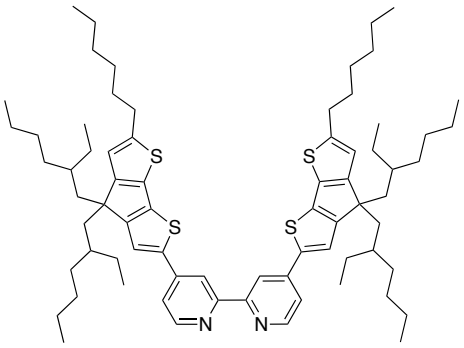

Compound building block (250 mg, 0.51 mmol) was introduced in an oven dried Schlenk flask, and three cycles of vacuum-argon were realized. Under argon steam, dry THF (5 mL) was then introduced with a syringe and the resulting solution

stirred at room temperature until the complete dissolution of the starting material. Next, the Schlenk flask was immerged in a H_20/NaCl ice bath at -10°C. Afterward, a 1.6 M solution of nBuLi in THF/hexane (0.45 mL, 0.72 mmol) was added drop by drop with a syringe to the solution at -10°C and the mixture stirred for 2h at the addition temperature. Next, tributyltin chloride (0,19 mL, 0.70 mmol) was added dropwise and the mixture stirred at -10°C for additional 2h before allowing it to warm to room temperature. The mixture was then stirred at room temperature overnight under argon. Finally, few drops of a saturated aqueous NH_4Cl solution were added to quench the reaction. After dilution in a copious amount of hexane, the solution was dried over $MgSO_4$, filtrated and solvents evaporated. The crude product was used without further purification in the next reaction step (yield was supposed to be quantitative).

^{1}H-NMR (300 MHz, $CDCl_3$), δ (ppm): 6.89 (s, 1H), 6.21 (s, 1H), 2.81 (t, 3J = 7 Hz, 2H), 1.96-1.77 (m, 4H), 1.74-0.70 (m, 59H), 0.69-0.52 (m, 9H).

In the second instance, the stannyl compound (303 mg, 390 µmol) and 4,4'-dibromo-2,2'-bipyridine (41 mg, 131 µmol) were dissolved in dry toluene (20 mL) in an argon flushed two-necked flask. The solution was degassed vigorously by bubbling argon through a needle/septum for 30 min. Afterward, $Pd(PPh_3)_4$ (45 mg, 38.9 µmol) was introduced in the flask and the solution heated while keeping a gentle argon bubbling. Once refluxing, the solution was let under inert atmosphere (Ar) and the reflux maintained for 3 days. After cooling down to room temperature, toluene was evaporated under reduced pressure and the crude purified by chromatography column on silica gel (eluent: CH_2Cl_2 containing 1% of MeOH and 0.2% of Et_3N), followed by GPC (Eluent: toluene), to afford **31** (61 mg, 54.2 umol) in a 41% yield as a black-yellowish oil.

Ligand (34) and Ligand (35)

General procedure :

Step 1 : Racemic mixtures of alcohols.

Commercially available 4,4'-dimethyl-2,2'-bipyridine was introduced in an oven dried 50 mL Schlenk flask, and then three cycles of vacuum-argon were realized. Afterwards, THF (5 mL) was introduced under argon with a syringe, and the resulting solution stirred at room temperature until the complete dissolution of the material. Next, the mixture was cooled at –78°C for 10 min, and then a 2M

commercial solution of LDA in heptane/THF (0.27 ml, 0.54 mmol) was added with a syringe to the colorless solution, which turned brown immediately. The solution was let to reach -60°C within 30 min, and then warmed at -10°C for additional 25 min (during this period of time the solution progressively turned from brown to deep dark black-reddish). The solution was cooled again at -78°C, and then a solution of aldehyde 2 (351 mg, 0.68mmol) in THF (5mL) was transferred under argon in the Schlenk flask with a cannula (the solution progressively turned bright orange). At the end of the addition, the mixture was stirred at -60°C for 2h, and then warmed at -10°C for additional 30 min. Finally, few drops of an aqueous saturated NH_4Cl solution were added to quench the reaction. After 10 min of stirring, the reaction mixture was diluted in CH_2Cl_2 (40 mL), successively dried over Na_2SO_4, filtered through a small plug of Celite, and then the solvents evaporated to dryness under reduced pressure. The crude orange oil was purified by flash chromatography column on SiO_2 using first CH_2Cl_2 100% as eluent until the disappearance of staring material (aldehyde 2), then CH_2Cl_2/MeOH/Et_3N (100:5:1)

As was obtained as complex racemic mixtures of alcohols, characterization was done on the next compound, see next step (compound **32** and **33**).

- Ruthenium Complex Intermeciate (**32**)

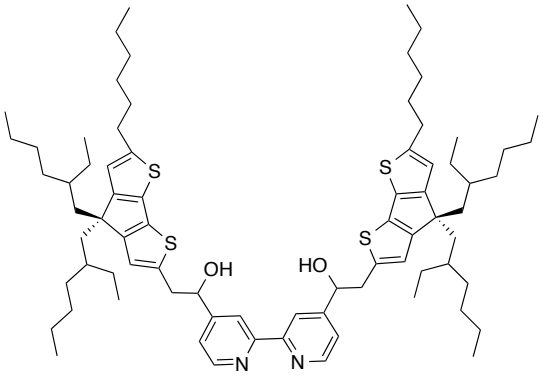

To afford in 89% yield (288 mg, 0.24 mmol) as a bright yellowish viscous solid.

- Ruthenium Complex Intermeciate (**32**)

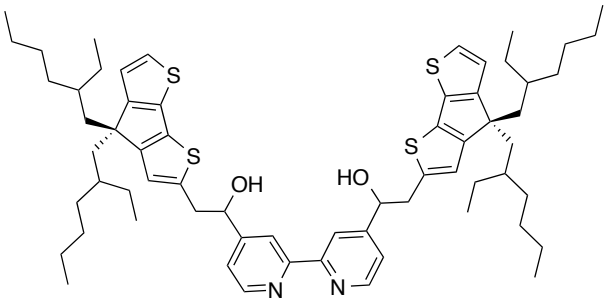

To afford in 89% yield (145 mg, 0.24 mmol) as a bright yellowish viscous solid.

Step 2 : Synthesis of Ligands- Dehydration. (**34** and **35**)

- Ligand **L-232** (**34**)

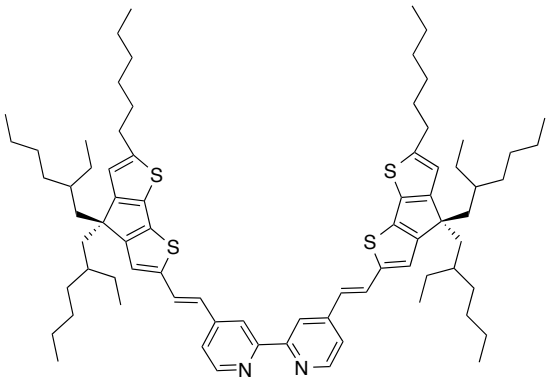

A solution of **32** (288 mg, 0.24 mmol), PPTS (50 mg, 0.20 mmol) and a catalytic amount of I_2 (~2 mol%) in dry toluene (20 mL) was refluxed in a Dean-Stark apparatus for 36h under Ar. After cooling to room temperature, Et_3N (≈ 0.5 mL) was added to the

solution, and then the solvents evaporated to dryness under reduced pressure. The crude was purified by successive chromatography columns (SiO_2; eluent: CH_2Cl_2/MeOH/Et_3N, 100:0.5:0.1), followed by gel permeation chromatography (eluent: toluene). Purification was achieved by trituration in MeOH (twice) to afford **4** in 50% yield (141 mg, 0.12 mmol) as a dark brown-yellowish viscous solid.

^{1}H-NMR (300 MHz, $CDCl_3$), δ (ppm): 8.63 (d, 3*J*= 5 Hz, 2H, 2Ar*H* bipy), 8.50 (s, 2H, 2Ar*H* bipy), 7.59 (d, 3*J*trans= 16 Hz, 2H, 2C=C*H*), 7.31 (d, 3*J*= 5 Hz, 2H, 2Ar*H* bipy), 7.00 (s, 2H, 2Ar*H* CDT), 6.84 (d, 3*J*trans= 16 Hz, 2H, 2C=C*H*), 6.66 (s, 2H, 2Ar*H* CDT), 2.84 (t, 3*J*= 7 Hz, 4H, 2C*H*2(α) hexyl chains), 1.94-1.78 (m, 8H, 4C*H*2(α) ethylhexyl chains), 1.75-1.61 (m, 4H, 4C**H* ethylhexyl chains), 1.47-0.52 (m, 78H, 24C*H*2 + 10C*H*3).

^{13}C-NMR (75 MHz, $CDCl_3$), δ (ppm): 158.4 (2 signals), 156.6 (3s), 156.4, 149.4, 147.5(3s), 145.9, 140.6 (3s), 139.0 (2s), 133.9, 127.7(3s), 123.4, 122.2 (2s), 120.5, 119.8, 117.4, 53.7, 43.2(3s), 35.1, 34.3, 34.2, 31.9, 31.6, 30.9 (2s) 29.7, 28.7, 28.6, 28.5, 27.4, 27.3, 22.8, 22.8, 22.6, 14.1, 10.7.

MS MS (MALDI-TOF): *m/z* (%): 1177.8 (100) [M+H]+. HRMS (MALDI-TOF) *m/z*: calcd for C76H109N2S4: 1177.7468 [M+H]+; found: 1177.7465.

UV-Vis: λ_{max}(CH_2Cl_2)/nm = 282 (25 860), 431 (60 650).

- Ligand **L-233** (**35**)

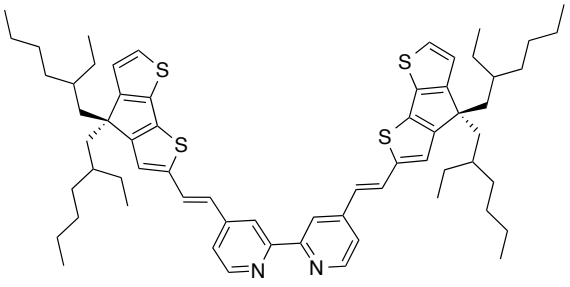

^{1}H-NMR (300 MHz, $CDCl_3$), δ (ppm): 8.63 (d, 3*J*= 5 Hz, 2H, 2Ar*H* bipy), 8.50 (s, 2H, 2Ar*H* bipy), 7.59 (d, 3*J*trans= 16 Hz, 2H, 2C=C*H*), 7.31 (d, 3*J*= 5 Hz, 2H, 2Ar*H*

bipy), 7.00 (s, 2H, 2Ar*H* CDT), 6.84 (d, 3*J*trans= 16 Hz, 2H, 2C=C*H*), 6.66 (s, 2H, 2Ar*H* CDT).

^{13}C-NMR (75 MHz, $CDCl_3$), δ (ppm): 158.4 (2 signals), 156.6 (3s), 156.4, 149.4, 147.5(3s), 145.9, 140.6 (3s), 139.0 (2s), 133.9, 127.7(3s), 123.4, 122.2 (2s), 120.5, 119.8, 117.4.

MS MS (MALDI-TOF): *m/z* (%): 1177.8 (100) [M+H]+. HRMS (MALDI-TOF) *m/z*: calcd for C76H109N2S4: 1177.7468 [M+H]+; found: 1177.7465.

UV-Vis: $\lambda_{max}(CH_2Cl_2)$/nm = 282 (25 860), 431 (60 650)

2.5.2 Synthesis of Ruthenium Complex :

General procedure for the microwave-assisted synthesis and purification of the ruthenium complexes.

In a 10 mL flask topped with a condenser, the appropriate bipyridine ligand (1.0 eq) and dichloro(*p*-cymene)-ruthenium(II) dimer (0.55–0.65 eq, *i.e.* 1.1–1.3 eq of formal "Ru(II)") were dissolved under Ar in a 1:1 mixture of $CHCl_3$ and EtOH (4 mL). The obtained solution was stirred and heated to reflux (c.a. 60–70 °C) under microwave irradiation (15–30 W) for 45 min in the dark. After removing the solvents under reduced pressure, the crude mononuclear ruthenium complex intermediates Ru[L] were obtained as bright deep-red oils. All these crude intermediates were characterized by ^{1}H NMR ($CDCl_3$), and then used as well in the next step. Next, the above-mentioned crude intermediate was dissolved in PhCl (0.5 mL) under argon, and then a solution of 4,4'-dicarboxylic acid-2,2'-bipyridine "dcbpy" (appropriate excess 1.2–1.6 eq) in dry DMF (4.5 mL) was added. The solution was irradiated under MW (80–115 W) to reach gradually 130–140 °C (reflux) within c.a. 10–15 min. The MW irradiation was then regulated automatically to maintain this range of temperature for additional 45 min. After cooling back to room temperature, NH_4NCS (50–75 equivalents) was added to the resulting deep dark-green solution, and then irradiated again at 130–140 °C (reflux) for additional 40 min, affording a deep dark brown-red solution. Finally, DMF was removed from the reaction flask by high-vacuum rotary evaporation to afford a deep dark-red pasty solid. This paste was then triturated with a 0.05 M HCl aqueous solution (≈25 mL), and the resulting fine black suspension was successively filtrated, washed with a copious amount of a 0.05 M HCl aqueous solution, air-dried, and washed with

the necessary amount of MeOH until the disappearance of a red-coloured filtrate (N3 dye). The filtrates were discarded and the remaining insoluble black solid recovered by dissolution in a mixture of THF/MeOH 7:3. After evaporation of solvents, crude was purified by gel permeation chromatography (Bio-rad Bio-beds® SX-1, eluent: THF/MeOH (7:3). The main fraction was evaporated to dryness and purification achieved by trituration in MeOH. The resulting fine dark black suspension was filtrated and washed with MeOH. The filtrates were discarded and the insoluble remaining product recovered with a mixture of CH_2Cl_2/MeOH 7:3.

2.5.4.1 Synthesis of the Ru(II) complexes based on BDT

- Ruthenium Complex **TT-221** (**36)**

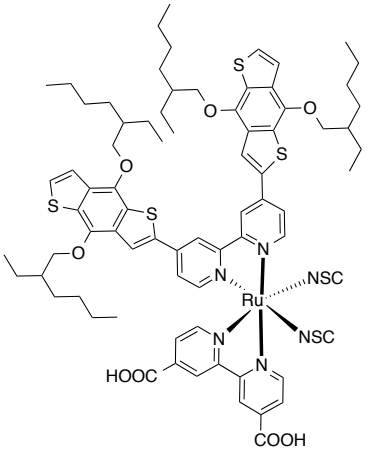

Prepared and purified according to the general procedure described for the microwave-assisted synthesis of ruthenium complexes, from **L221** (20 mg, 19.1 µmol), dichloro*(p*-cymene)-ruthenium(II) dimer (6.5 mg, 10.6 µmol), dcbpy (5.9 mg, 24.2 µmol) and NH_4NCS (100 mg, 1314 µmol), to afford **TT221** (27 mg, 17.9 µmol) in 94 % yield as a fine black powder.

^{1}H-NMR (300 MHz, $CDCl_3$), δ (ppm): . 9.61 (d, ^3J = 6 Hz, 1H), 9.51 (d, ^3J = 6 Hz, 1H), 8.93 (s, 1H), 8.79 (s, 1H), 8.54 (s, 1H), 8.40 (s, 1H), 8.21 (d, ^3J = 6 Hz, 1H), 8.17 (s, 1H), 8.04 (d, ^3J = 6 Hz, 1H), 7.93 (s, 1H), 7.73 (d, ^3J = 6 Hz, 1H), 7.60 (d, ^3J = 6 Hz, 1H), 7.56–7.36 (m, 5H), 7.34 (d, ^3J = 6 Hz, 1H), 4.31 (d, ^3J = 5 Hz, 2H), 4.26 (d, ^3J = 5 Hz, 2H), 4.20 (d, ^3J = 5 Hz, 2H), 4.26 (d, ^3J = 5.5 Hz, 2H), 2.07–0.62 (m, 60H).

MS (MALDI-TOF; DCTB): *m/z* found (%) 1448.4 (67) $[M\text{-}(NCS)]^+$, 1506.4 (100) $[M]^+$.

HRMS (MALDI-TOF, DCTB + PEGNa1500): *m/z* calc (%) for $^{96}RuC_{76}H_{88}N_6O_8S_6$: 1500.4058 (9), $^{102}RuC_{76}H_{88}N_6O_8S_6$: 1506.4043 (100); found 1500.4110 (9), 1506.4047 (100) $[M]^+$.

UV-Vis: λmax(CH2Cl2)/nm= 282 (*e* /dm^3 mol^{-1} cm^{-1}: 70 100), 314 (58 600), 338 (49 900), 425 (35 500), ≈560 (br sh, 19 000).

- Ruthenium Complex **TT-229** (**37**)

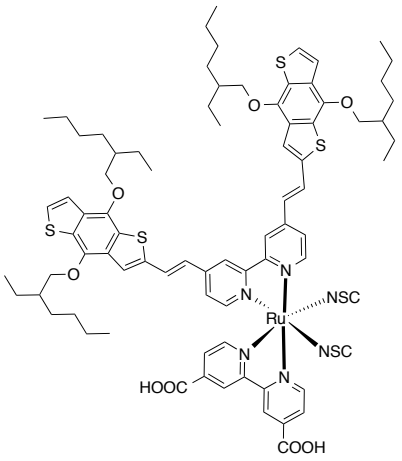

Prepared and purified according to the general procedure described for the microwave assisted one-pot synthesis of ruthenium complexes, from **L-229** (21.0 mg, 19.1 µmol), dichloro(*p*-cymene)-ruthenium(II) dimer (7.0 mg, 11.4 µmol), dcbpy (6.6 mg, 27.0 µmol) and NH_4NCS (70 mg, 920 µmol), to afford **TT-229** (18.7 mg, 12.0 µmol) in 76 % yield as a fine black powder.

^{1}H NMR (300 MHz, $CDCl_3$), δ (ppm): 9.62 (d, ^3J = 5 Hz, 1H), 9.22 (d, ^3J = 6 Hz, 1H), 8.80 (s, 1H), 8.65 (s, 1H), 8.14 (s, 1H), 8.03 (s, 1H), 7.96 (bs, 1H), 7.80–7.60 (m, 2H), 7.55 (d, ^3J = 5 Hz, 1H), 7.50 (d, ^3J = 6 Hz, 1H), 7.49–7.46 (m, 2H), 7.43 (bs, 2H), 7.43–7.39 (m, 1H), 7.34 (d, ^3J = 5 Hz, 1H), 7.29 (bs, 1H), 7.21 (d, ^3J = 5 Hz, 1H), 6.93 (d, ^3J = 5 Hz, 1H), 7.67 (d, $^3J_{trans}$ = 16 Hz, 1H), 7.56 (d, $^3J_{trans}$ = 16 Hz, 1H), 4.29 (d, ^3J = 5 Hz, 2H), 4.21 (d, ^3J = 5 Hz, 4H), 4.29 (bs, 2H), 2.00–1.18 (m, 36H), 1.18–0.67 (m, 24H).

MS (MALDI-TOF; DCTB): *m/z* found (%) 1500.4 (55) $[M\text{-}(NCS)]^+$, 1558.4 (100) $[M]^+$.

HRMS (MALDI-TOF, DCTB + PEGNa2000): $^{96}RuC_{80}H_{92}N_6O_8S_5$: 1552.4371 (9), $^{102}RuC_{80}H_{92}N_6O_8S_5$: 1558.4357 (100); found 1552.4401 (5), 1558.4345 (100) $[M]^+$.

UV-Vis: $\lambda_{max}(CH_2Cl_2)$/nm = 294 (e / dm^3 mol^{-1} cm^{-1} 36 100), 322 (40 600), 362 (43 800), 446 (38 200), ≈560 (br sh, 15 900).

- Ruthenium Complex **TT-222** (**38**)

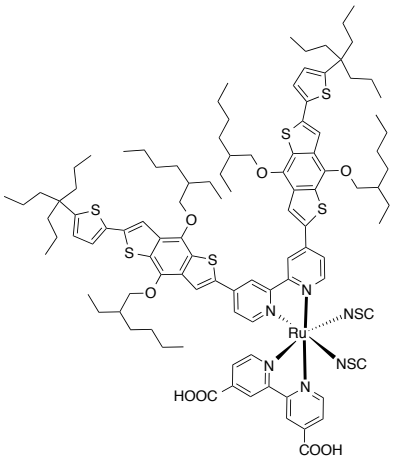

Prepared and purified according to the general procedure described for the microwave assisted synthesis of ruthenium complexes, from **L-222** (20 mg, 13.4 µmol), dichloro(*p*-cymene)-ruthenium(II) dimer (5.2 mg, 8.50 µmol), dcbpy (5.0 mg, 20.5

μmol) and NH_4NCS (30 mg, 394 μmol), to afford **TT-222** (13.4 mg, 6.87 μmol) in 51 % yield as a fine black powder.

^{1}H-NMR (300 MHz, $CDCl_3$), δ (ppm): 9.67 (d, ^3J = 6 Hz, 1H), 9.48 (d, ^3J = 6 Hz, 1H), 8.91 (s, 1H), 8.76 (s, 1H), 8.50 (s, 1H), 8.37 (s, 1H), 8.22 (d, ^3J = 6 Hz, 1H), 8.16 (s, 1H), 8.02 (d, ^3J = 6 Hz, 1H), 7.92 (s, 1H), 7.76 (d, ^3J = 6 Hz, 1H), 7.59 (dd, ^3J = 6 Hz and ^4J = 1.5 Hz, 1H), 7.44 (s, 1H), 7.44–7.42 (m, 1H), 7.36 (s, 1H), 7.32 (d, ^3J = 6 Hz, 1H), 7.15 (d, ^3J = 3.5 Hz, 1H), 7.10 (d, ^3J = 3.5 Hz, 1H), 6.73 (d, ^3J = 3.5 Hz, 1H), 6.70 (d, ^3J = 3.5 Hz, 1H), 4.30 (d, ^3J = 5 Hz, 2H), 4.25 (d, ^3J = 5 Hz, 2H), 4.19 (d, ^3J = 5 Hz, 2H), 4.15 (d, ^3J = 5 Hz, 2H), 1.96–0.64 (m, 102H).

MS (MALDI-TOF; DCTB): *m/z* found **(%)** 1892.7 (55) $[M\text{-}(NCS)]^+$, 1950.7 (100) $[M]^+$, 3846.4 (6) ($[(M)_2\text{-}(NCS)]^+$).

HRMS (MALDI-TOF, DCTB + PEGNa2000): *m/z* calc (%) for $^{96}RuC_{104}H_{132}N_6O_8S_8$: 1944.6943 (7), $^{102}RuC_{104}H_{132}N_6O_8S_8$: 1950.6934 (100); found 1944.6909 (5), 1950.6943 (100) $[M]^+$.

UV-Vis: λmax(CH_2Cl_2)/nm= 238 (*e* /dm^3 mol^{-1} cm^{-1}: 65 600), 285 (51 000), 320 (42 900), 373 (52 600), 441 (46 800), 559 (br, 21 600).

Ruthenium Complex TT-223 (39)

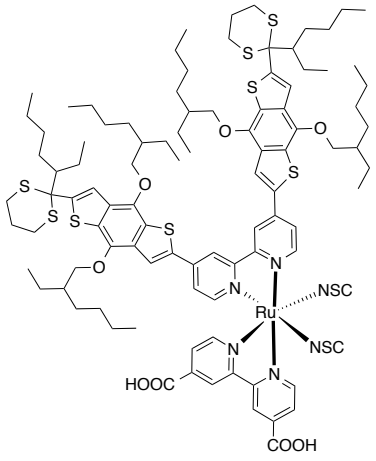

Prepared and purified according to the general procedure described for the microwave assisted synthesis of ruthenium complexes, from **L-223** (20.1 mg, 13.6 µmol), dichloro(*p*-cymene)-ruthenium(II) dimer (5.1 mg, 8.33 µmol), dcbpy (4.9 mg, 20.1 µmol) and NH_4NCS (50 mg, 657 µmol), to afford **TT-223** (19.3 mg, 9.95 µmol) in 73% yield as a fine black powder.

^{1}H-NMR (300 MHz, $CDCl_3$), δ (ppm): 9.67 (d, ^3J = 6 Hz, 1H), 9.50 (d, ^3J = 6 Hz, 1H), 8.94 (s, 1H), 8.79 (s, 1H), 8.57 (s, 1H), 8.43 (s, 1H), 8.24 (d, ^3J = 6 Hz, 1H), 8.21 (s, 1H), 8.09–8.01 (bs, 1H), 7.97 (s, 1H), 7.78 (d, ^3J = 6 Hz, 1H), 7.70 (m: s+d, 2H), 7.63 (s, 1H), 7.61 (d, ^3J = 6 Hz, 1H), 7.35 (bs, 1H), 4.33 (d, ^3J = 5 Hz, 2H), 4.26 (d, ^3J = 5 Hz, 2H), 4.23 (d, ^3J = 5 Hz, 2H), 4.17 (d, ^3J = 5 Hz, 2H),), 3.22 (d, ^2J = 14 Hz, 2H), 3.19 (d, ^2J = 14 Hz, 2H), 3.04 (d, ^2J = 14 Hz, 2H), 2.94 (d, ^2J = 14 Hz, 2H), 2.10–0.66 (m, 94H).

MS (MALDI-TOF; DCTB): *m/z* found (%) 1882.6 (33) $[M-(NCS)]^+$, 1938.6 (99), 1939.6 (95), 1940.6 (100) $[M]^+$.

HRMS (MALDI-TOF, DCTB + PEGNa2000): $^{96}RuC_{98}H_{128}N_6O_8S_{10}$: 1932.6071 (7), $^{102}RuC_{98}H_{128}N_6O_8S_{10}$: 1938.6059 (99), found 1932.6059 (8), 1938.6055 (99) $[M]^+$.

UV-Vis: λmax(CH_2Cl_2)/nm= 225 (*e* /dm^3 mol^{-1} cm^{-1}: 65 900), 285 (48 300), 307 (sh, 40 900), 317 (sh, 39 500), 352 (39 700), 437 (30 000), 565 (br, 16 100).

2.5.4.1 Synthesis of the Ru(II) complexes based on CDT

Rutenium Complex TT-230 (40)

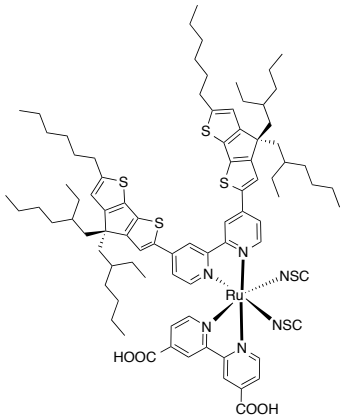

In an argon flushed flask, the free ligand **27** (21.5 mg, 19.1 μ mol) and dichloro(*p*-cymene)-ruthenium(II) dimer (7.05 mg, 11.5 μ mol) were dissolved in a 1:1 mixture of CHCl3/EtOH (4 mL) and the solution stirred under microwave irradiation at 65-70 $^{\circ}$ C for 45 min. Next, the solvents were removed under reduced pressure and the obtained crude intermediate re-dissolved in PhCl (0.5 mL). Subsequently, a solution of 4,4'- dicarboxylic acid-2,2'-bipyridine (6.61 mg, 27.1 μ mol) in dry DMF (4.5 mL) was added and the solution heated under MW at 135–140 °C for 45 min. Next, NH4NCS (80 mg, 1.05 mmol) was added to the obtained deep dark green solution and the reaction mixture irradiated again at 135–140 °C for additional 40 min, affording a deep dark brown-red solution. Finally, DMF was removed from the reaction flask by high-vacuum rotary evaporation to afford a black- reddish pasty solid. Afterwards, this solid was triturated with a 0.05 M HCl aqueous solution and the obtained fine black suspension filtrated, air-dried, and washed with the necessary amount of a 3:1 MeOH/H2O mixture until the disappearance of a red-coloured filtrate (N3 dye). The filtrate was discarded and the remaining insoluble black solid dissolved in a THF/MeOH mixture (7:3). After evaporation of solvents, crude was purified by Gel Permeation Chromatography (Bio-rad, Bio-beds SX-1, eluent: THF/MeOH 7:3). After evaporation to dryness of the main fraction, the remaining solid was dried under vacuum and purification achieved by trituration in hexane. The resulting fine dark black

suspension was filtrated and washed with a copious amount of hexane. The hexane filtrates were discarded and the solid recovered with a CH2Cl2/MeOH mixture (7:3). **TT-230** (11.6 mg; 7.58 μ mol) was obtained in 40 % yield as a fine black powder.

^{1}H and 2D-COSY NMR (300 MHz, CDCl3/MeOD 7:4), δ (ppm): 9.67 (d, 3J = 5.5 Hz, 1H), 9.26 (d, 3J = 6 Hz, 1H), 8.91 (s, 1H), 8.77 (s, 1H), 8.37 (br. s, 1H), 8.23 (br. s, 2H), 7.93-7.78 (m, 2H), 7.74 (s, 1H), 7.65-7.59 (m, 1H), 7.54-7.48 (m, 1H), 7.22-7.17 (m, 1H), 7.16-7.10 (m, 1H), 7.74 (s, 1H), 7.68 (s, 1H), 2.88 (t, 3J = 7 Hz, 2H), 2.83 (t, 3J = 7 Hz, 2H), 2.06-1.93 (m, 4H), 1.92-1.79 (m, 4H), 1.68 (m, 3J = 7 Hz, 4H), 1.45-1.19 (m, 12H), 1.11-0.80 (m, 36H), 0.80-0.50 (m, 30H).

MS (MALDI–TOF; DCTB): *m/z* (%) found 1528.7 (40) [M-(NCS)]+, 1586.6 (100) [M]+.

HRMS(MALDI–TOF; DCTB + PEGMeNa750 + PEGNa2000): *m/z* calcd for $_{96}RuC_{86}H_{112}N_6O_8S_{10}$: 1580.6140 (8.5), $_{102}RuC_{98}H_{128}N_6O_8S_{10}$: 1586.6127 (100), found 1580.6164 (8), 1586.6077 (100) [M]+.

UV-Vis: $\lambda_{max}(CH_2Cl_2)$/nm = 305 (/dm^3 mol^{-1} cm^{-1} 25 700) ; 317 (25 500) ; 439 (51 100) ; 581 (br sh, 19 500).

Ruthenium Complex TT-232 (41)

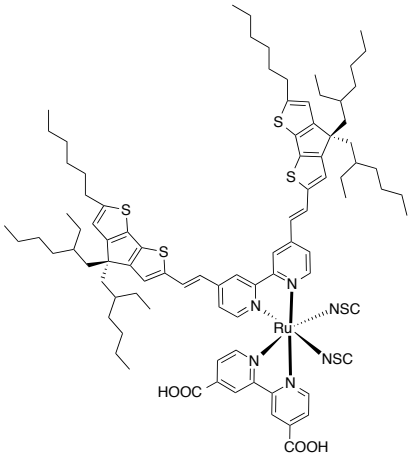

Ligand (19.0 mg, 16.1 μ mol), dichloro(*p*-cymene)ruthenium(II) dimer (5.94 mg, 9.70 μ mol), dcapy (5.67 mg, 23.2 μ mol), and NH_4NCS (50 mg, 657 μ mol). After removal of DMF under high-vacuum distillation, the remaining pasty solid was triturated in a copious amount of an aqueous 0.1 M HCl solution. The remaining fine black suspension was successively filtered-off, air-dried, and then washed with a copious amount of an aqueous 0.1 M HCl solution, followed by a minimum amount of cold MeOH. The filtrates were discarded, and the remaining solid was recovered by dissolution in CH2Cl2/MeOH mixtures. After evaporation of solvents to dryness, the crude complex was purified on gel permeation chromatography column (eluent: THF/MeOH mixtures). Purification was achieved by trituration in hexanes to afford **TT232** (18.6 mg, 11.3 μ mol) in 70% yield as a dark black powder.

^{1}H and 2D-COSY NMR (300 MHz, CDCl3/MeOD 7:4), δ (ppm): .71 (br d, 3*J*~ 5 Hz, 1H, Ar*H* bipy), 9.23 (d, 3*J*= 6 Hz, 1H, Ar*H* bipy), 8.85 (s, 1H, Ar*H* bipy), 8.70 (s, 1H, Ar*H* bipy), 8.25 (s, 1H, Ar*H* bipy), 8.15 (br s, 1H, Ar*H* bipy), 8.10 (s, 1H, Ar*H* bipy), 7.81-7.65 (m, 2H, 2Ar*H* bipy), 7.65-7.49 (m, 3H, Ar*H* bipy+2Ar*H* CDT), 7.27-7.07 (m, 3H, Ar*H* bipy+2C=C*H*), 6.92-6.50 (m, 5H, Ar*H* bipy+2Ar*H* CDT+2C=C*H*) , 2.93-2.73 (m, 4H, 2C*H*2(α) hexyl chains), 2.08-1.77 (m, 8H, 4C*H*2(α) ethylhexyl

chains), 1.77-1.61 (br s, 4H, 4C*H ethylhexyl chains), 1.45-0.46 (m, 78H, 24CH2+10CH3).

MS (MALDI–TOF; DCTB): *m/z* (%) found 1581.6 (40) $[M-(NCS)]^+$, 1638.6 (100) $[M]^+$

HRMS(MALDI–TOF; DCTB): *m/z* calcd $RuC_{90}H_{116}N_6O_4S_6$: 1638.6441 (100) [M]+; found 1638.6402 (100) .

UV-Vis: $\lambda_{max}(CH_2Cl_2)$/nm = 318 (26 000), 473 (47 700), 582 (br sh, 24 100).

Ruthenium Complex TT-232 (42)

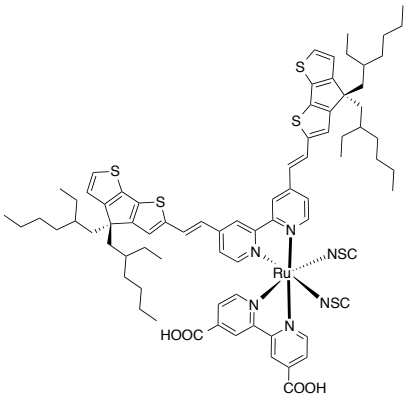

Ligand (20.0 mg, 16.1 μ mol), dichloro(*p*-cymene)ruthenium(II) dimer (5.94 mg, 9.70 μ mol), dcapy (5.67 mg, 23.2 μ mol), and NH_4NCS (50 mg, 657 μ mol). After removal of DMF under high-vacuum distillation, the remaining pasty solid was triturated in a copious amount of an aqueous 0.1 M HCl solution. The remaining fine black suspension was successively filtered-off, air-dried, and then washed with a copious amount of an aqueous 0.1 M HCl solution, followed by a minimum amount of cold MeOH. The filtrates were discarded, and the remaining solid was recovered by dissolution in CH2Cl2/MeOH mixtures. After evaporation of solvents to dryness, the crude complex was purified on gel permeation chromatography column (eluent: THF/MeOH mixtures). Purification was achieved by trituration in hexanes to afford **TT233** (21 mg, 11.3 μ mol) in 70% yield as a dark black powder.

^{1}H and 2D-COSY NMR (300 MHz, CDCl3/MeOD 7:4), δ (ppm): .71 (br d, 3*J*~ 5 Hz, 1H, Ar*H* bipy), 9.23 (d, 3*J*= 6 Hz, 1H, Ar*H* bipy), 8.85 (s, 1H, Ar*H* bipy), 8.70 (s, 1H, Ar*H* bipy), 8.25 (s, 1H, Ar*H* bipy), 8.15 (br s, 1H, Ar*H* bipy), 8.10 (s, 1H, Ar*H* bipy), 7.81-7.65 (m, 2H, 2Ar*H* bipy), 7.65-7.49 (m, 3H, Ar*H* bipy+2Ar*H* CDT), 7.27-7.07 (m, 3H, Ar*H* bipy+2C=C*H*), 6.92-6.50 (m, 5H, Ar*H* bipy+2Ar*H* CDT+2C=C*H*) , 2.93-2.73 (m, 4H, 2C*H*2(α) hexyl chains), 2.08-1.77 (m, 8H, 4C*H*2(α) ethylhexyl chains), 1.77-1.61 (br s, 4H, 4C**H* ethylhexyl chains), 1.45-0.46 (m, 78H, 24C*H*2+10C*H*3).

MS (MALDI–TOF; DCTB): *m/z* (%) found 1581.6 (40) $[M-(NCS)]^+$, 1638.6 (100) $[M]^+$

HRMS(MALDI–TOF; DCTB): *m/z* calcd $RuC_{90}H_{116}N_6O_4S_6$: 1638.6441 (100) [M]+; found 1638.6402 (100) .

UV-Vis: λ_{max}(CH_2Cl_2)/nm = 318 (26 000), 473 (47 700), 582 (br sh, 24 100).

CHAPTER 3: MESO-SUBSTITUTED PORPHYRINS FOR DYE-SENSITIZED SOLAR CELLS

3.1 INTRODUCTION

3.1.1 Introduction

In the photosynthetic cores of bacteria and plants, solar energy is collected at chromophores based on porphyrin;[191] the captured radiant energy is converted efficiently to chemical energy. Inspired by this efficient energy transfer in naturally occurring photosynthetic reaction centers, numerous porphyrins have been designed and synthesized for DSSC applications.[192-197] The intrinsic advantages of porphyrin-based dyes are their rigid molecular structures with large absorption coefficients in the visible region and their many reaction sites (*i.e.* four meso- and eight β- positions) available for functionalization: fine-tuning of the optical, physical, electrochemical and photovoltaic properties of porphyrins thus becomes feasible. In particular, advances in optimization of the device performance for OC8 "alkoxy wrapped" push-pull Zn(II)-porphyrin sensitizers using a cobalt-based electrolyte to enhance photovoltage, lead to an unprecedented power conversion efficiency of η = 13%,[198] which is superior to devices based on Ru complexes.[57,199,200] The successive breakthroughs and success of porphyrins as an highly-efficient class of sensitizers for DSSC have stimulated huge interest for further investigation and development.

The common core structure to all porphyrins is the porphin, which is shown in Figure 3.1. Along with the general IUPAC nomenclature to describe substituent patterns of porphyrins.[201] The four pyrrole units are connected via methine bridges leading to a macrocycle with 22 conjugated π electrons. The porphyrin's aromatic system is commonly described by 18 delocalized π electrons as shown in Figure 3.1 b[202]

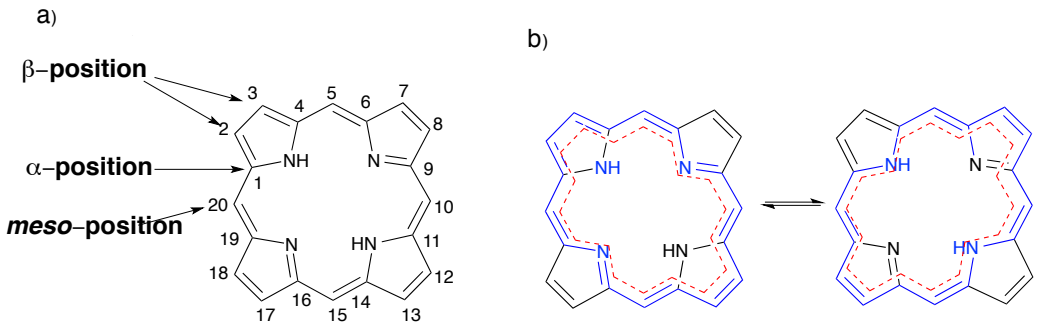

Figure 3.1. Structure of a porphyrin showing the four meso-, the eight β- and the four α-position. a) Numbering of the positions according to IUPAC nomenclature; b) illustration of the aromatic diaza[18]annulene structure (blue-red) in porphyrins.

At room temperature, their exchange is fast compared to the NMR time-scale leading to only one ^{1}H resonance around δ = -1.4 to -4.4 ppm.[203] The characteristic up-field shift is caused by the strong ring currents of the porphyrin macrocycle. [204]

The parcial acidic nature of the porphyrin is most obvious by the formation of the deprotonated di-anion upon complexation of metal ions within the porphyrin cavity. The rich coordination chemistry of porphyrins is well-known: Zn, Mg, Cu, Fe, Ni, Pd, Mn, Co; Ti, Zr, V, Nb, Cr, Mo, W, Tc, Rs, Ru; Os, Rh, Ir, Pt, Ag, Ge, Sn, P, As, Sb for which porphyrin complexes are currently known.[205]

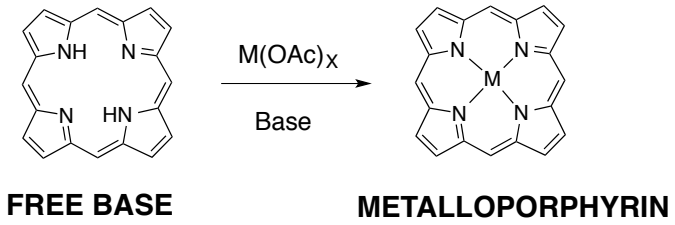

Figure 3.2. Metallacion of porphyrin.

A porphyrin features eight β and four meso positions that are potentially available for functionalization with one or more anchoring groups and other substituents. This extensive number of functionalizable positions of the macrocycle[206] offers a large panel of posible molecular designs for porphyrin dyes.

3.1.2 Photophysical Properties of Porphyrins

Porphyrins are intensively colored compounds which show intense and characteristic absorption pattern in the visible region an intense Soret band at around 420nm and two (metalloporphyrin) or four (free base) loss intense Q bands centered around 550 nm. There is of significant lack of absorption in the spectral region between these two features, as exemplified in Figure 3.3, which shows the UV/vis absorption spectra of a) the freebase *meso*-porphyrin H2Tetraphenylporphyrin (H_2TPP) and b) the *meso*-porphyrinato zinc(II) (Tetraphenylporphyrin) (ZnTPP) complex in chloroform.

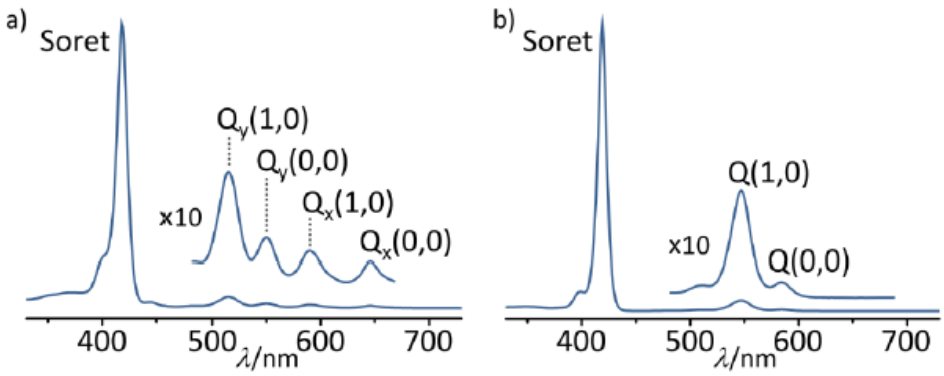

Figure 3.3. UV/vis absorption spectra of a) freebase *meso*- Tetraphenylporphyrin and b) *meso*-Tetraphenylporphyrinato zinc(II) in chloroform solutions.

Porphyrin-based dyes provide a highly flexible platform for the development of panchromatic sensitizers.[207 - 209] The most efficient porphyrin dyes has typically a donor/π-bridged chromophore/acceptor structure (D–π–A), well-known as "push-pull". Dialkylamine or diarylamine are usaly acting as strong donors, in conjunction with an ethynylbenzoic acid as the strong acceptor conterpart, yielding dyes with an intense vivid green colour, bereft of absorption between 500–600 nm.[209 - 213]

The a absorption spectra (metallo-)porphyrins can be explained by the Goutermann orbital model[214-218] (Figure 3.2). In this model, the absorption bands are attributed to π,π* transitions between the two highest occupied molecular orbitals (HOMO and HOMO-1) and the two lowest unoccupied molecular orbitals (LUMO and LUMO+1). In the ground state, the highest-occupied molecular orbitals (HOMOs) (a_{1u} or a_{2u}) have their orbital density mostly localized at *meso* positions and the nitrogen

atoms with a small amount of electron density on the β-pyrrolic positions. In the excited state, the electrons go into the lowest-unoccupied molecular orbitals (LUMOs) (eg), which have their electron density over the β-pyrrolic and meso positions.

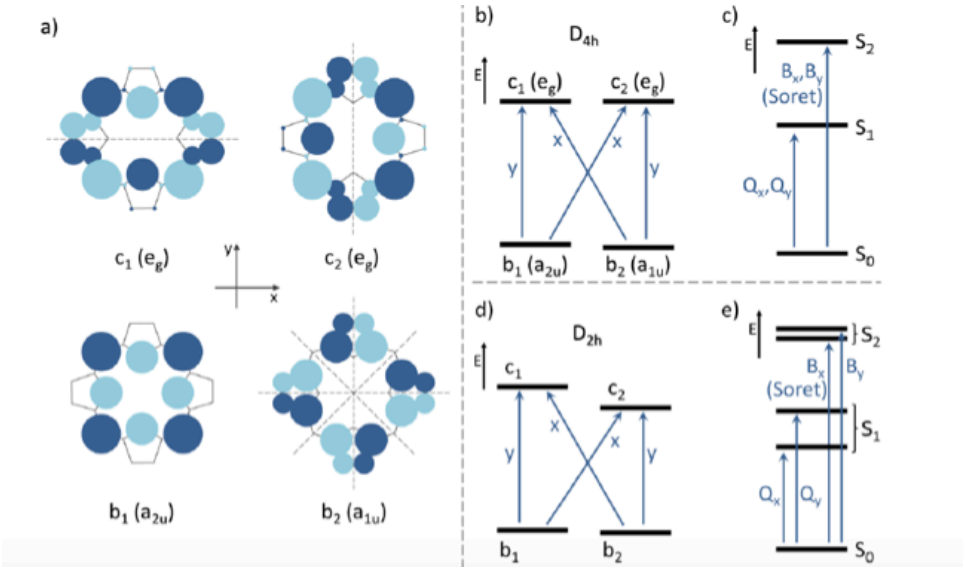

Figure 3.4. Schematic representation of the molecular frontier orbitals of porphin; top: LUMO and LUMO+1; bottom: HOMO and HOMO-1; b) to d) Simplified Gouterman's four orbital model: b) relative orbital energies and c) possible electronic transitions in metalloporphyrins; d) relative orbital energies and e) possible electronic transitions in free-base porphyrins.

For metalloporphyrins with an effective local *D4h* symmetry the two LUMOs are degenerated by symmetry whereas the two HOMOs are considered to be similar in energy as illustrated in Figure 3.8 e). Two of the possible one-electron exited states, 1(a1u,eg,y) and 1(a2u,eg,x), have x-polarisation while the other two, 1(a1u,eg,x) and 1(a2u,eg,y), show y-polarisation. Due to their similar energy and symmetry the x- and y-polarised exited states mix among each other resulting in:

- Two degenerate high-energy transitions with parallel transition dipoles leading to a high intensity (the Soret band or rather Bx and By absorption)
- Two degenerate low-energy transitions for which the nearly cancellation of the anti-parallel transition dipoles leads to lower intensity (the Qx and Qy absorption).

Vibronic progression of the Q-band transition often increases the number of the Q-bands observed (see Figure 3.3).

Most porphyrins, and especially Zn(II) porphyrins, display inherent suitable MOs levels to be efficient in TiO_2-DSSC, which constitute a remarkable advantage for this class of sensitizers: (i) the LUMO level is usually located well-above the conduction band of TiO_2, which is required for electron injection of the excited dye into the TiO2 CB; (ii) the HOMO level is below to the potential of the I_3^-/I_2 redox couple, traditionally used as shuttle in the electrolyte, which is required for an efficient dye-regeneration.[219] Besides strong changes in the optical properties, introducing a donor and acceptor groups at the *meso* positions of a porphyrin deeply influence the MO energy levels, which is useful to tune the HOMO and LUMO at adequate levels, with respect to those of the semi conducting oxide and the redox couple shuttle, in order to improve the performances of the dye in DSSC. For instance, it is well known that the presence of a *meso*-ethynyl carboxyphenyl group, acting as anchoring and acceptor group, strongly shift the electronic density of the porphyrin macrocycle toward it. On the other hand, *meso*-diarylamino groups are one of the best donor that are fully conjugated with the porphyrin macrocycle because of the direct N-bonded link. In consequence, in the ground state, the electron density for the highest occupied molecular orbital (HOMO) and HOMO-1 is shared by the diarylamino donor moiety and the π-system of the porphyrin ring. In other words, the oxidized radical cation formed after photoinuded charge separation is stabilized because the positive charge can be delocalized over both the donor and porphyrin macrocycle.

3.1.3 Synthesis of Porphyrins

The relative ease of synthesis and high-versatility of their molecular structure[220] offer many possible designs for meso-porphyrin dyes (Figure 3.5). Free base porphyrin (H_2-Por) and zinc porphyrin (Zn(II)-Por) remain by far the most studied in DSSCs. Zinc porphyrin dyes are usually preferred to other metallo-porphyrins, such as Cu, Pt, Mg, Mn, Sn, and other metals for many reasons. First, metallo-porphyrin dyes (and in particular Zn(II)-Pors) usually exhibit higher short circuit current (J_{SC}) in TiO_2-sensitized cells than their free-base porphyrin analogue, which most often results in higher PCE.

Depending on the substitution pattern, three main types of porphyrins may be distinguished: *meso*-substituted, β-substituted and *dodeca*-substituted porphyrins (Figure 3.10).

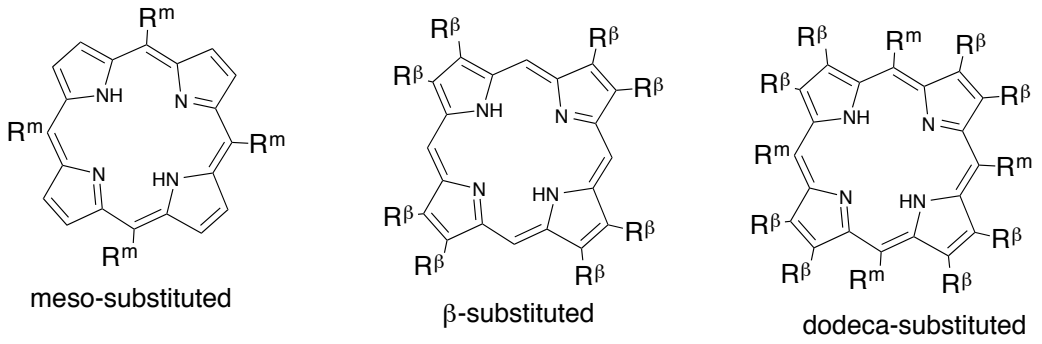

Figure 3.5. Different substitution patterns of porphyrins.

In the great majority, synthetic routes to porphyrins are based on the condensation of pyrrole or dipyromethane derivatives with aldehydes. Therefore β -substituents are most often introduced via the respective pyrrole derivatives, which may not be easily accessible. Functionalization of the *meso*-position can be achieved by use of different aldehydes whose chemistry is much more established.

The first synthetic route to *meso*-substituted A_4-porphyrins published by Rothemund and Adler-Longo is based on the condensation of pyrrole with different aldehydes in formic acid at elevated temperatures.[221] The procedure has been further optimized by Lindsey using Brønsted or Lewis acid catalysis in organic solvents leading to yields up to 30–50%.[222]

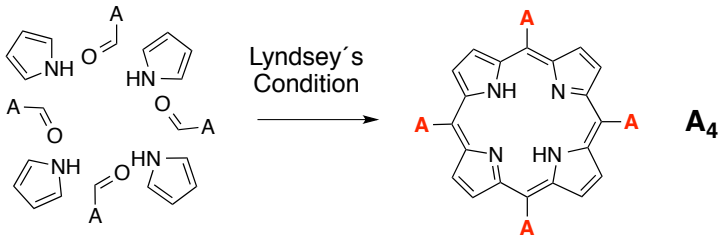

Figure 3.6. Synthesis of an A_4-type meso-porphyrin under Lindsey's classical conditions.

Unsymmetrically substituted meso-porphyrins may be synthesized by statistical condensation between pyrrole and different aldehydes under acid catalized conditions (tipically BF_3 OEt_2 or TFA), usually obtained in the range of 5-20% yield. This method remains commonly used for unsymmetrical A_3B-type porphyrin, for which yields in the range of 5-20% are usually obtained (Figure 3.7). However, for lower symmetrical porphyrins, the yields are usually too low and separation from other porphyrins formed

during the reaction can be challenging. Therefore, rational synthetic routes have been developed for the other types of unsymmetrical *meso*-substituted porphyrins. The different approaches *trans*-A_2B_2 type porphyrin by Lindsey *et al*.[223] Possible rational routes to *trans*- A_2B_2- and A_2BC-porphyrins are exemplarily in the next section.[224] Methods for the preparation of *cis*- A2B2, *cis*- A_2BC, and even recently ABCD type porphyrin involve different multi-steps procedures that will be mentioned but not detailed herein.

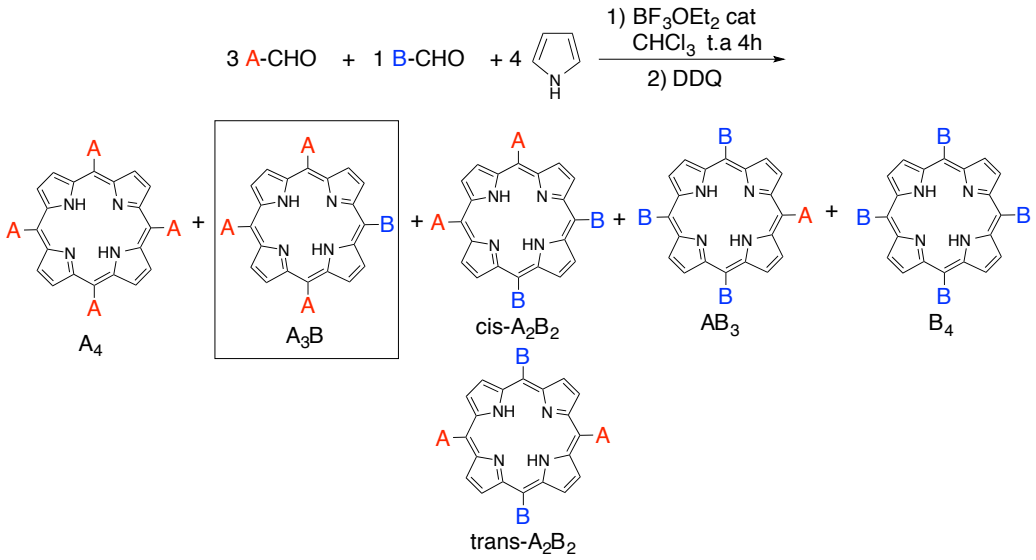

Figure 3.7. Unsymmetrically substituted porphyrins A_3B.

The synthesis of *trans*-A_2B_2 porphyrins involves the condensation between a dipyrromethane bearing one of the *meso*-substitutent (A) and an aldehyde bearing the other (B). This method requires the preparation of a dipyrromethane derivative that has to be synthesized beforehand.[223,224] Although this method require two steps, *trans*-A_2B_2 porphyrin can be obtained in excellent yield (up to c.a. 40–50%) depending mostly of the stability of the dipyrromethane toward acidolisis (backward reaction of formation). *Trans*-A_2BC porphyrins are obtained following a similar method but involves this time a statistical condensation between a dypyrometane bearing the meso subtituent A and two different aldehyde bearing the others (B and C). Therefore, the yields for the target A_2BC porphyrin is typically much less (ca 10–25%), because of the concurrent formation of the other porphyrins (A_2B_2 and A_2C_2).

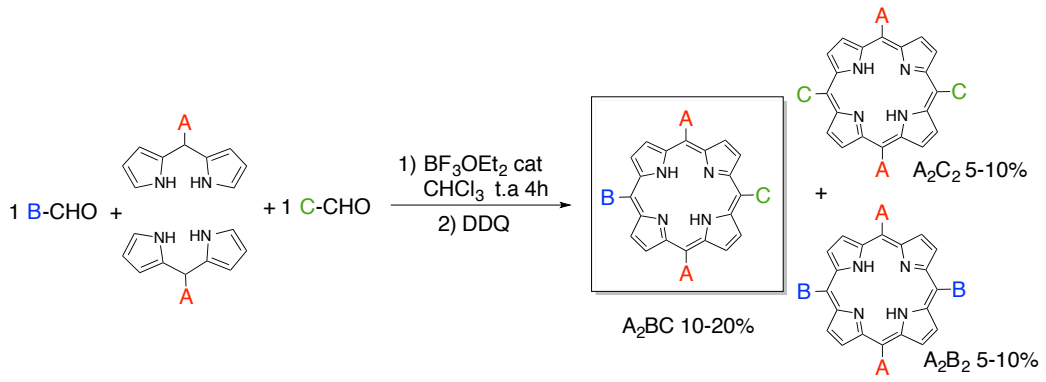

Figure 3.8. Synthesis of an A_2BC -type *meso*-porphyrin (or A_2B_2 if B=C) under Lindsey's classical conditions, and the different porphyrins obtained during the reaction.

3.1.4 Type of design for meso-subsituted porphyrin dyes

3.4.1. A_4-Type

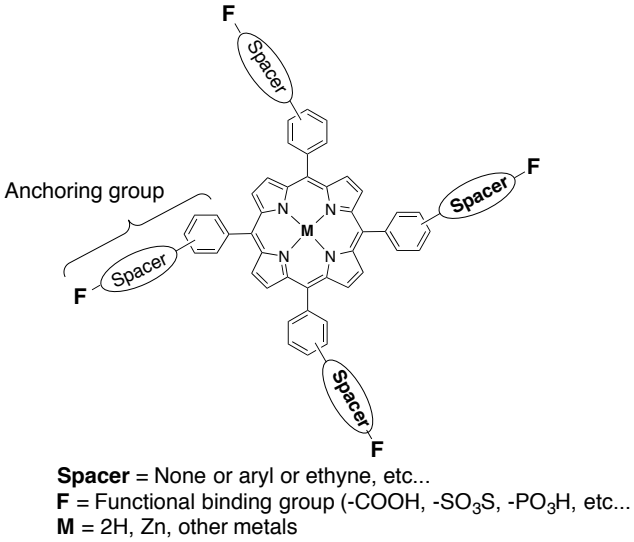

Figure 3.9. Common design for A_4-type tetrakis(phenyl)-substituted meso-substituted porphyrin dyes

The simplest design to build a porphyrin dye, and the easiest from the synthetic point of view, is the highly symmetrical A_4-type, for which the four *meso* positions are grafted with the same substituents (Figure 3.9). To date, almost all A_4-type porphyrin

dye reported and studied in DSSC are tetrakis-(phenyl)-substituted, easily obtained by condensation of the corresponding aryl aldehyde "A-CHO" and pyrrole under acidic conditions (Lindsey or Adler-Longo methods).[225] Anchors with various types of functional binding groups have been used and tested for porphyrin dyes[226,227] such as carboxylic, phosphonic, or sulfonic acid; the most commonly and widely used remains however carboxyl-based. (Figure 3.10)

The use of phosphonic/phosphinic acid anchor groups and their type of bonding to the TiO_2 surface are less known in porphyrin-based DSSCs. For Ruthenium-polypyridyl complexes, it was evidenced that dyes anchored through phosphonic acid groups bind much stronger to the TiO_2 surface than through carboxylic acid (about 80 times stronger) but give similar cell efficiencies.[228] However, unlike carboxyl-anchored dyes, phos-phonic analogues are not displaced by water and show excellent performance over a wide range of pH up to 9. Recently, Duarte et al. reported a series of phthalocyanine dyes anchored through either carboxylic or phosphinic acid groups. Their results showed that the carboxylic acid anchor leads to a higher amount of adsorbed dye than does the phosphinic acid analogue, thus giving slightly higher solar conversion effciency of the sensitizer in DSSC. However, the phosphinic acid anchor was shown to have stronger binding properties than the carboxylic one, which is a major advantage to improve the durability of a DSSC.

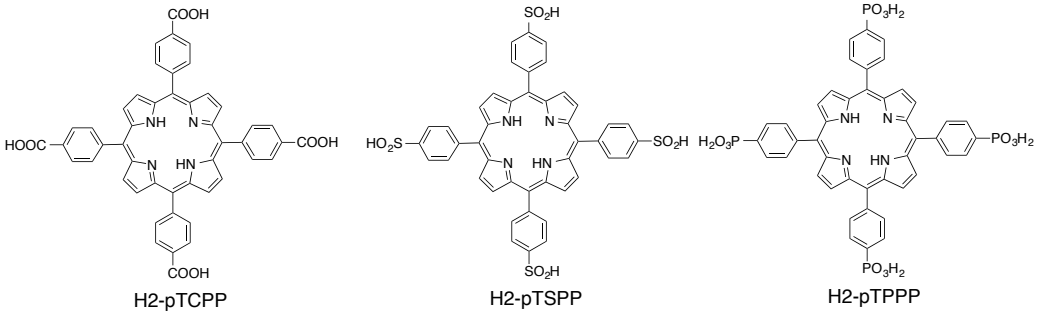

Figure 3.10. Tetrakis(phenyl)-substituted free base porphyrin dyes with anchoring groups of different nature.

Odobel et al. reported a series of phosphonato- and carboxy- phenyl functionalized porphyrin dyes claimed that the nature of the functional group ($-PO_3H$ or $-COOH$) has a little influence toward the performance of the cells in comparison with the substitution position of the anchoring group.[229] It is indeed known and well-established that apart from the intrinsic nature of the binding group the substitution

position have a drastic influence toward the performances of the cell, caused by changes in both the binding geometry of the dye onto the TiO_2 surface and electronic interactions between dye and TiO_2 (mediated through the spacer linking binding group and porphyrin)

3.4.2 A_3B-Type and A_2B-Type

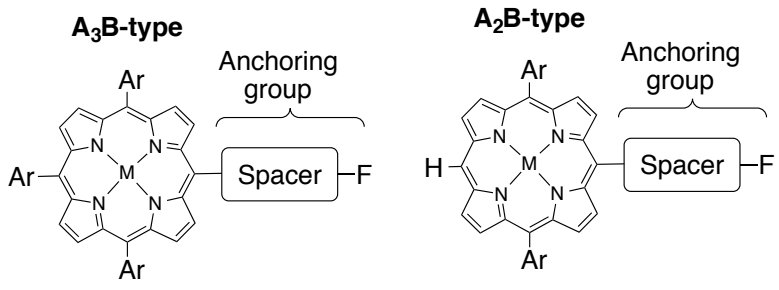

Figure 3.11. Common design for A_3B-type and A_2B-type meso-substituted porphyrin dyes

The synthetic versatility of meso-substituted porphyrins allows access quite easily to the lower-symmetrical A_3B-type porphyrins. This loss of symmetry disturbs the π-delocalized electrons system of the macrocycle creating a dipole moment that affects notably the photophysical and electrochemical properties of the porphyrin. In DSSC, this permanent and electron injection of the excited dye into the TiO_2 conduction band.

An example of an A_2B-type ADMPZn-C2-COOH, was reported by Sykes et al. had an energy conversión efficiency of 5.1% (Figure 3.12). The effective electronic coupling between DMPZn-C2-COOH and TiO_2 nanoparticles may also play a significant role for better photovoltaic performance. The short distancebetween the porphyrin ring and the surface of TiO_2 NPs may alsoplay an important role. the distance between the Ti atom and the edge of the porphyrin is ≈ 6.12 Å, which is shorter than that in benzoic acid modifiedporphyrin TPPZn-COOH (≈ 8.58 Å).

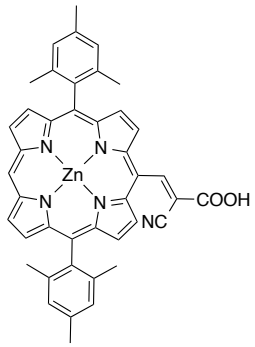

DMPZn-C2-COOH

Figure 3.12. Molecular structures of A_2B-type zinc porphyrin dyes reported by Sykes et al.[230]

This design offers various advantages counterbalanced by some disadvantages compared to the A_4:

1. From the synthetic point of view, the access to A_3B type porphyrins is less straightforward than A_4. The most commonly used and simple strategy to synthesize A_3B-type porphyrins remains the statistical condensation of aldehydes A-CHO (3eq), B-CHO (1 eq) and pyrrole (4eq) under the conditions optimized by Lindsey, leading to a mixture of six different porphyrins (A_4, A_3B, trans- and cis- A_2B_2, B_3A, and B_4). Consequently, various (and often tedious) chromatographic separations are required to isolate the desired A_3B-type porphyrin in much lower yields (typically 10−20% yield) than or A4 type (40−50%).
2. The reduced number of available anchoring groups, which might decrease the amount of adsorbed dyes on TiO_2. The most common A_3B-type porphyrin dyes (Figure 3.4) incorporate three bulky groups (“A”), acting as solubilizing and and one anchoring group (“B”). However, the presence of only one carboxyl binding group is usually sufficient to ensure an efficient adsorption of many

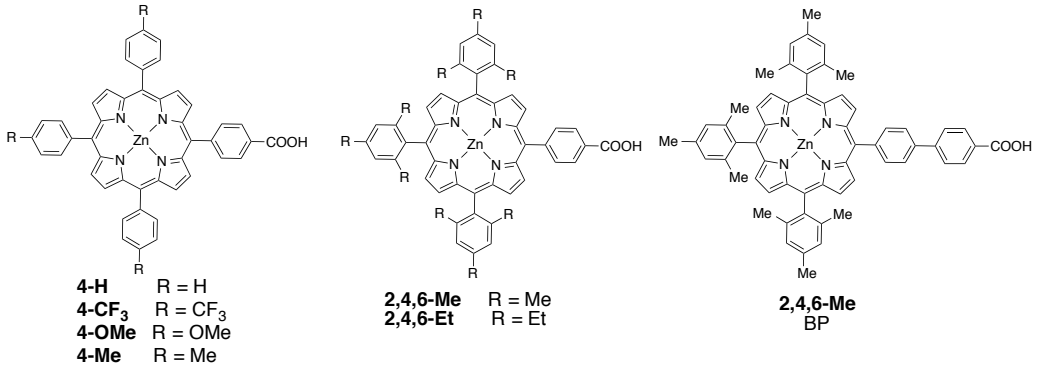

Figure 3.13. Molecular structures of A_3B-type zinc porphyrin dyes reported by Imahori et al.[231]

Imahori et al. reported a systematic study of the efect of porphyrin meso-substituents and adsorption conditions on photovoltaic properties in a series of phenyl tetra-substituted zinc porphyrins sensitized in TiO_2-DSSCs (Figure 3.13).[231] First, the drivingforce efects (ΔG_{inj}) from the porphyrin excited singlet state to the TiO_2 CB on the photovoltaic properties of 4-CF_3-, 4-OMe-, 4-H-, and 4-Me-sensitized TiO_2 cells were evaluated. Except for 4-H, the increase of the driving force upon introducing electron-donating substituents (−0.52 (4-CF_3) <−0.56 (4-OMe) < −0.57 (4-H) < −0.61 eV (4-Me)) matches well with the increase of photovoltaic performances in the same order 4-CF_3 (ηmax = 3.0%) < 4-OMe (ηmax = 3.5%) < 4-Me (ηmax = 3.8%). The drastic drop of performances for 4-H cells (ηmax = 1.2%) is ascribed to both an inherent strong tendency of 4-H to aggregate due to small steric hindrance of the unsubstituted phenyl groups, and by lower dye surface coverage.

3.4.3 A_2B_2-Type

A_2B_2-type porphyrin can exist under two regioisomers, namely trans- and cis-A_2B_2. However, the synthesis of pure regioisomer is, by far, much easier in the case of the trans-type. Typically, a trans-A_2B_2 porphyrin is readily synthesized regioselectively from the condensation of an aldehyde with a dipyrromethane under acid-catalyzed conditions.[232,233] Although some methods have been developed for the regioselective synthesis of cis-A_2B_2 porphyrins,[233] they require, however, multi-steps and most often tedious procedures. Hence, cis-A_2B_2 porphyrins are usually obtained as secondary products from statistical reactions involving pyrrole/aldehydes condensations, and are isolated in low yields after tedious chromatographic separations of a statistical mixture of porphyrins (HPLC is most often required to separate cis/ trans-A_2B_2 isomers under

his procedure). In principle, this molecular design should take advantage of the A_4-type and A_3B-type aforementioned designs, that is, the possibility to incorporate two anchoring groups for multibonds attachments, two solubilizing (or bulky) groups, and fynally the relative ease to graft coupled π-conjugated spacers at the meso positions. Given the fact that trans A_2B_2- type porphyrins are synthetically much more accessible than cis type, it implies in such design, that the two anchoring groups are located in an opposite way.

At first sight, this geometric orientation does not appear to be the most appealing to favor a possible multibond attachment of the dye on the TiO2 surface, limiting somehow the interest of such design. Moreover, given the fact that the synthetic access to trans-A_2B_2-type porphyrins is similar to trans-A_2BC without any particular higher dilculties, the A_2BC-type desing. One example is the dye ZnPDCA, (Figure 3.14).

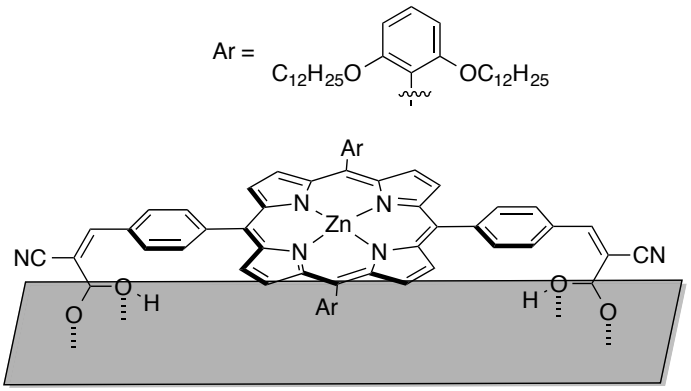

Figure 3.14. Molecular structures of dyes ZnPDCA (η = 5.5%) reported by Hupp and co-workers and schematic bonding mode attachment onto the TiO_2 surface proposed by the authors[234]

The dye ZnPDCA combines various favorable geometric and electronic factors:

1. A suitable length and geometry of the spacer that can allow a double-binding mode attachment to the surface.
2. Two coupled π-spacers that extend the conjugation with the porphyrin macrocycle and enhance the electronic communication dye-TiO_2 through the anchoring groups.
3. Two bulky (dodecyloxy)phenyl groups tethered at the two other (5,15)meso-positions protecting the porphyrin core against CR processes and aggregation.

The authors based on the following statements suggested the possible double-binding mode attachment to the surface of ZnPDCA. ZnPDCA display (1) a 5-fold stronger binding constant to TiO_2 and (2) an important blue-shift of the Q-bands of ZnPDCA was observed going from solution to TiO_2 films, suggesting that the environment on the TiO_2 surface is distinc from that of ZnPCA. Interestingly, this dye display indicate that the bridge-anchoring group must induce a coplanar/face-to-face orientation of the dye to the surface in both cases. DFT computational studies evidenced that the LUMOs of both dyes are fully delocalized over the porphyrin ring and entire ethyne-linked spacers. As expected, the extension of π-conjugation of the porphyrin macrocycle caused important broadening and redshifts of the Soret and Q bands, accompanied by higher molecular absorption coeficients. and more pronounced for ZnPDCA.

3.4.4 Trans-A_2BC-Type

Similar to A_2B_2-, A_2BC-type porphyrins can exist in principle under two different regioisomeric forms, cis ("AABC") or trans ("ABAC"). With the exception of two recent examples of cis-A_2BC-type porphyrin dyes reported by Kurotobi et al. only trans-A_2BC-type have been reported in DCCSs.

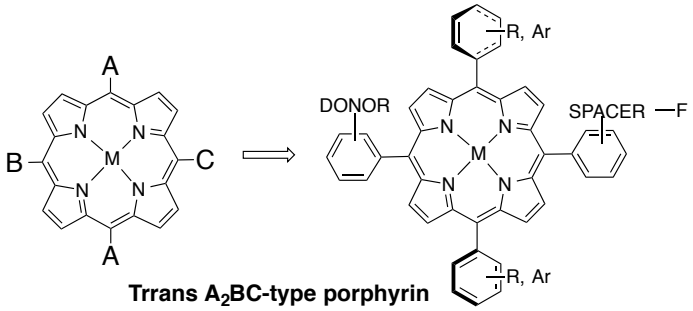

Figure 3.15. Common design for A_2BC-type meso-porphyrin dyes, (F = functional binding group).

This design is relatively new for porphyrin dyes and offers extremely high flexibility and versatility regarding the molecular structure of the porphyrin (electronic and geometric). In particular, the possibility to introduce a donor at opposite meso position of the acceptor/anchoring group allows the access to donor-bridge chromophore-acceptor (D-B-A) and donor-(π-bridged chromophore)-acceptor (D-π-A) structures, enhancing the permanent dipole moment. The donor that "pushes" the

electron density toward the macrocycle, and on the opposite site the acceptor moiety that "pulls" the electron to the TiO_2, are expected to strongly promote the electron injectio process through this ballistic way.

In order to take a maximum advantage and optimize the four meso-positions of a porphyrin, one could wonder why the two extra 5,15-meso-positions are not occupied by additional donor groups that would increase the electronic density and/or light-harvesting capability of the porphyrin dye. In an ideal case, these donors would be additionally systems that are strongly π-coupled to the porphyrin, and bulky enough to impede aggregation decrease, protect the zinc center metal ion of the porphyrin core against the electrolyte, and reduce recombination rate between oxidized species of the redox shuttle and photoinjected electron into the TiO_2 and recombination processes. The complexity of synthesis of such architectures, including fully conjugated multi donors- and acceptor-components in the same porphyrin dye.

3.1.5 Strategies to improve the performing of push-pull for dyes

In the state-of-the-art design for trans-A_2BC-type "push−pull" porphyrins (Figure 3.16), Diau and co-workers pioneered the incorporation of π-conjugated donors (ethyne- or amino-linked), as an eficient acceptor/anchoring group, both strongly coupled to the porphyrin ring and bulky groups, to impede eficiently the π−π stacking aggregation of porphyrins. These remarkable and highly sophisticated designs lead to the best-performing porphyrin dyes to date in TiO_2-DSSCs, the best performins during the years is:

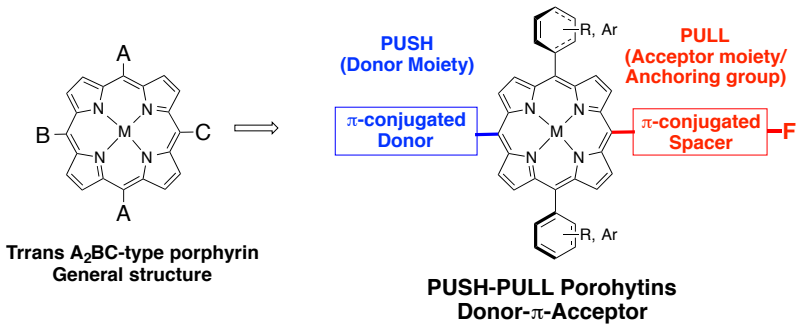

Figure 3.16. Common design for A_2BC-type "push-pull" meso-porphyrin dyes, (F = functional binding group).

3.1.5.1 Modification of the donor group.

Ethyne-Linked Donor "Push−Pull" porphyrins anchored through an ethynylcaboxyphenyl group.

Various "push−pull" porphyrin dyes achieving remarkably high eficiencies in DSSCs, which incorporate in their molecular structure an ethynylcaboxyphenyl as anchoring group, and ethyne-linked EDG or EWG, including aryl/phenyl, N,N-dialkylaminophenyl or triphenylamine derivatives.[235,-241] Lin and co-workers in 2011 achieving a PCE of 9.34% in DSSC (**LD13**).[237] which was successively improved.

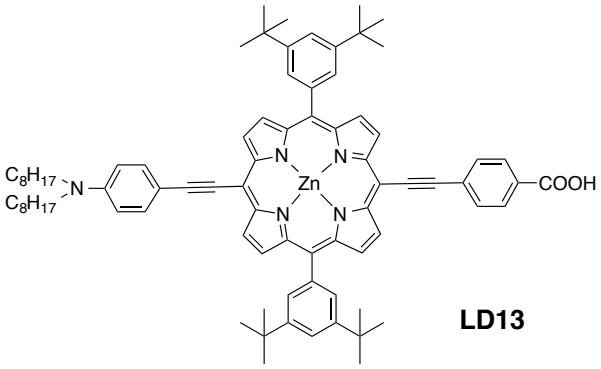

LD13

Figure 3.17. Ethyne-linked EDG (or EWG), ethynylcaboxyphenyl anchored, "push−pull" porphyrins reported

Amino-Linked Donor "Push−Pull" porphyrins anchored through an ethynylcarboxyphenyl group.

Diarylamino groups revealed to be one of the best efficient donors to date in push− pull porphyrin dyes, allowing strong conjugation with the π-conjugated porphyrin macrocycle and a strong "electron- pushing" effect. It was evidenced that diarylamino groups, directly N-bonded at the meso-position of the porphyrin, allow a delocalization of the positive charge of the oxidized dye over both the diarylamino moiety and porphyrin ring. Moreover, the extension of π-conjugation of the porphyrin over the both the donor (diarylamino group) and acceptor part (ethynylcarboxy-phenyl), both strongly coupled to the macrocycle, significantly widens and redshifts the absorption bands of the dye.

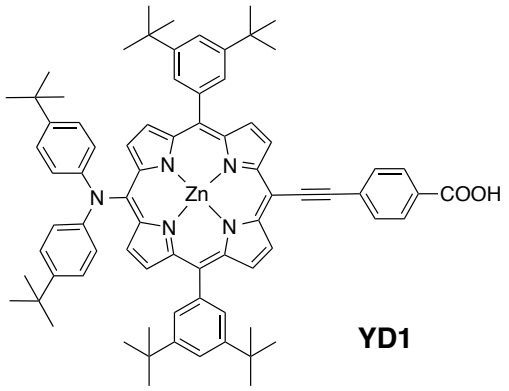

Figure 3.18. Diarylamino-linked donor, ethynylcarboxyphenyl anchored, "push−pull" porphyrin dyes **YD1**.[242]

Panchromatic response toward the Near-IR region through π-extended donor Systems in "Push− Pull" porphyrins

In order to expand the spectral window and improve the light-harvesting properties of a "push-pull" porphyrin dye (especially in the visible (red) and NIR regions, where porphyrins lack of absorption), many strategies have been attempted. For instance, the expansion of π-conjugation by fusion or annulation of a porphyrin with aromatic systems such as naphtalene,[243] antracene,[244-246] perylene,[247] or another porphyrin[248] confers to the resulting system wider and broader absorption in the visible and/or NIR regions.

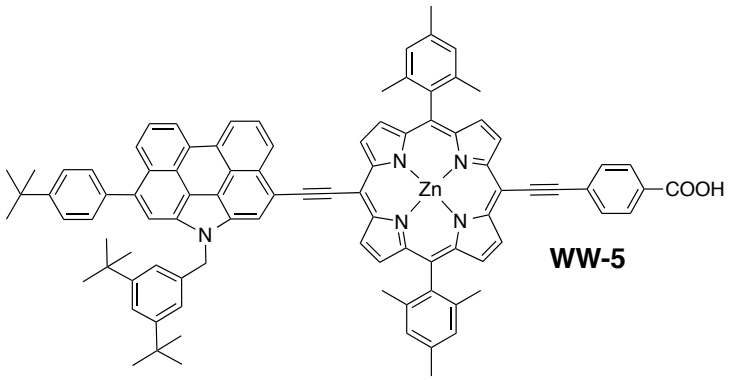

Figure 3.19. Molecular structure of dye **WW-5**

3.1.5.2 Modification of the donor group.

Panchromatic response toward the Near-IR region and improvement of charge-transfer ability through modification of the acceptor moiety in "Push-Pull" porphyrins

In the great majority, the best performing push−pull porphyrin dyes to date are A2BC-type anchored through an ethynylcarboxyphenyl group, which still show lack of absorption in the green (500−600 nm), red, and NIR regions (600−920 nm). If systematic investigations concerning the molecular structure and nature of the donor moiety ("pushing effect"), as well as the effect of the lateral 5,15-meso substituents, have been reported extensively in push−pull porphyrins, very few works, however, have been addressed to the acceptor/anchor moiety. For instance, the ethynylcarboxyphenyl anchoring group could be logically modiffed to lower slightly the LUMO to get a panchromatic response, and design new generations of effcient porphyrin dyes. Moreover, the concerns about improving the charge transfer ability ("pulling effect") of the acceptor/anchor moiety have been scarcely considered so far. On this scope, Imahori and co-workers reported in 2011 two similar-structured push−pull porphyrins **ZnPF** and **ZnPH**, diering ethynylcarboxytetrafluorophenyl or ethynylcar- boxyphenyl anchoring group, respectively) and studied the electron-withdrawing efect on the performances of these dyes in TiO_2-DSSCs (Figure 3.20).[249]

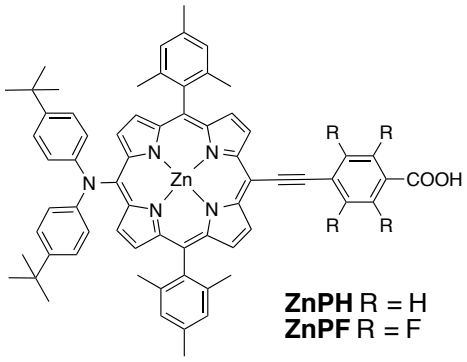

Figure 3.20. Molecular structures of dyes **ZnPH** and **ZnPF**

The introduction of a diarylamino donor group on one hand, and electron-withdrawing fluorine atoms in the phenylene bridge of the acceptor moiety in **ZnPF** on

the other hand, enhances the CT character ("push−pull effect") of this dye. Consequently, the fluoro-substituted porphyrin **ZnPF** displays slightly improved light-harvesting properties in solution compared to **ZnPH**, due to a stronger charge-transfer effect

Diau and co-workers reported a series of porphyrin dyes anchored through ethynylcarboxyphenyl (**YD20**[250]) or ethy-nylcarboxynaphthyl groups (**YD12**[251]) and their corresponding cyanoacrylic acid analogues (**YD12CN**[251] and **YD2,**[250] respectively; Figure 3.21163) and drew similar conclusions regarding the relationship geometry-performances. They evidenced that the introduction of a cyanoacrylic acid moiety causes slight redshifts of the porphyrin absorption bands but diminished the absorption coeficients, decreased the amount of adsorbed dye (Γ), IPCE and J_{SC}, and accordingly achieved lower overall PCE in comparison with their carboxylic acid analogues. They suggested that the flexible double bond of the cyanoacrylic spacer might induce a more tilted and loosely orientation, while the rigidly and linearly oriented ethynylcar-boxyacenyl groups must allow a densely packed and well-organized arrangement of the dyes on the surface. Thus, the titled and relatively planar orientation of dyes **YD12CN** and **YD21**, and the short distance between the porphyrin ring and TiO_2 surface, should increase the electron recombination rates through space between oxidized dyes and TiO_2-injected electrons leading to poorer charge collection effciencies.

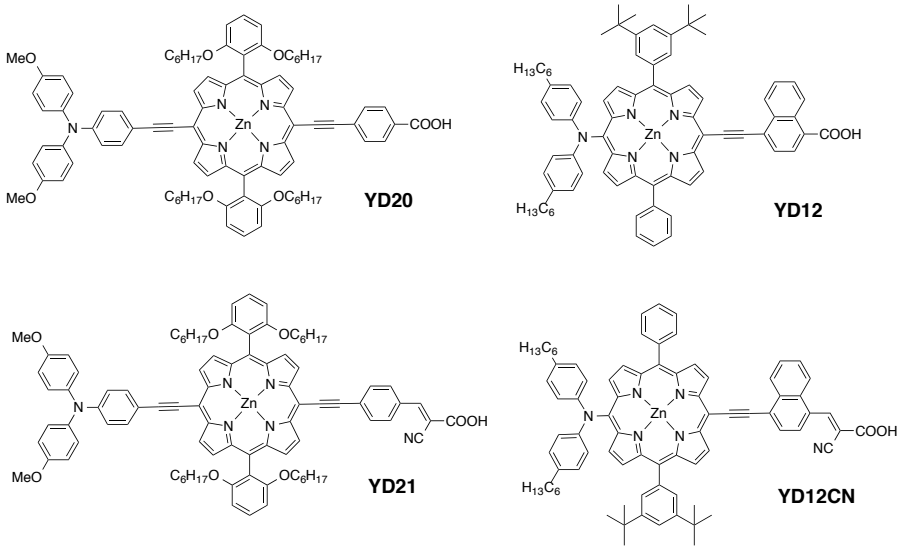

Figure 3.21. Molecular structures of dyes **YD20, YD21, YD12** and **YD12CN**

3.1.5.3 Strategies to suppress dye aggregation

In the state-of-the-art design for A_2BC push−pull porphyrin dyes, the donor and acceptor moieties are located at two opposite meso-positions of the porphyrin, while the two others are occupied by bulky groups (decoupled systems). The role of these latter is to impede dye aggregation, protect the zinc center metal ion of the porphyrin core against the electrolyte, and reduce recombination rate between oxidized species of the redox shuttle and photoinjected electron into he TiO_2. In order to take a maximum advantage and optimize the four meso-positions of a porphyrin, one could wonder why additional donor groups that would increase the electronic density and/or light-harvesting capability of the porphyrin dye do not occupy the two extra 5,15-meso-positions. In an ideal case, these donors would be additionally systems that are strongly π-coupled to the porphyrin, and bulky enough to impede aggregation and decrease recombination processes. The complexity of synthesis of such architectures, including fully conjugated multi donors- and acceptor-components in the same porphyrin dye, is however challenging and admirable.

Coadsorbent

To block this main recombination pathway and improve the performances of a DSSC, many strategies have been applied successfully. A first one consists in the incorporation of an adequate additive the addition of a coadsorbent in the dye solution during the fabrication of the device, such as cholic acids or salts,[252-254]which in some cases can improve simultaneously V_{OC}, J_{SC}, and FF The use of a coadsorbent (such as chenodoxycholic acid, abreviated as “CDCA” or “CHENO”)

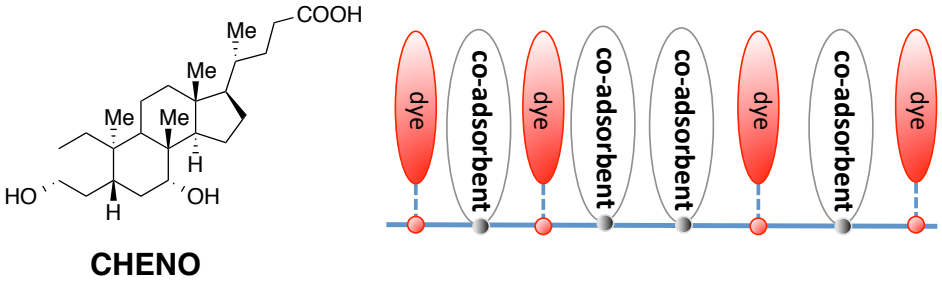

Figure 3.22. Molecular structures of coadsorbent CHENO and Schematic representation of a absortion of a dye whit a co-adsorbent.

Enveloping porphyrins with bulky groups

The great performance of porphyrins such as **YD2** was due to their superior light-harvesting ability through introduction of an EDG or a p-extended chromophore at the meso-position of the porphyrin ring. V_{OC} of those highly efficient porphyrin dyes was reported, however, to be significantly less than that of the commonly used ruthenium dye **N719**. The significantly diminished electron lifetime was reported to account for the smaller V_{OC} of porphyrins, and I_3 in the electrolyte might become attached to the positively charged Zn-center of the porphyrin core for effcient electron interception from the TiO_2 surface.[255]

As known for YD2 and other porphyrins, the 3,5-di-tert-butylphenyl bulky groups impede efficiently π–π- aggregation of porphyrins, but one can expect that they cannot protect efficiently the porphyrin core from the electrolyte in the DSSC.

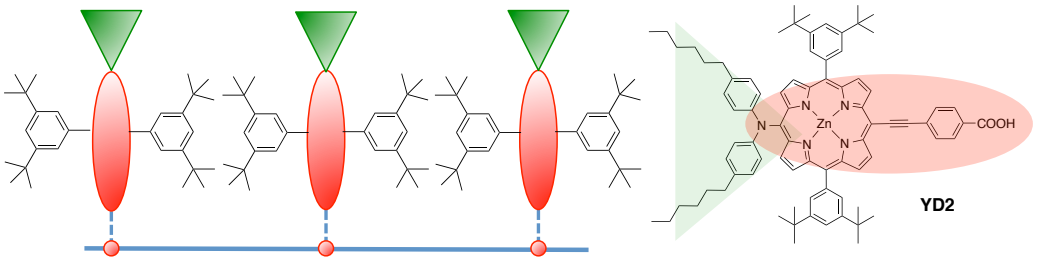

Figure 3.23. Schematic representation of dye **YD2**.

Alkoxy Wrapped Push−Pull" porphyrins, enveloping porphyrins with long alkoxy chains

On this line, the long and judiciously tailored alkoxy chains of **YD2-o-C8**[207] present a 2-fold advantage: they also impede efficiently the π–π aggregation, which reduce dipole−dipole deexcitation channels (hence improving the charge injection of the dye) and additionally protect the porphyrin core against the electrolyte, which on the other hand retards the charge recombination process with the oxidized species of the redox shuttle.

Tian and co-workers concluded that V_{OC} can be improved on decreasing the charge recombination and increasing the efficiency of electron injection with an

appropriate design of an organic dye.[256] To tackle this problem for porphyrins, a new concept was introduced to design a zinc- porphyrin sensitizer with long alkoxyl chains to protect the porphyrin core for retarded charge recombination and also to decrease effectively the dye aggregation for an efficient electron injection. One representative example is **YD2-o-C8**.

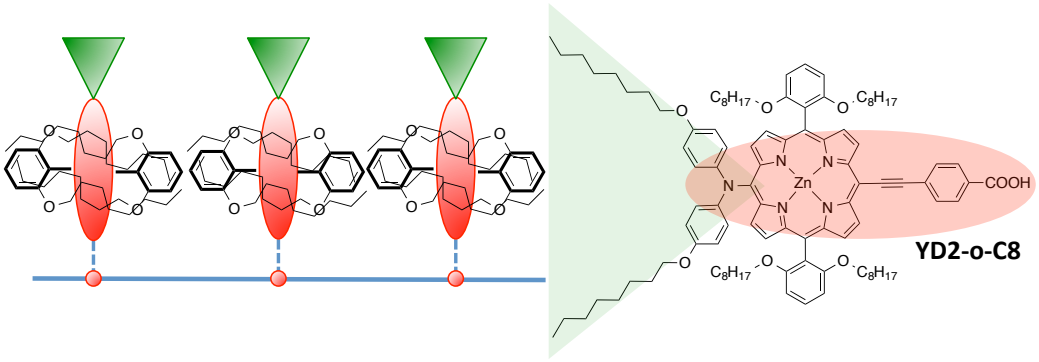

Figure 3.24. Schematic representation of dye YD2-o-C8.

3.1.5.4 Co-sensitizations

Co-sensitization is an effective approach to enhance the device performance through a combination of two or more dyes with complementary spectral features sensitized on semiconductornphotocurrents of the devices. Many co-sensitization systems, such as ruthenium complex plus organic dye,[257,258] metal-free organic dye,[259] phthalocyanine plus organic dye.[260]

One example is based on the aforementioned background, a nonplanar butterfly-shaped phenothiazine (PTZ) moiety[261] and a thiophenyl cyanoacrylic acid moiety were employed as the electron donor and acceptor, respectively. And an electron-deficient diketopyrrolo-pyrrole (DPP) moiety [262] was introduced as the auxiliary acceptor to construct cosensitizers **XS1**,**XS2** and **XS3** (Figure 3.25)

Hexyloxyl and hexyl groups were introduced to these dyes for suppressing the dye aggregation effect. Compared with **XS1**, an additional ethynylene bridge was introduced into **XS2** to expand the π-conjugation framework and enhance the absorption.[263] In addition, a hexyl group was introduced into the thiophenyl unit of **XS3** to further suppress the dye aggregation effect.[264] As expected, these dyes really exhibit a broad peak around 400 nm in addition to that around 520 nm, which may simultaneously fill up both absorption valleys of typical porphyrin dyes. Hence, XS (1, 2 and 3) were applied as cosensitizers for efficient porphyrin dyes **XW3** and **XW4**,[265]

thus achieving strong panchromatic light harvesting and the highest efficiency of 10.75% for XS3+XW4 cosensitized cells.

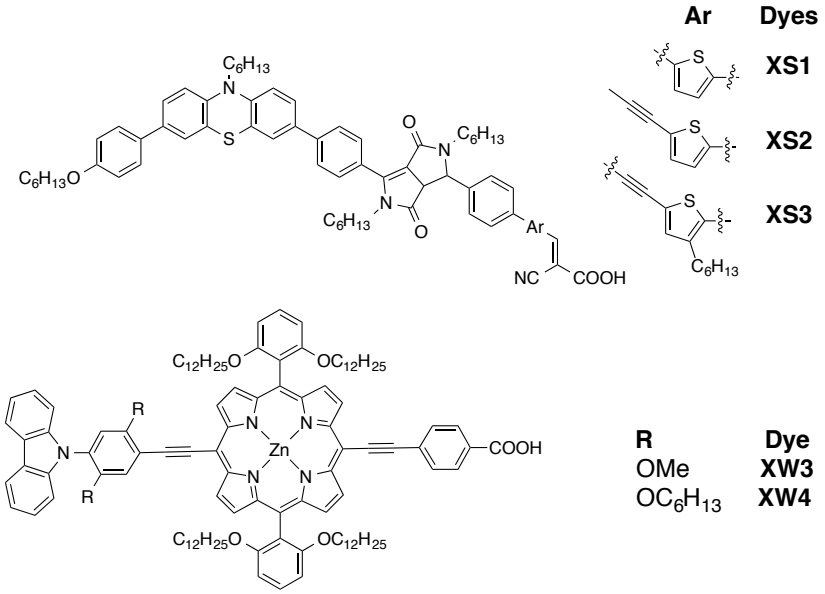

Figure 3.25. Molecular structures of zinc porphyrin dyes and Co-sensitization reported by Yongshu et al.[266]

These results provide an effective approach for developing cosensitizers to simultaneously fill up both of the absorption valleys of porphyrin dyes, especially for highly efficient panchromatic cosensitized DSSCs. Successful application of a lot of cosensitizers to porphyrin dyes indicates the general applicability of this to encrease the efficiency of the dyes .

3.2 OBJECTIVES

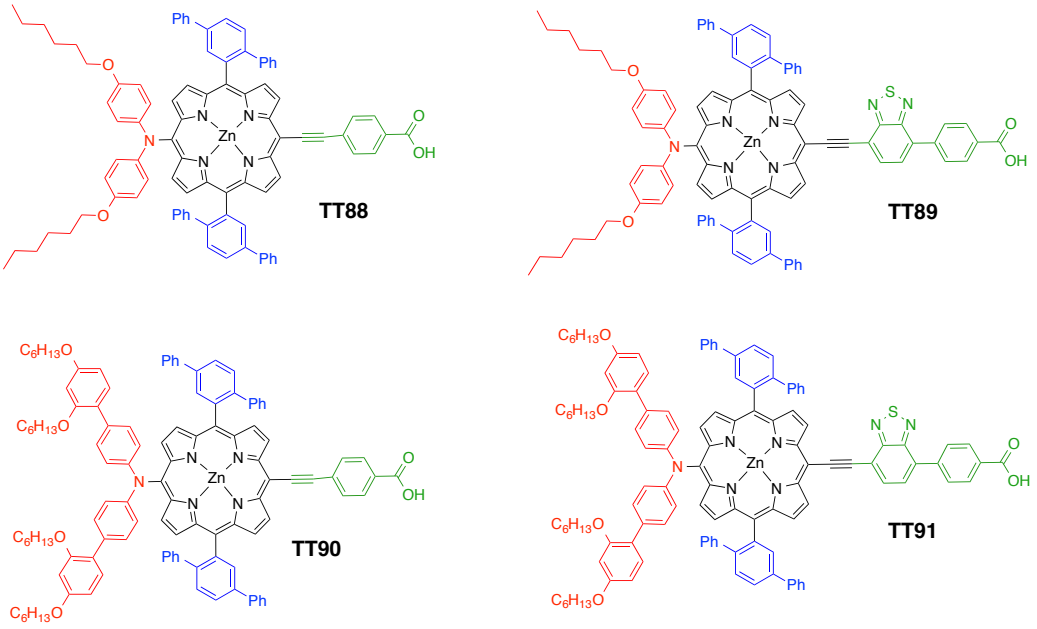

Figure 3.26. Four new push-pull Zn(II)–porphyrins

Our objective in this second part of the Thesis comprises the design, synthesis and characterization of appropriately unsymmetrically substituted push-pull porphyrins and their application as photosensitisers in DSSCs.

For this goal, four novel push-pull Zn(II)–porphyrins (see Figure 3.26) will be prepared. The design of these molecules is based on the structural features of "champion" porphyrin dyes **SM315**, **SM371** and **GY50** showing unprecedented efficiencies of 12-13%. (Figure 3.27)

Thus, we will prepare porphyrin dyes **TT88**, **TT89**, **TT90** and **TT91** with 2,5-diphenylbenzene bulky substituents at the 5,15 meso positions acting at the same time as solubilizing and disaggregating groups, which will protect the porphyrin core against oxidized species of the electrolyte that could provoke deactivation of the excited state of the porphyrins and, consequently, a loss of efficiency.

This kind of bulky substituent has not been used in the preparation of porphyrins for this purpose, and are inspired on the recent work of our group about non-aggregated Zn(II) (bearing 2,6-diphenylphenoxy moieties) substituted phthalocyanines, that

reached PCE over 6%[267] in DSSC without using any co-adsorbent, which is very important for this kind of sensitizers. This design is a pioneer attempt for the preparation of non-aggregated porphyrins.

Regarding the push-pull system, we will use the well-known donor bulky diphenyl amines bearing bulky substituents and also non-substituted analogue. On the other hand, the acceptor unit of the designed phthalocyanines will be the ethynyl phenyl carboxylate, with and without a (benzo[*c*][1,2,5]thioadiazole) (BDT) moiety as spacer.

The photovoltaic studies using these dyes as photosensitisers will be performed at EPFL in Lausanne (Switzerland) within the group of Prof. Michael Graetzel and Md. Nazeeruddin.

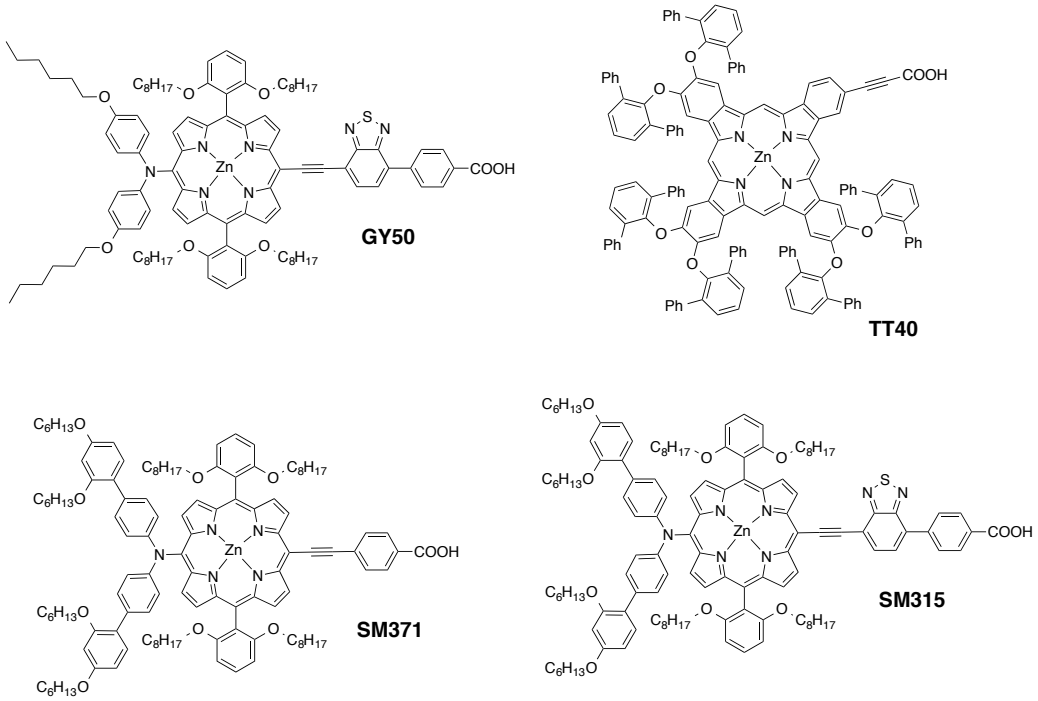

Figure 3.27. Some promising dyes in last years.

3.3 RESULTS AND DISCUSSION

3.3.1 Synthesis of the aldehyde and dipyromethane precursors

The synthesis of the two families of 5,15-disubstituted A_2B_2-type porphyrins involves a [2+2] condensation bettwen a dipyrromethane and the respective aldehyde carrying the meso substituent.[268,269,270]Thus, the first steps were the synthesis of the bulky aldehydes on one hand, and the dipyromethane on the other hand. The synthesis of the aldehyde derivative started obtaining the stannyl derivative **43** in quantitative yields by treatment with nBuLi. The aldehyde **44** was further obtained from a Stille coupling between this stannyl derivative **43** and 2,5-dibromobenzaldehyde.

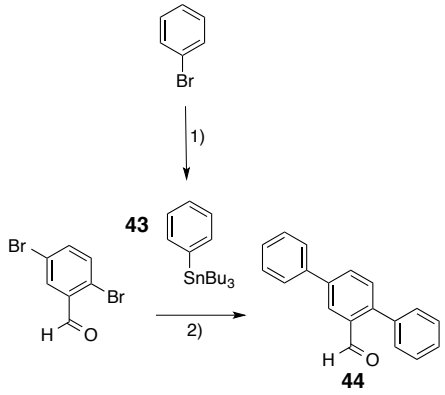

Scheme 3.1. a) *n*BuLi (2.5eq), THF, -78°C to -60°C, 1–2h followed by b) $SnBu_3Cl$ (1.5eq), -60°C to rt 2) $Pd(PPh_3)_3$ Toluene 4 days. (70%)

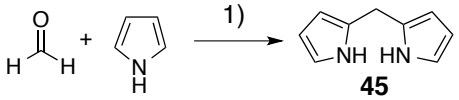

Scheme 3.2. Synthesis of dipyrromethane whitout sustutuyents 1) Paraformaldehyde, pyrrole and BF_3 Et_2O in DCM/EtOH. (60%)

Next, the dipyrromethane **45** was produced with syntetized under modified procedures previously reported in the literature. A suspention of paraformaldehyde in absolute ethanol and the suspension was refluxed until a clear solution was obtained. After cooling down to room temperature, a solution of pyrrole (20 eq) in freshly

distilled CH_2Cl_2 were added and the mixture was degassed by bubbling argon for 5-10 min in order to remove oxygen. Next a commercial solution of BF_3 Et_2O in Et_2O (0.5 mL) was then added and the resulting mixture stirred at room temperature under inert atmosphere in the darkness overnight. After workup and purification, dipyrromethane **45** was obtained in a 58.0% yield (2.54 g) as a white crystalline solid (Scheme 3.4). This dipyromethane is known to be relative unstable in time under ambient conditions so it needed to be stored under inert atmosphere (Argon) and at low temperature (-10ºC) in the absence of light, and used quickly in the next step of the synthesis. Under these conditions, it could used within 2 weeks..

3.3.2 Synthesis of the diarilamines (donor moieties):

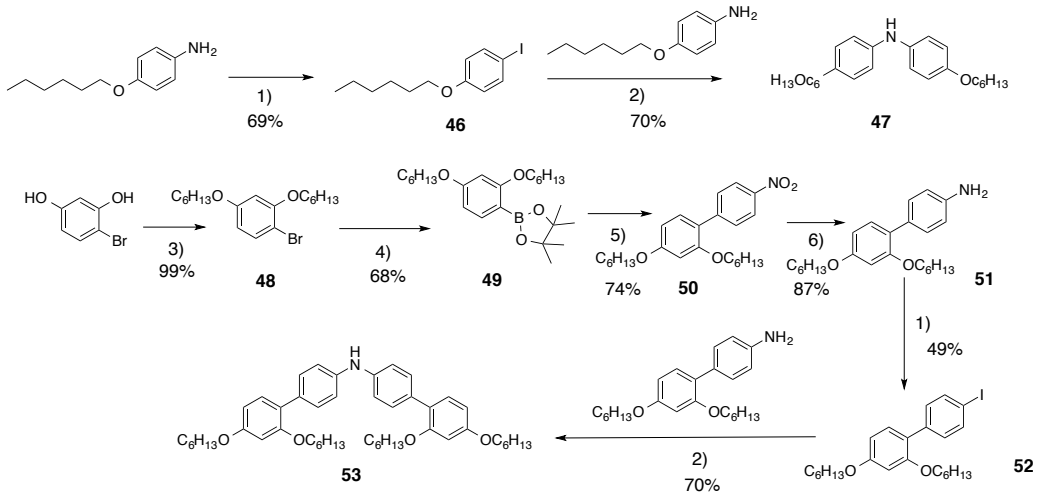

Scheme 3.3. H_2SO_4, $NaNO_2$, KI, H2O (**46**: 69% and **52**: 49%) (2) $Pd_2(dba)_3$, *t*BuONa, *t*-tertBuP, Toluene, reflux (**47**: 70% and **53**: 70%) (3) 1-bromohexane, K_2CO_3, DMF (99%); (4) *n*-BuLi, THF, isopropyl pinacol borate (68%); (5) 4-bromo-nitrobenzene, $Pd(PPh_3)_2Cl_2$, Cs_2CO_3, DMF, H_2O (74%); (6) Zn, NH_4Cl, acetone, H_2O (87%).

First of all, the synthesis started whit a diazonium salt to afford the iododerivatives **46** and **52**, followed by a paladium cross coupling reaction. This step is common for both of them to obtain the diamines in a good yield. In both cases it was necessary to caractarise the final products **47** and **53** by mass spectrometry to discart the presence of triamine. To obtain the iododerivative of compound **52** was produced with an alkylation of alcoxy grups (**48**) followed by a borilation (**49**). The next step was a

Suzuki cross coupling reaction (**50**) to finally afford the amine derivative by a reduction of the nitro group (**51**). In both cases we must did a mas spectra to differentiate the trisutituted than the disustituted.

3.3.2 Synthesis of the anchoring/acceptor groups

This compound was produced with a reaction between stannyl derivative **54** by treatment with *n*BuLi followed by $SnBu_3Cl$. The bromoderivative **55** was further obtained from a Stille coupling between the stannyl derivative **54** and dibromo derivative.

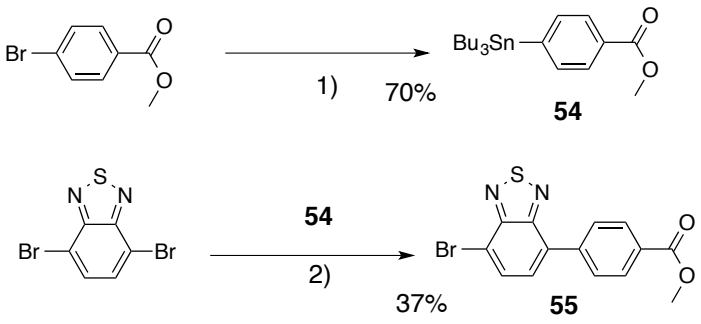

Scheme 3.4. bistributyltin, $Pd(PPh_3)_4$ in Toluene, reflux t=5h (70%) 2) $PdCl_2$, *t*-Bu_3P, CuI in DMF t=45°C for 1 hour (37%).

3.3.3 Synthesis of the porphyrins

The Lindsey conditions involve a two-step sequence starting with a 2+2 condensation of dipyrromethane **55** followed by oxidation (Scheme 3.5, step 1). This procedure is useful for making a wide variety of symmetric and asymmetric porphyrins. The original "Lindsey 2+2" approach involved the condensation of [1,1':4',1"-terphenyl]-2'-carbaldehyde, in this case, with unsubstituted dipyrromethane **55**, affording a non-aromatic dication intermediate called a porphodimethene salt 56-1 as shown in *Scheme 3.6.*

These intermediate chromophores exhibit a deep red color typical of dipyrromethene species with a characteristic visible spectrum. The condensations were catalyzed by a Lewis acid such as boron triflouride dietherate. Various oxidizing agents including molecular oxygen, iodine and quinones in this case to afford compound **56** and a subsequent metallation with salts such as zinc(II) acetate then readily convert into the corresponding zinc porphyrin. (**57**)

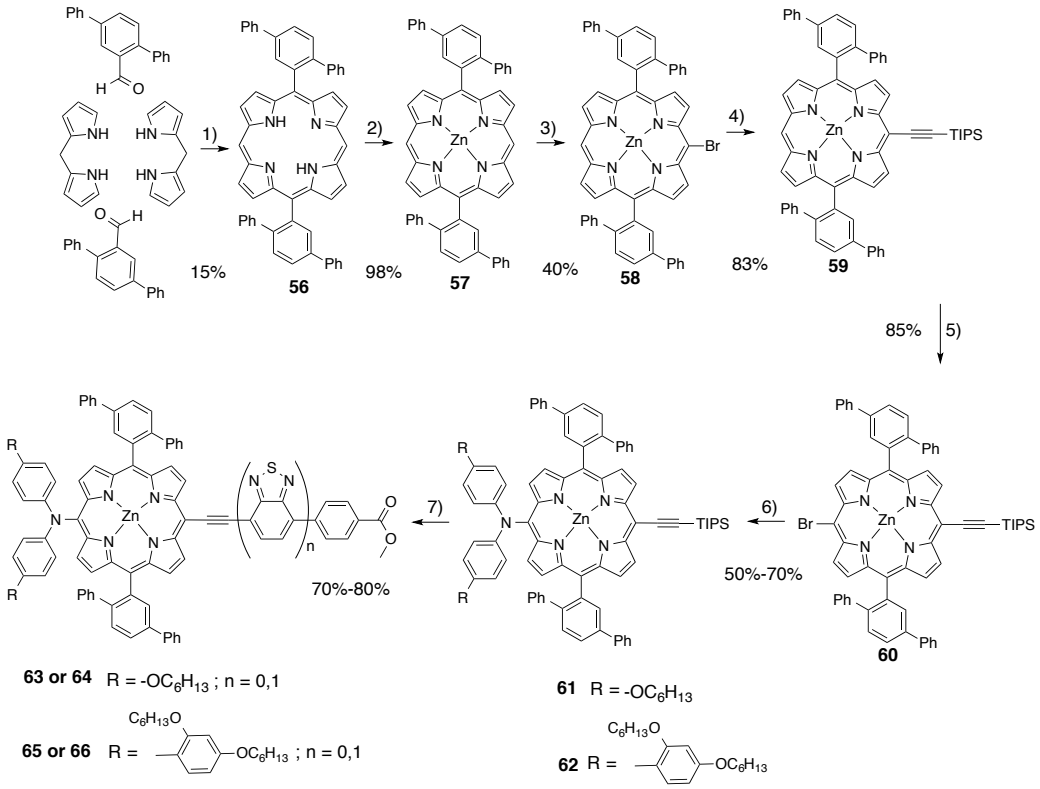

Scheme 3.5. General conditions scheme for the synthesis of the push-pull porphyrins **63**, **64**, **65** and **66**

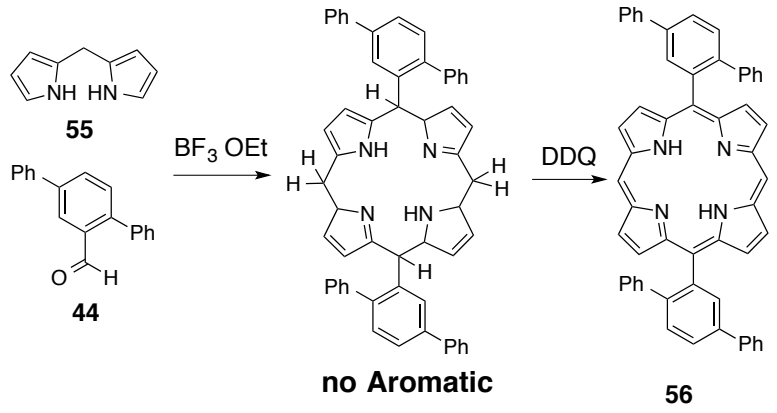

Scheme 3.6. Formation of the porphyrin 57 by a [2+2] condensation bettwen aldehyde **44** and dipyromethane **55**

As a representative example of the ^{1}H-NMR features of these derivatives, the spectrum of porphyrin **57** is shown in Figure 3.29.

Surprisingly, the protons located at the unsubstituted 1,10-meso positions of the porphyrin appear magnetically non equivalent in the NMR spectrum of **57** at 298 K, showing two different singlet signals instead of one unique singlet signal expected. Moreover, an unexpected complex multiplet was also observed for the ortho aromatic protons of the meso-phenyl groups between 8.1-8.2 ppm, whereas the metha and para ones appears as quite well-resolved doublets.

These observations supports that porphyrin **57**, as well as the other ones, exists under two atropoisomeric forms due to the restricted rotation of the meso phenyl substituents. This was also suspected during the purifications on chromatographic column (SiO_2) of all porphyrins, because TLC analysis of the different purified fractions revealed, in most cases, two distinct very close spots (sometimes an unresolved unique large one instead), however too close to be separated. To discard the possible presence of any other unexpected products (higher- or lower- weighted porphyrins), we purified afterwards these compounds by size-exclusion chromatography (bio-beds, biorad SX1. Eluent: Toluene).

In all cases, only one unique band was collected, which discard the presence of any other unexpected products.

Finally, MS and HRMS spectrometry experiments were performed for all compounds and in every cases, the expected molecular ion peak was observed.

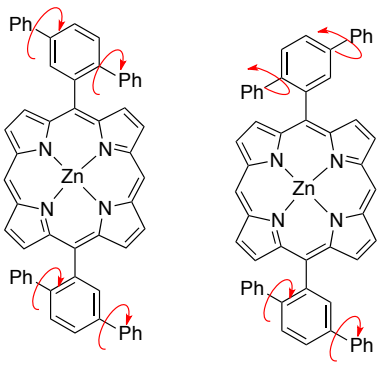

Figure 3.28. The two differents atropoisomers of porphyrin **57**

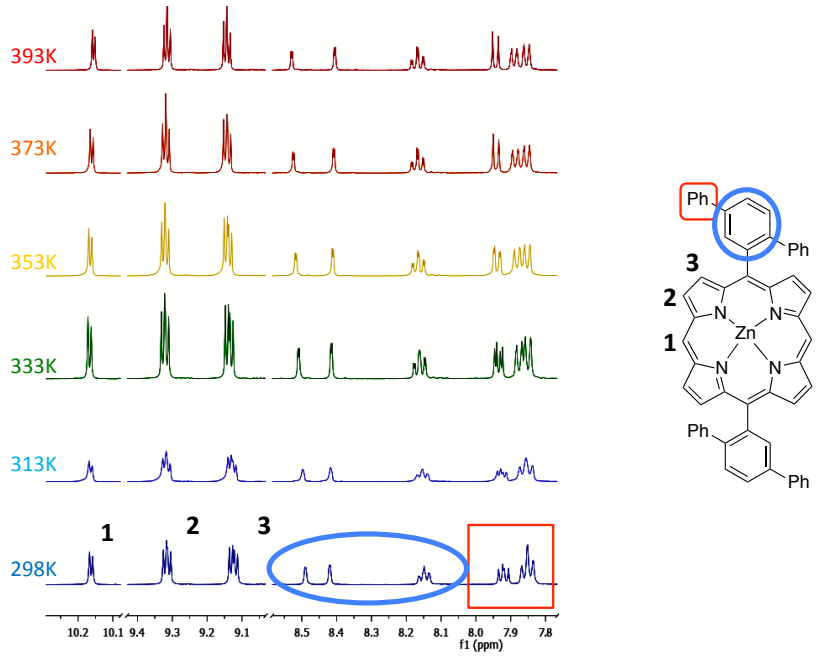

Figure 3.29. ^{1}H-NMR of Zn porphyrin (**57**) in $C_2D_2Cl_4$ (aromatic region) at different temperatures.

To corroborate this theory, the model analogous of a compound **57**, but whitout isomer which hold two 3,5-diphenylbenzene bulky groups in two of the meso position of the macrocycle in para position one to the other, to suppress agregation, was synthesise. The procedure of syntehsis is the same describe previusly in the synthesis of compound **57**

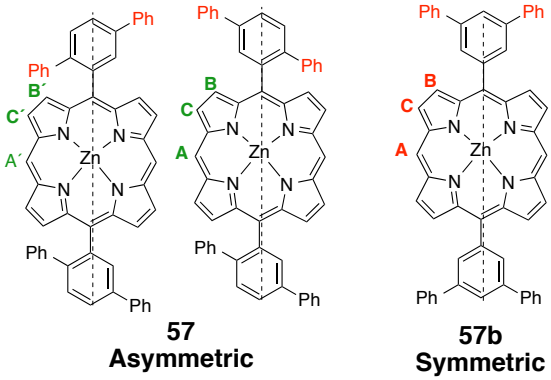

Figure 3.30. Two porphyrins to corroborate the topoisomers. **Asymetric** (**57**) would had a more difficult spectrum of RMN than **Symetric (57b)**.

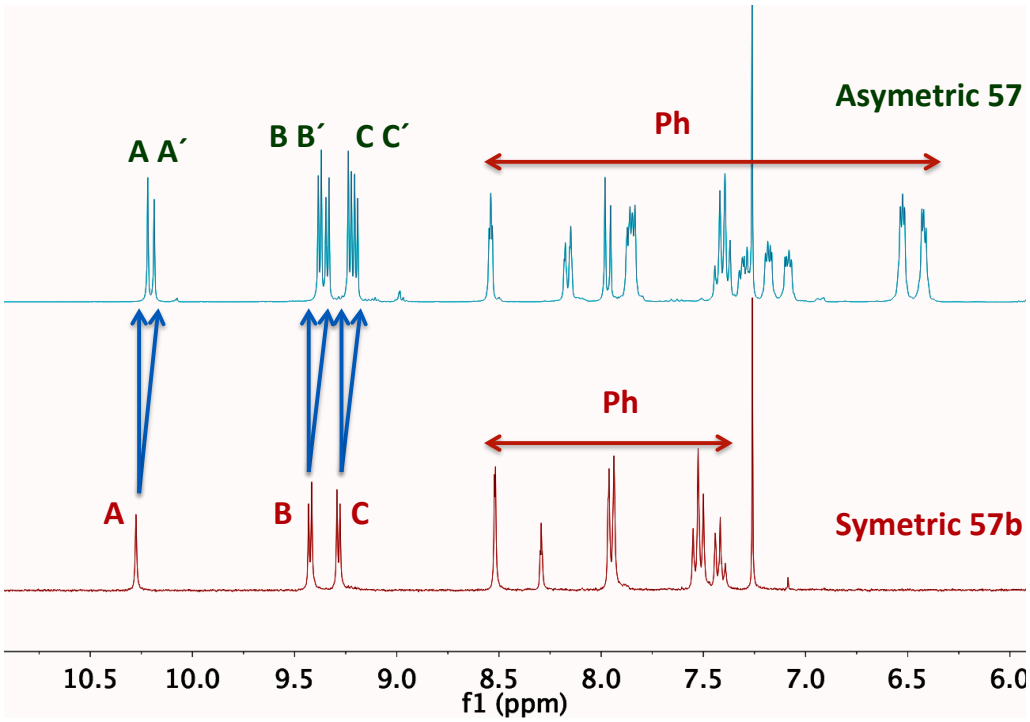

Figure 3.31. Aromatic part of the spectrum of porphyrins **Asymmtric** and **Symetric** in $CDCl_3$.

When the symmtrie was broken the complexity of the spectra increase and all the signals was duplicate the multiciplity. In the Figure 3.31 for example, the two doblets for meso protons of the Symmetric porphyrin (**1**), transform to two doble doblets in the Asymmetric porphyrin (**A**).

Bromination of the Zn porphyrin (**58**) with N-bromosuccinimide (NBS, 1 equiv.) in chloroform yielded a mixture of mono- and di-bromoporphyrin, and starting material (**58)**. The mixture of bromoporphyrins was subjected to a Pd-catalized Sonogashira cross-coupling reaction with triisopropylacetylene using $Pd(PPh_3)_2Cl_2$ and CuI as catalyst to yield intermediate **60**.

The next step was the bromination of porphyrine **60** whit NBS, to give **61** in satisfactory yield Subsequently, a Buchwald-Hartwig reaction bettwen bromo porphyrin **61** and diaryamine **47** or **53** was performed using a modified literature procedure[207] to yield porphyrins **62** and **63,** respectively**,** in beter yields and shorter times. Deprotection of the TIPS group of **62** or **63** with TBAF in (DCM) followed by a

Sonogashira coupling with methyl 4-iodobenzoate or **55**-linker (Scheme 3.3) allowed to obtain porphyrins **65**, **66**, **67** and **68**.

Intersingly, a deep changes in colours were observed during all these reactions in the mixture reaction, and of the purified compounds both in solution and solid state. (Figure 3.32)

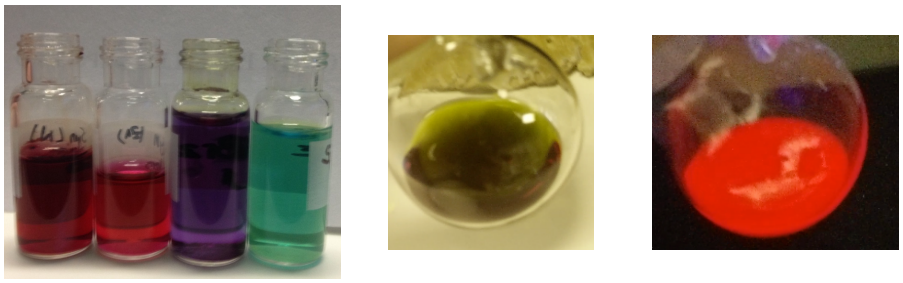

(A) **(B)** **(C)**

Figure 3.32. Left to right: compounds **57**, **58**, **59** and **61** in DCM solution (B) and (C) Porphyrin **63** in DCM solution and under UV lamp, respectively.

The last step to obtain the porphyrin dyes was the saponification of the ester group to obtain the corresponding carboxylic acid. This was realized by refluxing for 2h a solution of the different ester in THF/MeOH 3:2 in the presence of a 20 % w/w solution of NaOH in water. As well as the intermediates, the final compounds showed drastic changes of colors: dark green for porphyrin **59**, and dark brown-greenish (**61**) as typically observed for such push-pull porphyrins, also known as “green dyes”

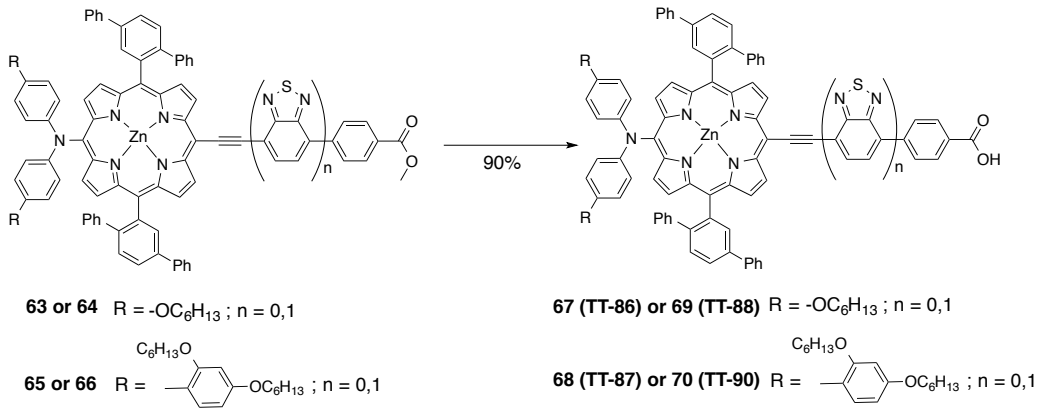

Figure 3.33. Synthesis of the Push-Pull Dyes 67, 68, 69 and 70: NaOH 20% w/w in THF/MeOH (3:2) (Yield: 70-80%)

3.3.1 Spectral properties

The absorption spectra of this serie of porphyrines are presented in Figure 3.6 in DCM, the UV/Vis spectra of all of them are nearly identical, as expected, which breflects that the ankory group has little effect on the photophysical properties. All absorption spectrum typical of porphyrins functionalized with a diarylamine donor and ethynylbenzoic acid acceptor, with maxima from the Soret band (B-band) at 447 nm and from the Q-bands at 580 nm and 646 nm. All colorants exhibit a Soret band at with similar molar absorption coefficients.

Figure 3.35 shows the solution absorption spectra, in DCM, of the two series (A) and serie (B) sensitizers. The donor group bis(2′,4′- bis(hexyloxy)-[1,1′-biphenyl]-4-yl)amine was specifically used in serie B and the splitting of the Soret band in **63** (0 (B) red line) can be rationalizedas with the incorporation of this especial donor group.

On the other hand, the introduction of the BTD acceptor unit had a significant impact on the absorption spectrum of the porphyrines in Figure 3.35 in compare with, most evident by the splitting of the Soret band, resulting in a shoulder at 440 nm on the maximum at 454 nm, independently of the donor group.

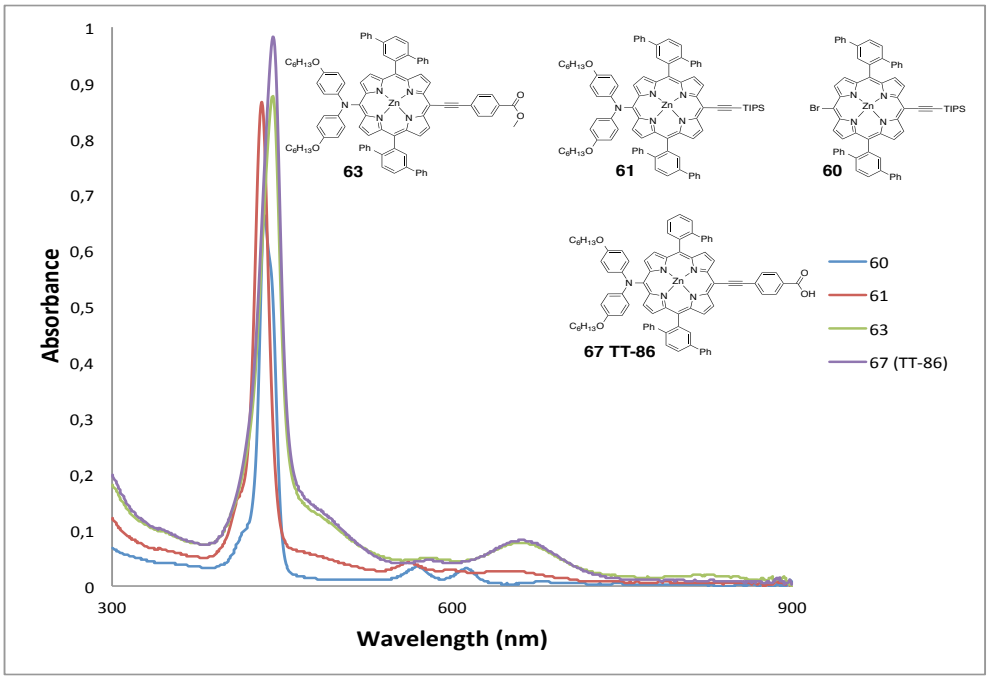

Figure 3.34. Uv spectrum of porphyrins **61**, **62**, **64** and **68** in DCM

Both the spectral splitting and the redshifting of absorbance maxima for both series are consistent with previously reported porphyrin–BTD ensembles.[271,272] The splitting of the Soret band can be rationalized using point-dipole exciton coupling theory.[272] The Soret band (B-band) is a composition of two perpendicularly polarized transitions within the molecule, denoted Bx and By, where the x-axis has the greatest degree of conjugation, ts formed for the hipotetic donor-porphyrin-acceptor axis.[273,274]In a symmetrical zinc tetraphenylporphyrin the Bx and By transitions are degenerate. Functionalization of the porphyrin with donor and acceptor moieties to afford these tipes of dyes increased the conjugation and charge transfer (CT) character along the donor-porphyrin-acceptor axis of the dye, causing the Soret absorption originating from the Bx transition to be redshifted with increased molar absorptivity. Overall, the Soret band in these porphyrins appears both broad and redshifted, as the Bx and By transitions are no longer degenerate. The presence of the BTD-functionalized acceptor further increased the electronic asymmetry and CT character of the dye, causing a redshifted Bx transition, which resulted in the Soret band appearing as two

distinguishable maxima in the absorbance spectrum. strength for the Bx transition, rationalizing the differences in molar absorptivity between the two Soret máxima.

The presence of the BTD acceptor increased the x-axis polarizability, indicative of increased oscillator

Furthermore, the absorption of Figure 3.34 between the Soret and Q-bands (450–550 nm) displayed significant enhancement compared to Figure 3.34, between leading to the panchromatic character of the BTD-functionalized dye.

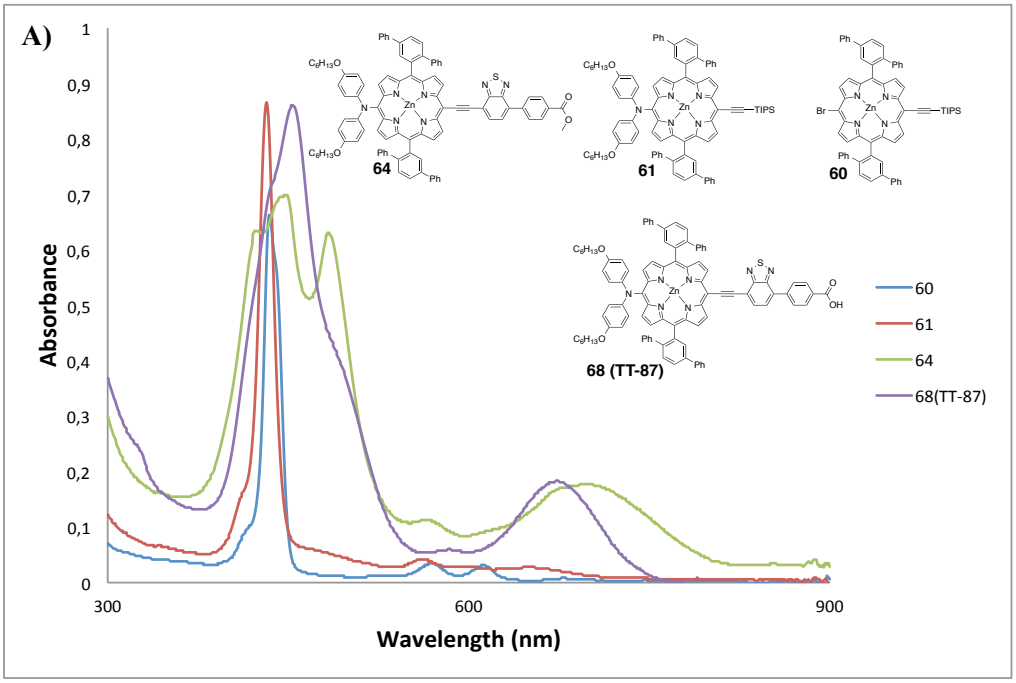

Figure 3.35. Uv spectrua: A) Linker wihttout BDT and B) with BDT in DCM

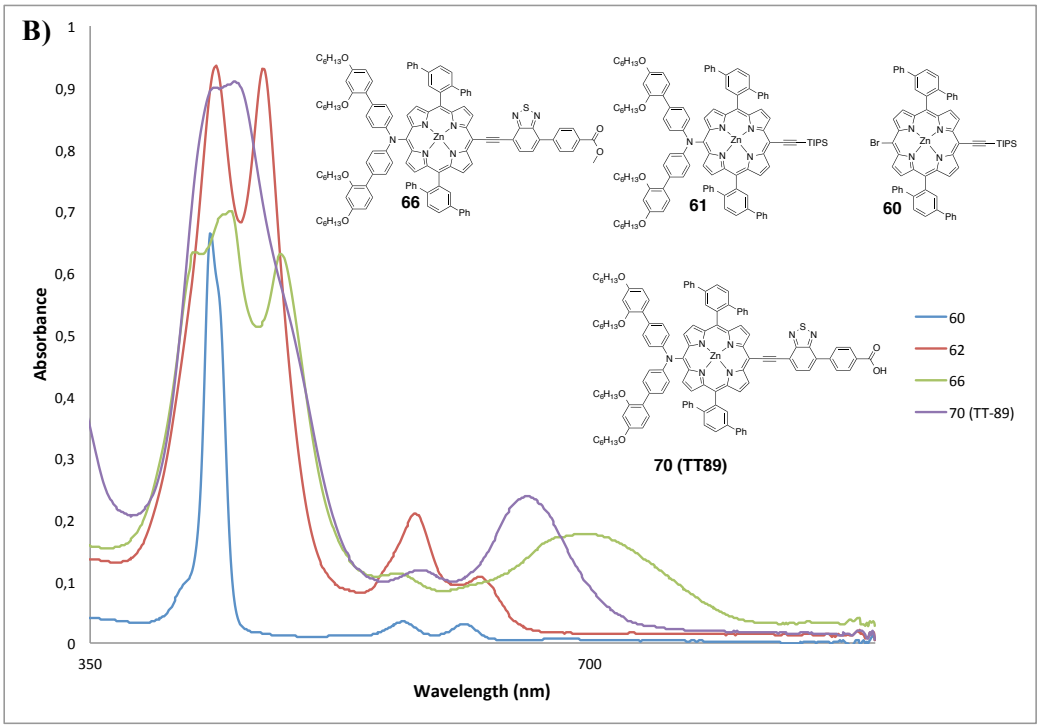

Figure 3.35. Uv spectrua: A) Linker wihttout BDT and B) with BDT in DCM

3.4 SUMMARY AND CONCLUSIONS

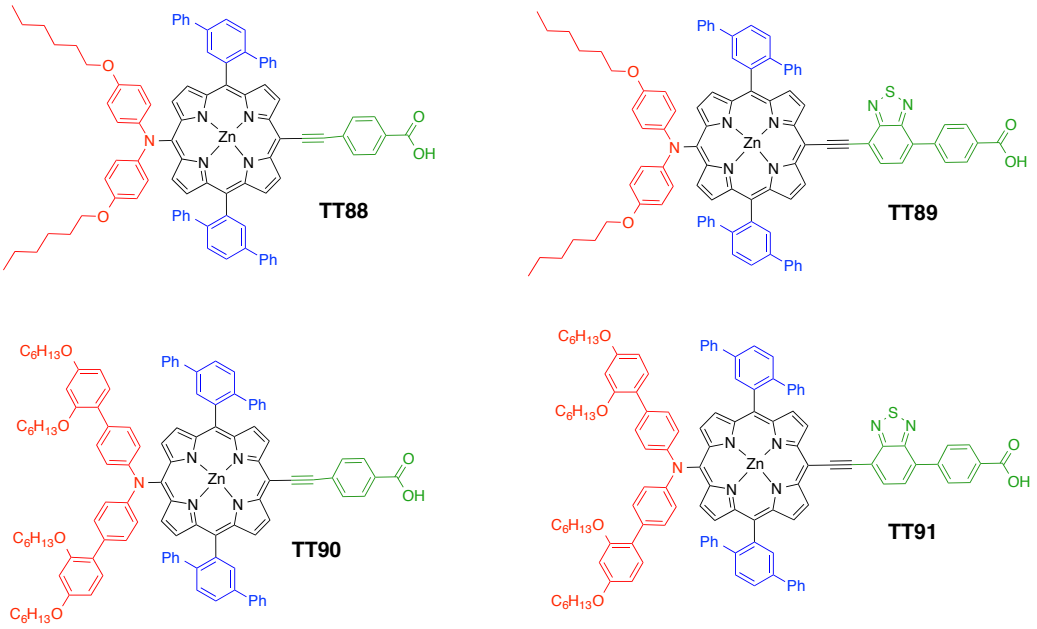

Figure 3.1. Four new push-pull Zn(II)–porphyrins

Four unsymetrically functionalized, carboxyethynylphenyl or BDT-carboxyethynylphenyl containing porphyrins (**TT88**, **TT89**, **TT90** and **TT91**) have been prepared in the search for new structural parameters that can bring about higher efficiencies in DSSCs based on porphyrin dyes. A comparison of the optical l features between BDT- and different lamino-substituted derivatives indicates that the former have close to those of the best porphyrin dyes reported in the literature with maximal electron- injection and dye-regeneration abilities. In addition, the presence of 2,5-diphenylbenzene bulky groups hinders the aggregation of the macrocycles an also had different isomer, which is also beneficial. In this way, functionalization with 2,5-diphenylbenzene moieties at the meso positions of carboxyporphyrins arises as a plausible substitution pattern for obtaining efficient dyes for DSSCs. The construction and measurements of DSSCs based on these derivatives is currently underway in EPFL in Lausanne (Switzerland) within the group of Prof. Michael Graetzel and Md. Nazeeruddin.

3.4 RESUMEN Y CONCLUSIONES

Cuatro porfirinas funcionalizadas asimetricamentes con grupos BDT-carboxietinilfenil y carboxietinilfenil (**TT88**, **TT89**, **TT90** and **TT91**) han sido preparadas para investigar como afecta sus parámetros estructurales a las eficiencias de los dispositivos en las medidas fotovoltaicas en las células solares. Comparando los valores ópticos obtenidos de estas con los que existentes en la literatura que actualmente poseen los record ya comentados en este capitulo (SM315, SM371 and GY50) podrian tener unos valores de inyecion y regeneracion en celulas solares parecidos. Por otro lado, la incorporacion de nuevos grupos como 2,5-diphenylbenceno como grupos dadores voluminosos ha dado lugar a isomeros de posicion y sera veneficioso para evitar la agregación de los macrociclos en el dispositivo y aumentar su eficiencia en ultimo termino. La construcción y desarrollo de estos dispositivos esta todavía en pogreso en el grupo de Lausanne (Switzerland) bajo la dirección de Prof. Michael Graetzel and Md. Nazeeruddin.

3.5 EXPERIMENATAL SECTION

3.5.1 Synthesis of the aldehyde and dipyromethane precursors

Compound (43)

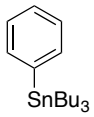

The bromobenzene (2,5 gr 17 mmol),was introduced in an oven-dried Schlenk flask, and then three cycles of vacuum-argon were realized. Under argon steam, dry THF (150 ml) was added by syringe in the flask through a septum/needle, and the resulting solution stirred at room temperature until the full mixing of the starting material. Next, the flask was immerged in an acetone/N_2 (l) bath and cooled at -78°C for 5 min. Afterwards, a solution of *n*BuLi in THF/hexane 0.25 M *n*BuLi solution in hexanes (10.5 mL, 10.5 mmol) was added drop by drop by syringe to the solution through a septum/needle. At the end of the addition, the mixture was stirred for additional 60–90 min at the addition temperature and then tributyltin chloride (5.7 mL, 18.7 mmol), was added dropwise. The mixture was stirred at -60°C for an additional hour, and then allowed to warm slowly to room temperature within 1–2 hours. Finally, few drops of a saturated aqueous NH_4Cl solution were added to quench the reaction. The reaction mixture was diluted in a copious amount of hexane, then successively dried over $MgSO_4$, filtrated, and solvents evaporated to dryness. The crude yellow oil was used without further purification in the next step (yield supposed to be quantitative for this step).

Compound (44)

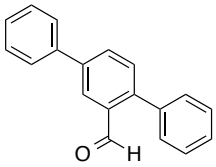

The stannyl compound (**43**) and 2,5-dibromobenzaldehyde (1.5 gr, 131 µmol) were dissolved in dry toluene (20 mL) in an argon flushed two-necked flask. The solution was degassed vigorously by bubbling argon through a needle/septum for 30

min. Afterward, $Pd(PPh_3)_4$ (45 mg, 38.9 μmol) was introduced in the flask and the solution heated while keeping a gentle argon bubbling. Once refluxing, the solution was let under inert atmosphere (Ar) and the reflux maintained for 3 days. After cooling down to room temperature, toluene was evaporated under reduced pressure and the crude purified by chromatography column on silica gel (eluent: Hexane 100% to Hexane/AcOEt 1:1), to afford **44** (1.2 g) in a 70% yield as a white solid.

^{1}H-NMR (300 MHz, $CDCl_3$), δ (ppm): 10.1 (s, 1H), 7.97 (s, 1H), 7.81 (d, *J* = 11.7 Hz, 2H), 7.65 (s, 4H), 7.51 (d, *J* = 159.2 Hz, 6H)

^{13}C-NMR (50 MHz, $CDCl_3$), δ (ppm): 126.46, 126.80, 127.23, 127.23, 128.60, 128.60, 128.60, 128.60, 128.87, 128.87, 128.87, 128.87, 128.92, 128.92, 137.61, 137.61, 139.46, 139.46, 192.37.

Compound (45)

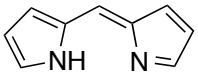

Paraformaldehyde (0.9 g, 30 mmol in formaldehyde) was suspended in 20 mL of absolute ethanol and the mixture was refluxed until clear solution appeared. After cooling down, 20-fold of pyrrole (42 mL, 600 mmol purified by alumina) and 1 L of dry CH_2Cl_2 were added and the mixture was stirred for 5 min to assure that oxygen was removed. Catalyst $BF_3{\cdot}O(Et)_2$ (0.5 mL) was then added and stirred at room temperature under argon atmosphere in the darkness overnight. After finishing the reaction, removing the solvent under vacuum .excess pyrrole was distilled under reduced pressure. The crude product was purified by silica gel chromatography with an eluent of CH_2Cl_2 and obtained 2.7 g (65%) of the colorless crystalline product.

^{1}H-NMR (300 MHz, $CDCl_3$), δ (ppm): 7.44 (dd, *J* = 2.7, 1.6 Hz, 2H), 6.10 (m, 4H), 3.92 (s, 2H)

3.5.2 Synthesis of the diarilamines (donor moieties):

Compound (46)

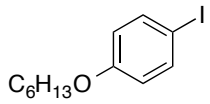

A suspension of 4-(hexyloxy)aniline (5.0 g, 35 mmol) in H_2SO_4 2.5 M (70ml) was cooled to -10 ºC and a solution of $NaNO_2$ (2.8 g, 39 mmol) in water (10 ml) was added dropwise under stirring. After total addition, the mixture was further stirred at 0ºC for 30 min and then poured over a solution of KI (6.5 g, 39 mmol) in cold water (40 ml). The resulting mixture was stirred at room temperature for 45 min and the Brown solid was filtered, washed with water and dissolved in CHCl3 (200 ml). This solution was then washed with a saturated solution of $Na_2S_2O_3$ (30 ml) and water (30 ml), and dried over Na_2SO_4. After filtration of the drying agent, the solvent was evaporated and the yellow oil obtained was subjected to column chromatography on silica gel using CH_2Cl_2 as eluent. Compound **46** was obtained (6.1 g, 24 mmol) as a white solid. Yield: 69%.

^{1}H-NMR (300 MHz, $CDCl_3$), δ (ppm): 7.08– 6.97 (m, 2H), 4.012 (m, 2H), 1.811 (t, *J* = 7.4 Hz, 2H), 1.36 (p, *J* = 7.5 Hz, 2H), 1.24– 1.27 (m, 6H), 0.86 (t, *J* = 7.0 Hz, 3H).

Compound (47)

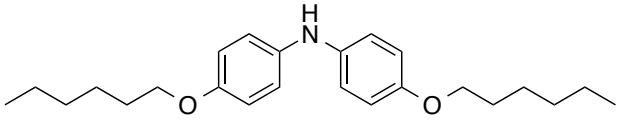

To a 50ml Schlenck flasck containing 1-(hexyloxy)-4-iodobenzene (400mg, 1.31mmol, 1.1eqv),4-(hexyloxy)aniline (231.1mg, 1.2mmol, 1eqv), $Pd_2(dba)_3$ (11.4mg, 0.01eqv), tri-t-butylphosphine (1.2, 0.03eqv), sodium t-butoxide (230mg, 1.7eqv) and 5ml of anhydrous toluene were added under argón atmosfere. The suspensión was refluxed for 1h. The mixture was filtered under celite and contrated under reduced pressure. The crude product was purified by silica gel column chromatography eluted with Hexane/CH_2Cl_2 (1:1) to give a white solid (70%)

^{1}H-NMR (300 MHz, $CDCl_3$)), δ (ppm): 6.96 – 6.87 (m, 2H), 6.86 – 6.75 (m, 2H), 3.91 (t, *J* = 6.6 Hz, 2H), 1.76 (dq, *J* = 8.1, 6.6 Hz, 2H), 1.44 (s, 2H), 1.33 (ddd, *J* = 7.3, 4.5, 3.2 Hz, 4H), 0.90 (td, *J* = 5.8, 4.6, 2.5 Hz, 3H).

MS (MALDI) : m/z (%) calculated $C_{24}H_{35}NO_2$ 369.2675 found 369.2668 (100) $[M]^+$

Compound (48)

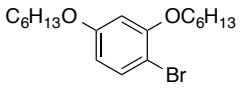

A mixture of 4-bromobenzene-1,3-diol (5 g, 26.5 mmol), 1-bromohexane (20 mL, 142 mmol) and K_2CO_3 (30 g, 217 mmol) in 30 mL of DMF was stirred at 90 °C for 3 h. After cooling to room temperature, the mixture was poured into 100 mL water and extracted with CH_2Cl_2. The combined organic phase was evaporated under vacuum to remove the solvent. The residue was subjected to silica gel column chromatography, eluting with a mixture of hexane and CH_2Cl_2 to give a colorless oil (9.4g, 99%).

^{1}H NMR (400 MHz, $CDCl_3$), δ (ppm): 7.38 (d, 1H, J = 8.8 Hz), 6.47(d, 1H, J = 2.8 Hz), 6.38(dd, 1H, J1 = 8.8 Hz, J2 =2.8 Hz), 4.00(t, 2H, J = 6.4 Hz), 3.93 (t, 2H, J = 6.4 Hz), 1.84(m, 4H), 1.49(m, 12H), 0.91(t, 6H, J = 6.8 Hz).

^{13}C NMR (100.6 MHz, $CDCl_3$) δ (ppm): 159.7, 156.2, 133.0, 106.7, 103.0, 101.7, 69.2, 68.4, 31.6, 31.5, 29.2, 25.7, 25.6, 22.6, 14.0

Compound (49)

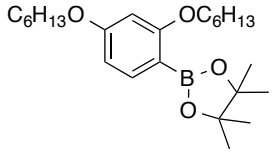

To a cold solution of **48** (5.9 g, 16.4 mmol) in 150 mL THF at -78 °C was added *n*-butyl lithium (17.5 mmol) under Argon. The mixture was stirred for 1 h at the same temperature and then isopropyl pinacol borate (3.35g, 18 mmol) was added dropwise, the resulting mixture was allowed to warm to room temperature and stirred for another 6 h. The reaction was quenched by adding 20 mL saturated NH_4Cl aqueous solution, the resulting mixture was poured into 100 mL water, and the solution was extracted with ethyl acetate. The extract was dried over $MgSO_4$. After removing the solvent under reduced pressure, the residue was treated by column chromatography

over silica gel with mixture of hexane and ethyl acetate (20:1) to yield a colorless oil (4.5 g, 68%).

^{1}H NMR (400 MHz, $CDCl_3$), δ (ppm): 7.58(d, 1H, J = 8.0 Hz), 6.46 (dd, 1H, J1 = 8.0 Hz, J = 2.0 Hz), 6.38 (d,1H, J = 2.0 Hz), 3.9 (m, 4H), 1.78 (m, 4H), 1.53 (m, 24H), 0.91 (m, 6H).

^{13}C NMR (100.6 MHz, $CDCl_3$) δ (ppm): 165.6, 163.1, 137.8, 105.2, 99.5, 83.0, 68.3, 67.9, 31.7, 29.3, 25.7, 24.8, 22.7, 22.6, 14.1, 14.0

Compound (50)

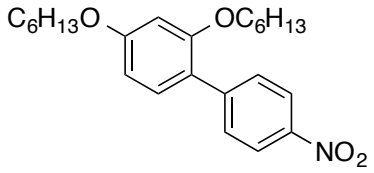

A mixture of **49** (1.73 mmol), 4-bromo-nitrobenzene (420 mg, 2.1 mmol), $Pd(PPh_3)_2Cl_2$ (70 mg, 0.1 mmol), Cs_2CO_3 (700 mg, 2.15 mmol), 2 mL H_2O in 10 mL DMF was heated at 120 °C for 9 h under inert atomosphere. The resulting solution was cooled to room temperatura and extracted with CH_2Cl_2 (2 x 100 mL) and water (100 mL). The combined extracts were evoporated and purified by column chromatography on silica gel (hexane/CH_2Cl_2 5:2) to yield a yellow oil (510 mg 74%).

^{1}H NMR (400 MHz, $CDCl_3$), δ (ppm): 8.23(d, 2H, J = 8.8 Hz), 7.69(d, 2H, J = 8.8 Hz), 7.27(d, 1H, J = 8.0 Hz), 6.59(m, 2H), 4.02(m, 4H), 1.83(m, 4H), 1.37(m, 12H), 0.94(m, 6H).

^{13}C NMR (100.6 MHz, $CDCl_3$) δ (ppm): 161.0, 157.2, 146.1, 145.6, 131.2, 130.0, 123.1, 120.9, 105.7, 100.3, 68.5, 68.2, 31.6, 31.4, 29.2, 29.0, 25.7, 25.7, 22.6, 22.5, 14.0, 13.9.

Compound (51)

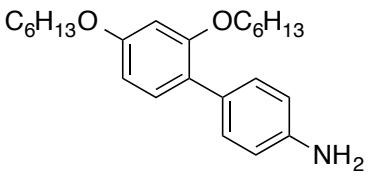

To a stirred solution of **50** (500 mg, 1.25 mmol) in mixture of actone (5 mL) and water (1 mL) was added zinc poder (800 mg, 12.3 mmol) and NH_4Cl (1.0 g, 18.9 mmol), and then the mixture was heated to 60 °C for 30 min. After cooling to room temperature, the solid was filtered off. The filtrate was extracted with CH_2Cl_2 (2 x 50 mL) and water (50 mL). The organic phase was combined and the solvent was removed by rotary evoparation. The product was purified by column chromatography using a hexane/CH2Cl2 (1:1) to CH2Cl2 gridient to yield a colorless oil (410 mg, 87%)

^{1}H NMR (400 MHz, $CDCl_3$), δ (ppm): 7.35(d, 2H, J = 8.8 Hz), 7.21(d, 1H, J = 7.2 Hz), 6.72(d, 2H, J = 8.8 Hz), 6.53(m, 2H), 3.98(m, 4H), 3.65(b, 2H), 1.80(m, 4H), 1.36(m, 12H), 0.92(m, 6H).

^{13}C NMR (100.6 MHz, $CDCl_3$) δ (ppm): 159.1, 156.9, 144.7, 130.6, 130.3, 128.9, 123.6, 114.7, 105.2, 100.5, 68.3, 68.0, 31.6, 31.4, 29.3, 29.1, 25.8, 22.6, 22.5, 14.0, 13.9

Compound (52)

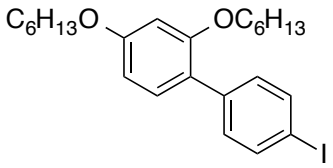

A suspension of **51** (400 mg, 1.08 mmol) in H_2SO_4 2.5 M (70ml) was cooled to -10 ºC and a solution of $NaNO_2$ (2.8 g, 39 mmol) in water (10 ml) was added dropwise under stirring. After total addition, the mixture was further stirred at 0ºC for 30 min and then poured over a solution of KI (6.5 g, 39 mmol) in cold water (40 ml). The resulting mixture was stirred at room temperature for 45 min and the Brown solid was filtered, washed with water and dissolved in $CHCl_3$ (200 ml). This solution was then washed with a saturated solution of $Na_2S_2O_3$ (30 ml) and water (30 ml), and dried over Na_2SO_4 . After filtration of the drying agent, the solvent was evaporated and the yellow oil obtained was subjected to column chromatography on silica gel using CH_2Cl_2 as eluent. Compound **51** was obtained as a yellow oil Yield: 49%.

^{1}H NMR (400 MHz, $CDCl_3$), δ (ppm): 77.69(d, 2H, J = 8.4 Hz), 7.27(d, 2H, J = 8.4 Hz), 7.20(d, 1H, J = 9.2 Hz), 6.54(m, 2H), 3.98(m, 4H), 1.80(m, 4H), 1.37(m, 2H), 1.35(m,6H), 1.30(m, 4H), 0.92(m, 6H)

^{13}C NMR (100.6 MHz, $CDCl_3$) δ (ppm): 160.1, 156.9, 138.1, 136.8, 131.4, 130.9, 122.2, 105.4, 100.4, 100.0, 91.7, 68.4, 68.1, 31.6, 31.4, 29.3, 29.0, 25.7, 22.6, 22.5, 14.0, 13.9.

Compound (53)

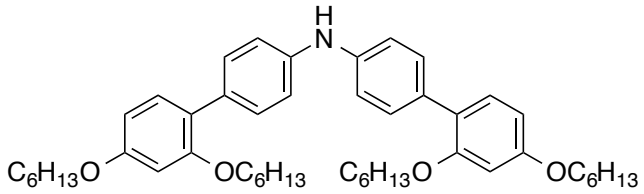

Procedure previous reportet in Compound **(47)**. (70%)

^{1}H-NMR (300 MHz, $CDCl_3$), δ (ppm): 7.46 (s, 3H), 7.27 (d, *J* = 2.2 Hz, 3H), 7.12 (d, *J* = 8.2 Hz, 4H), 6.55 (p, *J* = 5.0, 3.9 Hz, 4H), 5.76 (s, 1H), 3.97 (dt, *J* = 12.3, 5.8 Hz, 8H), 1.86 – 1.69 (m, 8H), 1.48 – 1.24 (m, 23H), 0.98 – 0.83 (m, 12H).

^{13}C NMR (100.6 MHz, $CDCl_3$) δ (ppm): 160.1, 156.9, 138.1, 136.8, 131.4, 130.9, 122.2, 105.4, 100.4, 100.0, 91.7, 68.4, 68.1, 31.6, 31.4, 29.3, 29.0, 25.7, 22.6, 22.5, 14.0, 13.9.

MS (MALDI): m/z (%) found 721.5 (100) $[M]^+$

3.5.3 Synthesis of the anchoring/acceptor groups

Compound (54)

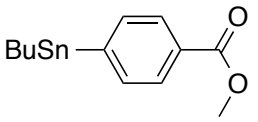

Methyl 4-iodobenzoate (300 mg, 1.15 mmol), bistributyltin (1.15 mL, 2.29 mmol) and $Pd(PPh_3)_4$ (70 mg, 0.06 mmol) was degassed by vaccum/argon cycles (three times), then degassed toluene (12mL) was added into the flask. The reaction mixture was heated to 120 oC for 5 h. The solvent was removed under reduced pressure and the

product was purified by silica flash gel chromatography eluting with 50:1 hexane/EtOAc to afford the product as colorless oil (330 mg, 70 %).

^{1}H NMR (400 MHz, $CDCl_3$), δ (ppm): 7.96 (d, J = 8.0 Hz, 2H), 7.56 (d, J = 8.0 Hz, 2H), 1.57 - 1.51 (m, 6H), 1.37 - 1.30 (m, 6H),1.10 - 1.07 (t, J = 9.0 Hz, 6H), 0.88 (t, J = 7.0 Hz, 9H).

^{13}C NMR (100.6 MHz, $CDCl_3$) δ (ppm): 167.5, 149.6, 136.4, 129.5, 128.3, 52.0, 29.0, 27.3, 13.6, 9.6.

Compound (55)

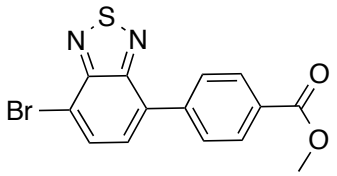

Compound **53** (210 mg, 0.702 mmol, 1.25 equiv), 4,7-bromo-2,1,3-benzothiadiazole (165 mg, 0.562 mmol), CsF (212 mg, 1.404 mmol, 2 equiv), PdCl2 (5 mg, 0.0281 mmol, 5mol%), *t*-Bu_3P (56 µL, 1M in toluene, 0.0562 mmol, 10mol%), CuI (5 mg, 0.0281 mmol, 5mol%) and DMF (2.4 mL) were stirred at 45°C for 1 hour, upon which no more stannane starting material was detected by TLC (silica, Dioxane/Heptane, 1:4). The reaction mixture was diluted with EtOAc (50 mL) and washed with water (5. 50 mL), dried (Na_2SO_4) and evaporated prior to purification using column chromatography (silica, Dioxane/Heptane, 1:4) to afford the desired product **54** as a yellow solid (73 mg, 37%)

^{1}H NMR (400 MHz, $CDCl_3$), δ (ppm): 8.20 (d, *J* = 8.4 Hz, 2H), 7.99 (d, *J* = 8.4 Hz, 2H), 7.96 (d, *J* = 7.6 Hz, 1H), 7.64 (d, *J* = 7.6 Hz, 1H), 3.97 (s, 3H).

^{13}C NMR (100.6 MHz, $CDCl_3$) δ (ppm): 166.7, 153.9, 152.8, 140.9, 132.8, 132.2, 129.9, 129.1, 128.7, 127.2, 114.2, 52.3.

3.5.3 Synthesis of Porphyrines:

Compound (56)

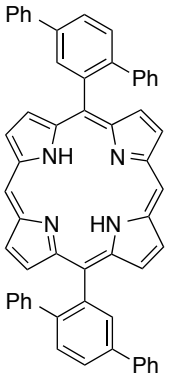

To a degassed solution of dipyrromethane (6.04 g, 41.4 mmol) and Donor 2 (**45**) (15 g, 41.4 mmol) in DCM (5.4 L) was added $BF_3 \cdot O(Et)_2$ (2.75 mL, 37.3 mmol). After the solution was stirred at r.t. under argon for 4 h, DDQ (14.1 g, 62.1 mmol) was added and the mixture was stirred for an additional 1 h. The mixture was basified with Et_3N (7 mL) and filtered through silica. The solvent was removed under reduced pressure and the residue was purified by column chromatography (silica gel) using DCM/Heptane 1:2 as eluent to obtein a red solid (15%)

^{1}H-NMR (300 MHz, $CDCl_3$), δ (ppm): 10.13 (s, 2H), 9.24 (d, *J* = 4.6 Hz, 4H), 9.04 (d, *J* = 4.6 Hz, 4H), 8.37 (d, *J* = 2.0 Hz, 1H), 8.15 (dd, *J* = 8.1, 2.0 Hz, 2H), 7.96 (d, *J* = 8.1 Hz, 2H), 7.85 – 7.80 (m, 4H), 7.47 – 7.39 (m, 3H), 7.39 – 7.31 (m, 2H), 7.20 – 7.11 (m, 4H), 6.54 (dd, *J* = 5.0, 1.8 Hz, 6H), -3.16 (s, 2H).

^{13}C-NMR (50 MHz, $CDCl_3$), δ (ppm): 147.57, 145.18, 143.99, 143.85, 141.46, 141.29, 140.52, 140.48, 140.15, 140.10, 138.41, 135.22, 134.87, 133.78, 131.75, 131.12, 130.45, 130.31, 129.70, 129.57, 129.13, 129.08, 128.38, 127.70, 127.67, 127.59, 127.52, 127.48, 127.26, 127.26, 126.08, 125.95, 122.79, 121.39, 118.20, 118.20, 105.23, 105.18, 100.14, 77.36, 29.86.

HRMS(FAB$^+$; NBA): *m/z* calcd $RuC_{90}H_{116}N_6O_4S_6$: 1638.6441 (100) [M]+; found 1638.6402 (100) .

UV-Vis: λmax(CH_2Cl_2)/nm= 414 (*e* /dm^3 mol^{-1} cm^{-1}: 307126), 285 (13846,13376), 544 (3832), 585 (3869), 641 (609).

Compound (57)

A suspension of **57** (2.3 g, 2.18 mmol) and $Zn(OAc)_2$ (4.79 g, 21.82 mmol) in a mixture of DCM (450 mL) and MeOH (220 mL) was stirred at r.t. for 2 h. The reaction was quenched with water (100mL), and the mixture was extracted with DCM (2 x 100 mL). The combined extracts were washed with water and dried over anhydrous $MgSO_4$. The solvent was removed under reduce pressure to give the product (2.39 g, 98%).

^{1}H-NMR (300 MHz, $CDCl_3$), δ (ppm): 10.20 (d, *J* = 9.3 Hz, 2H), 9.36 (dd, *J* = 11.3, 4.5 Hz, 4H), 9.21 (dd, *J* = 9.3, 4.5 Hz, 4H), 8.54 (t, *J* = 2.4 Hz, 2H), 8.19 – 8.13 (m, 2H), 7.97 (d, *J* = 8.1 Hz, 2H), 7.89 – 7.80 (m, 4H), 7.40 (q, *J* = 7.5 Hz, 4H), 7.29 (dd, *J* = 8.6, 4.4 Hz, 2H), 7.19 – 7.13 (m, 2H), 7.08 (dd, *J* = 6.7, 2.9 Hz, 2H), 6.55 – 6.49 (m, 3H), 6.44 – 6.38 (m, 3H).

^{13}C-NMR (50 MHz, $CDCl_3$), δ (ppm): 151.02, 150.95, 149.87, 149.82, 144.48, 144.34, 142.18, 142.02, 141.81, 141.76, 140.95, 140.89, 139.84, 138.49, 138.47, 135.11, 134.77, 133.02, 132.96, 132.41, 130.56, 130.46, 129.97, 129.82, 129.40, 129.35, 127.94, 127.81, 127.67, 127.45, 127.39, 126.33, 126.24, 119.50, 119.39, 114.67, 106.58, 77.79.

HRMS(MALDI; DCTB + PPGNa 790): *m/z* calcd $C_{56}H_{36}N_4Zn_1$: 828,22 (100) [M]+; found 828.2226 (100) .

UV-Vis: λmax(CH_2Cl_2)/nm= 419 (ε/dm^3 mol^{-1} cm^{-1}: 371161), 511 (13223), 564 (3363), 586 (3794), 613 (814).

Compound (58)

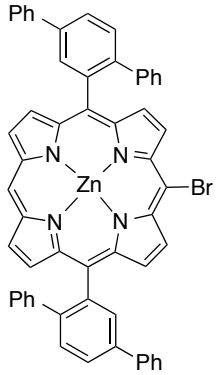

To a stirred solution of porphyrin **58** (3.5 g, 3.59 mmol) in DCM (1500 mL) wasslowly added a solution of NBS (0.671g, 3.77 mmol) in DCM (400 mL) in a period of 6 h at 0 °C under dinitrogen. After the reaction was quenched with acetone (30 mL), the solvent was removed under reduced pressure. The residue was purified by percolated (silica gel) using DCM/hexanes 1:2 as eluent. To obtain a mixture of products (monobromo, dibromo and some starting material **57**) as a purple powder. The mixture was used without further purification in the next step (yield supposed to be calculated whit the ^{1}H-NMR spectra for this step around 40%).

Compound (59)

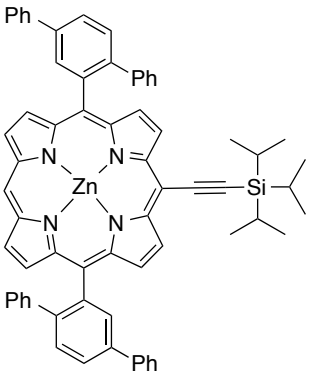

A mixture of the zinc complex of **59** (0.91 g, 0.81 mmol), triisopropylacetylene (0.37mL, 2.04 mmol), $Pd(PPh_3)_2Cl_2$ (0.11 g, 0.16 mmol), CuI (0.047 g, 0.24 mmol), THF (30 mL) and NEt3 (5 mL) was gently refluxed for 4 h under dinitrogen. The solvent was removed under vacuum. The residue was purified by column chromatography (silica gel) using DCM/hexanes 1:4 to as eluent to give the product (0.82 g, 83%) as a purple solid.

^{1}H-NMR (300 MHz, $CDCl_3$), δ (ppm): 9.97 (d, *J* = 7.5 Hz, 1H), 9.77 (d, *J* = 4.7 Hz, 2H), 9.17 (dd, *J* = 8.0, 4.5 Hz, 2H), 9.07 (d, *J* = 4.6 Hz, 2H), 8.96 (dd, *J* = 6.8, 4.5 Hz, 2H), 8.35 (dd, *J* = 9.4, 1.9 Hz, 2H), 8.11 (dd, *J* = 8.1, 2.0 Hz, 2H), 7.92 – 7.78 (m, 6H), 7.49 – 7.28 (m, 6H), 7.19 (dd, *J* = 6.7, 3.0 Hz, 1H), 7.06 – 7.02 (m, 2H), 6.51 – 6.46 (m, 2H), 6.42 – 6.37 (m, 4H), 1.53 – 1.41 (m, 22H).

^{13}C-NMR (50 MHz, $CDCl_3$), δ (ppm): 152.34, 152.32, 150.80, 150.70, 150.37, 150.35, 149.39, 149.33, 143.84, 143.71, 141.89, 141.57, 141.23, 141.20, 140.56, 140.47, 138.11, 134.33, 134.20, 132.80, 132.44, 132.41, 132.06, 131.38, 130.04, 130.01, 129.59, 129.41, 129.03, 128.98, 127.60, 127.44, 127.31, 127.27, 127.06, 126.94, 125.97, 125.88, 120.15, 120.11, 109.83, 107.34, 100.14, 97.55, 77.36, 63.06, 32.05, 22.87, 22.83, 19.31, 12.13.

HRMS (MALDI, DCTB+PPG1000): m/z (%) found $C_{67}H_{56}N_4Si_1Zn_1$ 1008.3560 (100) [M]+; found 1008.3521 (100) .

UV-Vis: λmax(CH_2Cl_2)/nm= 570 (ε/dm^3 mol^{-1} cm^{-1}: 105 2644), 570 (53 882), 613 (47 179).

Compound (60)

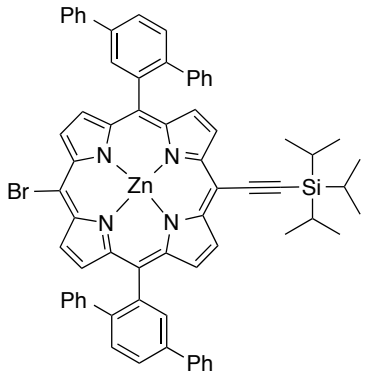

To a stirred solution of porphyrin **60** (0.82 g, 0.67 mmol) in DCM (250 mL) and dry pyridine (10 mL) was added NBS (0.14 g, 0.80 mmol) at r.t.. After stirring for 0.5 h, the reaction was quenched with water (25 mL). The mixture was extracted with DCM, dry and the solvent was removed under reduced pressure. The residue was purified by column chromatography (silica gel) using DCM/hexanes 1:4 to as eluent to give the product as a green solid. (0.74 g, 85%).

^{1}H-NMR (300 MHz, $CDCl_3$), δ (ppm): 9.65 (dd, *J* = 4.7, 1.2 Hz, 2H), 9.53 (t, *J* = 4.9 Hz, 2H), 8.96 (dd, *J* = 4.6, 1.1 Hz, 2H), 8.87 (t, *J* = 4.5 Hz, 2H), 8.31 (t, *J* = 2.4 Hz, 2H), 8.13 – 8.03 (m, 2H), 7.87 (dd, *J* = 8.1, 3.2 Hz, 2H), 7.82 – 7.75 (m, 4H), 7.42 (ddd, *J* = 8.0, 6.7, 1.8 Hz, 4H), 7.33 (d, *J* = 7.3 Hz, 1H), 7.12 (dd, *J* = 7.6, 2.0 Hz, 2H), 7.08 – 6.99 (m, 2H), 6.46 (ddd, *J* = 9.7, 4.8, 2.1 Hz, 6H), 1.55 – 1.31 (m, 22H).

^{13}C-NMR (50 MHz, $CDCl_3$), δ (ppm): 153.18, 151.31, 151.25, 150.74, 150.72, 149.37, 149.34, 143.75, 143.66, 143.22, 141.64, 141.42, 141.04, 141.01, 140.47, 140.41, 138.12, 134.30, 134.16, 133.22, 133.00, 131.71, 130.09, 129.56, 129.43, 129.05, 129.02, 127.65, 127.44, 127.18, 127.10, 125.99, 122.54, 121.31, 109.48, 106.17, 100.64, 98.03, 77.58, 77.36, 77.16, 76.74, 29.87, 19.27, 12.08, 12.06, 1.19.

HRMS (MALDI, DCTB+PPG1000): m/z (%) found $C_{67}H_{56}N_4Si_1Zn_1Br$ 1088.2655 (100) [M]+; found 1088.2618 (100) .

UV-Vis: λmax(CH2Cl2)/nm= 434 (ε/dm^3 mol^{-1} cm^{-1}: 105 2644), 570 (53 882), 613 (47 179).

Buchwald-Hartwig Cross Coupling Reaction

General Procedure:

To a 20ml Schlenck flasck containing porphyrine (1eqv), Donor 1 (1.5eqv), $Pd_2(dba)_3$ (0.01eqv), tri-t-butylphosphine (0.03eqv), sodium t-butoxide (2.5eqv) and anhydrous toluene were added under argón atmosfere. The suspensión was refluxed for 30min. The mixture was filtered under celite and concentrated under reduced pressure. The crude product was purified by silica gel column chromatography eluted with Hexane/CH_2Cl_2 (1:1) to give a disered product. Yield: 50-70%

Compound (61)

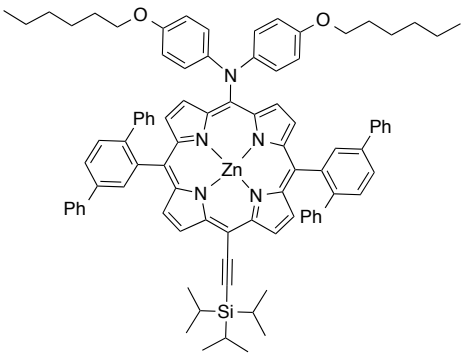

^{1}H-NMR (300 MHz, $CDCl_3$), δ (ppm): 9.59 (dd, *J* = 4.6, 2.9 Hz, 2H), 9.12 (dd, *J* = 6.0, 4.6 Hz, 2H), 8.91 (t, *J* = 4.4 Hz, 2H), 8.71 (q, *J* = 4.9, 4.1 Hz, 2H), 8.31 (dt, *J* = 5.4, 2.6 Hz, 2H), 8.07 (dd, *J* = 8.1, 2.1 Hz, 2H), 7.89 – 7.76 (m, 6H), 7.51 – 7.29 (m, 6H), 7.22 (d, *J* = 7.9 Hz, 1H), 7.15 – 7.06 (m, 4H), 7.00 (dt, *J* = 7.8, 2.8 Hz, 2H), 6.82 – 6.61 (m, *J* = 8.0 Hz, 4H), 6.56 (p, *J* = 4.0, 3.5 Hz, 3H), 6.52 – 6.37 (m, 3H), 4.03 – 3.64 (m, 4H), 1.79 – 1.58 (m, 4H), 1.44 (q, *J* = 4.2 Hz, 22H), 1.35 (d, *J* = 2.9 Hz, 5H), 1.29 (dt, *J* = 7.3, 3.3 Hz, 8H), 0.87 (td, *J* = 6.8, 3.1 Hz, 6H).

^{13}C-NMR (50 MHz, $CDCl_3$), δ (ppm): 153.15, 153.15, 152.90, 152.52, 152.39, 150.49, 150.46, 149.87, 149.82, 147.00, 143.70, 143.53, 141.58, 141.40, 140.91, 140.85, 140.51, 140.46, 138.15, 138.07, 134.34, 134.01, 132.97, 132.93, 132.77, 131.25, 131.11, 131.04, 130.15, 130.03, 129.56, 129.40, 129.05, 129.00, 127.62, 127.52, 127.46, 127.37, 127.11, 127.04, 126.01, 125.89, 125.00, 124.87, 123.78, 123.66, 123.42, 120.72, 120.68, 115.19, 115.14, 100.18, 97.75, 97.74, 77.36, 68.40, 53.58, 31.73, 29.47, 25.87, 22.73, 19.27, 14.17, 12.05, 12.03.

HRMS (MALDI, DCTB+PMMANa1000): m/z (%) found $C_{91}H_{89}N_5O_2Si_1Zn_1$ 1377.6085 (100) [M]+; found 1377.6156 (100) .

UV-Vis: λmax(CH_2Cl_2)/nm= 432 (ε/dm^3 mol^{-1} cm^{-1}: 1199 581), 561 (33017), 599 (20398), 649 (19771)

Compound (62)

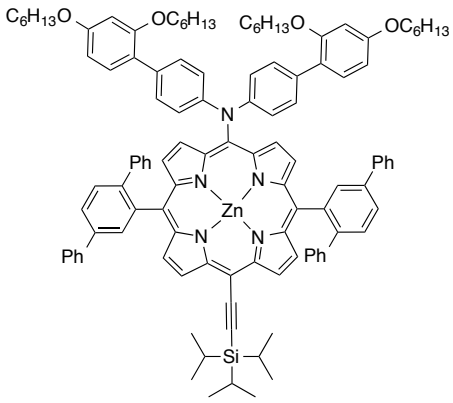

^{1}H-NMR (300 MHz, $CDCl_3$), δ (ppm): 9.59 (dd, *J* = 4.6, 2.9 Hz, 2H), 9.12 (dd, *J* = 6.0, 4.6 Hz, 2H), 8.91 (t, *J* = 4.4 Hz, 2H), 8.71 (q, *J* = 4.9, 4.1 Hz, 2H), 8.31 (dt, *J* = 5.4, 2.6 Hz, 2H), 8.07 (dd, *J* = 8.1, 2.1 Hz, 2H), 7.89 – 7.76 (m, 6H), 7.51 – 7.29 (m, 6H), 7.22 (d, *J* = 7.9 Hz, 1H), 7.15 – 7.06 (m, 4H), 7.00 (dt, *J* = 7.8, 2.8 Hz, 2H), 6.82 – 6.61

(m, *J* = 8.0 Hz, 4H), 6.56 (p, *J* = 4.0, 3.5 Hz, 3H), 6.52 – 6.37 (m, 3H), 4.03 – 3.64 (m, 4H), 1.79 – 1.58 (m, 4H), 1.44 (q, *J* = 4.2 Hz, 22H), 1.35 (d, *J* = 2.9 Hz, 5H), 1.29 (dt, *J* = 7.3, 3.3 Hz, 8H), 0.87 (td, *J* = 6.8, 3.1 Hz, 6H).

^{13}C-NMR (50 MHz, $CDCl_3$), δ (ppm): 153.15, 153.15, 152.90, 152.52, 152.39, 150.49, 150.46, 149.87, 149.82, 147.00, 143.70, 143.53, 141.58, 141.40, 140.91, 140.85, 140.51, 140.46, 138.15, 138.07, 134.34, 134.01, 132.97, 132.93, 132.77, 131.25, 131.11, 131.04, 130.15, 130.03, 129.56, 129.40, 129.05, 129.00, 127.62, 127.52, 127.46, 127.37, 127.11, 127.04, 126.01, 125.89, 125.00, 124.87, 123.78, 123.66, 123.42, 120.72, 120.68, 115.19, 115.14, 100.18, 97.75, 97.74, 77.36, 68.40, 53.58, 31.73, 29.47, 25.87, 22.73, 19.27, 14.17, 12.05, 12.03.

HRMS (MALDI, DCTB+PMMANa1000): m/z (%) found $C_{91}H_{89}N_5O_2Si_1Zn_1$ 1377.6085 (100) [M]+; found 1377.6156 (100) .

UV-Vis: λmax(CH_2Cl_2)/nm= 432 (ε/dm^3 mol^{-1} cm^{-1}: 1199 581), 561 (33017), 599 (20398), 649 (19771)

Cross Coupling Reaction whit out Cu

General Procedure:

To a solution of porphyrin (1eqv.) in dry THF was added TBAF (1M in THF, 2.5eqv.) and the resulting solution stirred for 30 minutes at room temperature. Water (25 mL) was added and the organics extracted with DCM (2 x 25 mL). The organics were dried (Na_2SO_4) filtered and evaporated. To the porphyrinic residue (1eqv) was added the corresponding Linker (1.5eqv), Pd(PPh_3) (0.01eqv), and finally with argon-degassed benzene and triethylamine. The green solution was heated at 60 °C until complete consumption of the starting material (determined by TLC), and then the solvent was evaporated under vacuum. The residue was treated with water and extracted with dichloromethane. The organic extracts were washed with water and then brine and dried over magnesium sulfate. The solvent was removed by evaporation. The residue was purified by chromatography on silica using DCM/Heptane 4:1 and a solid which was further purified by GPC (eluent toluene) to afford a green-brown solid. Yield: 70-80%

Compound (63)

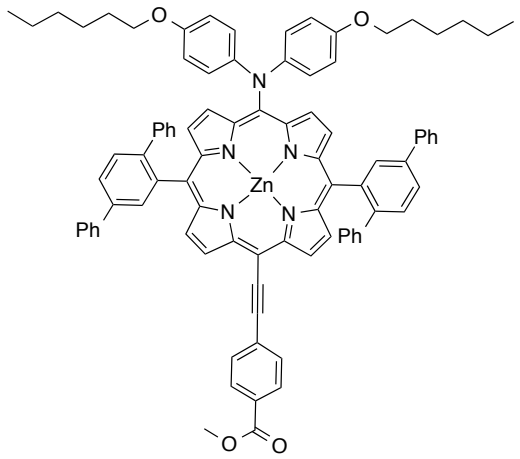

^{1}H-NMR (300 MHz, $CDCl_3$), δ (ppm): 9.57 – 9.51 (m, 2H), 9.13 (dd, *J* = 4.7, 3.5 Hz, 2H), 8.88 (dd, *J* = 11.6, 4.7 Hz, 3H), 8.73 (t, *J* = 5.0 Hz, 2H), 8.28 (d, *J* = 1.9 Hz, 2H), 8.21 – 8.12 (m, 3H), 8.09 – 7.98 (m, 5H), 7.87 – 7.74 (m, 8H), 7.74 – 7.65 (m, 3H), 7.50 – 7.27 (m, 19H), 7.21 – 6.98 (m, 13H), 6.79 – 6.66 (m, 4H), 6.60 – 6.54 (m, 4H), 6.41 (d, *J* = 7.1 Hz, 3H), 3.96 – 3.77 (m, 7H), 1.68 (dd, *J* = 14.2, 7.0 Hz, 7H), 1.36 – 1.13 (m, 17H), 0.93 – 0.70 (m, 13H).

^{13}C-NMR (50 MHz, $CDCl_3$), δ (ppm): 166.75, 153.12, 152.56, 152.49, 152.35, 150.31, 150.24, 150.03, 147.11, 147.02, 143.72, 143.64, 141.71, 141.47, 141.02, 140.96, 140.45, 138.11, 138.10, 134.34, 134.17, 133.00, 132.95, 132.73, 132.71, 131.38, 131.33, 131.17, 130.93, 130.69, 130.13, 130.05, 129.83, 129.61, 129.43, 129.06, 129.02, 127.64, 127.47, 127.41, 127.36, 127.11, 127.01, 125.97, 125.88, 125.43, 123.46, 120.92, 120.89, 115.20, 77.36, 68.41, 52.33, 32.09, 31.73, 29.86, 29.82, 29.52, 29.47, 25.87, 22.86, 22.83, 22.72, 14.29, 14.16, 1.19.

HRMS (MALDI, DCTB+PMMANa1000): m/z (%) found $C_{90}H_{75}N_5O_4Zn_1$ 1355.5119 (100) [M]+; found 1355.5110 (100) .

UV-Vis: λmax(CH_2Cl_2)/nm= 442 (ε/dm^3 mol^{-1} cm^{-1}: 3861951), 664 (102620)

Compound (64)

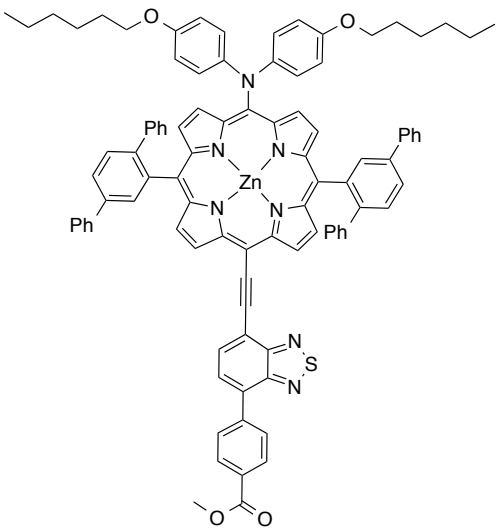

^{1}H-NMR (300 MHz, $CDCl_3$), δ (ppm): 9.14 (dd, *J* = 4.7, 1.1 Hz, 3H), 8.95 (dq, *J* = 9.8, 4.7 Hz, 3H), 8.74 (dd, *J* = 4.6, 2.2 Hz, 3H), 8.37 – 8.31 (m, 3H), 8.12 – 8.00 (m, 7H), 7.84 (ddd, *J* = 15.0, 7.7, 2.5 Hz, 14H), 7.48 – 7.31 (m, 11H), 7.21 – 7.01 (m, 14H), 6.82 – 6.37 (m, 19H), 3.97 – 3.44 (m, 11H), 1.64 (d, *J* = 20.2 Hz, 8H), 1.26 (s, 16H), 0.87 (tt, *J* = 7.0, 4.1 Hz, 15H).

^{13}C-NMR (50 MHz, $CDCl_3$), δ (ppm): 166.78, 153.07, 153.03, 152.61, 152.38, 152.33, 150.30, 150.24, 149.95, 146.95, 143.61, 143.48, 141.53, 141.34, 140.83, 140.80, 140.38, 140.33, 138.04, 138.00, 133.93, 133.13, 133.09, 132.61, 132.60, 131.09, 130.08, 129.97, 129.34, 129.09, 129.05, 128.95, 128.90, 127.52, 127.40, 127.34, 127.03, 126.95, 125.89, 125.82, 123.33, 121.02, 120.98, 115.14, 77.24, 68.31, 31.97, 31.60, 29.74, 29.70, 29.41, 29.35, 29.31, 25.72, 22.74, 22.60, 14.17.

HRMS (MALDI, DCTB+PMMANa1000): m/z (%) found $C_{96}H_{77}N_{7O}4S1Zn_1$ 1489.5058 (100) [M]+; found 1355.5110 (100) .

UV-Vis: λmax(CH_2Cl_2)/nm= 449 (ε/dm^3 mol^{-1} cm^{-1}: 3961481), 484 (3611952), 700 (7181).

Compound (65)

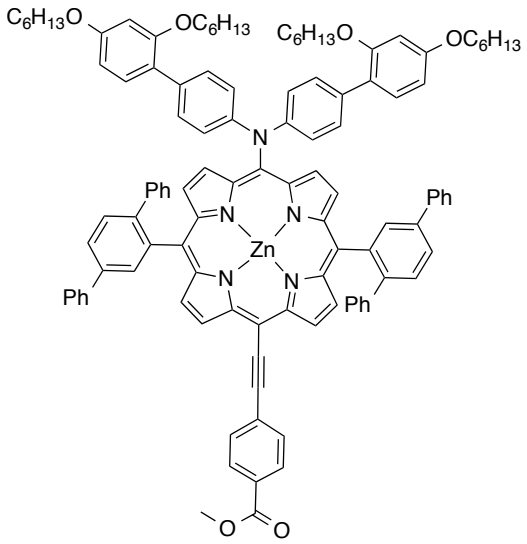

^{1}H-NMR (300 MHz, $CDCl_3$), δ (ppm): 9.57 (dd, *J* = 6.6, 4.6 Hz, 1H), 9.24 (dd, *J* = 4.7, 3.4 Hz, 1H), 8.90 (t, *J* = 5.0 Hz, 1H), 8.79 (dd, *J* = 4.6, 2.4 Hz, 1H), 8.34 – 8.25 (m, 1H), 8.14 – 7.93 (m, 4H), 7.93 – 7.75 (m, 5H), 7.75 – 7.66 (m, 2H), 7.54 (ddt, *J* = 9.1, 5.4, 2.5 Hz, 4H), 7.46 – 7.27 (m, 10H), 7.25 – 7.00 (m, 6H), 6.92 – 6.73 (m, 2H), 6.58 – 6.39 (m, 5H), 4.08 – 3.72 (m, 9H), 1.70 (dddd, *J* = 26.5, 15.3, 10.9, 6.1 Hz, 4H), 1.48 – 1.30 (m, 8H), 1.18 (ddd, *J* = 23.1, 7.3, 3.5 Hz, 6H), 0.99 – 0.70 (m, 8H).

^{13}C-NMR (50 MHz, $CDCl_3$), δ (ppm): 168.18, 166.71, 159.40, 157.06, 157.03, 152.48, 152.21, 150.94, 150.91, 150.35, 143.81, 143.62, 141.78, 141.49, 141.06, 140.55, 140.46, 138.14, 138.11, 137.84, 135.89, 135.05, 134.97, 134.88, 132.94, 132.16, 131.85, 131.54, 131.38, 131.13, 130.87, 130.79, 130.10, 130.05, 129.85, 129.72, 129.66, 129.46, 129.10, 129.04, 128.99, 128.06, 127.99, 127.92, 127.61, 127.47, 127.35, 125.97, 125.86, 123.84, 123.22, 123.02, 121.92, 121.80, 120.95, 105.58, 105.48, 105.40, 100.82, 100.69, 100.62, 100.55, 77.36, 68.57, 68.52, 68.47, 68.22, 68.19, 52.48, 52.37, 52.28, 51.66, 32.08, 31.72, 31.55, 31.50, 31.45, 29.85, 29.51, 29.41, 29.13, 25.86, 25.78, 25.75, 22.73, 22.63, 22.54, 14.16, 14.09, 14.00.

HRMS (MALDI, DCTB+PMMANa1000): m/z (%) found $C_{114}H_{107}N_5O_6Zn_1$ 1707.7533 (100) [M]+; found 1707.7512 (100) .

UV-Vis: λmax(CH_2Cl_2)/nm= 449 (ε/dm^3 mol^{-1} cm^{-1}: 3961481), 484 (3611952), 700 (7181).

Compound (66)

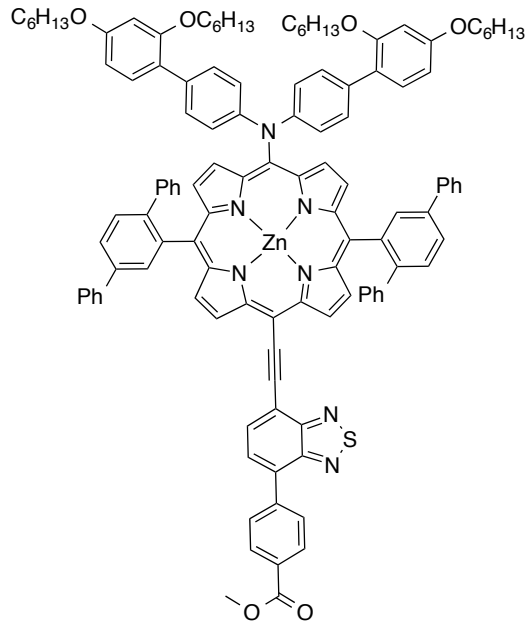

^{1}H-NMR (300 MHz, $CDCl_3$), δ (ppm): 9.57 (dd, *J* = 6.6, 4.6 Hz, 1H), 8.90 (t, *J* = 5.0 Hz, 1H), 8.36 – 8.24 (m, 1H), 8.19 – 7.97 (m, 5H), 7.97 – 7.78 (m, 5H), 7.78 – 7.64 (m, 4H), 7.61 – 6.95 (m, 34H), 6.86 (d, *J* = 8.0 Hz, 1H), 6.58 – 6.37 (m, 7H), 3.99 – 3.73 (m, 12H), 1.70 (dddd, *J* = 26.5, 15.3, 10.9, 6.1 Hz, 6H), 1.49 – 1.28 (m, 15H), 1.19 – 1.03 (m, 5H), 1.01 – 0.60 (m, 13H)

^{13}C-NMR (50 MHz, $CDCl_3$), δ (ppm): 166.92, 157.09, 152.63, 152.46, 150.91, 150.54, 150.36, 143.87, 143.70, 141.67, 141.48, 140.96, 140.47, 138.15, 134.32, 134.02, 133.25, 132.97, 131.41, 131.28, 130.88, 130.20, 130.08, 129.69, 129.62, 129.47, 129.22, 129.05, 127.63, 127.48, 127.40, 127.11, 126.01, 123.18, 121.83, 115.25, 105.42, 100.61, 77.36, 68.46, 68.22, 52.09, 32.09, 31.74, 31.49, 29.86, 29.44, 29.13, 25.89, 25.79, 22.85, 22.74, 22.63, 22.55, 14.28, 14.17, 14.10, 14.01, 1.18.

HRMS (DCTB+PEGMeNa2000): m/z (%) found $C_{120}H_{109}N_7O_6S_1Zn_1$ 1841.7472 (100) [M]+; found 1840.7414 (100) .

UV-Vis: λmax(CH_2Cl_2)/nm= 449 (ε/dm^3 mol^{-1} cm^{-1}: 3961481), 484 (3611952), 700 (7181).

Desprotection to the final push-pull dyes

General Procedure

The porphyrine was dissolved in a mixture THF/MeOH 3:2 and a solution of NaOH (20 % w/w in water) was added. The solution was heated at 40°C for 2 hours upon which TLC (silica, DCM) indicated complete hydrolysis of the ester. The reaction mixture was diluted with Et_2O (100 mL) washed with water (100 mL), HCl (1M, 120 mL), water (100 mL), the organics dried (Na_2SO_4) and evaporated. The residue was loaded onto a short column (silica, DCM then 1:9 MeOH/DCM) to afford the final product as a green-brown solid.

Compound (67) TT-86

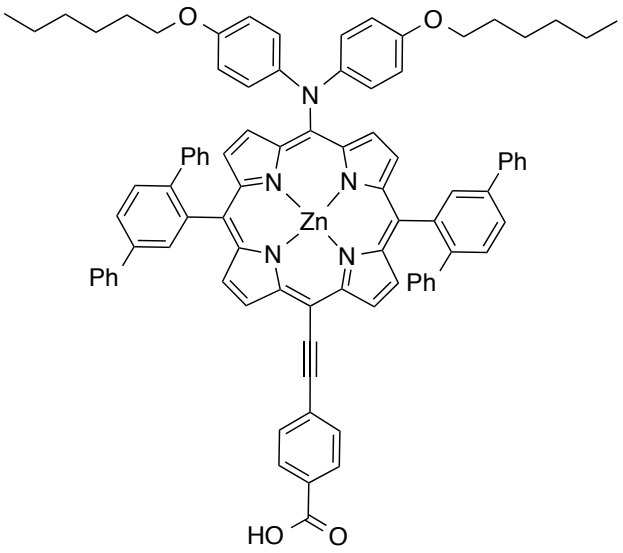

^{1}H-NMR (300 MHz, $CDCl_3$), δ (ppm): 9.57 – 9.51 (m, 2H), 9.13 (dd, *J* = 4.7, 3.5 Hz, 2H), 8.88 (dd, *J* = 11.6, 4.7 Hz, 3H), 8.73 (t, *J* = 5.0 Hz, 2H), 8.28 (d, *J* = 1.9 Hz, 2H), 8.21 – 8.12 (m, 3H), 8.09 – 7.98 (m, 5H), 7.87 – 7.74 (m, 8H), 7.74 – 7.65 (m, 3H), 7.50 – 7.27 (m, 19H), 7.21 – 6.98 (m, 13H), 6.79 – 6.66 (m, 4H), 6.60 – 6.54 (m, 4H), 6.41 (d, *J* = 7.1 Hz, 3H), 3.96 – 3.77 (m, 7H), 1.68 (dd, *J* = 14.2, 7.0 Hz, 7H), 1.36 – 1.13 (m, 17H), 0.93 – 0.70 (m, 13H).

HRMS (MALDI, DCTB + PPGNa 1000 + PPGNa 2000): m/z (%) found $C_{89}H_{73}N_5O_4Zn_1$ 1341.4962 (100) [M]+; found 1341.4923 (100) .

UV-Vis: λmax(CH_2Cl_2)/nm= 443 (ε/dm^3 mol^{-1} cm^{-1}: 5952299), 662 (7085)

Compound (68) TT-87

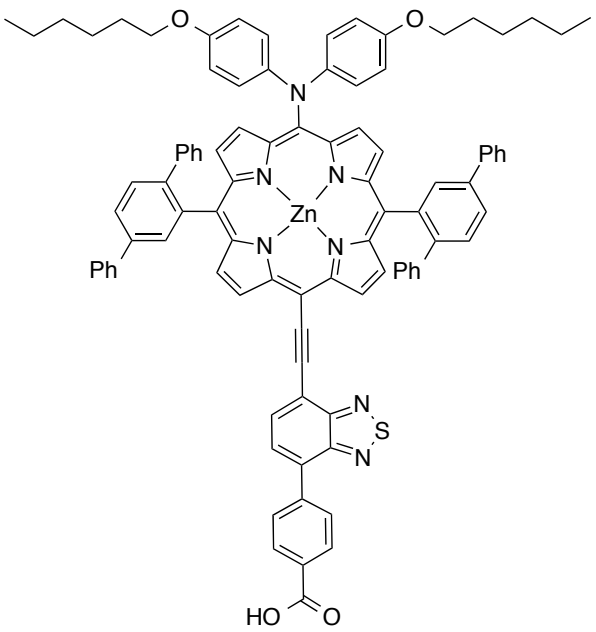

HRMS (MALDI, DCTB+PMMANa2100): m/z (%) found $C_{95}H_{75}N_7O_4SZn$ 1475.4901 (100) [M]+; found 1475.4904 (100) .

UV-Vis: λmax(CH_2Cl_2)/nm= 449 (ε/dm^3 mol^{-1} cm^{-1}: 3961481), 484 (3611952), 700 (7181).

Compound (69) TT-88

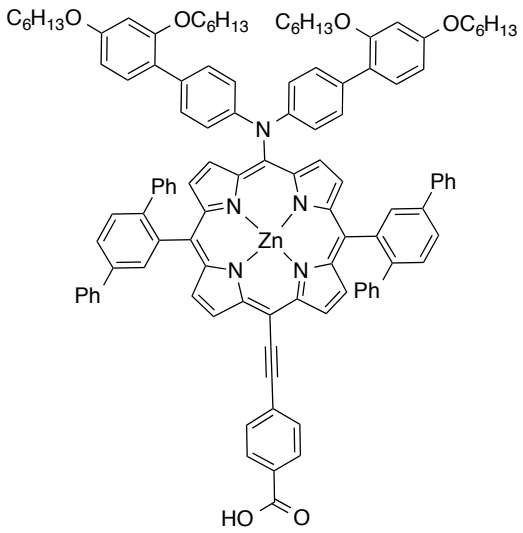

^{1}H-NMR (300 MHz, $CDCl_3$)), δ (ppm): 9.57 (dd, *J* = 6.6, 4.6 Hz, 1H), 9.24 (dd, *J* = 4.7, 3.4 Hz, 1H), 8.90 (t, *J* = 5.0 Hz, 1H), 8.79 (dd, *J* = 4.6, 2.4 Hz, 1H), 8.34 – 8.25 (m, 1H), 8.14 – 7.93 (m, 4H), 7.93 – 7.75 (m, 5H), 7.75 – 7.66 (m, 2H), 7.54 (ddt, *J* = 9.1, 5.4, 2.5 Hz, 4H), 7.46 – 7.27 (m, 10H), 7.25 – 7.00 (m, 6H), 6.92 – 6.73 (m, 2H), 6.58 – 6.39 (m, 5H), 4.08 – 3.72 (m, 9H), 1.70 (dddd, *J* = 26.5, 15.3, 10.9, 6.1 Hz, 4H), 1.48 – 1.30 (m, 8H), 1.18 (ddd, *J* = 23.1, 7.3, 3.5 Hz, 6H), 0.99 – 0.70 (m, 8H).

HRMS (MALDI, DCTB+PMMANa1000): m/z (%) found $C_{114}H_{107}N_5O_6Zn_1$ 1707.7533 (100) [M]+; found 1707.7512 (100) .

UV-Vis: λmax(CH_2Cl_2)/nm= 452 (ε/dm^3 mol^{-1} cm^{-1}: 1259806), 484 (66495).

Compound (70) TT-89

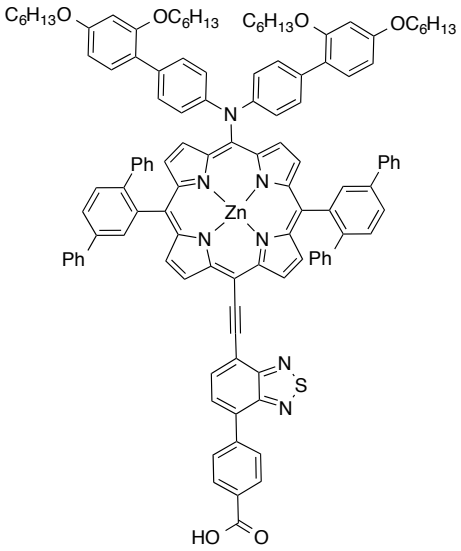

^{1}H-NMR (300 MHz, $CDCl_3$), δ (ppm) 9.57 (dd, *J* = 6.6, 4.6 Hz, 1H), 8.90 (t, *J* = 5.0 Hz, 1H), 8.36 – 8.24 (m, 1H), 8.19 – 7.97 (m, 5H), 7.97 – 7.78 (m, 5H), 7.78 – 7.64 (m, 4H), 7.61 – 6.95 (m, 34H), 6.86 (d, *J* = 8.0 Hz, 1H), 6.58 – 6.37 (m, 7H), 3.99 – 3.73 (m, 8H), 1.70 (dddd, *J* = 26.5, 15.3, 10.9, 6.1 Hz, 6H), 1.49 – 1.28 (m, 15H), 1.19 – 1.03 (m, 5H), 1.01 – 0.60 (m, 13H)

HRMS (DCTB + PPGNa 2000**): m/z (%) found** $C_{119}H_{107}N_7O_6SZn$ 1827.7315 (100) [M]+; found 1827.7242 (100) .

UV-Vis: λmax(CH_2Cl_2)/nm= 452 (ε/dm^3 mol^{-1} cm^{-1}: 1259806), 484 (66495).

CHAPTER 4: ANNEX

4.1 BULK HETEROJUNCTION DEVICES (BHJ)

4.1.1 Introduction.

The seminal work by Tang about PHJ,103 paved the way for the development of other donor/acceptor type architectures, including the solution processed BHJ typearchitecture with increased donor/acceptor interfacial areas (Figure 4.1). These BHJ devices present a unique blended film of a donor and an acceptor as active layer, this feature overcoming the diffusion problem. The great advantage in comparison to PHJ is that, upon controlling the morphology of the active layer into an interpenetrating, bicontinuous network of the donor and the acceptor, one can achieve, first, high interfacial area within the BHJ active layer for efficient exciton dissociation and, second efficient collection of charges. The BHJ architecture relies on finding a balance between charge generation and transport, and can be limited by charge carrier lifetimes. All these factors are significantly affected by the morphology of the layer at the nanoscale, which is probably the major challenge in BHJ devices.

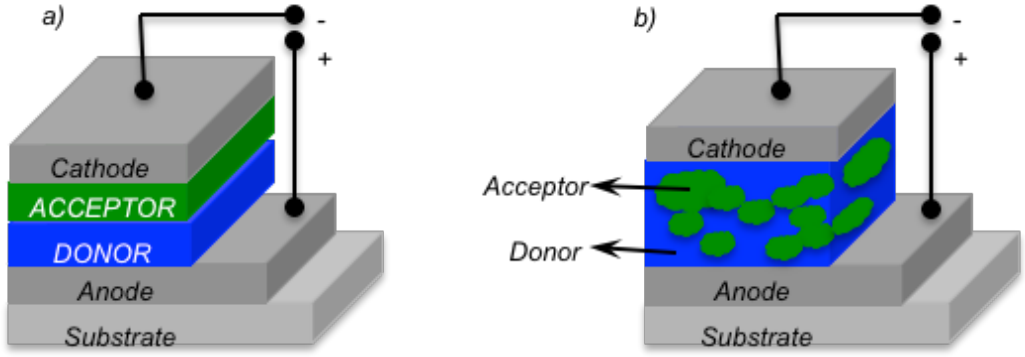

Figure 4.1. Comparative, schematic representations of a) a planar and b) bulk heterojunctiodevices.

Several techniques and a variety of materials have been used to sort out these morphological problems, like changing the fullerene derivative for other acceptor molecule or polymer as aforementioned. An alternative approach includes active layer made of polymers. many reports exemplify efforts to increase the lightharvesting properties of the p-type donor phase in a bulk heterojunction solar cell by incorporating

strongly light-absorbing chromophores into the backbone of the conjugated polymer phase. The first example of the synthesis and polymer solar cell applications of conjugated polymers with porphyrins as a unit of the main chain was reported by Bo et al. in 2008, [275] employing conjugated alternating porphyrin-dithienothiophene copolymers (both units are electron-rich) as active materials obtained (efficiencies were lower than 0.4%) promoted the incorporation of electronacceptor units, i.e. benzothiadiazole, to have novel low bandgap conjugated copolymers.

Obviously, phthalocyanines are a good alternative to porphyrins, since they can increase the absorption in the red/near infrared region of the solar spectrum owing to their high extinction coefficients; however, the studies about Phthalocianines(Pc)-containing polymers to be employed in BHJ solar cells are only a few and the tendency is the incorporation of Pc macrocycles as pendant groups. Torres et al . have studied n- and p-type conjugated PPV oligomers, bearing pendant Zn(II)Pcs linked through an oxygen atom and different linkers, with potential applications in organic solar cells.[276] Later, the p-type oligomers have been employed together with SWCNTs, where the Zn(II)Pc wraps around the nanotube,[277] and graphene.[278,279]

4.1.2 Objectives : Phthalocyanines as monomers for copolymerization

A interesting approach is to incorporate Pcs into the main chain of conjugated, polymeric structures. To this end, tert-butylated Zn(II)Pcs substituted in two β-positions of the same isoindole with Br derivative groups, will be synthesized for further coupling with appropriate monomers (Figure 4.4).

Another objective is to move the reactive position towards the exterior of the the Pc macrocycle aiming at facilitating the polymerization process. Then, copolymerization with will be performed in collaboration with Prof. McCulloch at Imperial College.

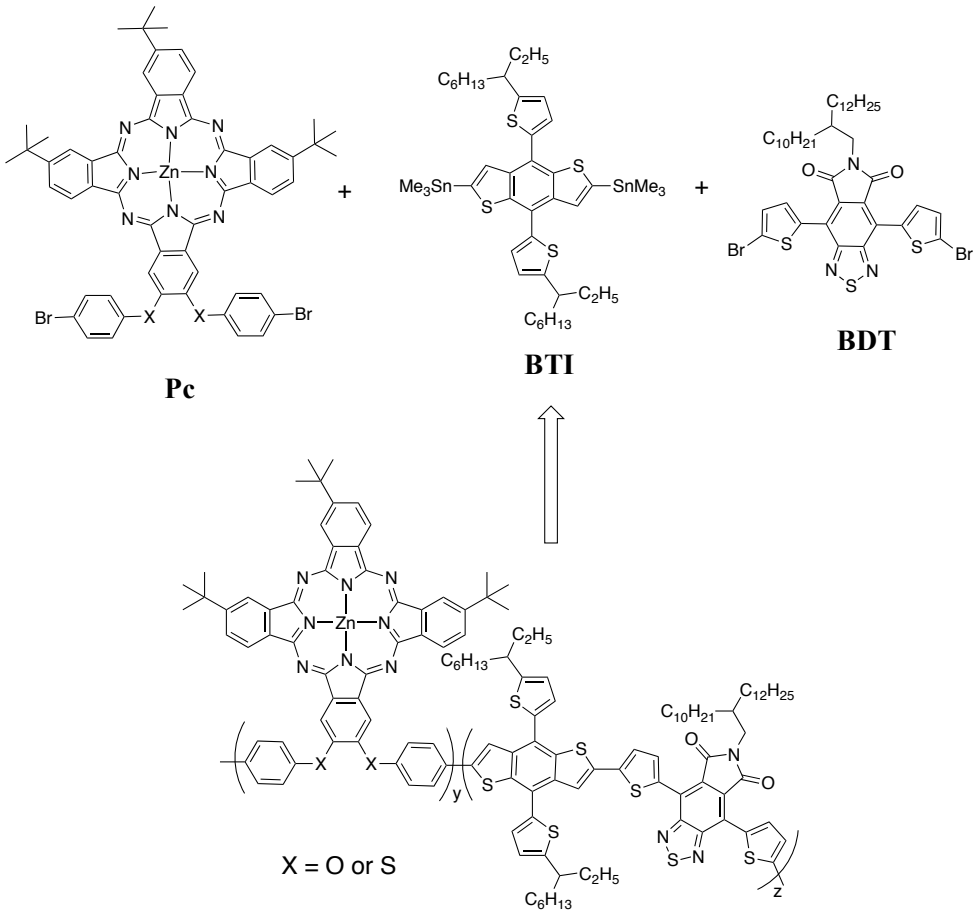

Figure 4.2. Structure of phthalocyanines with 2 β-positions occupied by good Br derivative groups. Asshown the retrosynthesis, 2 different phthalocyanines are proposed.

4.1.2 Results and discussion

The preparation of Pc holding bromo deritative groups at the periphery for the polimer architecture. The synthesis started with the preparation of 4,5-dichlorophthalonitrile (**71**)[280] in four steps (Scheme 10). The quantitative dehydration of 4,5-dichlorophthalic acid yielded the cyclic anhydride **72**, which was reacted with formamide, followed by the treatment with ammonium hydroxide to give phthalamide **73**. The latter compound was dehydrated with thionyl chloride to afford 4,5-dichlorophthalonitrile (**74**) in 87% yield. Then, the dicyano compounds **75** or **76** , bearing 4-bromophenol moieties or 4-bromobenzenethiol moieties, was obtained in good yields by reaction of **7** with the bromo derivative.

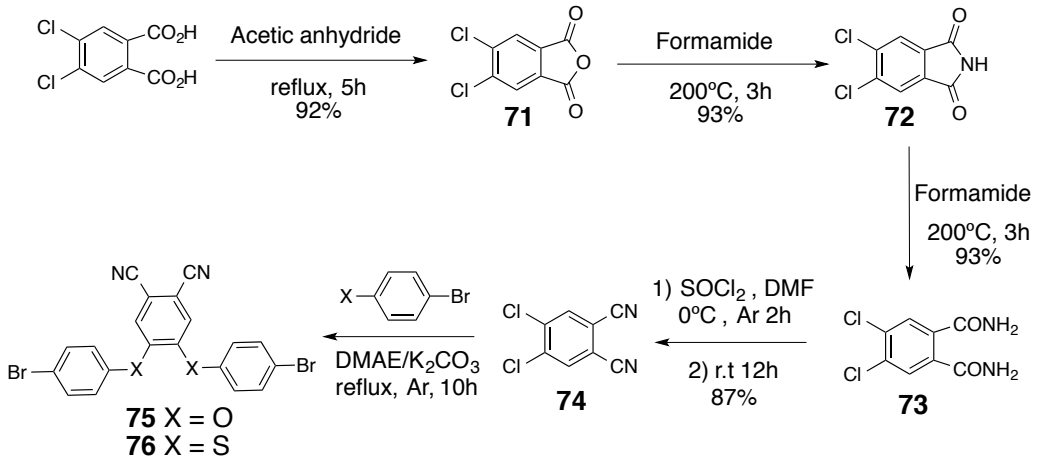

Scheme 4.1. Synthesis of phthalonitriles: **75** and **76**

The similar synthesis of bromo Pc derivatives by cyclic tetramerization of the corresponding phthalonitriles or diiminoisoindoles precursors had been previously reported wiht solvents for the condensation reaction with high-boiling solvents like DMAE, was used in this case. Therefore, this procedure has been employed in the synthesis of the unsymmetrically substituted Zn(II)Pcs **77** and **78** (Scheme 5.3), bearing three terbutil groups and one dibromophenil moiety that will be further converted into the conexión wiht the polimer. Thus, the condensation reaction of a 1:3 molar ratio of phthalonitriles **75** or **76** and 4-(*tert*-butyl)phthalonitrile was carried out in the presence of $Zn(OAc)_2$. The statistical mixture of Pcs was purified by column chromatography, leading to the isolation of the symmetrically substituted as the major component (A_4), followed by a small amount of the desired compound Pc **77** or **78** (A_3B). However, the chromatographic purification was specially arduous in this case due to the very similar polarities of the two Pcs.

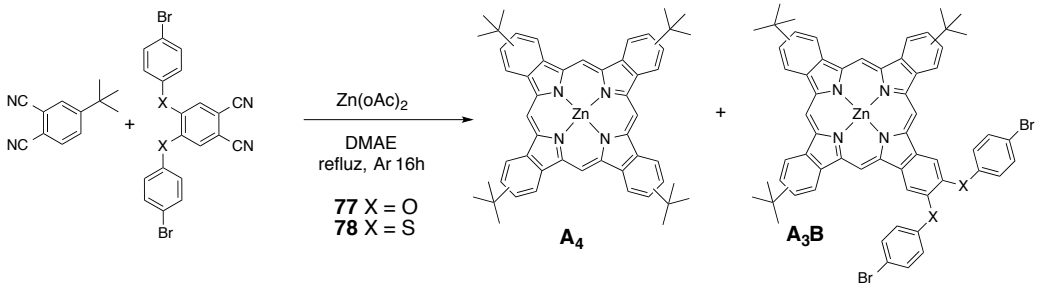

Scheme 4.2. Routes for the synthesis of Zn(II)Pc **77** and **78**

Main-chain Pc-copolymers: Testing copolymerization conditions

Another plausible route towards the preparation of conjugated polymers containing Pc units for BHJ devices is the incorporation of the macrocycle into the main chain of the polymer.

For that reason our final objective is the preparation of a copolymer incorporating Pcs and other electroactive units such as, for instance, BDT and BTI, which have been succesfullyincorporated in low-band gap polymers and in small-molecule structures for BHJ(Scheme 25).[281] Following this strategy the Pc units will be incorporated into the main chain, but connected through one bromo benzene unit with one heteroatom (O or S).

The copolymerization of Pc monomers with BTI and BDT (or other analogous) species will be performed by the group of Iain McCulloch at Imperial College in the framework of EU-funded network, since they have a demonstrated expertise in the polymerization of different units by metal-catalyzed coupling reactions to obtain low bandgap polymers. We have provided them with Pc´s **78** and **79** to perform copolymerizations with BTI/BDT organometallic and halogenated derivatives in different conditions and ratio of the comonomers

However, we performed in our laboratories an optimization of the coupling condition with simple organometallic thiophenes in order to find the optimal conditions to be applied in the polymerization reactions (Scheme 4.3). Among the immense variety of Suzuki conditions, the ones depicted in Scheme 4.3 and Table 4.1 were selected because they worked successfully with Pcs in other related coupling reactions. The use of $Pd(PPh_3)_4$ in DME resulted in a clean transformation, providing the dithiophene derivative in 47% isolated yield (Scheme 4.3 and Table 4.1, entry 1), whereas the use of DMF as solvent (Table 4.1, entry 2) was found to be less effective, because the starting Zn(II)Pc was not completely consumed after 24h. Interestingly, $Pd_2(dba)_3$ (Table 4.1, entry 3) resulted to be totally ineffective, affording just starting material. In an attempt to improve the yield of this cross-coupling reaction, a higher reactive form of thiophene derivative, 2-(tributylstannyl)thiophene. The Stille conditions used (Scheme 4.3) gave Pc wiht thiophenes in a better, yield (74%).

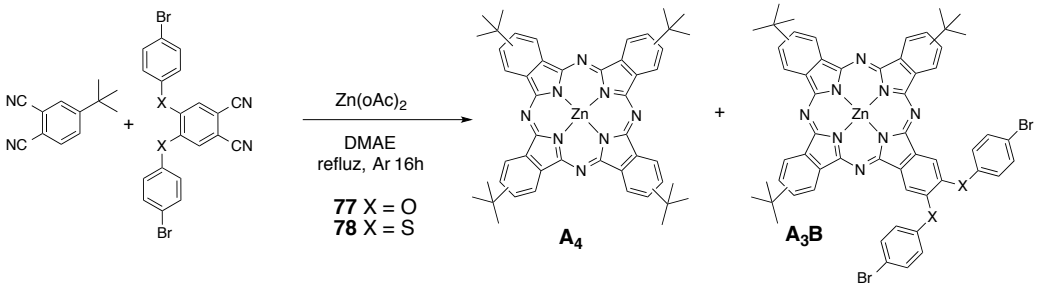

Scheme 4.3. Test of two possible palladium-catalyzed reactions

Table 4.1. Different conditions for the Suzuki reaction Zn(II)Pc 21 and thiophene-2-boronic acid pinacol ester.

Entry	Pd source	Base	Solvent	Others
1	$Pd(Ph_3)_4$	Na_2CO_3	DME	
2	$Pd(Ph_3)_4$	Na_2CO_3	DMF	
3	$Pd_2(dba)_3$	K_3PO_4	Toluene	S-Phos

Incorporation of Pc 78 (UAM 13) into Semiconducting Polymers

Three polymers synthesised with 0%, 5% and 10% incorporation of Pc (**78**)

Table 4.2. Polymers synthesised

Entry	Phthalocianine	BTI	BDT
1 (CN330)	0%	50%	50%
2 (CN332)	5%	45%	50%
3 (CN331)	10%	40%	50%

UV-vis of the crude reaction mixtures indicate that much of the Pc is not incorporated into the polymer but around 680nm it show the absoriton of the phthalocainine. From the UV-vis of the purified polymers (Figure 4.3 righ), it is evident that Phthalocianine is indeed incorporated into the polymer chain, but the actual ratio is lower than the feed ratio.

•

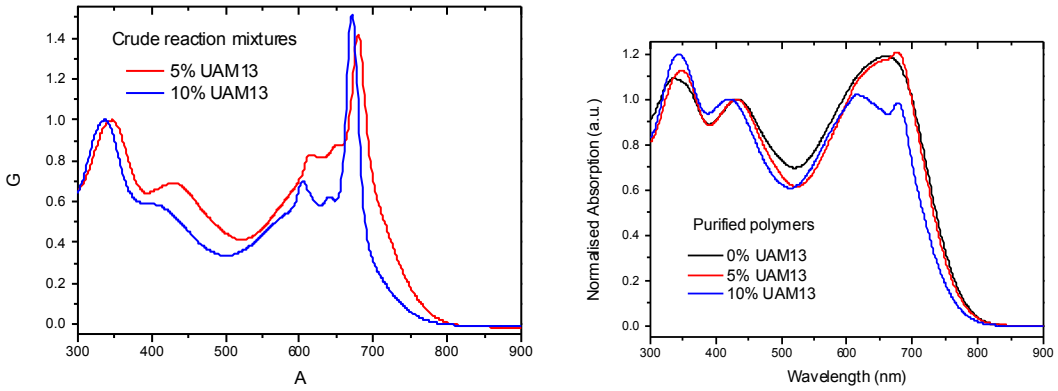

Figure 4.3. UV-vis of the crude reaction (on the left) and UV-vis of the purified polymers (on the right)

4.1.4 Summary and Conclusions

Table 4.3. Polymers synthesised with **UAM13**

Entry	Phthalocianine	Mw	Mn	PDI
1 (CN330)	0%	115k	49k	3.06
2 (CN332)	5%	64k	23k	2.80
3 (CN331)	10%	26k	12k	2.16

Thre polymers were synthesise with different grade of incorporate of Pc into the chain of the polymer. As expected, polymer molecular weight decreases with increasing amount of **UAM13** and tht conjugation of the polymer was breaker.

4.1.5 Experimenatal section

4.1.5.1 Synthesis of pthalonitriles

Compound 71

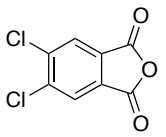

A solution of 4,5-dichlorophthalic acid (65.0 mmol, 15.3 g) in acetic anhydride (25.0 mL) was heated to reflux. After 5h, the suspended solid was filtered and washed with hexane. The grey solid obtained was stirred in hexane over 12h, obtaining a solid that was filtered and thoroughly washed with the same solvent (100 mL). In this way, 13.0 g of anhydride **72** (60.2 mmol) were obtained. Yield: 92%.

Mp: 181-183 ºC (reported:242 184-186 ºC).

^{1}H-NMR (300 MHz, $CDCl_3$), δ (ppm) 8.12 (s, 2H; H-3, H-6).

^{13}C-NMR (50 MHz, $CDCl_3$), δ (ppm): 160.6 (CO), 141.7 (C-4, C-5), 130.0 (C-1, C-2), 127.3 (C-3, C-6).

Compound 72

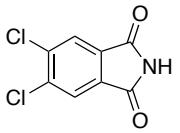

A mixture of 4,5-dichlorophthalic anhydride (**72**) (60.2 mmol, 13.0 g) and formamide (19.0 mL) was heated to 200 ºC over 3h. After cooling to room temperature, the solid obtained was filtered, washed with water (40 mL) and vacuum-dried, yielding 12.0 g of 4,5-dichlorophthalamide (**73**) (55.5 mmol) as a white solid. Yield: 93%.

Mp: 193-195 ºC (reported:242 193-195 ºC).

^{1}H-NMR (300 MHz, $CDCl_3$), δ (ppm) 8.12 (s, 2H; H-3, H-6).

^{13}C-NMR (50 MHz, $CDCl_3$), δ (ppm): 160.6 (CONH), 141.7 (C-4, C-5), 130.0 (C-1, C-2), 127.3 (C-3, C-6).

Compound 73

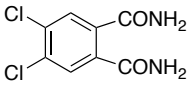

A suspension of 4,5-dichlorophthalimide (**73**) (55.5 mmol, 12.0 g) in 25% aqueous ammonia (168 mL) was stirred at room temperatura for 24h. At that time, a 33% ammonium hydroxide solution (56.0 mL) was added and the mixture was further stirred for 24h. The white solid obtained was filtered, washed with water (50 mL) and vacuum-dried. In so doing, 11.4 g of 4,5-dichlorophthalamide (**74**) (48.9 mmol) were isolated as a white solid. Yield: 88%.

Mp: 240-242 ºC (reported:242 245-247 ºC).

^{1}H-NMR (300 MHz, $CDCl_3$), δ (ppm) 7.95 (br s, 2H; NH_2), 7.72 (s, 2H; H-3, H-6),7.45 (br s, 2H; NH_2).

^{13}C-NMR (50 MHz, $CDCl_3$), δ (ppm): 169.6 ($CONH_2$), 136.6 (C-4, C-5), 131.9 (C-1, C-2), 129.2 (C-3, C-6).

Compound 74

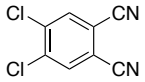

Thionyl chloride (41.0 mL) was cautiously poured over dry DMF (58.0 mL) at 0 ºC under argon atmosphere. The mixture was vigorouslystirred at that temperature for 2h and then 4,5-dichlorophthalamide (**74**) **(**48.9 mmol, 11.4 g,) was added. After stirring at room temperature for 12h, the reaction mixture was poured onto crushed ice (100 mL), resulting in the precipitation of a slightly grey solid which was filtered and washed with water (20 mL). Upon recrystallization from methanol, 8.4 g (42.5 mmol) of compound **75** were obtained. Yield: 87%.

Mp: 180-183 ºC (reported:242 182-184 ºC).

^{1}H-NMR (300 MHz, $CDCl_3$), δ (ppm) 7.94 (s, 2H; H-3, H-6).

^{13}C-NMR (50 MHz, $CDCl_3$), δ (ppm): 138.2 (C-4, C-5), 135.7 (C-3, C-6), 115.0, 114.6, 114.0 (C-1, C-2, CN).

MS (EI): m/z = 196 [M]+ (100%)

Compound 75 and Compound 76

General procedure:

A solution of 4,5-dichlorophthalonitrile (**75**) (1.0 eq) in freshly distilled DMAC (5.0 mL) was heated to 100 ºC, and oven-dry K_2CO_3 (9 eq), was added in five portions over 30 min. Then, 2-ethylhexane-1-thiol (2.4 eq, 3.1 mmol, 0.53 mL) was added, and the resulting mixture was stirred at 100 ºC for 10h. It was then allowed to reach room temperature, poured in water (15 mL) and extracted with DCM (3x15 mL). Combined organic layers were dried over $MgSO_4$ and evaporated

Compound 75

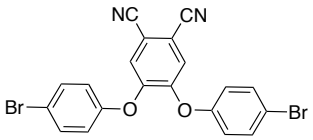

The residue was purified by column chromatography (SiO_2 , hexane/DCM, 1:1) to give **76** (1.01 mmol, 0.42 g) as a white solid. Yield: 80%.

^{1}H-NMR (300 MHz, $CDCl_3$), δ (ppm) 7.64 – 7.51 (m, 4H), 7.22 (s, 2H), 6.94 (d, *J* = 8.8 Hz, 4H).

^{13}C-NMR (50 MHz, $CDCl_3$), δ (ppm): 111.02, 113.34, 115.85, 116.70, 120.02, 133.25, 156.04, 147,00.

Compound 77

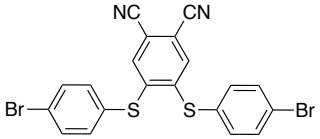

The residue was purified by column chromatography (SiO_2 , hexane/DCM, 1:1) to give **77** (1.01 mmol, 0.42 g) as a white solid. Yield: 80%.

^{1}H-NMR (300 MHz, $CDCl_3$), δ (ppm) 7.64 – 7.51 (m, 4H), 7.22 (s, 2H), 6.94 (d, *J* = 8.8 Hz, 4H).

^{13}C-NMR (50 MHz, $CDCl_3$), δ (ppm): 111.4, 115.8, 126.84, 127.49, 128.39, 132.69, 136.60, 137.33.

4.1.4.2 Synthesis of phthalocyanines : Compound 77 (UAM13) and Compound 78 (UAM14)

General procedure: 4-tert-butylphthalonitrile (3.0 eq, 3.84 mmol, 709 mg), phthalonitrile (1.0 eq, 1.28 mmol, 300 mg) and Zn(OAc)2 (1.3 eq, 1.66 mmol, 305 mg) in DMAE (5.0 mL) were heated to reflux under an argon atmosphere for 16h. After cooling to room temperature, the reaction mixture was treated with MeOH/Water (3:1, 200 mL), and the solid obtained was filtered, washed with MeOH (75 mL) and vacuum dried. The resulting blue solid was purified by column chromatography on silica gel using hexane/dioxane (2:1) as the carrier phase. The symmetrically tert-butyl substituted phthalocyanine was eluted first, and obtained as a blue solid. It was followed by the unsymmetrical derivatives **78** and **79**, as a green solid. (Yield: 15%).

Compound 77 (UAM 13)

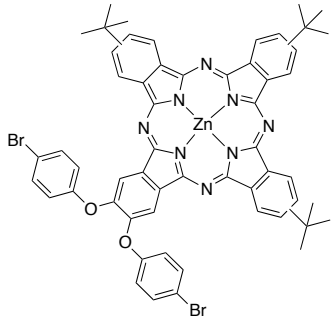

^{1}H-NMR (300 MHz, $CDCl_3$), δ (ppm): 9.66 – 9.08 (m, 7H), 9.08 – 8.67 (m, 3H), 8.55 – 8.13 (m, 4H), 7.78 – 7.58 (m, 4H), 7.41 – 7.16 (m, 4H), 2.18 – 1.78 (m, 35H).

HRMS (DCTB + PEGNa 1000): m/z (%) found $C_{56}H_{46}Br_2N_8O_2Zn_1$ 1088.1366 (100) [M]+; found 1088.1365 (100) .

UV-Vis: λmax(CH_2Cl_2)/nm= 672 (ε/dm^3 mol^{-1} cm^{-1}: 83909)

Compound 78 (UAM 14)

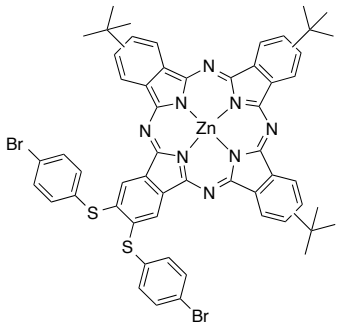

^{1}H-NMR (300 MHz, $CDCl_3$), δ (ppm): 9.66 – 9.08 (m, 7H), 9.08 – 8.67 (m, 3H), 8.55 – 8.13 (m, 4H), 7.78 – 7.58 (m, 4H), 7.41 – 7.16 (m, 4H), 2.18 – 1.78 (m, 35H).

HRMS (DCTB): m/z (%) found $C_{56}H_{46}Br_2N_8S_2Zn_1$ 1120.1 (100) [M]+; found 1120.1 (100) .

UV-Vis: λmax(CH_2Cl_2)/nm= 624 (ε/dm^3 mol^{-1} cm^{-1}: 24908), 675 (109998), 691 (151393)

4.2 SYNTHESIS OF PHTHALOCYANINES CONNECTED VIA A NITROGEN ATOM TO AN AMINO PHENYL GROUPS

Pc-based multi-macrocyclic assemblies, featuring different types of linkers (in terms of chemical composition and geometry) have been reported to study the electronic interactions between chromophores and their unique properties[282]. In the literature reported the use of a wide variety of Pd-catalyzed coupling reactions (Sonogashira, Suzuki, Heck) using Pc-halide monomers [283].

Incorporating an amino in the Pc structure strongly affects its properties. Pcs have also been functionalized with amine groups to permit covalent conjugation[284]. Pd-catalyzed C–N cross-coupling reactions are an important technology both in industrial and academic research. The use of Pd-catalyst has also emerged as a versatile and efficient synthetic technique for carbon–nitrogen bond formation through the crosscoupling reaction of aryl halides with amines (Buchwald– Hartwig amination) [13]. This method has been used for the synthesis of amino porphyrin derivatives. As compared to the Sonogashira and Suzuki coupling reactions, studies on the Buchwald–Hartwig[285] reaction involving Pcs are limited. Only a few studies have been reported including the synthesis of functionalized trisulfonated Pcs[286], **N** -linked Porphyrin–Pc dyads[287] and triades of Pcs.

4.1.2 Objectives : Buchwald–Hartwig amination in Phthalocyanines

Methods for the preparation of a variety of covalently linked Pc– N -aryl will be developed. The palladium catalyzed intermolecular carbon–nitrogen coupling reaction (Buchwald–Hartwig) between differents Pc-iodo (neutral = tertbutil grups in the peripheria; dador = terbutylphenoxy groups and acceptor = sulfonyl groups) and secundary amino derivatives was used for these studies. (Figure 4.4)

With this general procedure for the Pd-catalyzed intermolecular C–N bond formation involves coupling of an iodo-Pc with amines to afford the desired unsymmetrical substituted Pc excellent yield This approach was used for the synthesis of a series of ZnPc derivatives. In the direct linked molecules, the two Pc rings are

attached directly through an **N** –atom at different same of the Pc-phenyl ring. The desired new Pc–Ar dimers were prepared as shown in Figure 4.4

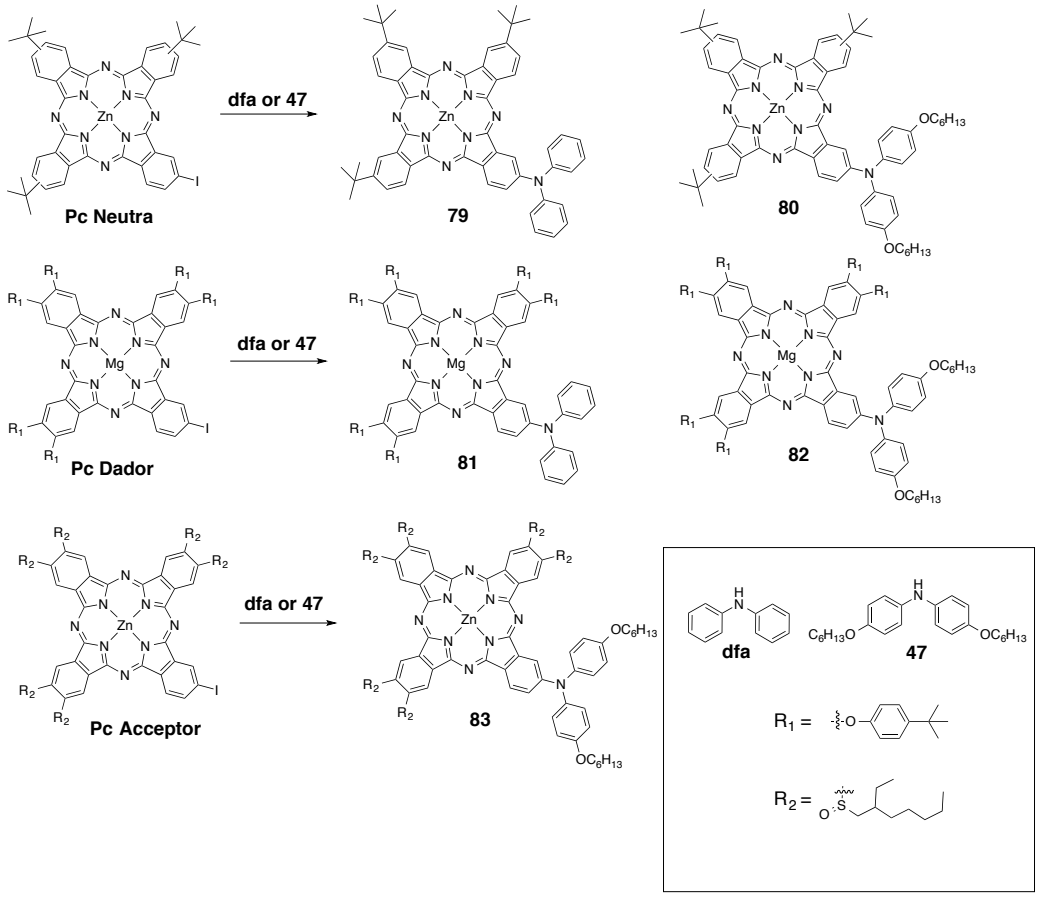

Figure 4.4. Structure of phthalocyanines with, Pc– N -aryl were developed. 2 different amines are proposed (**dfa** and **47**).

4.1.3 Results and discussion

We used a method involving meta mono-iodo ZnPc whit three diffrent types of sustytuyents (**Neutro, Dador and Acceptor**)[288,289] and the corresponding di-amino (**dfa or 47**) see Figure 4.4. Pc was coupled with Amin in toluene under argon at 90 ºC for 30min using tris(dibenylidene-acetone) dipalladium (Pd_2dba_3) as catalyst, tri-t-butylphosphine as a ligand and sodium t -butoxide as base.

After silica gel column chromatography, products were isolated in 80% yield of desired products (**79, 80, 81, 82 and 83** see: Figure 4.4) along with any amount of

reduced Pc. The assigned structures were confirmed by spectral analysis: MS, MALDI-TOF, and characteristic UV-vis absorption Q-band máxima.

Spectral properties

The optical properties of the Pc-Amin chromophores in DCM differ from those of the corresponding starting materials (Figure 4.4). The UV-vis spectra gave the characteristic B-band at about 350 nm and a more intense Q-band. (Figure 4.2)

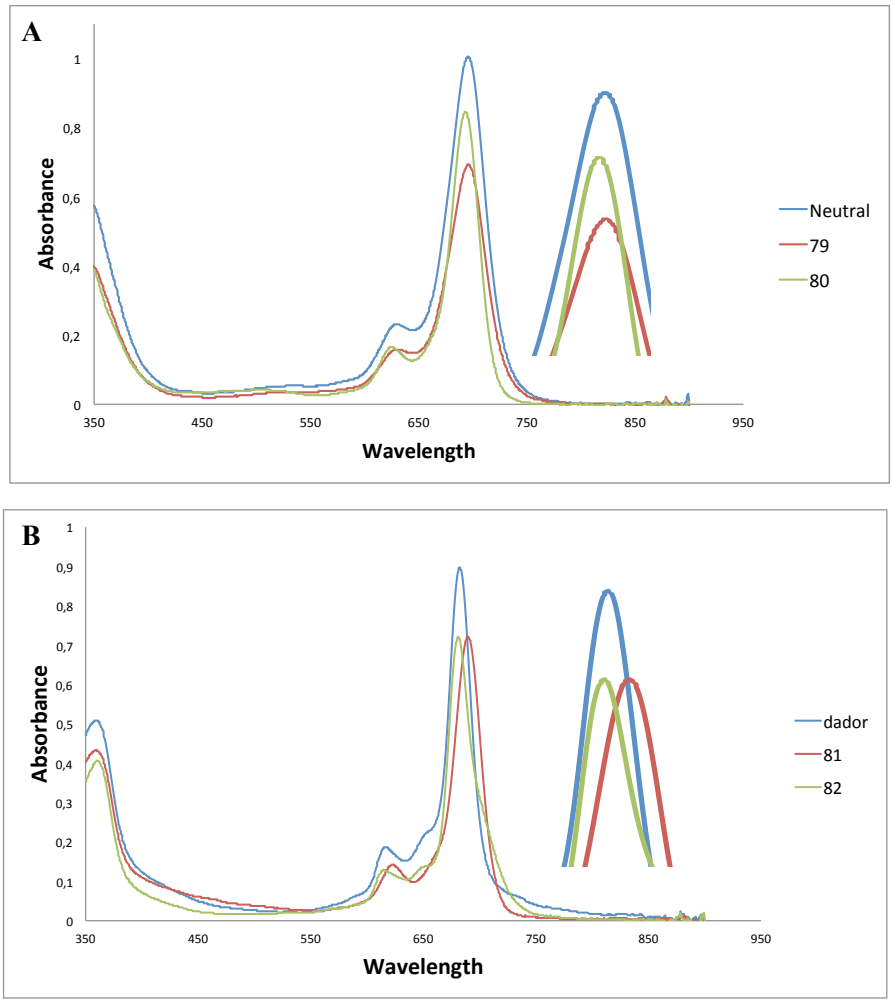

Figure 4.2. Electronic spectra of Pc–N(Ar) derivatives (DCM) **A**) N(Ar) = **dfa** and **B**) N(Ar) = **47**

Iodo Pc **Neutro** and **Dador** gave sharp Q-bands at λ_{max} 693 and 683 nm, respectively. In all cases the new Pc-NAr gave split Q-bands, featuring a bathochromic shift with respect to the corresponding whitout nitrogen bound. (Figure 4.3)

Figure 4.3. Resultos of electronic spectra of Pc–N(Ar) derivatives (DCM)

Pc	Amin	λ(Pc)	λ(Pc-Amin)
Neutral	**dfa**	693	**699**
Neutral	46	693	696
Dador	**dfa**	683	**689**
Dador	46	683	684

4.1.4 Summary and Conclusions

With this novel general procedure for the Pd-catalyzed intermolecular C–N bond formation involves coupling of different iodo-Pc with amines to afford the desired unsymmetrical substituted Pc excellent yield This approach was used for the synthesis of a series of ZnPc derivatives with any amount of reduced Pc.

On the other hand, this conditions was tested whit a label metal like Mg to probe it, giving favorable results.

4.1.5 Experimenatal section

General Procedure:

To a 10ml Schlenck flasck containing iodo-phthalocyanine (1eqv), Amin (1.5eqv), $Pd_2(dba)_3$ (0.01eqv), tri-t-butylphosphine (0.03eqv), sodium t-butoxide (2.5eqv) and anhydrous toluene (2 ml) were added under argón atmosfere. The suspensión was refluxed for 30min. The mixture was filtered under celite and concentrated under reduced pressure. The crude product was purified by silica gel column chromatography eluted with Hexane/Dioxane (4:1) to give a disered product.

Compound 79

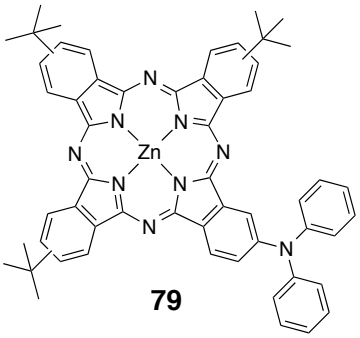

79

^{1}H-NMR (300 MHz, $CDCl_3$), δ (ppm): 9.58 – 9.48 (m, 1H), 9.44 – 9.29 (m, 1H), 8.27 (t, *J* = 8.9 Hz, 1H), 7.45 – 7.29 (m, 2H), 7.04 (dq, *J* = 11.4, 5.2, 4.0 Hz, 5H), 1.03 – 0.75 (m, 27H).

HRMS (DCTB): m/z (%) found $C_{56}H_{49}N_9Zn_1$ 911.3 (100) [M]+; found 911.4 (100) .

UV-Vis: λmax(CH_2Cl_2)/nm= 699 (ε/dm^3 mol^{-1} cm^{-1}: 70257,02814).

Compound 80

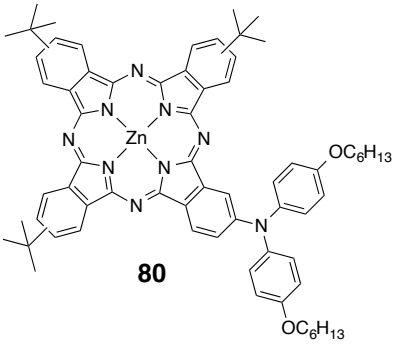

80

^{1}H-NMR (300 MHz, $CDCl_3$), δ (ppm): 9.56 – 9.43 (m, 4H), 9.41 – 9.31 (m, 4H), 9.31 – 8.99 (m, 6H), 8.35 – 8.15 (m, 6H), 7.91 – 7.65 (m, 5H), 7.46 (td, *J* = 6.7, 6.0, 2.8 Hz, 15H), 7.40 – 7.18 (m, 7H), 7.18 – 7.03 (m, 3H), 1.33 – 1.02 (m, 17H), 0.98 – 0.78 (m, 7H).

HRMS (DCTB): m/z (%) found $C_{68}H_{73}N_9O_2Zn_1$ 1111.5 (100) [M]+; found 1111.6 (100) .

UV-Vis: λmax(CH_2Cl_2)/nm= 696 (ε/dm^3 mol^{-1} cm^{-1}: 147579).

Compound 81

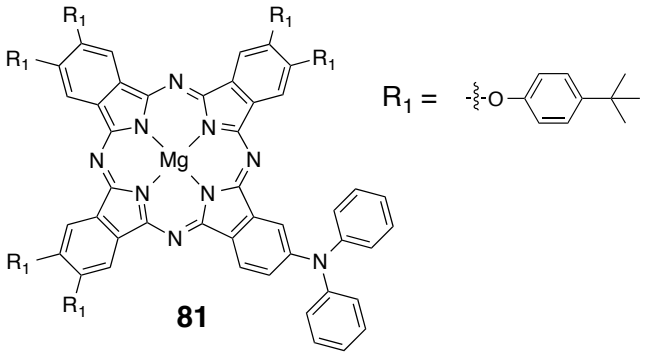

81

^{1}H-NMR (300 MHz, $CDCl_3$)), δ (ppm): 7.23 – 7.15 (m, 19H), 7.15 – 6.98 (m, 35H), 6.78 (tt, *J* = 7.2, 1.2 Hz, 13H), 1.57 (dd, *J* = 13.7, 3.2 Hz, 14H), 1.52 – 1.33 (m, 32H), 1.33 – 1.28 (m, 22H), 1.28 – 1.06 (m, 29H), 0.97 – 0.77 (m, 22H).

HRMS (DCTB + PEGNa 1500): m/z (%) found $C_{104}H_{97}Mg_1N_9O_6$ 1592.7436 (100) [M]+; found 1592.7430 (100) .

UV-Vis: λmax(CH_2Cl_2)/nm= 689 (ε/dm^3 mol^{-1} cm^{-1}: 26822).

Compound 82

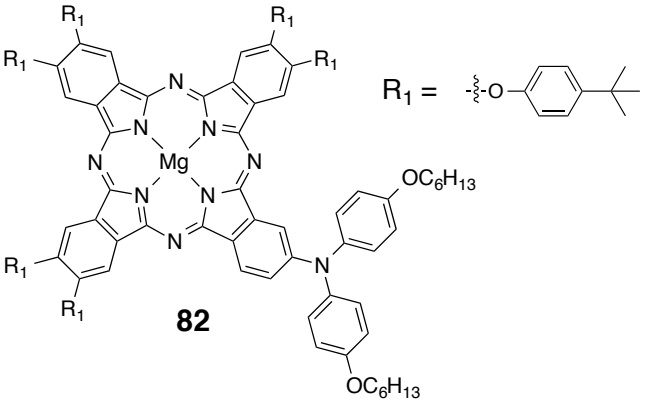

82

^{1}H-NMR (300 MHz, $CDCl_3$), δ (ppm): 9.58 – 9.48 (m, 1H), 9.44 – 9.29 (m, 1H), 8.27 (t, *J* = 8.9 Hz, 1H), 7.45 – 7.29 (m, 2H), 7.04 (dq, *J* = 11.4, 5.2, 4.0 Hz, 5H), 1.03 – 0.75 (m, 27H).

HRMS (DCTB): m/z (%) found $C_{116}H_{121}Mg_1N_9O_8$ 1792.9213 (100) [M]+; found 1792.9301 (100) .

UV-Vis: λmax(CH_2Cl_2)/nm= 684 (ε/dm^3 mol^{-1} cm^{-1}: 119620).

Compound 83

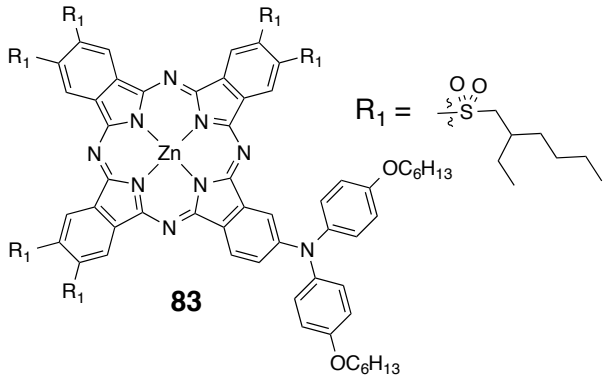

HRMS (DCTB): m/z (%) found $C_{68}H_{73}N_9O_2Zn_1$ 1111.5 (100) [M]+; found 1111.6 (100) .

UV-Vis: λmax(CH_2Cl_2)/nm= 696 (ε/dm^3 mol^{-1} cm^{-1}: 147579).

REFERENCES

[1] a) R. F. Service, *Science* **2005**, *309*, 548; b) J. Potocnik, *Science* **2007**, *315*, 810.

[2] Q. Schiermeier, J. Tollefson, T. Scully, A. Witze, O. Morton, *Nature* **2008**, *454*, 816.

[3] C. Richter, D. Lincot, C. Gueymard (eds.), *Solar Energy*, Springer, New York, **2013**.

[4] B. Norton, *Harnessing Solar Heat*, Lecture in Energy 18, Springer, Dordrecht, **2014**.

[5] M. A. Green, *Philos. Trans. R. Soc. A* **2013**, *371*, 20110413.

[6] T. Saga, *NPG Asia Mater*. **2010**, *2*, 96.

[7] a) A. W. Hains, Z. Liang, M. A. Woodhouse, B. A. Gregg, *Chem. Rev*. **2010**, *110*, 6689; b) J. Roncali, *Acc. Chem. Res*. **2009**, *42*, 1719; c) P. M. Beaujuge, J. M. J. Frechet, *J. Am. Chem. Soc*. **2011**, *133*, 20009; d) Z. X. Wang, F. J. Zhang, J. Wang, X. W. Xu, J. Wang, Y. Liu, Z. Xu, *Chin. Sci. Bull*. **2012**, *57*, 4143; e) M. Pfannmoller, W. Kowalsky, R. R. Schroder, *Energy Environ. Sci*. **2013**, *6*, 2871; f) J. Yu, Y. Zheng, J. Huang, *Polymers* **2014**, *6*, 2473; g) F. C. Krebs, N. Espinosa, M. Hosel, R. R. Sondergaard, *Adv. Mater*. **2014**, *26*, 29; h) T. R. Andersen, H. F. Dam, M. Hosel, M. Helgesen, J. E. Carle, T. T. Larse-Olsen, S. A. Gevorgyan, J. W. Andreasen, J. Adams, N. Li, F. Machui, G. D. Spyropoulos, T. Ameri, N. Lemaitre, M. Legros, A. Scheel, D. Gaiser, K. Kreul, S. Berny, O. R. Lozman, S. Nordman, M. Valimaki, M. Vilkman, R. R. Sondergaard, M. Jorgensen, C. J. Brabec, F. C. Krebs, *Energy Environ. Sci.* **2014**, *7*, 2925.

[8] M. A. Green, *Third Generation Photovoltaics*, Springer-Verlag, Berlin, **2003**.

[9] C. A. Nelson, N. R. Monahan, X. –Y. Zhu, *Energy Environ. Sci*. **2013**, *6*, 3508.

[10] a) F. G. Brunetti, R. Kumar, F. Wudl, *J. Mater. Chem*. **2010**, *20*, 2934; b) J. L. Delgado, P.-A. Bouit, S. Filippone, M. A. Herranz, N. Martin, *Chem. Comm*. **2010**, *46*, 4853; c) K. A. Mazzio, C. K. Luscombe, *Chem. Soc. Rev*. **2015**, *44*, 78; d) J. Yan, B. R. Saunders, *RSC Adv*. **2014**, *4*, 43286.

[11] G. Yu, J. Gao, J. C. Hummelen, F. Wudl, A. J. Heeger, *Science* **1995**, *270*, 1789.

[12] a) M. Hiramoto, H. Fujiwara, M. Yokoyama, *Appl. Phys. Lett*. **1991**, *58*, 1062; b) J. J. M. Halls, C. A. Walsh, N. C. Greenham, E. A. Marseglia, R. H. Friend, S. C. Moratti, A. B. Holmes, *Nature* **1995**, *376*, 498.

[13] a) C. J. Brabec, N. S. Saricifti, J. C. Hummelen, *Adv. Funct. Mat*. **2001**, *11*, 15; b) J. Peet, M. L. Senatore, A. J. Heeger, G. C. Bazan, *Adv. Mater*. **2009**, *21*, 1521; c) C. J. Brabec, S. Gowrisanker, J. J. M. Halls, D. Laird, S. Jia, S. P. Williams, *Adv. Mater*. **2010**, *22*, 3839; d) D. Gendron, M. Leclerc, *Energy Environ. Sci*. **2011**, *4*, 1225; e) J. Peet, A. J. Heeger, G. C. Bazan, *Acc. Chem. Res*. **2009**, *42*, 1700.

[14] a) J. Roncali, P. Frere, P. Blanchard, R. de Bettignies, M. Turbiez, S. Roquet, P. Leriche, Y. Nicolas, *Thin Solid Films* **2006**, *511-512*, 567; b) B. Walker, C. Kim, T.-Q. Nguyen, *Chem. Mater*.

[15] T. M. Clarke, J. R. Durrant, *Chem. Rev*. **2010**, *110*, 6736.

[16] a) R. N. Marks, J. J. M. Halls, D. D. C. Bradley, R. H. Friend, A. B. Holmes, *J. Phys. Condens. Matter* **1994**, *6*, 1379; b) P. B. Miranda, D. Moses, A. J. Heeger, *Phys. Rev. B* **2001**, *64*, 081201.

[17] V. Coropceanu, J. Cornil, D. A. S. Filho, Y. Oliver, R. Silbey, J.-L. Bredas, *Chem. Rev*. **2007**, *107*, 926.

[18] B. A. Gregg, M. C. Hanna, *J. Appl. Phys*. **2003**, *93*, 3605.

[19] J. You, L. Dou, K. Yoshimura, T. Kato, K. Ohya, T. Moriaty, K. Emery, C.-C. Chen, J. Gao, G. Li, Y. Yang, *Nat. Commun*. **2013**, *4*, 1446.

[20] Heliatek GmbH, *Heliatek consolidates its technology leadership by establishing a new world record for organic solar technology with a cell efficiency of 12%*, **2013**. Available at: http://www.heliatek.com/newscenter/latest_news/neuer-weltrekord-fur-organische-solarzellen-heliatek-behauptet-sich-mit-12-zelleffizienz-als-technologiefuhrer/?lang=en (Accessed Jan. 2015)

[21] Mitsubishi Chemical Corporation, *Achieved power conversion efficiency of 11.7%, the highest in the world!*, Available at: http://www.mkagaku.co.jp/english/r_td/strategy/technology/topics/opv/index.html (Accessed Jan. 2015).

[22] a) A. Hagfeldt, G. Boschloo, L. Sun, L. Kloo, H. Pettersson, *Chem. Rev*. **2010**, *110*, 6595; b) M. K. Nazeeruddin, E. Baranoff, M. Gratzel, *Solar Energy* **2011**, *85*, 1172.

[23] B. O'Regan, M. Gratzel, *Nature* **1991**, *353*, 737.

[24] H. S. Jung, J.-K. Lee, *J. Phys. Chem. Lett*. **2013**, *4*, 1682.

[25] . Odobel, Y. Pellegrin, E. A. Gibson, A. Hagfeldt, A. L. Smeigh, L. Hammarstrom, *Coord. Chem. Rev*. **2012**, *256*, 2414.

[26] I. R. Perera, T. Daeneke, S. Makuta, Z. Yu, Y. Tachibana, A. Mishra, P. Bauerle, C. A. Ohlin, U. Bach, L. Spiccia, *Angew. Chem. Int. Ed*. **2015**, *54*, 3758.

[27] a) P. Docampo, S. Guldin, T. Leijtens, N. K. Noel, U. Steiner, H. J. Snaith, *Adv. Mater*. **2014**, *26*, 4013; b) A. Fakharuddin, R. Jose, T. M. Brown, F. Fabregat-Santiago, J. Bisquert, *Energy Environ. Sci*. **2014**, *7*, 3952.

[28] a) M. A. Halim, *Nanomaterials* **2013**, *3*, 22; b) M. R. Kim, D. Ma, *J. Phys. Chem. Lett*. **2015**, *6*, 85.

[29] a) H. J. Snaith, *J. Phys. Chem. Lett*. **2013**, *4*, 3623; b) M. A. Loi, J. C. Hummelen, *Nat. Mater*. **2013**, *12*, 1087; c) S. Kazim, M. K. Nazeeruddin, M. Gratzel, S. Ahmad, *Angew. Chem. Int. Ed*. **2014**, *53*, 2812; d) M. He, D. Zheng, M. Wang, C. Lin, Z. Lin, *J. Mater. Chem. A* **2014**, *2*, 5994; e) P. Gao, M. Gratzel, M. K. Nazeeruddin, *Energy Environ. Sci*. **2014**, *7*, 2448; f) M. A. Green, A. Ho-Baillie, H. J. Snaith, *Nature Photon*. **2014**, *8*, 506; g) H.-S. Kim, S. H. Im, N.-G. Park, *J. Phys. Chem. C* **2014**, *118*, 5615; h) G. Giorgi, K. Yamashita, *J. Mater. Chem. A* **2015**, DOI:

10.1039/c4ta05046k; i) W.-J. Yin, J.-H. Yang, J. Kang, Y. Yan, S.-H. Wei, *J. Mater. Chem. A* **2015**, DOI: 10.1039/c4ta05033a.

[30] A. Kojima, K. Teshima, Y. Shirai, T. Miyasaka, *J. Am. Chem. Soc*. **2009**, *131*, 6050.

[31] J. Burschka, N. Pellet, S.-J. Moon, R. Humphry-Baker, P. Gao, M. K. Nazeeruddin, M. Gratzel, *Nature* **2013**, *499*, 316

[32] G. E. Eperon, S. D. Stranks, C. Menelaou, M. B. Johnston, L. M. Herz, H. J. Snaith, *Energy Environ. Sci*. **2014**, *7*, 982.

[33] N. K. Noel, S. D. Stranks, A. Abate, C. Wehrenfennig, S. Guarnera, A.-A. Haghighirad, A. Sadhanala, G. E. Eperon, S. K. Pathak, M. B. Johnston, A. Petrozza, L. M. Herz, H. J. Snaith, *Energy Environ. Sci*. **2014**, *7*, 3061.

[34] Ardo, S.; Meyer, *Chem. Soc. Rev*. **2009**, *38*, 115-164.

[35] Martinson, A. B. F.; Hamann, T. W.; Pellin, M. J.; Hupp, J. T., *Chem. Eur. J.* **2008**, *14* (15), 4458-4467.

[36] [36] J. G. Vos, J. M. Kelly, *Dalton Trans.* **2006**, *41*, 4869-4883

[37] Green, M. A., Physica E **2002**, *14* (1-2), 11-17.

[38] W. W. Brandt, F. P. Dwyer, E. D. Gyarfas, *Chem. Rev.* **1954**, *54* (6), 959-1017.

[39] Y. Ooyama, S. Inoue, T. Nagano, K. Kushimoto, J. Ohshita, I. Imae, K. Komaguchi, Y. Harima, *Angew. Chem., Int. Ed.* **2011**, *50*, 7429.

[40] K. Kalyanasundaram; M. Gratzel, *Coord. Chem. Rev*. **1998**, *177*, 347-414.

[41] E. Galoppini, *Coord. Chem. Rev*. **2004**, *248* (13-14), 1283-1297.

G.J. Meyer, *Inorg. Chem*. **2001**, *40* (23), 6073-6079

[43] S. Altobello; C. A. Bignozzi; , S. Caramori; G. Larramona; S. Quici; G. Marzanni; Lakhmiri, R., *J. Photochem. Photobiol., A* **2004**, *166* (1-3), 91-98.

[44] P. Ghosh; T. G. Spiro, *J. Am. Chem. Soc*. **1980**, *102* (17), 5543-5549.

[45] A.Vittadini; A. Selloni; F. P Rotzinger; M. Gratzel, *J. Phys. Chem. B* **2000**, *104* (6), 1300-1306.

[46] T. J Meyer; G. J. Meyer; B. W. Pfennig,; J. R. Schoonover; J. C. Timpson; J. F. Wall; C. Kobusch; X. Chen; B. M. Peek, *Inorg. Chem*. **1994**, *33* (18), 3952-3964.

[47] J.N. Clifford; E. Palomares; M.K. Nazeeruddin; M. Grätzel; J. Nelson; X. Li; N.J. Long; J.R. Durrant, *J. Am. Chem. Soc*. **2004**, *126* (16), 5225-5233

[48] Y. Kageshima, H. Kumagai, T. Minegishi, T. Kubota; K. Dome, *Angewandte Chemie*. **2015**.

[49] Y. M. Yang, W. Chen, L. Dou, W. H. Chang, H. S Duan, B. Bob, Y. Yang, *Nature Photonics*. **2015**.

[50] J. R. Swierk, D. D. Méndez-Hernández, , N. S. McCool, P. Liddell, Y. Terazono, I. Pahk, T. E. Mallouk, *National Academy of Sciences* **2015** , *112*(6), 1681-1686.

[51] S. Altobello; R. Argazzi; S. Caramori; C. Contado; S. Da Fre; P. Rubino; C. Chone; G. Larramona; C. A. Bignozzi, *J. Am. Chem. Soc.* **2005**, *127*, 15342-15343.

[52] G. M. Hasselmann, G. J. Meyer, *J. Phys. Chem. B* **1999**, *103*, 7671-7675.

[53] S. Ferrere, *Inorg. Chim. Acta* **2002**, *329*, 79-92.

[54] E. A. M. Geary, K. L. McCall, A. Turner, P. R. Murray, E. J. L. McIness, L. A. Jack, L. J. Yellwleesa, N. Robertson, *Dalton Trans.* **2008**, 3701-3708.

[55] T. Bessho, C. Constable Edwin, M. Grätzel, A. Hernandez Redondo, E. Housecroft Catherine, E. Kylberg, M. K. Nazeeruddin, M. Neuburger, S. Schaffner, *Chem. Commun.* **2008**, 3717-3719.

[56] P. Persson, M. J. Lundqvist, *J. Phys. Chem. B* **2005**, *109,* 11918-11924

[57] M. K. Nazeeruddin, F. De Angelis, S. Fantacci, A. Selloni, G. Viscardi, P. Liska, S. Ito, B. Takeru, M. Gratzel, *J. Am. Chem. Soc*. **2005**, *127*, 16835.

[58] a) Y. Chiba, A. Islam, Y. Watanabe, R. Komiya, N. Koide, L. Han, *Jpn. Appl. Phys.* **2006**, *45*, L638; b) M. K. Nazeeruddin, P. Pechy, M. Gratzel, *Chem. Comm*. **1997**, 1705; c) M. K. Nazeeruddin, P. Pechy, T. Renouard, S. M. Zakeeruddin, R. Humphry-Baker, P. Comte, P. Liska, L. Cevey, E. Costa, V. Shklover, L. Spiccia, G. B. Deacon, C. A. Bignozzi, M. Gratzel, *J. Am. Chem. Soc*. **2001**, *123*, 1613.

[59] C.-Y. Chen, M. Wang, J.-Y. Li, N. Pootrakulchote, L. Alibabaei, C.-h. Ngoc-le, J.-D. Decoppet, J.-H. Tsai, C. Gratzel, C.-G. Wu, S. M. Zakeeruddin, M. Gratzel, *ACS Nano* **2009**, *3*, 3103.

[60] A. Hagfeldt, G. Boschloo, L. Sun, L. Kloo, H. Pettersson, Chem. Rev. 2010, 110, 6595-6663.

[61] a) L.-L. Li, E. W.-G. Diau, *Chem. Soc. Rev*. **2013**, *42*, 291; b) M. Urbani, M. Gratzel, M. K. Nazeeruddin, T. Torres, *Chem. Rev*. **2014**, *114*, 12330; c) T. Higashino, H. Imahori, *Dalton Trans*. **2015**, *44*, 448.

[62] M. Gouterman,, In Porphyrins, ed. Dolphin, D., Ed. New York, **1978**; Vol. 3, pp 1-166.

[63] C.-P. Hsieh, H.-P. Lu, C.-L. Chiu, C.-W. Lee, S.-H. Chuang, C.-L. Mai, W.-N. Yen, S.-J. Hsu, E. W.-G. Diau, C.-Y. Yeh, *J. Mater. Chem.* **2010**, *20*, 1127.

[64] T. Bessho, S. M. Zakeeruddin, C.-Y. Yeh, E. W.-G. Diau, M. Gratzel, *Angew. Chem. Int. Ed*. **2010**, *49*, 6646.

[65] T. Bessho, S. M. Zakeeruddin, C.-Y. Yeh, E. W.-G. Diau, M. Gratzel, *Angew. Chem. Int. Ed*. **2010**, *49*, 6646.

[66] A. Yella, C.-L. Mai, S. M. Zakeeruddin, S.-N. Chang, C.-H. Hsieh, C.-Y. Yeh, M. Gratzel, *Angew. Chem. Int. Ed*. **2014**, *53*, 2973

[67] S. Mathew, A. Yella, P. Gao, R. Humphry**-** Baker, B. F. E. Curchod, N. Ashari**-** Astani, I. Tavernelli,U. Rothlisberger, M. K. Nazeeruddin, M. Gratzel, *Nat. Chem* . **2014** , *6* , 242.

[68] a) M.**-** E. Ragoussi, J.**-** J. Cid, J.**-** H. Yum, G. de la Torre, D. Di Censo, M. Gratzel, M. K. Nazeeruddin, T. Torres, Angew. Chem. Int. Ed . 2012 , 51 , 4375; b) M.**-** E. Ragoussi, J.**-** H. Yum, A. K. Chandiran, M. Ince, G. de la Torre, M. Gratzel, MM. K. Nazeeruddin, T. Torres, ChemPhysChem 2014 , 15 , 1033.

[69] a) M.-E. Ragoussi, M. Ince, T. Torres, *Eur. J. Org. Chem*. **2013**, *29*, 6475; b) L. Martin-Gomis, F. Fernandez-Lazaro, A. Sastre-Santos, *J. Mater. Chem. A* **2014**, *2*, 15672; c) V. K. Singh, R. K. Kanaparthi, L. Giribabu, *RSC Adv*. **2014**, *4*, 6970.

[70] V. S. Manthou, E. K. Pefkianakis, P. Falaras, G. C. Vougioukalakis, *ChemSusChem* **2015**, *8*, 588.

[71] M. K. Nazeeruddin, R. Humphry-Baker, M. Gratzel, D. Wohrle, G. Schnurpfeil, G. Schneider, A. Hirth, N. Trombach, *J. Porphyrins Phthalocyanines* **1999**, *3*, 230.

[72] A. Morandeira, I. Lopez-Duarte, B. O'Regan, M. V. Martinez-Diaz, A. Forneli, E. Palomares, T. Torres, J. R. Durrant, *J. Mater. Chem*. **2009**, *19*, 5016.

[73] [73] Z. Zhang, N. Evans, S. M. Zakeeruddin, R. Humphry-Baker, M. Gratzel, *J. Phys. Chem. C* **2007**, *111*, 398.

[74] Z. Yao, M. Zhang, H. Wu, L. Yang, R. Li, P. Wang, *J. Am. Chem. Soc*. **2015**, DOI: 10.1021/jacs.5b01537.

[75] Some examples; a) M. Zhang, Y. Wang, M. Xu, W. Ma, R. Li, P. Wang, *Energy Environ. Sci*. **2013**, *6*, 2944; b) K. Kakiage, Y. Aoyama, T. Yano, T. Otsuka, T. Kyomen, M. Unno, M. Hanaya, *Chem. Comm*. **2014**, *50*, 6379.

[76] Y. Zhaoyang, Z. Min, Renzhi Li, Y. Lin, Q. Yongna, and W. Peng, *Angew. Chem. Int. Ed*. **2015**, *54*, 1 – 6

[77] M.-S. Kang, J. H. Kim, J. Won, N.-G. Park, N.-G.; S. Kang, *Chem. Commun*. **2005**, 889-891.

[78] P. Wang, S. M. Zakeeruddin, J. E. Moser, M. K. Nazeeruddin, T. Sekiguchi, M. Grätzel, *Nat.Mater*. **2003**, *2*, 402-407..

[79] P. Wang, S. M. Zakeeruddin, J. E. Moser, R. Humphrey-Baker, M. Grätzel, *J. Am. Chem. Soc.* **2004**, *126*, 7164-7165.

[80] P. Wang, Q. Dai, S. M. Zakeeruddin, M. Forsyth, D. R.;MacFarlane, M. Grätzel, M *J. Am. Chem. Soc*. **2004**, *126*, 13590-13591

[81] H. Nusbaumer, S. M. Zakeeruddin, J. E. Moser, M. Grätzel, *Chem. Eur. J.* **2003**, *9*, 3756-3763.

[82] Y. Sato, T. Azechi, T. Kitamura, Y. Hasegawa, Y. Wada, S. Yanagida, *Coord. Chem. Rev.* **2004**, *248*, 1469-1478.

[83] J. Krüger, R. Plass, L. Cevey, M. Piccirelli, M. Grätzel, U. Bach, *Appl. Phys. Lett.* **2001**, *79*, 2085.

[84] N. Papageorgiou, Y. Athanassov, M. Armand, P. Bonhote, H. Pettersson, A. Azam, M. Grätzel, , *J. Electrochem. Soc.* **1996**, *143*, 3099-3108.

[85] A. Hagfeldt, G. Boschloo, L. Sun, L. Kloo, H. Pettersson, *Chem. Rev*. **2010**, *110*, 6595-6663.

[86] T. Welton, *Chem. Rev*. **1999**, *99*, 2071-2084.

[87] S. A. Haque, E. Palomares, B. M. Cho, A. N. M. Green, N. Hirata, D. R. Klug, J. R. Durrant, *J. Am. Chem. Soc.* **2005**, *127*, 3456-3462

[88] R.C. Young, T.J. Meyer, D.G. Whitten, *J. Am. Chem. Soc.* , **1975**, *97* 4781–4782.

[89] A.J. Morris, G.J. Meyer, E. Fujita, *Acc. Chem. Res*., **2009**, *42*, 1983–1994.
[90] C.R. Bock, T.J. Meyer, D.G. Whitten, *J. Am. Chem. Soc*., **1974** ,*96,* 4710–4712.
[91] B. Schlicke, P. Belser, L. De Cola, E. Sabbioni, V. Balzani, *J. Am. Chem. Soc*.,**1999**, *121* 4207–4214.
[92] B. Schlicke, P. Belser, L. De Cola, E. Sabbioni, V. Balzani*, J. Am. Chem. Soc*., **1999**, *121* 4207–4214.
[93] Y.X. Zhao, J.R. Swierk, J.D. Megiatto, B. Sherman, W.J. Youngblood, D.D. Qin, D.M.Lentz, A.L. Moore, T.A. Moore, D. Gust, T.E. Mallouk, Proc. Nat. Acad. Sci. U.S.A109 **2012** 15612–15616.
[94] S.L.H. Higgins, K.J. Brewer, *Angew. Chem. Int. Ed*., **2012** ,*51,* 11420–11422.
[95] M.E. Hagerman, S.J. Salamone, R.W. Herbst, A.L. *Payeur, Chem. Mater*., **2003** ,*15* ,443–450.
[96] M. P. Dare-Edwards, J. B. Goodenough, *Faraday Discussions of the Chemical Society*, **1980**, 70:285.
[97] C. Y. Chen, M. Wang, J. Y. Li, N. Pootrakulchote, et al, *ACS Nano*, **2009**, *3*(10)3103.
[98] W. P. Griffith, *Chem. Soc. Rev*. **1992**, *21* (3), 179-185.
[99] J. J. Rack and Harry B. Gray. *Inorganic Chemistry*, **1999**, *38*, 2.
[100] G. D. Henry, *Tetrahedron* **2004**, *60* (29), 6043-6061
[101] F. Dumur, E. Dumas, C. Mayer, *Targ. Heterocycl. Syst*. **2007**, *130*, 70-103.
[102] C. Kaes, A. Katz, M. W. Hosseini, *Chem. Rev.* **2000**, *100* (10), 3553-3590.
[103] E. C. Constable, *Adv. Inorg. Chem. Radiochem.* **1986**, *30*, 69-121.
[104] W. W. Brandt, F. P. Dwyer, E. D. Gyarfas, *Chem. Rev.* **1954**, *54* (6), 959-1017.
[105] A. Goller, U. W. Grummt, *Chem. Phys. Lett.* **2000**, *321* (5,6), 399-405.
[106] Nakamoto, *J. Phys. Chem.* **1960**, *64* (10), 1420-1425.
[107] G. Albano, V. Balzani, E. C. Constable, M. Maestri, D. R. Smith, *Inorg. Chim. Acta* **1998,** *277* (2), 225-231.
[108] S. Leroy-Lhez, F. Fages, *C. R. Chim*. **2005**, *8* (8), 1204-1212.
[109] A. S. Polo, M. K. Itokazu, N. Y. Murakami Iha, *Coord. Chem. Rev*. **2004**, *248* (13-14), 1343-1361.
[110] K. K.-W. Lo, W.-K. Hui, C.-K. Chung, K. H.-K. Tsang, D. C.-M. Ng, N. Zhu, K.-K. Cheung, *Coord. Chem. Rev.* **2005**, *249* (13-14), 1434-1450..
[111] G. Chelucci, R. P. Thummel, *Chem. Rev*. **2002**, *102* (9), 3129-3170.
[112] V. Balzani, G. Bergamini, P. Ceroni, *Coord. Chem. Rev*. **2008**, *252* (23+24), 2456-2469.
[113] A. Hagfeldt, G. Boschloo, L. Sun, L. Kloo, H. Pettersson, *Che Rev,* **2010**, 6595–6663.
[114] YC. Qin, Q. Peng, *Artn*, **2012**, 291579
[115] . Balzani, G. Bergamini, S. Campagna, F. Puntoriero, *Top. Curr. Chem*. **2007**, *280*, 1-36.
[116] V. Balzani, A. Juris, M. Venturi, S. Campagna, S. Serroni, *Chem. Rev.* **1996**, *96* (2), 759-833.
[117] G. A. Crosby, *Acc. Chem. Res*. **1975**, *8* (7), 231-238.

[118] K. Kalyanasundaram, M. K. Nazeeruddin, *Chem. Phys. Lett.* **1992,** *193* (4), 292-297.
[119] G. R. Newkome, A. K. Patri, E. Holder, U. S. Schubert, *Eur. J. Org. Chem*. **2004**, (*2*), 235-254.
[120] N. E. Tokel-Takvoryan, R. E. Hemingway, A. J. Bard, *J. Am. Chem. Soc*. **1973**, *95* (20), 6582-6589.
[121] Anderson, P. A.; Strouse, G. F.; Treadway, J. A.; Keene, F. R.; Meyer, T. J., Inorg. Chem. 1994, 33 (18), 3863-3864.
[122] Keene, F. R., Coord. Chem. Rev. 1997, 166, 121-159.
[123] A. Juris, V. Balzani, F. Barigelletti, S. Campagna, P. Belser, A. Von Zelewsky, *Coord. Chem. Rev*. **1988**, *84*, 85-277.
[124] J. G. Vos, J. M. Kelly, *Dalton Trans*. **2006**, (*41*), 4869-4883
[125] A. Islam, H. Sugihara, H. Arakawa, *J. Photochem. Photobiol., A* **2003**, *158* (2-3), 131-138.
[126] K. Kalyanasundaram, M. Gratzel, *Coord. Chem. Rev*. **1998**, *177*, 347-414.
[127] T. J. Meyer, *Acc. Chem. Res.* **1989**, *22* (5), 163-170
[128] J. N. Demas, B. A. DeGraff, *J. Chem. Educ.* **1997**, *74* (6), 690-695
[129] K. K.-W. Lo, *Struct. Bond.* **2007,** *123*, 205-245.
[130] Y. Xiong, L.-N. Ji, *Coord. Chem. Rev*. **1999**, 185-186, 711-733.
[131] D. M. Roundhill. Plenum Press New York and London, **1994.**
[132] S. Ardo, G.J. Meyer, *Chem Soc Rev*, **2009**, *3 8*(1):115–164.
[133] Y. Cao, Y. Bai, Q. Yu, Y. Cheng, S. Liu, D. Shi, F. Gao, P. Wang, *J. Phys. Chem. C* , **2009**, *113*, 6290–6297
[134] A. Abbotto, C. Barolo, L. Bellotto, F. De Angelis, M. Grätzel, N. Manfredi, C. Marinzi, S. Fantacci, J. Yumd and M. K. Nazeeruddin *Chem. Commun*., **2008**, 5318–5320
[135] E. U. Condon. *Physics Review*, **1928**, *32*, 858-872.
[136] The metal-to-ligand charge transfer (MLCT) of d_ coordination compounds have emerged as the most e_cient for solar harvesting and sensitization of wide-bandgap semiconductor materials. As the name implies, light absorption promotes an electron from the Metal d orbitals to the Ligand π^*. orbitals, d(π) ➔ π^*.
[137] S. Anderson, E.C. Constable, M.P. Dare-Edwards, J.B. Goodenough, A. Hamnett, K.R. Seddon, R.D. Wright, *Nature*, **1979**, *280*(5723):571–573
[138] J. Desilvestro, M. Grätzel, L. Kavan, J. Moser, J. Augustynski, *J Am Chem Soc* , **1985**, *107*(10):2988–2990
[139] M.K. Nazeeruddin, P. Liska, J. Moser, N. Vlachopoulos, M. Grätzel, *Helv Chim Acta*, **1990** *73*(6), 1788–1803.
[140] M.K. Nazeeruddin, A. Kay, I. Rodicio, R. Humphry-Baker, E. Müller, P. Liska, N. Vlachopoulos, M. Grätzel, *J Am Chem Soc,* **1993**, *115*(14), 6382–6390
[141] M.K. Nazeeruddin, P. Pechy, M. Grätzel, *Chem Commun,* **1997**, *18*, 1705–1706.

[142] . Wang, S.M. Zakeeruddin, R. Humphry-Baker, J.E. Moser, M. Grätzel, *Adv Mater* , **2003**, *15*(24), 2101.
[143] M.K. Nazeeruddin, P. Pechy, M. Grätzel, *Chem Commun,* **1997**, *18*, 1705–1706.
[144] P. Wang, S.M. Zakeeruddin, R. Humphry-Baker, J.E. Moser, M. Grätzel, *Adv Mater*, **2003**, *15*(24), 2101.
[145] S.R. Jang, J.H. Yum, C. Klein, K.J. Kim, P. Wagner, D. Officer, M. Gratzel, M.K. Nazeeruddin, *J Phys Chem C* , **2009,** *113*(5), 1998–2003.
[146] . Gao, Y. Wang, D. Shi, J. Zhang, M. Wang, X. Jing, R. Humphry-Baker, P. Wang, S.M. Zakeeruddi, M. Grätzel, *J Am Chem Soc,* **2008**, *130*(32), 10720–10728.
[147] P. Wang, S.M. Zakeeruddin, J.E. Moser, R. Humphry-Baker, P. Comte, V. Aranyos, A. Hagfeldt, M.K. Nazeeruddin, M. Grätzel, *Adv Mater*, **2004**, *16*(20).
[148] C.Y. Chen, H.C. Lu, C.G. Wu, J.G. Chen, K.C. Ho, *Adv Funct Mater,* **2007**, *17*(1), 29–36.
[149] C.Y. Chen, J.G. Chen, S.J. Wu, J.Y. Li, C.G. Wu, K.C. Ho, *Angew Chem*, **2008**, *47*(38), 7342–7345.
[150] S.R. Jang, J.H. Yum, C. Klein, K.J. Kim, P. Wagner, D. Officer, M. Grätzel, M.K. Nazeeruddin, *J Phys Chem C* , **2009**, *113*(5), 1998–2003.
[151] K.S. Chen, W.H. Liu, Y.H. Wang, C.H. Lai, P.T. Chou, G.H. Lee, K. Chen, H.Y. Chen, Y. Chi, F.C. Tung, *Adv Funct Mater* , **2007**, *17*(15), 2964–2974.
[152] S.M. Zakeeruddin, M.K. Nazeeruddin, R. Humphry-Baker, P. Pechy, P. Quagliotto, C. Barolo, G. Viscardi, M. Grätzel, *Langmuir*, **2002**, *18*(3), 952–954.
[153] P. Wang, S.M. Zakeeruddin, J.E. Moser, M.K. Nazeeruddin, T. Sekiguchi, M. Grätzel, *Nat Mater,* **2003***, 2*(6):402–407.
[154] M.S. Kang, J.H. Kim, Y.J. Kim, J. Won, N.G. Park, Y.S. Kang, *Chem Commun*, **2005**, *7*, 889–891.
[155] JN Clifford, E Palomares, MK Nazeeruddin, M GrÄtzel, J Nelson, X Li, NJ Long, J Durrant *J Am Chem Soc,* **2004**, *126*, 16, 5225–5233.
[156] L. Schmidt-Mende, J. E. Kroeze, J. R. Durrant, M. K. Nazeeruddin, M. Grätzel, *Nano Letters*, **2005**, *5*, no. 7, pp. 1315–1320.
[157] J.N. Clifford, E. Palomares, M.K. Nazeeruddin, M. Grätzel, J. Nelson, X. Li, N.J. Long, J. Durrant, *J Am Chem Soc*, **2004**, *126*(16), 5225–5233.
[158] P. Coppo, D. C. Cupertino, S. G. Yeates, M. L. Turner, *Macromolecules* **2003**, *36*, 2705-271
[159] S.W. Wang, K.L. Wu, E. Ghadiri, M. Grazia Lobello, S.T. Ho,a Yun Chi, J.E. Moser, F. De Angelis, M. Grätzel, M. K. Nazeeruddin, *Chem. Sci.*, **2013**,*4*, 2423-2433
[160] K. C. D. Robson, B. D. Koivisto, A. Yella, *Inorganic Chemistry*, **2011**, *50*, 12, 5494–5508.
[161]O. Lohio, L. Viau, O. Maury, H. L. Bozec, *Tetrahedron Lett*. **2007**, *48*, 1229-1232.
[162]S. M. Zakeeruddin, M. K. Nazeeruddin, R. Humphry-Baker, P. Péchy, P. Quagliotto, C. Barolo, G. Viscardi, M. Grätzel, *Langmuir* **2002**, *18*, 952-954.

[163] Z. Zhu, D. Waller, R. Gaudiana, M. Morana, D. Mühlbacher, M. Scharber, C. Brabec, *Macromolecules,* **2007**, *40*, 1981-1986.

[164] Z. Zhu, D. Waller, R. Gaudiana, M. Morana, D. Mühlbacher, M. Scharber, C. Brabec, *Macromolecules,* **2007**, *40*, 1981-1986.

[165] G.Maerker, F. H. Case, *J. Am. Chem. Soc.* **1958,** *80*, 2745-2748.

[166] D. Wenkert, R. B. Woodward, *J. Org. Chem.* **1983**, *48*, 283-289.

[167]P. Wang, S. M. Zakeeruddin, J. E. Moser, M. K. Nazeeruddin, T. Sekiguchi, M. Grätzel, *Nat. Mater.* **2003**, *2*, 402-407.

[168]S. M. Zakeeruddin, M. K. Nazeeruddin, R. Humphry-Baker, M. Grätzel, V. Shklover, *Inorg. Chem.* **1998**, *37*, 5251-5259.

[169]N. Hirata, J.-J. Lagref, E. J. Palomares, J. R. Durrant, M. K. Nazeeruddin, M. Grätzel, D. Di Censo, *Chem. Eur. J.* **2004**, *10*, 595-602.

[170] F. Matar, T. H. Ghaddar, K. Walley, T. Dos Santos, J. R. Durrant, B. O'Regan, *J. Mater. Chem.* **2008**, *18*, 4246-4253.

[171] L. Spiccia, G. B. Deacon, C. M. Kepert, *Coord. Chem. Rev.* **2004**, *248*, 1329-1341.

[172] D. Dominguez-Gutierrez, G. De Paoli, A. Guerrero-Martinez, G. Ginocchietti, D. Ebeling, E. Eiser, L. De Cola, C. J. Elsevier, *J. Mater. Chem.* **2008**, *18*, 2762-2768.

[173] B. Therrien, *Coord. Chem. Rev.* **2009**, *253*, 493-519.

[174] K. Severin, *Chem. Commun.* **2006**, 3859-3867.

[175] K. Willinger, K. Fischer, R. Kisselev, M. Thelakkat, *J. Mat. Chem.* **2009**, *19*, 5364-5376.

[176] S. Rau, B. Schäfer, A. Grüßing , S. Schebesta, K. Lamm, J. Vieth, H. Görls , D. Walther, M. Rudolph, U. W. Grummt, E. Birkner, *Inorg. Chim. Acta* **2004**, *357*, 4496-4503.

[177] C. O. Kappe, *Angew. Chem.* **2004**, *116*, 6408-6443; *Angew. Int. Ed.* **2004**, *43*, 6250-6284.

[178] M. Garcia-Iglesias, L. Pelleja, J.-H. Yum, D. Gonzalez-Rodriguez, M. K. Nazeeruddin, M. Grätzel, J. N. Clifford, E. Palomares, P. Vazquez, T. Torres, Chem. Sci. 2011, 3, 1177-1184

[179] O. Lohio, L. Viau, O. Maury, H. L. Bozec, Tetrahedron Lett. 2007, 48, 1229-1232.

[180] P. Wang, S. M. Zakeeruddin, J. E. Moser, M. K. Nazeeruddin, T. Sekiguchi, M. Grätzel, Nat. Mater. 2003, 2, 402-407.

[181] F. Matar, T. H. Ghaddar, K. Walley, T. Dos Santos, J. R. Durrant, B. O'Regan, J. Mater. Chem. 2008, 18, 4246-4253

[182] M. Sánchez Carballo, M. Urbani, A. K. Chandiran, D. González- Rodríguez, P. Vazquez, M. Gratzel, M. K. Nazeeruddin, T. Torres, Dalton Trans. 2014, 43, 15085-15091.

[183] S. M. Zakeeruddin, M. K. Nazeeruddin, R. Humphry-Baker, P. Péchy, P. Quagliotto, C. Barolo, G. Viscardi, M. Grätzel, Langmuir 2002, 18, 952- 954.

[184] M. Sanchez Carballo, M. Urbani, A. K. Chandiran, D. Gonzalez-Rodriguez, P. Vazquez, M. Grätzel, M. K. Nazeeruddin, T. Torres, *Dalton Trans.* **2014**, *43*, 15085-15091.

[185] S. Amit Kuma, M. Urbani, M. Medel, M. Ince, D. Gonzalez-Rodriguez, A. K. Chandiran, A. N. Bhaskarwar, T. Torres, M. K. Nazeeruddin, M. Grätzel, *J. Phys. Chem. Lett.* **2014**, *5*, 501-505.

[186] A. Reynal, A. Forneli, E. Martinez-Ferrero, A. Sánchez-Díaz, A. Vidal-Ferran, B. C. O'Regan, E. Palomares, J. Am. Chem. Soc. 130 (2008) 13558.

[187] Peter, L. M. Dye-sensitized nanocrystalline solar cells. *Phys. Chem. Chem. Phys.* **2007,** *9*, 2630-2642.

[188] L. M. Peter, *Phys. Chem. Chem. Phys.* **2007,** *9*, 2630-2642.

[189] . Listorti, B. O'Regan, J. R. Durrant, *Chem. Mat.* **2011**, *23*, 3381-3399.

[190] . S. Ito, T. N. Murakami, P. Comte, P. Liska, C. Grätzel, M. K. Nazeeruddin, M. Grätzel, *Thin Solid Films* **2008**, *516* , 4613-4619.

[191] T. Hasobe, H. Imahori, P. V. Kamat, T. K. Ahn, S. K. Kim, D. Kim, A. Fujimoto, T. Hirakawa and S. Fukuzumi, *J. Am. Chem. Soc*., **2005**, *127*, 1216–1228.

[192] H. Imahori, T. Umeyama and S. Ito, *Acc. Chem. Res*., **2009**, *42*,1809–1818.

[193] I. Radivojevic, A. Varotto, C. Farley and C. M. Drain, *Energy Environ. Sci.,* **2010**, *3*, 1897–1909.

[194] M. V. Martínez-Díaz, G. de la Torrea and T. Torres, *Chem. Commun*., **2010**, *46,* 7090–7108.

[195] M. G. Walter, A. B. Rudine and C. C. Wamser, *J. Porphyrins Phthalocyanines*, **2010**, *14*, 759–792.

[196] M. J. Griffith, K. Sunahara, P. Wagner, K. Wagner, G. G. Wallace, D. L. Officer, A. Furube, R. Katoh, S. Mori and A. J. Mozer, *Chem. Commun*., **2012**, *48*, 4145–4162.

[197] H. Imahori, T. Umeyama, K. Kurotobi and Y. Takano, *Chem. Commun*., **2012***, 48*, 4032–4045.

[198] Mathew, S.; Yella, A.; Gao, P.; Humphry-Baker, R.; Curchod, B. F. E.; Ashari-Astani, N.; Tavernelli, I.; Rothlisberger, U.; Nazeeruddin, M. K.;Grätzel, M. Nat. Chem. 2014, 6, 242.

[199] Q. Wang, S. Ito, M. Grätzel, F. Fabregat-Santiago, I. Mora-Sero, J. Bisquert, T. Bessho, H. Imai, *J. Phys. Chem. B*, **2006**, *110*, 25210–25221.

[200] Q. J. Yu, Y. H. Wang, Z. H. Yi, N. N. Zu, J. Zhang, M. Zhang and P. Wang, *ACS Nano*, **2010**, *4*, 6032–6038

[201] G. P. Moss, *Pure Appl Chem* **1987**, *59*, 779–832.

[202] L. E. Webb, E. B. Fleischer, *J. Am. Chem. Soc.* **1964**, 667–669.

[203] N. Z. Mamardashvili, O. a Golubchikov, *Russ. Chem. Rev.* **2001**, *70*, 577–606.

[204] C. B. Storm, Y. Teklu, *J. Am. Chem. Soc.* **1972**, 1745–1747.

[205] J. K. M. Sanders, N. Bampos, Z. Clyde-Watson, S. L. Darling, J. C. Hawley, H.-J. Kim, C. C. Mak, S. J. Webb, in *Porphyr. Handb.* (Eds.: M. Kadish, K.M. Smith, R. Guillard), Academic Press, New York, **2000**, pp. 1–48.

[206] B.G. Kim, K. Chung, K. Kim, *Chem. Eur. J.,* **2013**, *19*, 5220.
[207] A.Yella, et al. *Science,* **2011**, *334*, 629–634.
[208] H. Imahori, T. Umeyama, S. Ito, *Acc. Chem. Res.,* **2009**, *42*, 1809–1818.
[209] T. Bessho, S. M Zakeeruddin, C. Y. Yeh, E. W. G. Diau, M. Grätzel, *Angew. Chem. Int. Ed.,* **2010**, *49*, 6646–6649
[210] Y. C Chang,. et al. *Chem. Commun.,* **2011**, *47*, 8910–8912.
[211] C. P. Hsieh, et al. *J. Mater. Chem.,* **2010**, *20*, 1127–1134
[212] S. L. Wu, et al. *Energy Environ. Sci.,* **2010**, *3*, 949–955.
[213] C. L. Wang, et al. *Energy Environ. Sci.,* **2012**, *5*, 6933–6940.
[214] M. Gouterman, *J. Chem. Phys.* **1959**, *30*, 1139–1161
[215] M. Gouterman, G. H. Wagnière, L. C. Snyder, *J. Mol. Spectrosc.* **1963**, *11*, 108–127.
[216] M. Gouterman, *J. Mol. Spectrosc.* **1961**, *6*, 138–163.
[217] M. Gouterman, G. H. Wagnière, L. C. Snyder, *J. Mol. Spectrosc.* **1963**, *11*, 108–127
[218] C. Weiss, H. Kobayashi, M. Gouterman, *J. Mol. Spectrosc.* **1965**, *16*, 415–450.
[219] W. M. Campbell, A. K. Burrell, D. L. Officer, K. W. Jolley, *Coord. Chem. Rev*. **2004**, *248*, 133 – 1379.
[220] F. Ambrosio, N. Martsinovich, A. Troisi, *J. Phys. Chem. Lett.,* **2012**, *3*, 1531.
[221] P. Rothemund, *J. Am. Chem. Soc.* **1936**, 625–627.
[222] J. S. Lindsey, K. A. Maccrum, J. S. Tyhonas, Y. Chuang, *J. Org. Chem.* **1994**, 579–587.
[223] J. S. Lindsey, *Acc. Chem. Res.* **2010**, *43*, 300–311.
[224] C.-H. Lee, J. S. Lindsey, *Tetrahedron* **1994**, *50*, 11427–11440.
[225] M. Guo, R. He, Y. Dai, W. Shen, M. Li, C. Zhu, S. H. Lin, *J. Phys. Chem. C,* **2012**, *116*, 9166.
[226] K. Ladomenou, T. N. Kitsopoulos, G. D. Sharma, A. G. Coutsolelos, *RSC Adv.* **2014**, *4*, 21379.
[227] M. J. Griffith, K. Sunahara, P. Wagner, P. Wagner, G. G. Wallace, D. L. Officer, A. Furube, R. Katoh, S. Mori, A. Mozer, *J. Chem. Commun.* **2012**, *48*, 4145.
[228] P. Pechy, F. P. Rotzinger, M. K. Nazeeruddin, O. Kohle, S. M. Zakeeruddin, R. Humphry-Baker, M. J Grätzel, *Chem. Soc., Chem. Commun.* **1995**, *65*
[229] F. Odobel, E. Blart, M. Lagrée, M. Villieras, H. Boujtita, N. El Murr, S. Caramori, C. A. Bignozzi, *J. Mater. Chem.* **2003**, *13*, 502.
[230] H. Hongshan, G. Ashim, S. Liping, G. S. Andrew, *Chem. Commun*., **2012**, *48*, 7619–7621
[231] H. Imahori, S. Hayashi, H. Hayashi, A. Oguro, S. Eu, T. Umeyama, Y.Matano, *J. Phys. Chem. C* **2009**, *113*, 18406.
[232] J. S. Lindsey, *Acc. Chem. Res*. **2009**, *43*, 300.
[233] P. D. Rao, S. Dhanalekshmi, B. J. Littler, J. S. J. Lindsey, *Org. Chem*. **2000**, *65*, 7323.
[234] S. Eu, S. Hayashi, T. Umeyama, A. Oguro, M. Kawasaki, N. Kadota, Y. Matano, H. Imahori, *J. Phys. Chem. C* **2007,** *111*, 3528.

[235] C. W. Lee, C.-W. Lu, C.-M. Lan, Y. L. Huang, Y.R. Liang, W. N. Yen, Y. C. Liu, Y.S. Lin, E. W. G. Diau, C.-Y. Yeh, *Chem. Eur. J.* **2009**, *15*, 1403.

[236] C.-P. Hsieh, H. P. Lu, C. L. Chiu, C. W. Lee, S. H. Chuang, C. L. Mai, W. N. Yen, S. J. Hsu, E. W. G. Diau, C. Y. Yeh, *J. Mater. Chem.* **2010,** *20*, 1127.

[237] Y. C. Chang, C. L. Wang, T. Y. Pan, S.H. Hong, C. M. Lan, H. H. Kuo, C. F. Lo, H. Y. Hsu, C. Y. Lin, , E. W. G. Diau *Chem. Commun*. **2011**, *47*, 8910.

[238238238] Wu, C.-H.; Pan, T.-Y.; Hong, S.-H.; Wang, C.-L.; Kuo, H.-H.; Chu, Y.-Y.; Diau, E. W.-G.; Lin, C.-Y. Chem. Commun. 2012, 48, 4329.

[239] C. L. Wang, Y. C. Chang, C. M. Lan, C. F. Lo, E. W. G. Diau, C. Y. Lin, *Energy Environ. Sci.* **2011**, *4*, 1788.

[240] C. F. Lo, S. J. Hsu, C. L. Wang, Y. H. Cheng, H. P. Lu, E. W. G. Diau, C.Y. J. Lin, *Phys. Chem. C* **2010,** *114*, 12018.

[241] C. L. Wang, C. M. Lan, S. H. Hong, Y. F. Wang, T.-Y. Pan, C. W. Chang, H. H. Kuo, M. Y. Kuo, E. W. G. Diau, C.-Y. Lin, *Energy Environ. Sci*. **2012**, *5*, 6933.

[242] C.P. Hsieh, H. P. Lu, C. L. Chiu, C.W. Lee, S. H. Chuang, C. L. Mai, W. N. Yen, S. J Hsu, E. W.G. Diau, C. Y. Yeh, *J. Mater. Chem.* **2010**, *20*, 1127.

[243] S. Hayashi, M. Tanaka, H. Hayashi, S. Eu, T. Umeyama, Y. Matano, Y. Araki, H. J. Imahori, *Phys. Chem. C* **2008**, *112*, 15576.

[244] J. M. Ball, N. K. S. Davis, J. D. Wilkinson, J. Kirkpatrick, J. Teuscher, R. Gunning, H. L. Anderson, H. Snaith, *J. RSC Adv.* **2012**, *2*, 6846.

[245] N. K. S. Davis, A. L. Thompson, H. L. Anderson, *Org. Lett.* **2010**, *12*, 2124.

[246] N. K. S. Davis, A. L. Thompson, H. L. Anderson, *J. Am. Chem. Soc.* **2011**, *133*, 30.

[247] C. Jiao, N. Zu, K. W. Huang, P. Wang, J. Wu, *Org. Lett.* **2011**, *13,* 3652.

[248] C.-L. Mai, W.-K. Huang, H.-P. Lu, C.W. Lee, C. L. Chiu, Y. R. Liang, E. W. G. Diau, C.-Y. Yeh*, Chem. Commun*. **2010,** *46*, 809.

[249] S. Mathew, H. Iijima, Y. Toude, T. Umeyama, Y. Matano, S. Ito, N. V. Tkachenko, H. Lemmetyinen, H. Imahori, J. *Phys. Chem. C* **2011**, *115*, 14415.

[250] T. Ripolles-Sanchis, B. C. Guo, H. P. Wu, T. Y. Pan, H. W. Lee, S. R. Raga, F. Fabregat-Santiago, J. Bisquert, C. Y. Yeh, E. W. G. Diau, *Chem. Commun*. **2012**, *48*, 4368.

[251] Y.-C. Chang, H. P. Wu, N. M. Reddy, H. W. Lee, H. P. Lu, C. Y. Yeh, E. W. G. Diau, *Phys. Chem. Chem. Phys.* **2013**, *15*, 4651.

[252] K. Hara, Y. Dan-oh, C. Kasada, Y. Ohga, A. Shinpo, S. Suga, K. Sayama, H. Arakawa, *Langmuir* **2004**, *20*, 4205.

[253] N. R. Neale, N. Kopidakis, J. van de Lagemaat, M. Grätzel, A. J. Frank, *J. Phys. Chem. B* **2005**, *109*, 23183.

[254] K. M. Lee, V. Suryanarayanan, K. C. Ho, K. R. Justin Thomas, J. T. Lin, *Sol. Energy Mater. Sol. Cells* **2007**, *91*, 1426.

[255] A. J. Mozer, P. Wagner, D. L. Officer, G. G. Wallace, W. M. Campbell, M. Miyashita, K. Sunahara and S. Mori, *Chem. Commun*., **2008**, 4741–4743.

[256] Z. J. Ning, Y. Fu and H. Tian, *Energy Environ. Sci*., **2010**, *3,* 1170–1181.

[257] L. Y. Han, A. Islam, H. Chen, C. Malapaka, B. Chiranjeevi, S. F. Zhang, X. D. Yang and M. Yanagida, *Energy Environ. Sci*., **2012**, *5*, 6057–6060.

[258] R. Y. Ogura, S. Nakane, M. Morooka, M. Orihashi, Y. Suzuki and K. Noda, *Appl. Phys. Lett*., **2009**, *94*, 073308.

[259] D. Kuang, P. Walter, F. Nuesch, S. Kim, J. Ko, P. Comte,S. M. Zakeeruddin, M. K. Nazeeruddin and M. Grätzel, *Langmuir*, **2007**, *23,* 10906–10909.

[260] M. Kimura, H. Nomoto, N. Masaki and S. Mori, *Angew. Chem., Int. Ed*., **2012**, *51*, 4371–4374.

[261] Y. Hua, S. Chang, D. Huang, X. Zhou, X. Zhu, J. Zhao, T. Chen, W. Y. Wong and W. K. Wong, *Chem. Mater*., **2013**, *25*, 2146-2153

[262] **(**a) L. Favereau, J. Warnan, F. B. Anne, Y. Pellegrin, E. Blart, D. Jacquemin and F. Odobel, *J. Mater. Chem. A*, **2013**, *1*, 7572; (b) J. Warnan, L. Favereau, F. Meslin, M. Severac, E. Blart, Y. Pellegrin, D. Jacquemin and F. Odobel, *ChemSusChem*, **2012**, *5*, 1568-1577

[263] (a) S. L. Wu, H. P. Lu, H. T. Yu, S. H. Chuang, C. L. Chiu, C. W. Lee, E. W. G. Diau, C. Y. Yeh, *Energy Environ. Sci*., **2010**, *3,* 949-955; (b) J. H. Delcamp, Y. Shi, J. H. Yum, T. Sajoto, E. Dell'Orto, S. Barlow, M. K. Nazeeruddin, S. R. Marder, M.Grätzel, *Chem. Eur. J.,* **2013**, *19*, 1819-1827; (c) J. Luo, M. Xu, R. Li, K. W. Huang, C. Jiang, Q. Qi, W. Zeng, J. Zhang, C. Chi, P. Wang, J. Wu, *J. Am. Chem. Soc*., **2014**, *136*, 265-272

[264] (a) K. Pei, Y. Z. Wu, W. J. Wu, Q. Zhang, B. Q. Chen, H. Tian, W. H. Zhu, *Chem. Eur. J.*, **2012**, *18*, 8190-8200; (b) Y. Z. Wu, M. Marszalek, S. M. Zakeeruddin, Q. Zhang, H. Tian, M. Grätzel, W. H. Zhu, *Energy Environ. Sci*., **2012**, *5*, 8261; (c) K. Pei, Y. Z. Wu, A. Islam, Q. Zhang, L. Y. Han, H. Tian, W. H. Zhu, *ACS Appl. Mater. Interfaces*, **2013**, *5,* 4986-4995; (d) W. H. Zhu, Y. Z. Wu, S. T. Wang, W. Q. Li, X. Li, J. Chen, Z. S. Wang, H. Tian, *Adv. Funct. Mater*., **2011**, *21*, 756-763.

[265] Y. Q. Wang, B. Chen, W. J. Wu, X. Li, W. H. Zhu, H. Tian, Y. S. Xie, *Angew. Chem. Int. Ed*., **2014**, *53*, 10779-10783

[266] X. Sun, Y. Wang,a X. Li, H. Ågren, W. Zhu, H. Tian, Y. Xie, *Chem. Commun*., **2014**, *50*, 15609-15612.

[267] M.E. Ragoussi, J.-H. Yum, A. K. Chandiran, M. Ince, G. de la Torre, M. Grätzel, M. K. Nazeeruddin, T. Torres, *ChemPhysChem* **2014**, *15*, 1033 – 1036

[268] K. Kalayansundaram, M. Grätzel, *Coord. Chem. Rev.* **1998**, *177*, 347.

[269] a) S. Ferrere, A. Zaban, B. A. Greg, *J. Phys. Chem. B* **1997**, *101*, 4490; b) S. Ferrere, B. A. Greg, *New J. Chem*. **2002**, *26,* 1155; c) Y. Shibano, T. Umeyama, Y. Matano, H. Imahori, Org. Lett. 2007, 9, 1971.

[270] a) A. Ehret, L. Stuhl, M. T. Spitler, *J. Phys. Chem. B* **2001**, *105*, 9960; b) S. Ushiroda, N. Ruzycki, Y. Lu, M. T. Spitler, B. A. Parkinson, *J. Am. Chem. Soc*. **2005**, *127*, 5158; c) S. Tatay, S. A. Haque, B.O_Regan, J. R. Durrant, W. J. H. Verhees, J. M. Kroon, A. Vidal-Ferran, P. GaviÇa, E. Palomares, *J. Mater. Chem*. **2007**, *17,* 3037.

[271] K. Susumu, T. V. Duncan, M. J. Therien, *J. Am. Chem. Soc*. **2005**, *127*, 5186–5195.

[272] M. Kasha, H. R. Rawls, M. A. El-Bayoumi, *Pure Appl. Chem*. **1965**, *11*, 371–392.

[273] M. Gouterman, *J. Chem. Phys*. **1959**, *30*, 1139–1161.

[274] M. Gouterman, *J. Mol. Spectrosc*. **1961**, *6*, 138–163.

[275] X. Huang, C. Zhu, S. Zhang, W. Li, Y. Guo, X. Zhan, Y. Liu, Z. Bo, *Macromolecules* **2008** , *41* , 6895.

[276] J.‐ J. Cid, C. Ehli, C. Atienza‐ Castellanos, A. Gouloumis, E.‐ M. Maya, P. Vazquez, T. Torres, D. M. Guldi, *Dalton Trans* . **2009** , *20* , 3955.

[277] a) J. Bartelmess, C.Ehli, J.‐ J. Cid, M. Garcia‐ Iglesias, P. Vazquez, T. Torres, D. M. Guldi, *Chem. Sci* . **2011** , *2* , 652; b) J. Bartelmess, C. Ehli, J.‐ J. Cid, M. Garcia‐ Iglesias, P. Vazquez, T. Torres, D. M. Guldi, *J. Mater. Chem* . **2011** , *21* , 8014.

[278] J. Malig, N. Jux, D. Kiessling, J.‐ J. Cid, P. Vazquez, T. Torres, D. M. Guldi, *Angew. Chem. Int. Ed* . **2011** , *50* , 3561.

[279] L. Brinkhaus, G. Katsukis, J. Malig, R. D. Costa, M. Garcia‐ Iglesias, P. Vazquez, T. Torres, D. M. Guldi, *Small* **2013** , *9* , 2348.

[280] D. Wohrle, M. Eskes, K. Shigehara, A. Yamada, *Synthesis* **1993** , *2* , 194.

[281] Discrete Pc‐ DPP molecules have been already reported. See for instance: D. Molina, A. Guerrero, G. Garcia‐ Belmonte, F. Fernandez‐ Lazaro, A. Sastre‐ Santos, *Eur. J. Org. Chem* . **2014** , 4585.

[282] (a) CG Claessens, D González-Rodriguez, MS Rodriguez-Morgade, A Medina, T.Torres *Chem.Rev*. **2014**; 114: 2192–2277. (b) PL Lo, X Ng DKP Leng. *Coordination Chem. Rev*. **2007**; *251*, 2334–2353. (c) N. Kobayashi *Coordination Chem Rev*. **2002**; *251*, 129–152. (d) WA Nevin, WL Hempstead, CC Leznoff, ABP Lever. *Inorg. Chem.* **1987**; *26*, 570–577. (e) CC Leznoff, H Lam, WA Nevin, N Kobayashi, P Janda, ABP Lever. *Angew. Chem., Int. Ed. Engl.* **1987**; *26,* 1021–1023. (f) A Lyubimtsev, Z Iqbal, M Hanack. *Aust. J. Chem*. **2008**; *61*, 273–278.

[283] H Ali, JE. van Lier *Tetrahedron Lett.* **1997**; *38* .1157–1160.

[284] (a) BN Yu, AM.Kolker *J. Phys. Chem. C* **2014**, *118*: 14403,1440. (b) G Meltem, D Mahmut, A. Devrim *J. Photochem. Photobiol A* **2013**, *266*, 37–46.

[285] (a) MM Khan, H Ali, JE. van Lier *TetrahedronLett.* **2001**; *42*,1615–1617. (b) Y Chen, XP. Zhang *J. Org. Chem*. **2003**, *68*, 4432–4438. (c) T Takanami, M Hayashi, F Hino, K Suda *Tetrahedron Lett.* **2003**, *44*, 7353–7357 (d) LJ Esdaile, MO Senge, DP. Arnold *Chem. Commun*. **2006**, 4192–4194. (e) K Ladomenou, T Lazarides, MK Panda, G Charalambidis, D Daphnomili, AG Coutsolelos. *Inorg. Chem*. **2012**, *51*, 10548–10556.

[286] H Tian, H Ali, JE. van Lier *Tetrahedron Lett* ., **2000**, *41*, 8435–8438.

[287] ARM Soares, MV Martınez-Dıaz, A Bruckner, AMVM Pereira, JPC Tome, CM Alonso, MAF Faustino, GPMS Maria, MGP Neves, AC Tome, AMS Silva, AS Jose, AS Cavaleiro, T Torres, DM Guldi. *Org. Lett***. 2007**, *9* : 1557–1560.

[288] C. R. Ganivet, A. Lennert, R. D. Costa, G. de la Torre, T. Torres, D. M. Guldi, *Angew. Chem. Int*., **2015**.

[289] C. R. Ganivet, B. Ballesteros. G. de la Torre, J. M. Clemente-Juan, E. Coronado, T. Torres, *Chem. Eur. J*. **2013** , *19*, 1475-1465.